Renormalization, Entanglement and Continuous Tensor Networks

by

Adrián Franco Rubio

A thesis
presented to the University of Waterloo
in fulfillment of the
thesis requirement for the degree of
Doctor of Philosophy
in
Physics

Waterloo, Ontario, Canada, 2020

Examining Committee Membership

The following served on the Examining Committee for this thesis. The decision of the Examining Committee is by majority vote.

External Examiner:	Paul Fendley Professor, Dept. of Physics, University of Oxford
Supervisor(s):	Guifré Vidal Faculty, Perimeter Institute for Theoretical Physics Adjunct Faculty, Dept. of Physics and Astronomy University of Waterloo
	Timothy Hsieh Junior Faculty, Perimeter Institute for Theoretical Physics Adjunct Faculty, Dept. of Physics and Astronomy University of Waterloo
Internal Member:	James Forrest Professor, Dept. of Physics and Astronomy University of Waterloo
Internal-External Member:	Achim Kempf Professor, Dept. of Applied Mathematics University of Waterloo
Other Member(s):	Beni Yoshida Junior Faculty, Perimeter Insitute for Theoretical Physics Adjunct Faculty, Dept. of Physics and Astronomy University of Waterloo

Author's Declaration

This thesis consists of material all of which I authored or co-authored: see Statement of Contributions included in the thesis. This is a true copy of the thesis, including any required final revisions, as accepted by my examiners.

I understand that my thesis may be made electronically available to the public.

Statement of Contributions

The following constitute my research contributions contained in this thesis:

Chapter 3 consists mostly of material from Reference [1], which I co-authored with Guifré Vidal. Dr. Vidal proposed the question, and I carried out the analysis and wrote most of the paper.

Chapter 4 consists mostly of material from Reference [2], which I co-authored with Guifré Vidal. The inspiration for the project came from conversations between both of us, while I carried out the analysis and the writing of most of the paper.

Chapter 5 consists mostly of currently unpublished material of which I am the sole author [3], and which is planned to be published in the near future.

Chapter 6 consists mostly of currently unpublished material which I co-authored with Qi Hu and Guifré Vidal [4], and which is planned to be published in the near future. The idea of the project was proposed by Dr. Vidal. Dr. Hu took the lead of the project, and I independently reproduced his analytical and numerical results (the latter using different, more efficient software) for confirmation. This is with the exception of the optimization procedure which is solely Dr. Hu's. The first draft of the paper was written by myself, which was then used as reference for a second draft written by Dr. Hu.

Chapter 7 consists mostly of material from Reference [5], which I co-authored with Qi Hu and Guifré Vidal. The idea for the project and most of its advances came during conversations among the three of us. Dr. Hu took the lead of the project and wrote the draft of the paper.

Abstract

The study of the ground states of local Hamiltonians in quantum many-body and quantum field theoretic systems is a source of many research problems of great complexity. Almost in its entirety, this thesis deals with constructions related to the field of tensor networks, which are efficient parametrizations of mathematical objects from quantum many-body theory (such as quantum states and operators) that exploit our knowledge of their entanglement structures in order to obtain improvements in our computational abilities. In the past decade, the new research program of *continuous* tensor networks has arisen with the goal of reproducing, in the setting of quantum field theory, the success that tensor network techniques have enjoyed on the lattice.

First, we present a number of results from research performed on non-interacting examples of the Continuous Multiscale Entanglement Renormalization Ansatz, or cMERA, a continuous tensor network that provides a variational wavefunctional for a quantum field theoretic ground state. Initially, we study the correlations and entanglement structure of cMERA states, providing evidence that such states can be interpreted as UV regularized versions of the physical states they approximate. After that, we study what modifications of the formalism are necessary in order to consider systems with gauge symmetry, or in the presence of boundaries and defects. We obtain prescriptions for the treatment of these cases which, we expect, may also hold in the interacting setting.

We then abandon briefly the area of continuous tensor networks to present a piece of research within a different though related research program: that of the study of manifestations of universal emergent behaviour in critical lattice systems. In particular we bring attention to the existence of an approximate representation of the Virasoro algebra supported on the eigenvectors of the reduced density matrices of critical lattice systems. We call this the *entanglement algebra*, and study its accuracy in the particular case of the Ising model.

Lastly, we present a proposal for a continuous version of the Tensor Network Renormalization (TNR) algorithm, which we dub continuous TNR, or cTNR. cTNR operates on UV regularized classical partition functions or quantum Euclidean path integrals, and generates a real-space renormalization group flow via continuous coarse-graining and rescaling operations. We show that a UV regularized version of the free boson path integral can be made a fixed point of such a renormalization flow, in a way that allows for recovery of the conformal data associated to the free boson conformal field theory.

Acknowledgements

First thanks has to go to my PhD supervisor: thank you, Guifré, for your guidance and support. Thanks for being there to give away physics insights, honest advice and occasional ironic remarks, in spite of having to deal with the many occupations of an active research career. Thanks for being reassuring and for raising concerns when each of them was needed. Thanks for teaching me about physics, about being a physicist, and a bit about life in general.

I am indebted to the whole tensor network monoid (there are no groups at Perimeter). Thanks to our postdocs Martin, Julián, Ash, Adam, Stefan and Jacob. Thanks to our visitors Siva and Ruoshui. Thanks to my fellow PhD students Markus, Nick and Yijian, and special thanks to Qi, for all those insightful hours spent discussing in front of blackboards: most of what is good in our collaborative work is due to you. I have learnt immensely from you all. You are truly first-class scientists and approachable, warm humans, and deserve every recognition.

Thanks to the La Caixa Foundation for sponsoring the first half of my PhD, and to Perimeter Institute and the University of Waterloo for sponsoring the other half. Thanks to all the different funding agencies that have supported my development as a physicist.

Thanks to the members of my PhD Thesis Committee for their time and effort, and for giving me useful feedback on this thesis.

Thanks to the Perimeter community: master students, PhD students, Bistro and administrative staff, and all other employees, for making it such an amazing, welcoming place. Thanks to Debbie for all the help. Thanks to the members of the Perimeter Orchestra during these years, for making me invariably stop whatever I was doing every Tuesday evening for a couple of hours of good fun. Thanks to Gang, Dan and Shira for being extraordinary friends, always sure to land a smile on my face and lend a helping hand when I needed it. Thanks to Christophe, for being a great officemate to talk to when work is not going as expected (and when it is). Thanks to Álvaro, Javier and Raimón, for dropping by PI in the past four years to cheer me up.

Thank you Supranta and Soham, my housemate and honorary housemate respectively, for the laughter, the food and the conversations, and for making our house feel like a home.

Thanks to the La Caixa Fellows, for turning the map of a once foreign and unfamiliar half-continent into a beaming constellation of friendships and good memories.

Thanks to Priyank, Chris, Tom, Camila and Sajin: as my non-physicist friends in Waterloo you were unknowingly tasked with keeping my sanity. I do not know how successful you were at that, but all the fun was definitely worth it.

Thanks to all the wonderful people I have met in my visits to research institutions, conferences and schools around the world, too numerous to list, who have kept me going along the way.

Thank you, Nitica, my best friend in Waterloo, with all my heart. Thanks for taking care of me, for being my confidant, someone I can always turn to. It is hard to overstate how much of a positive difference your friendship has made for me all these years, and I just hope I was able to reciprocate even if slightly.

Finally, infinitely many thanks to my family: you all have been there through every struggle and setback, in my moments of strongest need, within an endless supply of support and love from the other side of the ocean. I am extremely fortunate to have you.

Dedication

Para mis padres, Hipólito y Gloria. Para mi hermana Lorena.
Para mis abuelos, Hipólito, Maruja, Manolo y Gloria.

Table of Contents

List of Figures

Chapter 1

Introduction

This chapter's goal: In this chapter we give a general overview and motivation of the contents of the thesis, and we review some background concepts.

1.1 This thesis: what to expect

Quantum many-body systems and their emergent behaviours, as objects of study, are prodigal with great computational challenges. These are rooted in the fact that the scaling of computational resources required to naïvely simulate them is exponential with the system size, hence becoming unmanageable already for sizes much smaller than those of physical interest. In tackling this problem, an understanding of the *entanglement* structure of the quantum states of interest, mostly ground states of local Hamiltonians, has become one of our most important assets. Indeed, in addition to being a concept of undeniable theoretical value, entanglement has the potential to guide new advancements in the *efficient* simulation of such systems.

The present thesis fits within the general program we just described. Most of its contents are in particular aligned with the field of *tensor networks*, one of the most paradigmatic research avenues exploiting knowledge about entanglement to improve our computational capabilities. Additionally, we will also devote some time to the discussion of entanglement structures in critical lattice systems.

Tensor networks provide computationally efficient ways to parametrize and manipulate the mathematical objects involved in the quantum many-body problem, most notably

quantum states. In its now almost three decades of existence, the field of tensor networks has grown and evolved, jumping from its initially restricted playground of numerical simulations to become a useful tool also in theoretical analyses, its applications ranging from condensed matter physics and materials science to quantum chemistry, machine learning or even quantum gravity. Tensor networks have played an important role in the study of entanglement structures and real space renormalization group flows in quantum lattice systems in the past, and new methods based on them keep being developed, e.g. to address the simulation of lattice gauge theories in regimes outside the reach of Monte Carlo numerics, or to understand and classify topological phases of matter.

About a decade ago, the tensor network community began the pursuit of a new quest, namely the application of tensor network techniques in a *quantum field theoretic* setting. Quantum field theory (QFT), as opposed to lattice models, presents continuous degrees of freedom and symmetries, and is regarded as our best current description of the microscopic physics of the Universe, at least as an effective theory up to scales where quantum gravitational effects become relevant. Its applications range today from particle physics to condensed matter, and despite its ubiquity, much is still to be achieved in terms of our computational abilities. A lot of our current knowledge of strongly correlated regimes, where perturbation theory breaks, comes from the use of lattice discretization as a UV regulator of the theory at hand. The research program of continuous tensor networks was thus born with the aim of importing what was learned via tensor networks about discrete lattice models to the continuum of QFT.

Here we will focus on a particular subset of continuous tensor network constructions, the continuous multiscale entanglement renormalization ansatz (cMERA), and continuous tensor network renormalization (cTNR). Unsurprisingly from their names, both have strong ties to the renormalization group (RG): cMERA is a variational class of ansatz wavefunctionals for quantum field theoretic states that includes explicit information about the RG flow of the state; while cTNR is a proposed scheme that implements a real space RG flow on continuous tensor network representations of classical partition functions or Euclidean path integrals.

This thesis is organized as follows: in Chapters 2-5 we occupy ourselves with the cMERA. We introduce the cMERA class, along with the necessary background, in Chapter 2, and devote Chapter 3 to understanding the entanglement structure of cMERA wavefunctionals. Chapters 4 and 5 respectively explore the modifications required by the cMERA formalism in the presence of gauge symmetry and of boundaries and defects. After that, Chapter 6 serves as an interlude where we return to the discretuum and explore a phenomenon that, while somewhat further from the main line of the thesis, shares important conceptual ties with it: the emergence of universal entanglement structures in critical lat-

tice systems. Finally, in Chapter 7 we return to the realm of continuous tensor networks to introduce and discuss the cTNR proposal. We then conclude with a brief epilogue.

For the rest of this chapter, we would like to compile a few introductory concepts that either provide background to motivate the research carried out in this thesis or will be directly used in subsequent chapters. That said, we have mostly tried to keep important explanations until the moment they are about to become relevant, so the reader should not expect to be constantly referring back to this chapter while reading of the rest of the thesis. In Section 1.2 we introduce (discrete) tensor networks. While we will not be working with them, they provide the main motivation and starting point for most of the research presented below. Section 1.3 provides a first introduction to continuous tensor networks. Finally, Section 1.4 introduces a few conformal field theory (CFT) concepts that will later come in handy when addressing critical theories both in the continuum and on the lattice.

1.2 Tensor networks

When talking about tensor networks, the word *tensor* is used in the sense of multilinear algebra, that is, to describe a potentially multidimensional array of (for our purposes complex) numbers. More precisely, given a set of N natural numbers $d_1, \ldots, d_N$, a $(d_1, \ldots, d_N)$-dimensional tensor T is an element of the tensor product vector space

$$T \in \mathbb{C}^{d_1} \otimes \ldots \otimes \mathbb{C}^{d_N}. \tag{1.1}$$

The components of the tensor are denoted in the usual way via indices

$$T_{i_1 \ldots i_N} \qquad i_j = 1, \ldots, d_j \qquad j = 1, \ldots, N. \tag{1.2}$$

We call N the *rank* of the tensor. Tensors of rank 0, 1 and 2 are easily identified as, respectively, scalars, d_1-dimensional vectors and $d_1 \times d_2$ dimensional matrices.

Tensors arise naturally when working with vector spaces which have a tensor factorization. Indeed, given an element of such a vector space, its coefficients with respect to a tensor product basis can be expressed as a tensor. This is the case, for instance, of the wavefunction $|\psi\rangle$ of an N-particle quantum system, since the axioms of quantum mechanics state

$$|\psi\rangle \in \mathcal{H}_1 \otimes \ldots \otimes \mathcal{H}_N \tag{1.3}$$

where $\mathcal{H}_j$ denotes the Hilbert space of states of the j-th particle. Indeed, fixing a basis $|1\rangle, \ldots, |d_j\rangle$ for each $\mathcal{H}_j$, we can express

$$|\psi\rangle = \sum_{i_1,\ldots,i_N} T_{i_1 \ldots i_N} |i_1 \ldots i_N\rangle \tag{1.4}$$

where each index i_j takes values in the corresponding range $1, \ldots, d_j$. The component $T_{i_1 \ldots i_N}$ is thus nothing but the coefficient of the basis vector $|i_1 \ldots i_n\rangle$ in the basis expansion of $|\psi\rangle$.

The field of tensor networks benefits from a particularly handy *diagrammatic notation*, the Penrose notation, that represents tensors as polygons or circles with legs attached to them, each representing one index of the tensor:

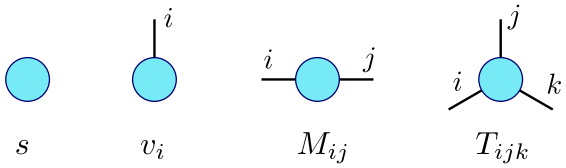

Due to this notation, a tensor of rank N is sometimes referred to as an *N-legged tensor*.

Tensor contraction is an operation that generalizes matrix multiplication. It produces an output tensor out of two input tensors by summing over one of their indices, and it is represented diagrammatically by joining the corresponding legs of the tensors, for example:

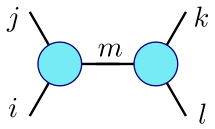

$$A_{ijkl} = \sum_m T_{ijm} T_{mkl}$$

Most common operations in linear algebra are tensor contractions of some kind, e.g. taking a trace, or acting a matrix on a vector:

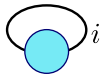

$$\operatorname{tr} M = \sum_i M_{ii}$$

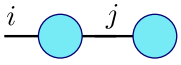

$$(Mv)_i = \sum_i M_{ij} v_j \, .$$

A *tensor network* represents a tensor as the result of multiple contractions of lower dimensional tensors. In quantum many-body theory, the paradigmatic example is the matrix product state (MPS) [6], a tensor network representation for a state of a 1-dimensional quantum many-body system, following (1.4), given by

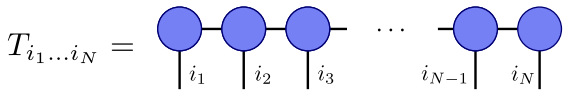

The contracted legs of this network are usually called *virtual* legs or bonds and the uncontracted ones, labeled $i_1, \ldots, i_N$, are called *physical* legs, since each of them is associated to the Hilbert space $\mathcal{H}_j$ of one of the physical degrees of freedom.

The example of the MPS will help us present one of the initial applications of tensor networks: as efficient parametrizations of very high-dimensional objects. Note that the MPS is composed of two- and three-legged tensors

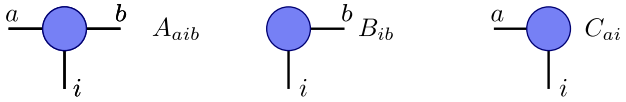

where we assume that the dimensions of each index are fixed: we call d the physical bond dimension and D the virtual bond dimension. In general, any quantum state of N qudits (degrees of freedom whose local Hilbert space dimension is d) on a line can be written as an MPS. However, generic states require the virtual bond dimension D to grow exponentially with N. Parameter counting provides an intuitive explanation for this fact. The number of parameters of a generic wavefunction in the many-body Hilbert space is d^N, that is, it grows exponentially with the number of degrees of freedom. On the other hand, the number of parameters in the MPS tensor network is just $(N-2)dD^2 + 2dD$, where the first term is the contribution from the three-legged tensors, and the second that of the two-legged tensors. This amount is linear in N.

Turning this argument around, we conclude that an MPS with fixed bond dimension D will not be able to represent arbitrary tensors, i.e., arbitrary states in the Hilbert space of the qudit chain, but only a particular subclass of them, which on the other hand only need a number of parameters linear in N to be specified. This would not be at all interesting were it not for the fact that the particular subclass that can be described by MPS is actually *physically relevant*. Indeed, the states that are expressible as MPS happen to be those that satisfy an *area law*[1], and are therefore lowly entangled. There is a (positive)

[1] A many-body quantum state satisfies the area law if the entanglement entropy of a spatial region $\mathcal{R}$ scales as the area of the boundary of $\mathcal{R}$. In one spatial dimension, this translates to the fact that the entanglement entropy of an interval saturates to a constant value independent of its length as we consider longer and longer intervals. Area-law states display a low amount of entanglement in comparison with generic states from the many-body Hilbert space. Indeed, a typical many-body state will satisfy a *volume law*, that is, the entanglement entropy of $\mathcal{R}$ will grow as the volume of $\mathcal{R}$ (in the one dimensional case, the entanglement entropy of an interval will scale proportionally to its length).

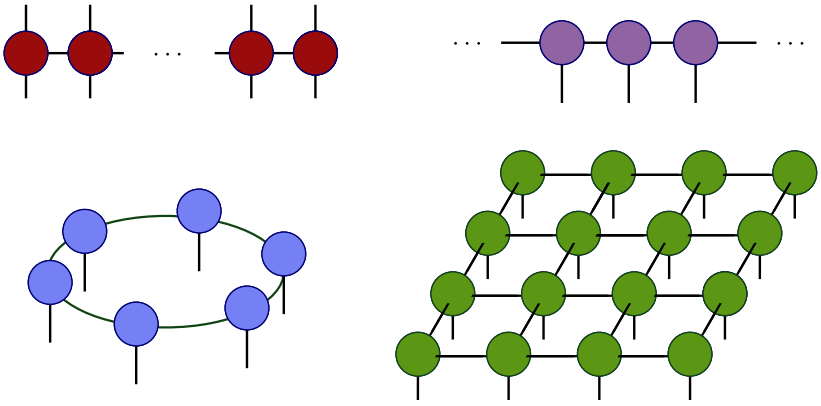

Figure 1.1: Top left: a matrix product operator (MPO). Top right: an infinite MPS. Bottom left: a periodic MPS. Bottom right: a two-dimensional PEPS.

correlation between how entangled a state is, and how big the bond dimension D necessary to represent it as an MPS is. This connection can be made precise, but intuitively we can already appreciate that the family of MPS with lowest bond dimension, $D = 1$, corresponds exactly with the family of product states, those which have no entanglement between different degrees of freedom.

Luckily for us, ground states of gapped Hamiltonians belong to this category of low entanglement states, which makes MPS useful tools to describe them with linearly (as opposed to exponentially) many parameters. With time, MPS techniques have grown to become an indispensable tool with abundant and diverse applications. Figure 1.1 shows a few tensor networks from the family of the MPS. A related tensor network, the matrix product operator (MPO), can be used to describe operators acting on the states of the qudit chain. The tensor network can also be given periodic boundary conditions (periodic MPS), and if the qudit chain is infinite, but translation invariant, we can use an analogous formalism based on the iMPS (infinite MPS), which just assumes that the tensors of the MPS continue on forever, to describe states in the thermodynamic limit with finitely many parameters. In higher dimensions, MPS are replaced by projected entangled pair states (PEPS) [7] which have a similar structure, but are significantly harder to work with, both from the computational complexity and the analytical points of view.

However, not all one-dimensional quantum states of interest have the entanglement structure that is hard-coded in an MPS with constant bond dimension. Most notably, ground states of *gapless* Hamiltonians present logarithmic violations of the area law (the

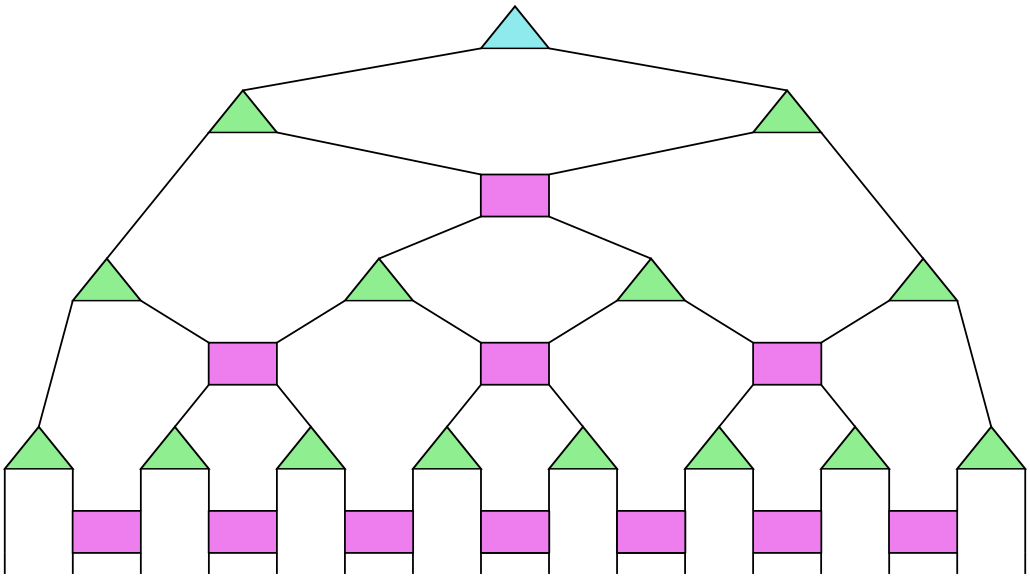

Figure 1.2: A MERA for a finite one-dimensional system

entanglement entropy of an interval scales as the logarithm of its length) due to them having an infinite correlation length, which allows for entanglement to be present at all length scales. The *multiscale entanglement renormalization ansatz* (MERA) [8] is a different tensor network that matches the entanglement pattern of these states. Its structure is more complex than that of the MPS, as can be seen in Figure 1.2: its most prominent feature when compared to MPS (and to PEPS, in higher dimensions) is that the network lives in one higher dimension than the state it represents. Thus for a one-dimensional state it displays a two-dimensional tree-like structure. This extra dimension has a very useful interpretation as one along which the renormalization group flow happens. MERA is the tensor network to whose continuous version we are going to devote the most space in this thesis. We shall introduce it at proper length in Chapter 2.

Even though it is the case that we will be mostly focusing on, tensor networks are not exclusively aimed at representing pure quantum states. We have already seen them used above to represent an operator as an MPO. Density matrices of quantum many-body systems are also usual targets for tensor network representation. In Chapter 7 we will look at tensor networks used to represent partition functions of 2-dimensional classical systems, where each tensor contains the information about the local Boltzmann weights. Alternatively, these tensor networks can also be interpreted as discrete versions of Euclidean path integrals for 1+1 quantum dimensional systems. The reader interested to learn more

about tensor networks is invited to consult reviews [9, 10], or the website [11], which additionally contains examples of algorithms coded in Matlab, Julia and Python.

1.3 Continuous tensor networks

Most of this thesis revolves around the idea of generalizing tensor network techniques to the setting of quantum field theory. The corresponding constructions are called *continuous tensor networks*. In the particular case of tensor networks that represent quantum states on the lattice, their continuous versions will be parametrizations of quantum states in the continuum, inside the Hilbert space of a quantum field theory.

Why should we care about continuous tensor networks? There are a few possible answers to this question. When working with a continuous system, one of the possible routes to take involves simply discretizing it and working on it with lattice techniques, e.g. discrete tensor networks. Conceptually, though, there are big differences between discrete and continuous systems: for instance, discretization will break continuous symmetries (such as those in the Poincaré group) to, at best, discrete subgroups thereof. It can also lead to artifacts, i.e. physical effects not present in the continuous model but arising when a lattice is introduced, such as fermion doubling. Hence, while it is early to say if there will be a computational advantage in keeping things mostly[2] continuous, there is definitely a conceptual one. Additionally, both for computational and theoretical reasons, it would be highly desirable to develop a variational approach to QFT, and to get a better grasp of the entanglement structure of QFT states. The former could give a new way to move past perturbative approaches and probe the strongly interacting regimes of quantum field theoretic systems, while the latter could bring in quantum information theoretic insight into QFT and contribute to the "emergent spacetime from entanglement" program in quantum gravity, stemming from the holographic principle and the AdS/CFT correspondence [12]. Tensor networks have proved themselves very handy in performing the analogous tasks on the lattice, and continuous tensor networks have the potential to do so in the continuum. Along these lines, one of the research fields where interest for discrete and continuous tensor networks saw faster growth is in fact the holographic and AdS/CFT communities [13–35], especially for their use as toy models. Finally, an understanding of continuous tensor networks might also bring new insights into the area of discrete tensor networks, helping design better tensor network algorithms to minimize lattice effects and ease generalizations

[2]Note that if we want to apply numerical computation, eventually we are going to have to discretize the information, introducing a finite basis since a digital computer cannot store truly continuous variables.

to higher dimensions (which may be more straightforward in the continuum than on the lattice).

Now that we have covered a few reasons *why*, let us talk briefly about *how*. Note that we have intentionally avoided speaking of "continuous limits" of tensor networks to describe continuous tensor networks. In fact, one could say there are two main types of continuous tensor networks, according to how one arrives at their definition: the ones that arise as *bona fide* continuous limits of discrete tensor networks and the ones that do not. For instance, the continuous MPS (cMPS), introduced in [36], can be defined as arising from a vanishing lattice spacing limit of a family of discrete MPS, whose tensors have components that depend on an infinitesimal quantity that goes to zero with the lattice spacing. The continuous tensor network states (cTNS) proposed in [37] can also be built in a relatively similar fashion as continuum limits of discrete PEPS.

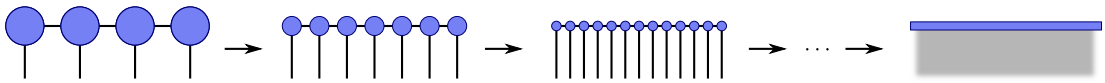

Figure 1.3: Schematic depiction of the limiting procedure that gives rise to the definition of the continuous matrix product state.

On the other hand, the MERA, the tensor network we introduce in the following chapter, does not give rise to a continuous MERA via a continuum limit of this sort, at least not naïvely. Indeed, the cMERA is defined in a way that does not involve an "$\varepsilon \to 0$ continuum limit". Rather, as we will see in Chapter 2, the construction is motivated by analogy, copying the philosophy of the lattice definition with the tools available in the quantum field theoretic setting. It is an open problem in the field whether there exists a meaningful[3] continuum limit of discrete tensor networks that gives rise to the continuous MERA. If that were the case, there could be applications for it in numerical algorithms. Indeed, this happens for the cMPS, for which algorithms exist that interpret the continuum object as an organizing structure that contains all possible discretizations at different lattice parameters, and thus operate by discretizing it with a certain relevant lattice parameter to an MPS, working on it via discrete MPS algorithms, then reinterpolating back to a cMPS, and iterating [38].

[3]By *meaningful* we mean that the corresponding discrete tensor networks have a certain degree of structure, and if possible a standalone physical interpretation. We specify this because in principle one could produce such a limit by just discretizing the operators that define the continuous MERA, but the resulting tensor networks would look little like MERA.

1.4 Criticality, CFT and conformal data

Critical phenomena are a major area of study in many-body physics, both classical and quantum. They underlie the theory of second-order phase transitions, and play an important role in the understanding of renormalization group flows and universality. At criticality, the long distance physics of a Lorentz invariant quantum system is described by a conformal field theory (CFT), a quantum field theory whose symmetries include the conformal group, and which is a fixed point of the renormalization group flow. In the next chapters we are going to be working with tensor network constructions that are intimately related to the renormalization group, and we will be recurrently referring to a few CFT-related concepts. Hence, we give in what follows a review of these. Our presentation is far from exhaustive, and we refer to other sources [39–42] for a more systematic introduction.

A conformal field theory is a quantum field theory that is symmetric under the conformal group, the group of diffeomorphisms that preserve the metric up to a (possibly spacetime dependent) scale factor:

$$g'_{\mu\nu}(x') = \Omega(x) g_{\mu\nu}(x) \tag{1.5}$$

In flat spacetime, the conformal group is generated by translations, rotations and/or boosts, scale transformations and so-called special conformal transformations (translations preceded and followed by an inversion with respect to the origin). Thus, in particular, CFTs are scale-invariant theories, thus being suitable to describe critical phenomena, where scale invariance plays a key role. As such, CFTs are also fixed points of the RG flow. But aside from their applicability to describe a lot of interesting emergent properties, a big motivation to look at CFTs is that the large amount of symmetry can be exploited to help in solving the theory. Indeed, many properties of the correlation functions are dictated solely by symmetry considerations, giving rise to a whole research program devoted to exploiting the consequences of these powerful symmetries, known as the *conformal bootstrap*.

One major problem in condensed matter physics involves the identification of the underlying CFT for critical systems whose microscopic description does not make it self-evident. A route towards this goal comes from the extraction of *conformal data* from the system at hand. Conformal data are parameters that can be used to describe the CFT, and whose knowledge amounts to being able to compute any correlation function. For us, they will be important since our continuous tensor network constructions will in many occasions be targeting critical systems, and the retrieval of correct conformal data from the examples that we can handle analytically will serve both as a sanity check and a proof of principle that such information could be extracted in less tractable cases from a successful continuous

tensor network implementation. We devote the rest of this section to the introduction of conformal data. It is important to remark that CFTs in $d = 2$ spacetime dimensions have a larger algebra of infinitesimal symmetries, and in consequence display more structure than CFTs in arbitrary dimensions. We thus present their specific features after introducing the general formulation.

1.4.1 Operator spectrum and operator product expansion (OPE)

When working in CFT we assume the existence of a family of local operators that transform in a simple way, called *quasiprimary* operators. Let us place ourselves in d dimensions and Euclidean signature, and consider a conformal transformation $x \to x'$ satisfying (1.5); its Jacobian will then have the form:

$$\frac{\partial x'^{\mu}}{\partial x^{\nu}} = \sqrt{\Omega(x)} M^{\mu}{}_{\nu}(x), \qquad M^{\mu}{}_{\nu}(x) \in \mathrm{SO}(d). \tag{1.6}$$

which reflects that the conformal transformation is just the combination of a local rotation and a local rescaling. The transformation law of a quasiprimary operator is

$$\mathcal{O}(x) \to \mathcal{O}'(x') = [\Omega(x)]^{-\frac{\Delta}{2}} \mathcal{R}\left[M^{\mu}{}_{\nu}(x)\right] \mathcal{O}(x) \tag{1.7}$$

where $\mathcal{R}\left[M^{\mu}{}_{\nu}(x)\right]$ is the rotation matrix corresponding to $M^{\mu}{}_{\nu}(x)$ in the representation $\mathcal{R}$ that $\mathcal{O}(x)$ transforms in according to its spin. Quasiprimary operators, each with their scaling dimension Δ and spin representation $\mathcal{R}$, form the *operator spectrum* of the CFT, except in the two-dimensional case, where this term is reserved for a more fundamental subclass of quasiprimary operators called *primary*[4] operators (see below). All local operators in the theory can be expressed in terms of quasiprimary operators and their *descendants* (i.e., their derivatives). The two-point functions of quasiprimary operators are fixed by conformal symmetry and, when properly normalized, depend only on their scaling dimensions. For example, in the scalar case:

$$\langle \mathcal{O}_1(x_1) \mathcal{O}_2(x_2) \rangle = \frac{\delta_{\Delta_1, \Delta_2}}{|x_1 - y_2|^{2\Delta_1}} \tag{1.8}$$

This power-law decay of correlators is, as we already mentioned when talking about MERA, a characteristic phenomenon of scale invariant theories.

[4]The reader should be warned that some texts on $d > 2$ CFT may want to abbreviate and call all quasiprimary fields "primary" since there is no distinction outside $d = 2$ (this is the case in [41]).

Another important aspect of CFTs is the fact that one can define an operator product expansion (OPE), where the product of two nearby operators is replaced by a series of local operators:

$$\mathcal{O}_1(x)\mathcal{O}_2(0) = \sum_{\mathcal{O}} c_{12\mathcal{O}} f_{12\mathcal{O}}(x, \partial_y)\mathcal{O}(y)|_{y=0}, \tag{1.9}$$

where the sum is over quasiprimary fields $\mathcal{O}$, and the functions $f_{12\mathcal{O}}(x, \partial_y)$ are fixed by conformal symmetry, leaving the constants $c_{12\mathcal{O}}$ as an extra piece of data that we need to specify the theory. These constants, also called *OPE coefficients*, show up in the three-point functions between quasiprimary fields. For instance, for three scalar quasiprimaries we have (assuming they are properly normalized so that (1.8) holds):

$$\langle \mathcal{O}_1(x_1)\mathcal{O}_2(x_2)\mathcal{O}_3(x_3)\rangle = \frac{c_{123}}{|x_1 - x_2|^{\Delta_1+\Delta_2-\Delta_3}|x_2 - x_3|^{\Delta_2+\Delta_3-\Delta_3}|x_1 - y_3|^{\Delta_1+\Delta_3-\Delta_2}}. \tag{1.10}$$

In fact, knowledge of the operator spectrum (including scaling dimensions and spins) and the OPE coefficients amounts to completely solving the theory, since n-point functions maybe reduced to 3-point functions via the OPE, and they computed with the help of (1.10) and its higher spin counterparts. Together, thus, they form the conformal data for the CFT.

1.4.2 Two-dimensional CFT

In two spacetime dimensions, conformal symmetry becomes a stronger property. Indeed, for $d > 2$, the conformal symmetry algebra is finite dimensional: d translations, $\frac{d(d-1)}{2}$ rotations/boosts, one dilation and d special conformal transformations give a total of $\frac{(d+2)(d+1)}{2}$ symmetry generators (in fact this algebra is isomorphic to $\mathfrak{so}(d+1,1)$). However, for $d = 2$, where the spacetime coordinates can be written in terms of complex variables

$$z \equiv x + iy, \quad \bar{z} \equiv x - iy \quad \Longrightarrow \quad x = \frac{z + \bar{z}}{2}, \quad y = \frac{z - \bar{z}}{2i}, \tag{1.11}$$

all *holomorphic* maps are conformal. While they cannot be considered part of the conformal *group* (a holomorphic function is generally not globally invertible), their infinitesimal versions (which satisfy the infinitesimal version of (1.5)) do generate an infinite-dimensional conformal *algebra* of infinitesimal symmetries which extends the symmetry algebra derived from the conformal group. Thus, conformal symmetry in two dimensions is much more restrictive that its higher dimensional counterpart [43].

The infinite dimensional conformal algebra of a 2d CFT is made of two commuting copies of the *Virasoro algebra* $\mathrm{Vir} \otimes \overline{\mathrm{Vir}}$, whose generators $\{L_n, \bar{L}_n\}_{n\in\mathbb{Z}}$ satisfy

$$[L_n, L_m] = (n-m)L_{n+m} + \frac{c}{12}(n^3 - n)\delta_{n+m,0}, \tag{1.12}$$

$$[\bar{L}_n, \bar{L}_m] = (n-m)\bar{L}_{n+m} + \frac{c}{12}(n^3 - n)\delta_{n+m,0}, \tag{1.13}$$

$$[L_n, \bar{L}_m] = 0. \tag{1.14}$$

These operators generate conformal transformations[5] on the Hilbert space of the CFT. The constant c is called the *central charge* of the theory. It is behind many important characteristics of the CFT: it can be related to monotonicity of the renormalization group, anomalies, stress-energy tensor transformation rules, and, something that we will make explicit use of, the scaling of the entanglement entropy of an interval of length L in the ground state of the theory on the real line [44, 45]

$$S(L) \propto \frac{c}{3} \log L. \tag{1.15}$$

In 2d CFT, the important family of local operators is that of *primary* operators, a subclass of quasiprimary operators, which transform as

$$\mathcal{O}(z, \bar{z}) \to \mathcal{O}'(z', \bar{z}') = \left(\frac{\partial z'}{\partial z}\right)^{-h} \left(\frac{\partial \bar{z}'}{\partial \bar{z}}\right)^{-\bar{h}} \mathcal{O}(z, \bar{z}) \tag{1.16}$$

under a conformal (holomorphic) map $z \mapsto z'$, where $h, \bar{h}$ are real numbers called the *conformal dimensions* of the field. Together with their descendants (which are obtained by the action of L_n and $\bar{L}_n$ for $n > 0$), primary fields span the space of local operators of the theory. Not all quasiprimary operators are primary. For instance, the stress-energy tensor is a quasiprimary but not a primary operator: it is in fact a descendant of the identity operator. Primary operators can however still be characterized by their scaling dimension $\Delta = h + \bar{h}$, and their conformal spin $s = h - \bar{h}$ (in 2d, representations of the rotation group are indexed by a single number s). Additionally, a 2d version of the OPE (1.9)

[5] Things are a bit more subtle than this: the Virasoro algebra is the central extension (which loosely amounts to the quantization) of the Witt algebra (its classical version). Not all generators of the Witt algebra correspond to actual conformal transformations of the complex plane: only those which preserve the condition $\bar{z} = z^*$ (where $*$ denotes the complex conjugate), i.e. $x, y \in \mathbb{R}$, do. This amounts to preserving the complex plane as the physical submanifold embedded in the $\mathbb{C}^2$ space where the complex coordinates $(z, \bar{z})$ take values. Nevertheless, we will not need this level of precision for the purposes of this thesis.

can be defined, where the sum runs over the subset of primary fields, as opposed to all quasiprimary fields, and the $f_{12\mathcal{O}}$ functions involve not only derivatives but also the action of general Virasoro generators. OPE coefficients c_{ijk}, where i, j, k label three primary operators, can be defined in an analogous way. It can then be checked that knowledge of the central charge c, the scaling dimensions and conformal spins of the primary fields Δ_i, s_i and their OPE coefficients c_{ijk} is enough to compute the correlation functions of the theory. These are then collectively referred to as conformal data, analogously with the higher dimensional case.

Chapter 6 is the most CFT-heavy of this thesis, since we will be dealing with emergent universal structures in critical lattice systems. In fact, for that particular chapter we will be working with a *boundary* CFT (BCFT), which arises from defining a CFT on a manifold with a boundary [46]. BCFTs are rather analogous to their boundaryless counterparts in many aspects, so for now, we postpone their introduction until the relevant chapter.

This chapter's takeaways:

- Exploiting the *entanglement structure* of quantum states can lead to better computational capabilities to solve the quantum many-body problem.
- *Tensor networks* are a set of computational tools that follow this philosophy on the lattice. They have also proven themselves capable of providing considerable theoretical insight on entanglement structures.
- *Continuous* tensor networks are aimed at reproducing the success of tensor network techniques in the setting of QFT. In this thesis we will be focusing on two such constructions: cMERA and cTNR.
- Conformal field theory (CFT) is remarkably useful to describe critical systems. CFTs are characterized by a set of parameters, the *conformal data*, which when extracted from a critical system can help identify its underlying CFT.

Chapter 2

MERA and cMERA

This chapter's goal: In this chapter we introduce the continuous multi-scale entanglement renormalization ansatz, or cMERA, the continuous tensor network construction that will be the subject of the next three chapters.

2.1 Introduction

So far, we have presented tensor networks as a family of efficient parametrizations of very high-dimensional objects, such as quantum states. There is nevertheless an additional aspect of tensor networks, which turns out to have great theoretical value: their connection with the renormalization group. This relationship lies at the heart of the definition of a particular tensor network that we will be focusing on in this chapter: the multi-scale entanglement renormalization ansatz, or MERA [8, 47].

MERA is a tensor network representation of quantum states that originates from a particular real space renormalization scheme, called *entanglement renormalization*. In one spatial dimension, it has been proved successful at approximating ground states of critical lattice Hamiltonians, and it allows for the extraction of a number of conformal data of their associated conformal field theory [48–51]. MERA can also be defined in higher dimensions, though the scaling of the computational cost with system size becomes less favorable as we increase the spatial dimension.

The continuous MERA, or cMERA, is a proposed continuous tensor network analogue of the MERA. As such, it provides an ansatz wavefunctional for the ground state of a quantum

field theoretic Hamiltonian, and it can be interpreted as arising from a continuous version of entanglement renormalization. Computational approaches to the cMERA are much less developed than in the discrete case, thus much of what we currently understand about the construction comes from analytical treatment of solvable examples, some of which will presented in the next three chapters.

This chapter is organized as follows: we begin by giving some context about the real space renormalization group in Section 2.2. We then move on to define the MERA tensor network in Section 2.3, and its continuum analogue, the cMERA, in Section 2.4. In Section 2.5 we present two examples of cMERAs for non-interacting theories, which will play a fundamental role in future chapters. We conclude in Section 2.6 with a summary of the current status of research in cMERA and how the contributions in this thesis fit into it.

2.2 Real space renormalization group methods

The renormalization group (RG) is one of the key concepts that have shaped theoretical physics in the past decades. It has allowed physicists to organize their understanding of the physics of a system scale by scale, moving between them by means of the renormalization group flow. In high energy physics, renormalization is key to deal with ultraviolet singularities and obtain meaningful physical predictions from formerly divergent quantities. In statistical physics, the RG flow helps formalize the idea of *universality*, the independence of the macroscopic physics from the microscopic description used to model the system, as long as it is chosen within the correct *universality class*, which has led to improved understanding of phase diagrams and phase transitions.

In quantum many-body physics, the ideas of renormalization found a useful application with the advent of *real space renormalization group* methods[1], an approach famously established by Wilson in his analysis of the Kondo problem [52, 53], and whose origins can be traced back to Kadanoff's ideas about spin blocking [54]. The goal of these methods, when applied to a complex quantum many-body system, is to identify the set of relevant *effective* degrees of freedom needed to explain the long distance, low energy physics of the system, and to find a characterization in terms of these. To achieve it, they rely on the implementation of the RG flow in the form of a *coarse-graining transformation*, that removes short distance information and produces an effective description of the system. More specifically, this coarse-graining map truncates the local Hilbert space of a set of neighbouring degrees of freedom (collectively referred to as a block $\mathcal{B}$), projecting it onto

[1] Here *real space* refers to position space, as opposed to momentum space.

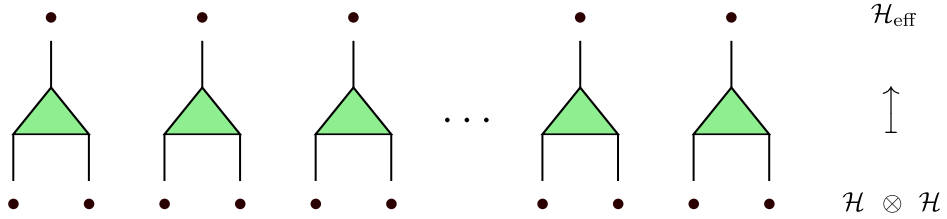

Figure 2.1: Each coarse-graining transformation maps the Hilbert space of a block of original degrees of freedom (in this case, just two neighbouring ones) to the Hilbert space of an effective degree of freedom.

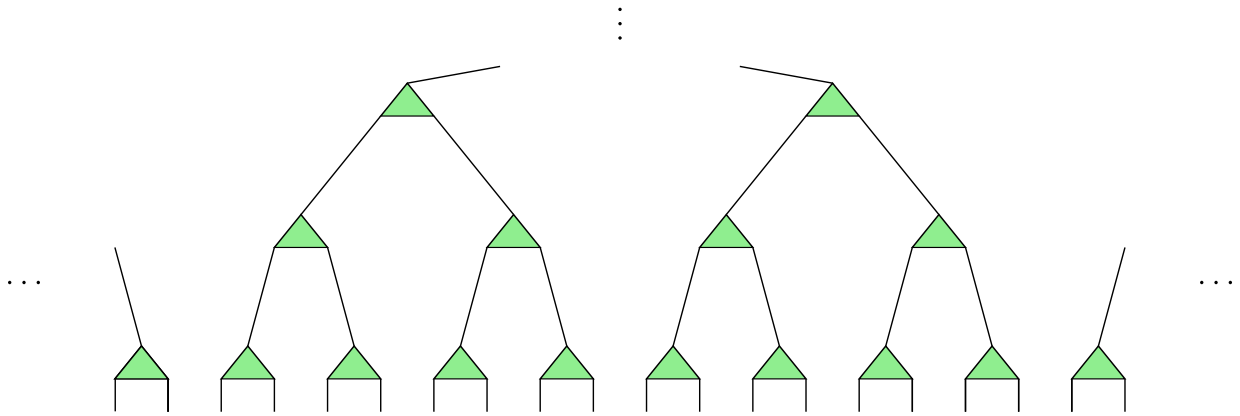

Figure 2.2: A binary tree tensor network for an infinite one-dimensional system.

a lower-dimensional subspace and thereby effectively reducing the number of degrees of freedom (see Figure 2.1).

Iterative application of the coarse-graining transformation is expected to yield the sought-after efficient description of the low energy physics of the system under study. Of course, the choice of the subspace $\mathcal{H}_{\text{eff}}$ on which we project is key to the success of the method. White [55] proved that, for fixed $\dim\mathcal{H}_{\text{eff}} = m$, the choice

$$\mathcal{H}_{\text{eff}} = \text{span}\{|v_1\rangle, \ldots, |v_m\rangle\} \tag{2.1}$$

where $|v_1\rangle, \ldots, |v_m\rangle$ are the m highest weight eigenvectors in the spectral decomposition of the reduced density matrix of site $\mathcal{B}$, is optimal, in the sense that the state after projecting is closest in norm to the original state. The resulting algorithm, the density matrix renormalization group or DMRG, has proved immensely successful in the study of 1d systems, and is nowadays the best tool for a lot of numerical computations.

This kind of algorithms has a close connection to tensor networks. In particular, we can build a tensor network representation for quantum states that reproduces the structure of iterative applications of the coarse-graining map that we have just discussed: the *tree tensor network* (TTN). Figure 2.2 shows the structure of a TTN in a 1-dimensional system where the blocking takes two degrees of freedom to one, i.e. a *binary* TTN. A TTN can be interpreted as a tensor network ansatz for a quantum state that also contains information about its RG flow as per a real space method such as the ones introduced in this section.

The definition of a TTN brings us one step closer to the definition of the MERA, which in fact also arises as the tensor network associated to a real space RG flow method, *entanglement renormalization*, that we introduce next.

2.3 Entanglement renormalization and MERA

Entanglement renormalization was introduced by Vidal [47] as a real space renormalization method specifically aimed at dealing with a particular set of shortcomings of DMRG and related methods; namely, their failure to give rise to the adequate fixed point structure expected from an RG flow, which should have scale-invariant (i.e. critical) systems as fixed points. Indeed, application of DMRG to a critical state requires the effective Hilbert space dimension for each blocking (we we called m in the previous section) to consistently grow as we keep coarse-graining in order to maintain the accuracy of the description. This precludes us from reaching a fixed point, and additionally thwarts our efforts to get an efficient description of the system, since computational complexity grows with the dimension of the Hilbert spaces involved.

The physical explanation for the growth of the effective block dimension relies on the fact that the coarse-graining step from Figure 2.1 is not able to remove all of the state's short-range entanglement. Part of this entanglement is instead "promoted" to longer-range entanglement and accumulated along the RG flow, leading to the growth of the effective dimension needed to keep the error caused by the coarse-graining transformation small. The proposal of entanglement renormalization involves adding a disentangling step prior to each coarse-graining step, via unitary maps (called *disentanglers*) acting across the block's boundaries, with the intention of removing as much short-range entanglement as possible, so that it does not accumulate during the RG flow. In other words, the action of the disentanglers removes entanglement so that the same accuracy after the coarse-graining step can be obtained while keeping a smaller number m of eigenvectors of the reduced density matrix, i.e. a smaller effective Hilbert space dimension.

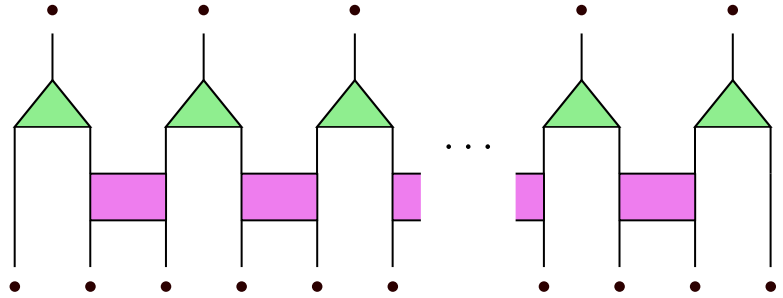

Figure 2.3: In entanglement renormalization, the coarse-graining map is now preceded by a disentangling step.

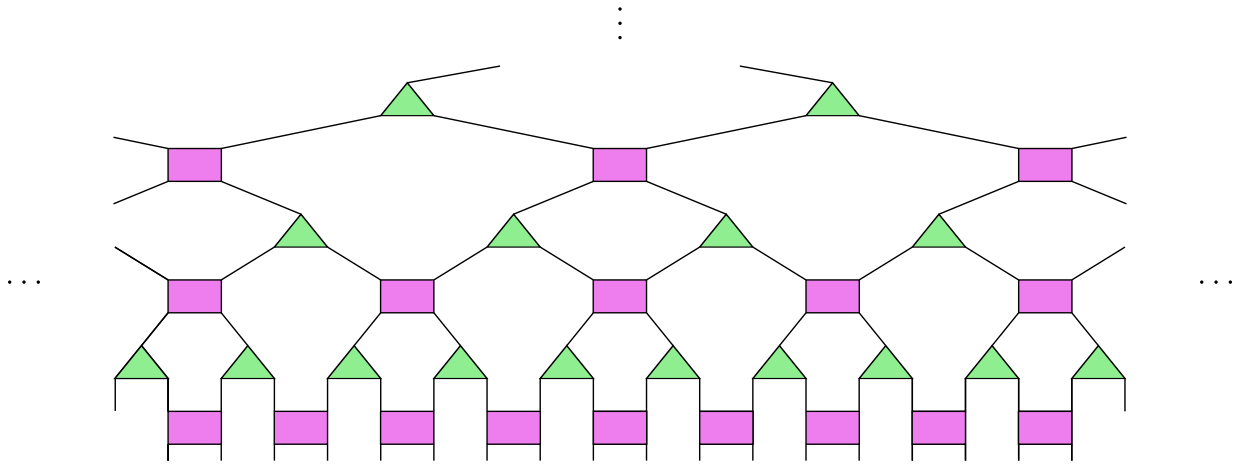

Figure 2.4: A MERA tensor network for an infinite one-dimensional system. Compare it with the TTN from Fig. 2.2.

As it happened before with the TTN, there is a tensor networks ansatz based on the structure of this RG flow algorithm, and consequently named multi-scale entanglement renormalization ansatz, or MERA. Figure 2.4 shows the structure of the network for an infinite 1d system[2], though it can be generalized to higher dimensions in a relatively straightforward manner. The network is made of alternating layers of isometries and disentanglers. The components of these tensors are the variational parameters of the ansatz. If we are interested in finding a MERA that approximates the ground state of a given Hamiltonian, there are algorithms that search for the optimal values of these tensors in order to minimize the expectation value of the Hamiltonian in the state parametrized by the MERA.

[2]Recall we showed the finite case in Fig. 1.2.

There are a few reasons MERA is an interesting tensor network. To begin with, MERA provides an *efficient* encoding of a quantum state: notice that the number of tensors of a MERA (and thus the number of parameters, if we assume tensors have constant sizes) grows linearly with the system size N. For example, in a MERA that maps two sites to one in each coarse-graining step, the lowermost layer has $\sim N$ tensors, the second lowest has $\sim N/2$ tensors, the third lowest has $\sim N/4$, and so on, giving a total of

$$N + \frac{N}{2} + \frac{N}{4} + \ldots\ldots \sim 2N$$

tensors. Moreover, MERA allows for efficient computation of reduced density matrices and expectation values of local observables [8]. This is due to the isometric and unitarity properties of the tensors, which provide great simplification whenever they meet their Hermitian conjugates:

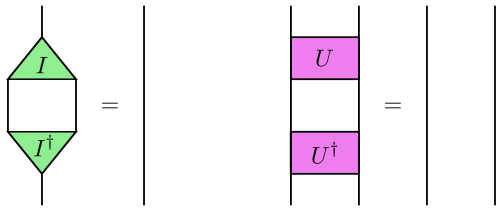

In fact, these properties allow us to define a certain causal structure on the MERA. For a given region $\mathcal{R}$ of the system, we know that the reduced density matrix $\rho_{\mathcal{R}}$ only depends on the tensors of the *causal cone* of $\mathcal{R}$, and all other tensors may be perturbed without affecting $\rho_{\mathcal{R}}$. We will see this concept in more detail in Chapter 5.

In addition to these computational properties, MERA is especially suited to describe ground states of critical Hamiltonians. This is because it can be proved that generic MERA states have the entanglement structure of critical grounds states, i.e., they display (i) power-law decay of correlations and (ii) logarithmic scaling of entanglement entropy (in 1d) or area law scaling of entanglement entropy (in higher dimensions) [8]. For comparison in the 1d case, MPS display exponentially decaying correlations (finite correlation length) and entanglement entropy that saturates to a constant (1d area law).

An optimized MERA for the ground state of a critical Hamiltonian can be used to extract conformal data of the underlying CFT [49,51]. It is usually imposed when working with such a system that the isometries and disentanglers are the same in all layers of the network (scale invariance). Consider for example the case of a 1d binary MERA. Each layer can be interpreted as implementing a finite scale transformation by a factor of 2.

We can use the optimized tensors to build a super operator that maps three-site operators on the original lattice to three-site operators in the coarse-grained lattice one layer above. If we then diagonalize it, the eigenvalues λ_j of this superoperator will be related to the scaling dimensions Δ_j of the underlying CFT (up to finite size errors):

$$\lambda_j \approx 2^{-\Delta_j} \tag{2.2}$$

and the eigenoperators will give a basis of lattice representations of the scaling operators of the CFT. After that, we can consider a pair of these scaling operators, and coarse-grain them until they fuse, then expand the result back in the basis of scaling operators, obtaining in this way approximations of the OPE coefficients of the theory.

As we have just summarized, the MERA is a tensor network that displays a number of interesting properties, which justify the search for a continuous version. To do that, we present now an alternative interpretation that is more suitable to generalization.

2.3.1 Quantum circuit interpretation of the MERA

So far, we have spoken of the MERA as the ansatz arising from applying entanglement renormalization to a quantum state. In this sense, the "vertical dimension" of the tensor network is interpreted as a scale direction, and we move from the bottom to the top.

However, the MERA has an alternate interpretation as a quantum circuit, where the vertical dimension corresponds to the time, or "pseudotime", which flows from the top to the bottom of the network, and along which unitary gates are applied to a quantum state to produce another quantum state. The key to move from the tensor network to the quantum circuit interpretation of MERA is the simple realization that any isometric map $I : \mathcal{H} \to \mathcal{H} \otimes \mathcal{H}$ can be written as a unitary map $U_I : \mathcal{H} \otimes \mathcal{H} \to \mathcal{H} \otimes \mathcal{H}$, one of whose inputs has been fixed to a reference state $|0\rangle$:

$$I\left(|\psi\rangle\right) = U_I\left(|\psi\rangle \otimes |0\rangle\right). \tag{2.3}$$

Figure 2.5 shows the result of performing this modification in all isometries. The result is that the MERA class consists of states that can be obtained from an initial product state (made of tensor copies of the reference state $|0\rangle$) by means of a unitary quantum circuit with a particular hierarchical structure, in which gates are applied first at long length scales, then progressively at shorter and shorter scales, until the last row of gates entangle nearest-neighbour degrees of freedom. Thus MERA states can be seen as the result of an entangling evolution in scale. Run backwards, this evolution is nothing but

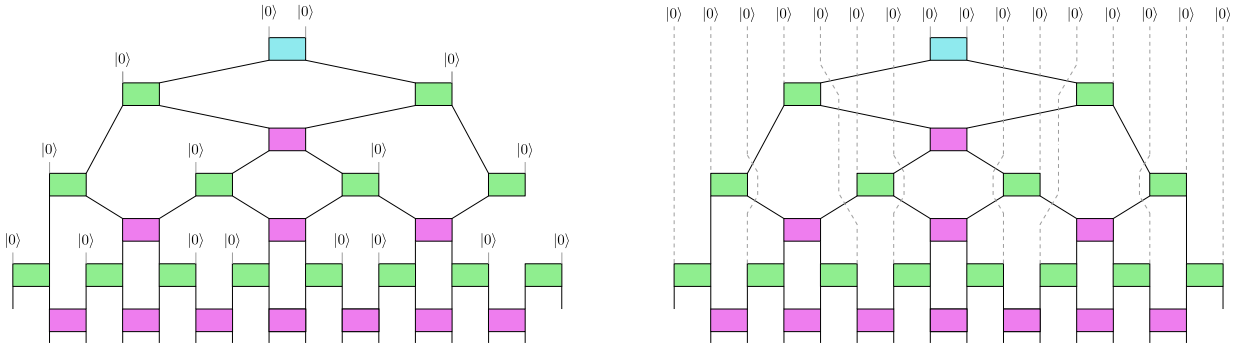

Figure 2.5: (left) The isometries of a MERA can be interpreted as unitary gates where one of the inputs is in a reference state $|0\rangle$, tensored with the rest of the system. Bringing all these reference states to the top of the network we obtain a quantum circuit (right).

the entanglement renormalization group flow described above, made unitary by keeping track of all the degrees of freedom that we have disentangled at each renormalization step (which remain in a product state with the rest of the system).

2.4 Generalization to the continuum: the cMERA

We now introduce the continuous MERA, or cMERA, which is a proposed analogous construction to the MERA in the setting of QFT. We concluded in the previous section that a MERA ansatz state is the result of the unitary evolution via a quantum circuit of an initial reference state. These satisfy the following two key properties:

(a) The initial state is a product state, i.e., there is no entanglement between the local degrees of freedom.

(b) The evolution is organized so that the initial gates introduce long-range entanglement in the system, while later gates introduce shorter and shorter-range entanglement.

A cMERA [56] (denoted $|\Psi^\Lambda(s)\rangle$ or $|\Psi^\Lambda\rangle$ depending on the context) is an ansatz QFT state that aims to approximate some target wavefunctional of interest, typically the ground state of a QFT Hamiltonian in d spatial dimensions. Mimicking the MERA, it is produced through a unitary evolution acting on an initial reference state, but this time the evolution is continuous, yielding a one-parameter family of cMERA states

$$|\Psi^\Lambda(s)\rangle \equiv \mathcal{U}(s,0)|\Omega\rangle. \tag{2.4}$$

Here $\mathcal{U}(s,0)$ is the unitary operator representing the entangling evolution up to pseudotime s, and $|\Omega\rangle$ is the initial state. They satisfy the following conditions:

(a) The initial state is taken to be unentangled, in the sense that its two-point correlation functions vanish when evaluated at different points:

$$\langle\Omega|\mathcal{O}(x)\mathcal{O}(y)|\Omega\rangle = 0, \qquad x \neq y. \tag{2.5}$$

We can think of $|\Omega\rangle$ as the continuum limit of a product state of a lattice system.

(b) The unitary evolution is generated by a Hermitian operator made of the sum of two contributions, L and $K(s)$, which take specific forms (see below) to ensure that entanglement is introduced during the evolution sequentially in scale, as in the discrete MERA. That is,

$$\mathcal{U}(s,0) \equiv \mathcal{P}\exp\left(-i\int_0^s ds'\ [L + K(s')]\right) \tag{2.6}$$

where $\mathcal{P}$ denotes the path-ordered exponential.

Let us elaborate on this last condition. The two contributions to the generator of the cMERA unitary evolution, L and $K(s)$, play two distinct roles. L is the generator of scale transformations that rescale both space and the field degrees of freedom. As such, L only depends on the field content of the theory under study, and not on the specific form of the Hamiltonian whose ground state we aim to approximate with the cMERA. For a generic field φ with (non-relativistic[3]) scaling dimension Δ_φ, we have

$$e^{isL}\varphi(\vec{x})e^{-isL} = e^{s\Delta_\varphi}\varphi(e^s\vec{x}). \tag{2.7}$$

On the other hand $K(s)$ is a quasilocal operator called the *entangler* (see Eqs. (2.12) and (2.16) below for examples in one spatial dimension). By *quasilocal* we mean that the operator, an integral of a quasi-local density, acts at a specific length scale. It is standard to denote this length scale as Λ^{-1}, where Λ is the corresponding momentum scale[4]. Intuitively, the entangling evolution in scale builds the cMERA wavefunctional

[3]The non-relativistic and relativistic scaling generators differ in the scaling dimensions they assign to the fields. This will not be essential for us, but the interested reader can check the Supplemental Material to the first arXiv version of [56] for an explanation.

[4]As the reader may have guessed, this Λ is what makes us denote the cMERA states as $|\Psi^\Lambda(s)\rangle$. Additionally, in a large fraction of the literature on cMERA, the initial state $|\Omega\rangle$ is denoted $|\Lambda\rangle$. The reason is that for the simplest example of cMERA, the one for the free scalar field (see Section 2.5), the right choice for the initial state (in order to get a good approximation of the target ground state) depends on Λ (via Eqs. (2.10) and (2.11)). In this thesis we have however preferred to keep the notation separate, for $|\Omega\rangle$ and Λ are two *a priori* different elements of the cMERA construction, that may or may not be related once we demand it be a good approximation to its target state.

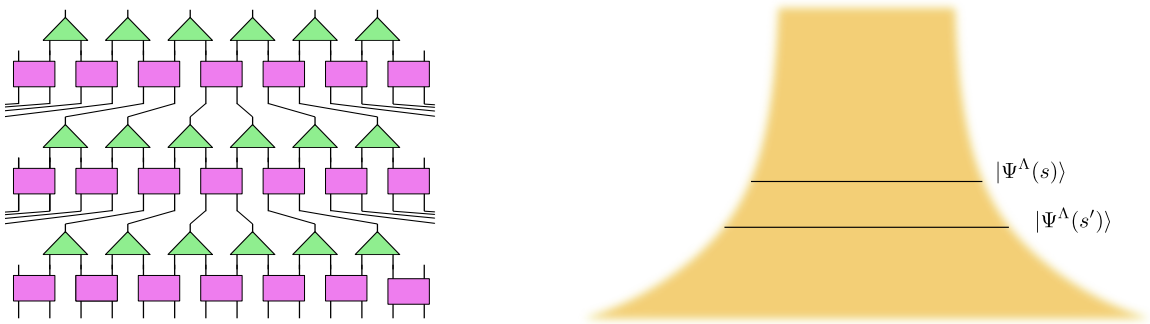

Figure 2.6: (left) A MERA tensor network, rescaled so that it keeps the same lattice spacing after each step. (right) The cMERA evolution.

from the initial uncorrelated state $|\Omega\rangle$ by progressively introducing entanglement at length scale Λ^{-1} as we keep "zooming in", rescaling both space and the fields. The resulting state will contain correlations at a range of length scales above Λ^{-1}, but will (partially) preserve the unentangled character of the initial state $|\Omega\rangle$ at shorter distances. This idea can be made more precise, and allows us to say that a cMERA state presents an entanglement UV cutoff at length scale Λ^{-1}, as we will see in Chapter 3. Thus the ansatz wavefunctional $|\Psi^\Lambda(s)\rangle$ aims to approximate its target state $|\Psi\rangle$ at distances x larger than Λ^{-1}, in the sense that e.g. the correlators agree to high accuracy for $\Lambda x \gg 1$. This UV cutoff length scale is in a certain sense the continuous version of the lattice spacing a. Note that it stays constant along the cMERA evolution; in the discrete case we could keep rescaling the lattice accordingly so that it also stays constant (see Fig. 2.6).

Of particular interest for us is the case where the entangler is independent of s, $K(s) \equiv K$. Then, in the limit $s \to \infty$, (assuming this limit exists) we obtain a fixed point wavefunctional known as a *scale invariant* cMERA $|\Psi^\Lambda\rangle$,

$$|\Psi^\Lambda\rangle \equiv \lim_{s\to\infty} e^{-is(L+K)}|\Lambda\rangle. \tag{2.8}$$

By construction, the fixed point wavefunctional $|\Psi^\Lambda\rangle$ is invariant under further evolution by $L + K$. We can think of $D^\Lambda \equiv L + K$ as a generator of an alternative notion of scale transformations, one that is adapted to the specific theory under study [57]. For instance, in the context of a free boson CFT (see below), D^Λ is the generator of (a quasi-local version of) relativistic scale transformations, whereas L generates non-relativistic scale transformations. Then we say that $|\Psi^\Lambda\rangle$ is invariant under this alternative notion of scale transformations, which is why we call $|\Psi^\Lambda\rangle$ a scale invariant cMERA wavefunctional.

Ideally, given a target QFT Hamiltonian, the specific form of the entangler $K(s)$ should

be determined variationally from a procedure such as energy minimization. While no general algorithms have been developed so far to determine the entangler variationally, in the particular case of free fields one can find examples of entanglers that give rise to interesting cMERA wavefunctionals. Below we present the two simplest examples, the cMERAs for the free boson and free fermion CFTs.

2.5 Examples of Gaussian cMERAs

2.5.1 Free boson cMERA

Let $\phi(\vec{x})$ denote a scalar field operator in d spatial dimensions and $\pi(\vec{x})$ its canonical momentum conjugate field, with $[\phi(\vec{x}), \pi(\vec{y})] = i\delta(\vec{x} - \vec{y})$. The free boson cMERA aims to produce a long distance approximation to the ground state of the massless Klein-Gordon Hamiltonian

$$H = \frac{1}{2} \int d^d x \ : \left(\pi(\vec{x})^2 + (\vec{\nabla}\phi(\vec{x}))^2 \right) : \tag{2.9}$$

The data defining this cMERA, originally proposed in [56] are given as follows:

(a) The initial unentangled state is defined by a set of local annihilation operators. In particular, define

$$\psi(\vec{x}) \equiv \sqrt{\frac{\Lambda}{2}} \phi(\vec{x}) + i \sqrt{\frac{1}{2\Lambda}} \pi(\vec{x}) \tag{2.10}$$

where Λ is the momentum scale introduced above, related to the length scale at which the generator K is introducing entanglement. Then the initial state is given by

$$\psi(\vec{x})|\Omega\rangle = 0 \qquad \forall \vec{x} \in \mathbb{R}^d \tag{2.11}$$

(b) The entangler is given by the translation and rotation invariant, quasi-local quadratic operator:

$$K = \frac{-i}{2} \int d^d x \, d^d y \ g(|\vec{x} - \vec{y}|) \psi(\vec{x}) \psi(\vec{y}) + \text{h.c} \tag{2.12}$$

and $g(x)$ is some real profile function that implements the required quasi-locality at length scale Λ^{-1}. Note that we assume the cMERA to be scale invariant (g does not depend on s), because the free boson is a CFT, and thus its ground state should be scale invariant. Simple examples are the profiles $g(x) \sim e^{-(\Lambda x)^2}$ used in [56] and $g(x) \sim e^{-\Lambda x}$, used in [58].

We have thus a family of free boson cMERAs, and different choices of g may result in better or worse approximations to the free boson ground state. In the next chapter we analyze in detail the cMERA states resulting from the choices above.

2.5.2 Free fermion cMERA

Consider now a Dirac spinor[5] $\vec{\psi}(\vec{x})$, with components $\psi_i(x)$, $i = 1, \ldots, 2^{\lfloor \frac{d}{2} \rfloor}$ obeying anti-commutation relations $\left\{\psi_i(\vec{x}), \psi_j^\dagger(\vec{y})\right\} = \delta_{i,j}\delta(\vec{x}-\vec{y})$ and $\left\{\psi_i(\vec{x}), \psi_j(\vec{y})\right\} = 0$. For simplicity, in the following we focus on $d = 1, 2$, for which the Dirac spinor has two components ψ_1, ψ_2. The free fermion cMERA aims to approximate the ground state of the free Dirac fermion Hamiltonian

$$H = \int d^d x \; \psi^\dagger(\vec{x})\gamma^0(-i\vec{\gamma}\cdot\vec{\partial})\psi(\vec{x}), \tag{2.13}$$

where γ^μ are the Dirac matrices satisfying the Clifford algebra

$$\{\gamma^\mu, \gamma^\nu\} = 2\eta^{\mu\nu}. \tag{2.14}$$

The data defining this cMERA (which is a generalization to arbitrary dimensions of the one proposed in [56]) are given as follows:

(a) The initial unentangled state is as before defined by a set of local annihilation operators. In particular, define

$$\psi_1(\vec{x})|\Omega\rangle = 0, \quad \psi_2^\dagger(\vec{x})|\Omega\rangle = 0, \quad \forall \vec{x}, \tag{2.15}$$

Note that, as opposed to the bosonic case, this initial state is independent of the momentum scale Λ.

(b) The entangler is given by the translation invariant, quasi-local quadratic operator:

$$K = \int d^d x \, d^d y \; h(|\vec{x}-\vec{y}|)\psi^\dagger(\vec{x})(\vec{\gamma}\cdot\vec{\partial})\psi(\vec{y}) \tag{2.16}$$

and $h(x)$ is again some real profile function that implements the required quasi-locality at length scale Λ^{-1}. This operator is not rotation invariant itself (it does not commute with the generator of rotations), but it can be checked that the cMERA evolution it generates with initial state $|\Omega\rangle$ only produces rotation invariant states.

[5] The symbol ψ being as overloaded as it usually is, we find that within a few paragraphs we use it twice, first as the bosonic annihilation operator, and later as the fermionic spinor components (which act as fermionic annihilation operators). We hope this will not lead the reader to confusion, since along this thesis we will always deal with bosonic and fermionic theories in a separate and orderly manner.

In the next chapter we analyze as well the cMERA states resulting from the choices above.

2.6 Current status of the cMERA programme

Already in their seminal paper [56], Haegeman *et al.* argue that *"the full power of the* [cMERA] *construction should emerge in the case of interacting theories"*. Indeed, the examples presented so far, in spite of their interesting properties, which will be discussed in the next chapter, correspond to theories that we can solve exactly. Thus, in principle, the cMERA wavefunctional does not bring any additional information about the theory itself, at least naïvely. In fact, we have made use of our knowledge of the solution of the theories in some of the choices made in defining the free boson and free fermion cMERAs above, rather than following a variational approach[6]. The real application for which cMERA could make a big difference in our understanding of particular quantum field theories would be variational optimization of cMERA for interacting field theories that we do not now how to solve (nonperturbatively) by other means.

However, this does not mean that studying the non-interacting cMERA is devoid of any interest. While numerical algorithms are developed to tackle the interacting case, examples cMERAs like the ones we just introduced can be the source of considerable insight on general properties of the construction. In fact, the non-interacting case provides a useful test case from which to derive prescriptions and guidance to use later when less restrictive algorithms are available. The work on cMERA presented on this thesis is representative of this line of research. We will use non-interacting examples to study the entanglement structure of cMERA states (Chapter 3), and to explore the nuances derived from applying the formalism in the presence of gauge invariance (Chapter 4) and in systems with boundaries or defects (Chapter 5). Before moving on to that, and for completeness, we review in what follows past and current work devoted to the interacting case.

Currently, our understanding of interacting cMERAs is limited. In [59], the authors build cMERAs with quadratic entanglers for interacting theories, resulting in a Gaussian approximation to the target ground states, in the spirit of mean field theory. Later, in [60,61], a scheme based on perturbation theory is proposed to generate cMERA approximations to interacting ground states in the weakly interacting regime, with an example

[6] In the Supplemental Material to the first arXiv version of [56] there are examples of entanglers found analytically by energy density minimization. However, these are restricted to a particular subclass of entangler profiles, and the corresponding method seems hard to generalize.

of its application to the ϕ^4 theory at 1-loop order. Though undoubtedly interesting, this approach relies from the beginning on the weakness of the interaction, and as such denies in advance the possibility of matching the applicability of lattice variational methods to strongly interacting systems. Finally, the authors of [62] build a family of non-Gaussian ansatz states derived from the cMERA: they use however a quadratic entangler, and apply a non-Gaussian transformation *after* the cMERA evolution, hence the proposal does not fit exactly within the formalism.

Another major research avenue in interacting cMERA stems from [58], where the concept of *magic* entanglement renormalization is introduced. A magic cMERA for the 1+1 dimensional free boson is given by a particular choice of the entangler in Eq. 2.12, namely

$$g(x) = \frac{\Lambda}{4} e^{-\Lambda|x|}. \tag{2.17}$$

The reason for this nomenclature is that this specific cMERA displays a few important characteristics that generic choices of the entangler will not give rise to. In particular, they are compatible with continuous matrix product states (cMPS) and operators (cMPO), in the sense that (i) magic cMERA states can be expressed as cMPS, and (ii) their entangling evolution can be represented via cMPOs. Interacting cMPS techniques being much more developed, this property makes magic cMERAs very promising for the construction of numerical schemes to treat non-Gaussian cMERA wavefunctionals for interacting QFTs. Magic cMERA will play an important role as well in our discussion of gauge invariant cMERAs in Chapter 4, hence we will postpone until then a deeper exposition of this topic.

This chapter's takeaways:

- The MERA is a tensor network for ground states of lattice Hamiltonians, whose origins lie in a real space RG method called entanglement renormalization. It can be interpreted as a *quantum circuit* that introduces correlations in a product state, scale by scale.
- The *continuous* MERA is an analogous construction to the MERA in the continuum, and provides a variational wavefunctional for ground states of QFT Hamiltonians. It is defined via a *unitary evolution* that introduces correlations in an initial unentangled state, scale by scale.
- For free bosonic and fermionic fields, there are examples of *Gaussian* cMERAs that can be manipulated analytically, and thus used to provide insight into expectedly general properties of the cMERA construction, as we will do in what follows.

Chapter 3

Entanglement structure and UV regularization in cMERA

This chapter's goal: In this chapter we analyze the properties of cMERA states, in particular how they look from the point of view of entanglement and correlations.

3.1 Introduction

In Section 2.5 of the previous chapter we introduced two important families of cMERAs for free bosonic and fermionic theories. Thanks to them being Gaussian, we can compute with relative ease anything we would like to know about the corresponding cMERA states. In this chapter we pick a particular *scale invariant* entangler for each of them, and explore in depth the entanglement structure of the fixed point state $|\Psi^\Lambda\rangle$ via the computation of correlation functions and entanglement entropy profiles, in 1 and 2 spatial dimensions. As we will see, the results evidence the existence of two different distance regimes, above and below the cutoff length scale Λ^{-1}, where the characteristics of the cMERA state differ significantly.

This chapter is organized as follows: in Section 3.2 we review the parametrization of Gaussian states in terms of their annihilation operators, which we will make heavy use of. Further, in Section 3.3 we review the particular aspects of the computation of correlation functions and entanglement entropy in Gaussian states that will be exploited later. Finally, Sections 3.4 and 3.5 study, respectively, the free bosonic and fermionic cMERAs.

3.2 Gaussian cMERA

For our purposes, a *Gaussian state* $|\Phi\rangle$ is such that it can be characterized (up to an irrelevant global phase) by a complete set of constraints, implemented by annihilation operators that are linear combinations of the bosonic/fermionic field operators[1]. When the Gaussian state is invariant under translations, each annihilation operator can be labeled by its momentum $\vec{k}$, and the linear constraints read

$$a(\vec{k})|\Phi\rangle = 0 \qquad \forall \vec{k} \in \mathbb{R}^d. \tag{3.1}$$

Both the free boson and free fermion cMERAs introduced in the previous chapter belong to the category of *Gaussian cMERAs*, i.e., those for which the whole evolution happens within the Gaussian state manifold. This is due to the fact that (a) our choice for the initial state $|\Omega\rangle$ is a Gaussian state (by Eqs. (2.10) and (2.11)), and (b) our choice for the entangler K is a quadratic operator, and hence the evolution generator $L+K$ is quadratic. Indeed, the evolution generated by a quadratic operator will preserve the manifold of Gaussian states, since it will map linear operators to linear operators. In particular,

$$\left.\begin{aligned} &a(\vec{k})|\Omega\rangle = 0 \\ &|\Psi^\Lambda(s)\rangle = \mathcal{U}(s,0)|\Omega\rangle \end{aligned}\right\} \implies \left(\mathcal{U}(s,0)a(\vec{k})\mathcal{U}(s,0)^\dagger\right)|\Psi^\Lambda(s)\rangle = 0 \tag{3.2}$$

where, recall, $\mathcal{U}(s,0)$ is the unitary evolution generated by $L+K$, which gives the cMERA state $|\Psi^\Lambda(s)\rangle$ when acting on the initial state $|\Omega\rangle$. Since $a(\vec{k})$ is a linear combination of field modes, by the previous statement, so is $\mathcal{U}(s,0)a(\vec{k})\mathcal{U}(s,0)^\dagger$, and we have that $|\Psi^\Lambda(s)\rangle$ is a Gaussian state. In fact, what $\mathcal{U}(s,0)$ is implementing is nothing but a canonical transformation between the modes. Using a Gaussian cMERA to approximate the ground states of the free boson and free fermion theories is a sensible choice given that said target ground states are themselves Gaussian.

The characterization in terms of annihilation operators is particularly useful to study the Gaussian cMERA. In our cases of interest, it will allow us to straightforwardly parametrize each state in terms of a single real function of the momentum coordinate (which we call $\alpha(\vec{k})$ in the bosonic case, and $\theta(\vec{k})$ in the fermionic case). Such an efficient characterization is not available for the ground state of a generic interacting QFT. Furthermore, an intuitive interpretation of the cMERA states is easy to state in these terms: below we show that the linear constraints of the cMERA are just an interpolation between those of

[1]Note that here we are talking of a *pure* Gaussian state. There is a bigger class of Gaussian mixed states, all of which satisfy Wick's theorem (see next section).

the unentangled state $|\Omega\rangle$ for large momenta ($|\vec{k}| \gg \Lambda$), and those of the target state $|\Psi\rangle$ at small momenta ($|\vec{k}| \ll \Lambda$). This was first pointed out in [57] for the 1+1 dimensional free boson theory. This interpolating character already hints at the UV regularized character of cMERA states: in $|\Psi^\Lambda\rangle$, the large momentum / short distance modes satisfy constraints similar to those of the unentangled initial state $|\Omega\rangle$, which is UV finite.

An additional major advantage of working with Gaussian states is that the correlation measures that we are going to analyze in this chapter for free boson and free fermion cMERAs are easy to compute for this kind of states, as we review in the next section.

3.3 Correlation measures in Gaussian states

The tools that we are going to use to probe the entanglement structure of the cMERA states are the two-point correlation functions and the entanglement entropy profile. Both are measures of the correlations between different degrees of freedom of the theory, and we can use them to study how these correlations depend on the scale at which we are looking. Here we speak briefly about their significance, and explain the standard procedure to compute entanglement entropies in Gaussian states. The familiar reader can skip directly back to cMERA topics in Section 3.4.

The two-point correlation functions of the theory are $\langle \mathcal{O}(x)\mathcal{O}'(y)\rangle$, where $\mathcal{O}(x), \mathcal{O}'(y)$ belong to the local algebra of linear[2] operators at their respective locations. Their role in theories with quadratic Hamiltonians, such as the free theories we deal with in this paper is particularly important, since they encode all the information of the N-point functions for the ground state of the theory. Indeed, only the correlation matrix of the field modes is needed to completely specify the state. This is due to Wick's theorem: given operators $\mathcal{O}_1(x_1), \ldots, \mathcal{O}_N(x_N)$ that are linear in the field modes, their N-point function with respect

[2]Note that as in the previous section, by this we mean operators that are linear *in the field modes*, as opposed to just linear as operators on the Hilbert space (nowhere in this thesis will we use the word *operator* for anything that is not linear in this last sense). That is, in the bosonic case

$$\mathcal{O}(x) \in \text{span}\{\phi(x), \pi(x)\},$$

while in the fermionic case

$$\mathcal{O}(x) \in \text{span}\{\psi_i(x), \psi_i^\dagger(x)\}, \qquad i = 1, \ldots, 2^{\lfloor \frac{d}{2} \rfloor}$$

to any Gaussian state satisfies

$$\langle \mathcal{O}_1(x_1) \dots \mathcal{O}_N(x_N) \rangle = \sum_{\sigma=(i_1,\dots,i_N)} s_\sigma \langle \mathcal{O}_{i_1}(x_{i_1}) \mathcal{O}_{i_2}(x_{i_2}) \rangle \dots \langle \mathcal{O}_{i_{N-1}}(x_{i_{N-1}}) \mathcal{O}_{i_N}(x_{i_N}) \rangle, \quad (3.3)$$

where the sum runs over all possible pairings of the operators, and s_σ is a sign that accounts for the commutation/anticommutation relations of the modes.

Our second witness for correlations is entanglement entropy. Given a certain spatial region $\mathcal{R}$, we may obtain its associated density matrix $\rho_\mathcal{R}$ by tracing out the degrees of freedom outside $\mathcal{R}$. The von Neumann entanglement entropy of region $\mathcal{R}$ is then defined as

$$S(\rho_\mathcal{R}) := -\operatorname{tr}(\rho_\mathcal{R} \log \rho_\mathcal{R}). \quad (3.4)$$

This computation can be extremely involved, more so in the case of quantum field theory. Working with Gaussian states, however, once again simplifies our task. The reduced state of a pure Gaussian state is a mixed Gaussian state (indeed, Wick's theorem for the former implies Wick's theorem for the latter). We then have the following strategy at hand: we look for a canonical transformation that maps the field modes inside $\mathcal{R}$ to a set of uncorrelated modes (we will be more specific about what this means below). The density matrix will then factor into the tensor product of the density matrices associated to said uncorrelated modes, and the total entropy of the state can be computed as a sum over contributions from each mode:

$$\rho_\mathcal{R} = \bigotimes_i \rho_i \implies S(\rho) = \sum_i S(\rho_i). \quad (3.5)$$

Note however that we cannot handle computations with infinitely many modes[3], so we will resort to discretizing the correlation matrix by sampling of the two-point functions with a certain lattice parameter a. We can then interpret it as the (approximate) correlation matrix for a discrete, finite set of bosonic/fermionic modes, and carry on from there, with the advantage that numerical computation then becomes available as a tool to produce the final results, and observe their behaviour as a function of a. We therefore proceed to review the entanglement entropy computation techniques we employ in Gaussian states of finitely many modes, and in particular the procedure needed to find the uncorrelated modes, which is different but analogous depending on whether we are speaking of bosons or fermions [63, 64].

[3] See however B.3 we perform some estimations while still in the continuum.

3.3.1 Bosonic theories

By discretizing a bosonic theory we obtain an algebra of operators $\{\phi_i, \pi_i\}$ that satisfy the canonical commutation relations (CCR):

$$[\phi_i, \pi_j] = i\delta_{i,j}\,, \qquad [\phi_i, \phi_j] = [\pi_i, \pi_j] = 0. \tag{3.6}$$

Linear transformations in this algebra that preserve the CCR form a group and are called canonical transformations. They map bosonic modes into bosonic modes. The group of canonical transformations for N bosonic modes is the symplectic group $\mathrm{Sp}(2N, \mathbb{C})$, which by definition is the subgroup of $\mathrm{GL}(2N, \mathbb{C})$ whose elements M satisfy

$$M \begin{pmatrix} 0 & \mathbb{1}_N \\ -\mathbb{1}_N & 0 \end{pmatrix} M^T = \begin{pmatrix} 0 & \mathbb{1}_N \\ -\mathbb{1}_N & 0 \end{pmatrix}. \tag{3.7}$$

Notice that this is precisely the condition that the CCR are preserved when the map M is applied to the column vector of modes $(\phi_1, \ldots, \phi_N, \pi_1, \ldots, \pi_N)$.

A Gaussian state, as stated above, is completely characterized by its Hermitian, positive definite correlation matrix:

$$C_{ij}^{\mathcal{O}\mathcal{O}'} = \langle \mathcal{O}_i \mathcal{O}'_j \rangle, \text{ with } \mathcal{O}, \mathcal{O}' \in \{\phi, \pi\},\ i, j = 1, \ldots N. \tag{3.8}$$

Given any such matrix, there exists a procedure, called *symplectic diagonalization*, by which we can find a symplectic transformation that maps our initial set of bosonic modes to a set of uncorrelated modes $\{\tilde{\phi}_i, \tilde{\pi}_i\}$, for which the correlation matrix decomposes as a direct sum [65]:

$$C = \bigoplus_{i=1}^{n} \begin{pmatrix} \langle \tilde{\phi}_i \tilde{\phi}_i \rangle & \langle \tilde{\phi}_i \tilde{\pi}_i \rangle \\ \langle \tilde{\pi}_i \tilde{\phi}_i \rangle & \langle \tilde{\pi}_i \tilde{\pi}_i \rangle \end{pmatrix}.$$

Consequently the density matrix factorizes as in (3.5). Each of the uncorrelated modes will be in a thermal state of the form

$$\rho_i = (1 - \zeta_i) \sum_{n=0}^{\infty} \zeta_i^n |n\rangle\langle n| \implies S(\rho_i) = -\frac{\zeta_i \log_2 \zeta_i}{1 - \zeta_i} - \log_2(1 - \zeta_i) \tag{3.9}$$

where $\zeta_i \in [0, 1)$ can be written in terms of the eigenvalues λ_i of the matrix

$$K_{ij} = C_{ik}^{\phi\phi} C_{kj}^{\pi\pi}, \tag{3.10}$$

that is, the product of the $\phi\phi$ and the $\pi\pi$ submatrices of the original correlation matrix[4]. Indeed, we have

$$\zeta_i = \frac{2\sqrt{\lambda_i} - 1}{2\sqrt{\lambda_i} + 1}. \tag{3.11}$$

This way we can easily compute the entanglement entropy of a spatial region from its correlation matrix.

3.3.2 Fermionic theories

If we start with a fermionic theory and discretize it we arrive at a set of fermionic modes $\psi_i, \psi_i^\dagger$ which in turn satisfy the canonical anticommutation relations (CAR):

$$\{\psi_i\,, \psi_j^\dagger\} = \delta_{i,j}\,, \qquad \{\psi_i, \psi_j\} = \{\psi_i^\dagger, \psi_j^\dagger\} = 0. \tag{3.12}$$

The group of canonical transformations will this time be composed of those maps that preserve the CAR. It can be seen that for N fermionic modes this group is isomorphic to $\mathrm{O}(2N)$, the orthogonal group of dimension $2N$. For our purposes it will nonetheless be enough to consider the $U(N)$ subgroup given by the transformations:

$$\psi_i \longmapsto U_{ij}\psi_j \tag{3.13}$$

where U_{ij} is a unitary matrix. Note that these are the transformations that leave invariant the total particle number operator

$$\psi_1^\dagger\psi_1 + \ldots + \psi_N^\dagger\psi_N. \tag{3.14}$$

The correlation matrix that characterizes our Gaussian state will now be of the form

$$C_{ij} = \langle\psi_i^\dagger\psi_j\rangle, \text{ with } i, j = 1, \ldots N, \tag{3.15}$$

and it can be proved that finding a canonical transformation that yields uncorrelated modes amounts to finding a unitary that diagonalizes this Hermitian matrix. The resulting modes will satisfy

$$\langle\tilde{\psi}_i^\dagger\tilde{\psi}_j\rangle = \lambda_i\delta_{i,j} \tag{3.16}$$

for $\lambda_i \in [0, 1]$ the eigenvalues of the correlation matrix. Thus we can easily compute the entanglement entropy of the state given its correlation matrix:

$$S(\rho) = \sum_{i=1}^{N} s(\lambda_i) = -\sum_{i=1}^{N} \left[\lambda_i \log\lambda_i + (1 - \lambda_i)\log(1 - \lambda_i)\right] \tag{3.17}$$

[4]The set $\{\sqrt{\lambda_i}\}$ is usually referred to as the *symplectic eigenvalues* of the correlation matrix $C_{ij}^{\mathcal{O}\mathcal{O}'}$.

where $s(\lambda_i)$ is the entropy of the state of a single fermionic mode $\tilde{\psi}_i$ whose density matrix is

$$\rho_i = (1-\lambda_i)|0\rangle\langle 0| + \lambda_i |1\rangle\langle 1| \tag{3.18}$$

in the basis of eigenstates of the number operator $\tilde{\psi}_i^\dagger \tilde{\psi}_i$.

3.4 Free boson cMERA

Finally we are in a position to begin our analysis of cMERA states, and we do so with the first example from Section 2.5, the free boson cMERA. We will begin by finding the characterization by annihilation operators of all relevant quantum states in the construction. Then we will proceed to compute their correlators and entanglement profiles and compare them to each other in order to extract conclusions about the nature of the fixed point states. Finally we will say a few words about cMERA states at finite s.

3.4.1 Meeting our bosonic Gaussian states

Recall that this cMERA is defined for a scalar field in d dimensions, denoted $\phi(\vec{x})$, whose conjugate momentum we denote $\pi(\vec{x})$, so that $[\phi(\vec{x}), \pi(\vec{y})] = i\delta(\vec{x}-\vec{y})$. Exploiting translational invariance, we will carry out part of our analysis in momentum space. Hence we define the momentum modes $\phi(\vec{k})$ and $\pi(\vec{k})$

$$\phi(\vec{k}) \equiv \frac{1}{(2\pi)^{d/2}} \int d^d x \; e^{-i\vec{k}\cdot\vec{x}} \phi(\vec{x}) \,, \qquad \pi(\vec{k}) \equiv \frac{1}{(2\pi)^{d/2}} \int d^d x \; e^{-i\vec{k}\cdot\vec{x}} \pi(\vec{x}) \,. \tag{3.19}$$

which satisfy $[\phi(\vec{k}), \pi(\vec{q})] = i\delta(\vec{k}+\vec{q})$. The *target state* of the cMERA is the ground state of the massless Klein-Gordon Hamiltonian in d spatial dimensions:

$$H = \frac{1}{2} \int d^d x \; : \left(\pi(\vec{x})^2 + (\vec{\nabla}\phi(\vec{x}))^2 \right) : \tag{3.20}$$

which we denote $|\Psi\rangle$.

Because of the Gaussian property (see 3.2), both the target state $|\Psi\rangle$ and all cMERA states $|\Psi^\Lambda(s)\rangle$ for all $s \in [0,\infty]$ can be written [57] as the common kernel of annihilation operators, i.e. in the form:

$$a(\vec{k})|\Psi\rangle = 0, \qquad a(\vec{k}) = \sqrt{\frac{\alpha(k)}{2}}\phi(\vec{k}) + i\sqrt{\frac{1}{2\alpha(k)}}\pi(\vec{k}) \qquad \forall \vec{k} \in \mathbb{R}^d \tag{3.21}$$

Here and in the rest of this chapter, $k = |\vec{k}|$. The function $\alpha : \mathbb{R} \to \mathbb{R}$ completely determines the Gaussian state (up to an irrelevant global phase). The fact that it only depends on the modulus of the momentum implies the state is rotation invariant. The two-point functions of such a state can be readily expressed in terms of $\alpha(k)$:

$$\langle \phi(\vec{k})\phi(\vec{q})\rangle = \frac{1}{2\alpha(k)}\delta(\vec{k}+\vec{q}), \qquad \langle \pi(\vec{k})\pi(\vec{q})\rangle = \frac{\alpha(k)}{2}\delta(\vec{k}+\vec{q}). \tag{3.22}$$

In agreement with Wick's theorem, the two-point functions[5] fully determine the state.

Let us now compute the α function for the target state $|\Psi\rangle$, the initial state $|\Omega\rangle$ and the cMERA fixed point $|\Psi^\Lambda\rangle$. The Hamiltonian (3.20) can be diagonalized as usual in momentum space via creation-annihilation operators

$$H = \frac{1}{2}\int d^d k \ : \Big(\pi(\vec{k})\pi(-\vec{k}) + k^2\phi(\vec{k})\phi(-\vec{k})\Big) : = \int d^d k \ k a^\dagger(\vec{k})a(\vec{k}) \tag{3.23}$$

where

$$a(\vec{k}) = \sqrt{\frac{k}{2}}\phi(\vec{k}) + i\sqrt{\frac{1}{2k}}\pi(\vec{k}), \qquad a^\dagger(\vec{k}) = \sqrt{\frac{k}{2}}\phi(-\vec{k}) - i\sqrt{\frac{1}{2k}}\pi(-\vec{k}). \tag{3.24}$$

Therefore, we can define the target state as a common kernel of the annihilation operators of the form (3.21) with

$$\alpha(k) = k \qquad \text{(target CFT ground state } |\Psi\rangle\text{)}. \tag{3.25}$$

Turning now to the cMERA, in momentum space the constraints that define the initial state $|\Omega\rangle$ (given by the bosonic annihilation operators $\psi(\vec{x})$ from Eq. (2.10)) read

$$\left(\sqrt{\frac{\Lambda}{2}}\phi(\vec{k}) + i\sqrt{\frac{1}{2\Lambda}}\pi(\vec{k})\right)|\Omega\rangle = 0 \qquad \forall \vec{k} \in \mathbb{R}^d. \tag{3.26}$$

That is,

$$\alpha(k) = \Lambda \qquad \text{(initial unentangled state } |\Omega\rangle\text{)}. \tag{3.27}$$

[5] In our discussion we will be omitting the remaining correlator

$$\langle \phi(\vec{k})\pi(\vec{q})\rangle = \frac{i}{2}\delta(\vec{k}+\vec{q})$$

which is the same for all states of the form (3.21), independently of α.

Finally, we can use the definition of the cMERA to find the constraints that annihilate $|\Psi^\Lambda(s)\rangle$ following Eq. (3.2). We define $\alpha(k,s)$ as follows:

$$\left(\sqrt{\frac{\alpha(k,s)}{2}}\phi(\vec{k}) + i\sqrt{\frac{1}{2\alpha(k,s)}}\pi(\vec{k})\right)|\Psi^\Lambda(s)\rangle = 0 \qquad \forall\vec{k} \tag{3.28}$$

and compute it by means of equation (2.6). For this theory, the generator of scale transformations is

$$L = \frac{1}{2}\int d^dk \left[\pi(-\vec{k})\left(\vec{k}\cdot\vec{\nabla}_{\vec{k}} + \frac{d}{2}\right)\phi(\vec{k}) + \text{h.c.}\right]. \tag{3.29}$$

and the entangler K introduced in (2.12) can be written in momentum space as follows (we already make the assumption that it is independent of scale):

$$K = \frac{1}{2}\int d^dk\; g(k)\phi(\vec{k})\pi(-\vec{k}) + \text{h.c.} \tag{3.30}$$

Thus we compute the evolution of the field operators

$$\partial_s\phi(\vec{k}) = -i[L+K,\phi(\vec{k})] = -\left(\vec{k}\cdot\vec{\nabla}_{\vec{k}} + \frac{d}{2} + g(\vec{k})\right)\phi(\vec{k}) \tag{3.31}$$

$$\partial_s\pi(\vec{k}) = -i[L+K,\pi(\vec{k})] = -\left(\vec{k}\cdot\vec{\nabla}_{\vec{k}} + \frac{d}{2} - g(\vec{k})\right)\pi(\vec{k}) \tag{3.32}$$

from which we can obtain a partial differential equation for $\alpha(k,s)$

$$\partial_s\alpha(k,s) = (k\partial_k - 2g(k))\alpha(k,s) \tag{3.33}$$

We solve this equation to obtain:

$$\alpha(k,s) = \alpha(ke^s,0)\exp\left(-2\int_0^s du\; g(ke^u)\right), \tag{3.34}$$

or, replacing the value of $\alpha(k,0) = \Lambda$ from the initial state,

$$\alpha(k,s) = \Lambda\exp\left(-2\int_0^s du\; g(ke^u)\right). \tag{3.35}$$

In particular, taking $s\to\infty$ the asymptotic fixed point is characterized by

$$\alpha(k) = \Lambda\exp\left(-2\int_0^\infty du\; g(ke^u)\right) \qquad \text{(cMERA fixed point } |\Psi^\Lambda\rangle\text{)}. \tag{3.36}$$

The time has now come to pick an entangler, fixing g to work with a particular cMERA. In this simple case, rather that resorting to a variational argument, we can argue *a priori* in favor of certain properties for the $\alpha(k)$ function of the cMERA, then choose a $g(k)$ that guarantees those properties.

Recall that cMERA states are obtained via an entangling evolution that introduces correlations scale by scale, trying to approximate the target state, in this case the massless free boson ground state. At long distances (compared to the cutoff Λ^{-1}, below which we barely introduce correlations), the physics of $|\Psi^\Lambda\rangle$ and $|\Psi\rangle$ should be similar for a successful cMERA. We conjecture (and we will see it is indeed the case) that this can be achieved by having their α functions match in the corresponding momentum range. On the other hand, since the short-distance properties of the initial state should be left mostly untouched by the cMERA entangling procedure, we would expect $|\Psi^\Lambda\rangle$ and $|\Omega\rangle$ to behave similarly in the ultraviolet, and this should be reflected in their α functions. In summary, we expect $\alpha(k)$ and by extension the cMERA state, to have an *interpolatory* character between the target state, at long distances, and the initial unentangled state at short distances. In momentum space, this reads

$$\alpha(k) = \begin{cases} k & \text{for } k \ll \Lambda, \\ \Lambda & \text{for } k \gg \Lambda. \end{cases} \tag{3.37}$$

Note from (3.36) that the second condition can be met by having $g(k)$ decay fast enough for $k \gg \Lambda$. This makes sense, since it implies that K does not act at scales shorter than Λ^{-1}, as we demanded it to. Along these lines, consider now the Gaussian profile

$$g(x) = \frac{1}{2} e^{-\frac{\sigma\Lambda^2}{4}x^2} \implies g(k) = \frac{1}{2} e^{-\frac{1}{\sigma}\frac{k^2}{\Lambda^2}} \tag{3.38}$$

This choice is almost exactly the one presented in the seminal paper [56], except for the presence of the constant σ, which is added here so that the cMERA $|\Psi^\Lambda\rangle$ properly matches the long-distance properties of its target state $|\Psi\rangle$. With this particular choice of $g(k)$, we have

$$\alpha(k) = \Lambda \exp\left(\frac{1}{2}\mathrm{Ei}\left(-\frac{1}{\sigma}\frac{k^2}{\Lambda^2}\right)\right) \tag{3.39}$$

where

$$\mathrm{Ei}(x) = \int_{-x}^{\infty} dt\, \frac{e^{-t}}{t} \tag{3.40}$$

is the exponential integral function [57]. In the infrared limit $k \ll \Lambda$, we have

$$\alpha(k) \sim \sqrt{\frac{e^\gamma}{\sigma}} k \tag{3.41}$$

where $\gamma \approx 0.57722$ is the Euler-Mascheroni constant. Hence we choose $\sigma = e^{\gamma}$ for $\alpha(k)$ to reproduce the behaviour of the target state at small k. With this we have that the function $\alpha(k)$ for the fixed point of the free boson cMERA, depicted in Figure 3.1, satisfies (3.37).

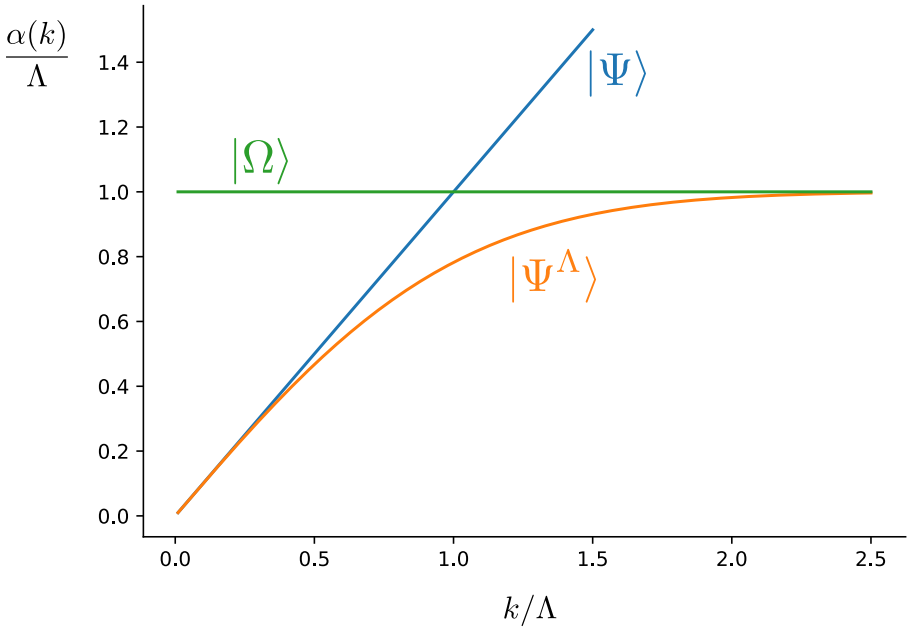

Figure 3.1: $\alpha(k)$ for the three states $|\Psi\rangle$, $|\Omega\rangle$ and $|\Psi^{\Lambda}\rangle$.

3.4.2 Entanglement structure of the cMERA state

To probe the entanglement structure of the cMERA state, we will investigate the scaling of two-point correlation functions and entanglement entropy. For comparison purposes we briefly review the scaling of two-point correlations and entanglement entropy in the two states $|\Psi\rangle$ and $|\Omega\rangle$ of which cMERA is an interpolation. Then we will move on to study the cMERA state in 1+1 and 2+1 dimensions.

Target state $|\Psi\rangle$

In the ground state $|\Psi\rangle$ of a free massless bosonic CFT in $d+1$ spacetime dimensions, the two-point correlation functions involving $\phi(\vec{x})$ and $\pi(\vec{x})$ show power-law decays:

$$\langle\phi(\vec{x})\phi(\vec{y})\rangle = \frac{\Gamma\left(\frac{d-1}{2}\right)}{4\pi^{\frac{d+1}{2}}}\frac{1}{|\vec{x}-\vec{y}|^{d-1}}, \qquad \langle\pi(\vec{x})\pi(\vec{y})\rangle = -\frac{\Gamma\left(\frac{d-1}{2}\right)}{4\pi^{\frac{d+1}{2}}}\frac{d-1}{|\vec{x}-\vec{y}|^{d+1}}, \tag{3.42}$$

except in $d=1$, where the first correlation function is instead, up to an additive constant,

$$\langle\phi(x)\phi(y)\rangle = -\frac{\log|x-y|}{2\pi}. \tag{3.43}$$

since $\phi(x)$ is not a primary operator in 2d. In turn, the entanglement entropy of a region of linear size x obeys the area law:

$$S(x) \sim \left(\frac{x}{a}\right)^{d-1} \tag{3.44}$$

where a is a UV cutoff, except in $d=1$, where the scaling is logarithmic, as we saw in Section 1.4:

$$S(L) \sim \frac{c}{3}\log\left(\frac{L}{a}\right) \tag{3.45}$$

with $c=1$ the central charge of the free boson CFT. Note that if we remove the UV cutoff by taking the limit $a \to 0$, the entanglement entropy in Eqs. (3.44)-(3.45) diverges.

Unentangled state $|\Omega\rangle$

In the case of the initial state $|\Omega\rangle$ we have

$$\langle\phi(\vec{x})\phi(\vec{y})\rangle = \frac{\delta(\vec{x}-\vec{y})}{2\Lambda}, \qquad \langle\pi(\vec{x})\pi(\vec{y})\rangle = \frac{\Lambda\delta(\vec{x}-\vec{y})}{2}, \tag{3.46}$$

i.e. there are no correlations between degrees of freedom at different points. It follows that the entanglement entropy of any interval is zero.

cMERA fixed point $|\Psi^\Lambda\rangle$ (1+1 dimensions)

The position space two-point functions of the cMERA state given by (3.36) in 1+1 dimensions are most easily computed by Fourier transforming the corresponding momentum

space correlators, which are given in terms of $\alpha(k)$ by (3.22). For instance,

$$\begin{aligned}\langle\phi(x)\phi(y)\rangle &= \int dk\, dq\ \frac{e^{i(kx+qy)}}{2\pi}\langle\phi(k)\phi(q)\rangle = \int dk\ \frac{e^{ik(x-y)}}{2\pi}\frac{1}{2\alpha(k)} = \\ &= \frac{1}{2\Lambda}\delta(x-y) + \int_{\mathbb{R}\setminus(-\varepsilon\Lambda,\varepsilon\Lambda)} dk\ \frac{e^{ik(x-y)}}{2\pi}\left(\frac{1}{2\alpha(k)} - \frac{1}{2\Lambda}\right) = \\ &= \frac{1}{2\Lambda}\delta(x-y) + f_\varepsilon(x-y). \end{aligned} \tag{3.47}$$

And equally,

$$\langle\pi(x)\pi(y)\rangle = \frac{\Lambda}{2}\delta(x-y) + \int_{\mathbb{R}\setminus(-\varepsilon\Lambda,\varepsilon\Lambda)} dk\ \frac{e^{ik(x-y)}}{4\pi}\left(\alpha(k)-\Lambda\right) = \frac{\Lambda}{2}\delta(x-y) + g_\varepsilon(x-y). \tag{3.48}$$

$f_\varepsilon, g_\varepsilon$ are continuous functions that depend on a parameter $\varepsilon \ll 1$. Here $\varepsilon\Lambda$ acts as an IR cutoff, needed to counter the well-known IR divergence of the 1+1 Klein-Gordon theory of a free massless scalar. Since the cMERA construction reproduces the infrared behaviour of the target state, it also displays such a divergence. Indeed, the integral that defines $f_\varepsilon(x-y)$ can be seen to diverge for $\varepsilon = 0$. We thus regulate this divergence by introducing an additional IR length scale $1/(\varepsilon\Lambda)$ and removing the degrees of freedom at length scales larger than $1/(\varepsilon\Lambda)$ from the integrals that translate from momentum space back into position space.

Figure 3.2 show the cMERA two-point correlators. Two very different regimes can be appreciated. First, at short distances $x \ll 1/\Lambda$, the correlators are practically constant. In contrast, at distances larger than $1/\Lambda$ (but smaller than the IR cutoff scale given by $1/(\varepsilon\Lambda)$) the correlators recover the scaling expected in the CFT:

$$\langle\phi(x)\phi(y)\rangle = -\frac{\log|x-y|}{2\pi} \qquad \langle\pi(x)\pi(y)\rangle \propto \frac{-1}{(x-y)^2} \tag{3.49}$$

From the numerically obtained cMERA correlations in the regime of distances x given by $1/\Lambda \ll x \ll 1/(\varepsilon\Lambda)$, $\varepsilon = 10^{-6}$, we can estimate the following values for the coefficient of the logarithmic decay and the exponent of the power law decay:

$$\langle\phi(x)\phi(y)\rangle \sim -p_1 \log|x-y| \qquad p_1 \approx 0.15904 \tag{3.50}$$

$$\langle\pi(x)\pi(y)\rangle \sim \frac{-1}{(x-y)^{p_2}} \qquad p_2 \approx 2.0078 \tag{3.51}$$

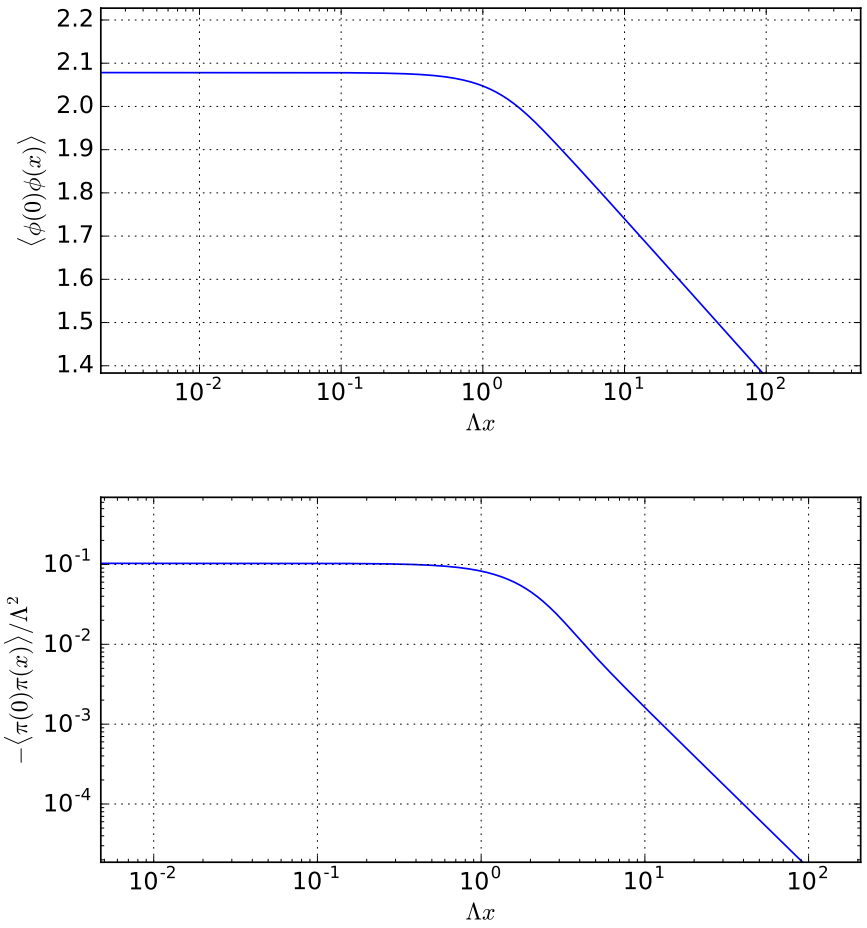

Figure 3.2: $\langle\phi(0)\phi(x)\rangle$ (top) and $\langle\pi(0)\pi(x)\rangle$ (bottom) correlators computed for a cMERA defined by 3.39. Notice the existence of two clearly different regimes delimited by $\Lambda x \sim 1$. These results were obtained with an IR regulator with $\varepsilon = 10^{-6}$.

which indeed are very close to their values for the target CFT theory, namely $1/(2\pi) = 0.15915$ and $2\Delta_\pi = 2$, where $\Delta_\pi = 1$ is the scaling dimension of π. The value of p_2 can in fact be obtained from the momentum space representation (3.22), prior to the numerics, via asymptotic analysis. Indeed, the fact that $\alpha(k)$ has a discontinuity in its first derivative at $k = 0$ imposes for the two-point function in position space an asymptotic power-law decay of the form $\langle \pi(x)\pi(y)\rangle \sim |x-y|^{-2}$. This discontinuity in $\alpha(k)$ was already there in the target theory, of which cMERA preserves the low momentum characteristics. By the same kind of arguments we can also compute the leading order asymptotic term of the difference between CFT and cMERA correlators. Since

$$\alpha_{\text{cMERA}}(k) - \alpha_{\text{CFT}}(k) = -\frac{k^3}{2\sigma\Lambda^2} + \dots \tag{3.52}$$

we have, at long distances

$$|\langle \pi(0)\pi(x)\rangle_{\text{cMERA}} - \langle \pi(0)\pi(x)\rangle_{\text{CFT}}| = \frac{3}{2\pi\sigma\Lambda^2 x^4} + \dots \tag{3.53}$$

We now turn to the entanglement entropy profile. In the CFT, the entanglement entropy of a finite interval is divergent. We can still obtain its characteristic scaling in Eq. (3.45) by discretizing the CFT into a lattice, where the lattice spacing provides the UV cutoff. Importantly, progressive fine-graining of the lattice brings in new degrees of freedom that contribute to the entropy, which therefore diverges as the lattice spacing is removed in the limit $a \to 0$.

Our procedure for numerically computing the entanglement entropy in the cMERA is also based on a lattice discretization. However, instead of discretizing and solving the full theory on the lattice, we will simply sample the continuum two-point correlation functions on a lattice with lattice spacing a.

This procedure yields discrete matrix versions of the correlation functions $C_{\phi\phi} = \langle \phi(x)\phi(y)\rangle$ and $C_{\pi\pi} = \langle \pi(x)\pi(y)\rangle$, from which one can easily extract the entanglement entropy following Section 3.3. We apply the following discretization conventions

$$\begin{aligned} C_{\phi\phi}(x,y) &= \frac{1}{2\Lambda}\delta(x-y) + f_\varepsilon(x,y) \quad &\longrightarrow\ (C_{\phi\phi})_{ij} &= \frac{1}{2\Lambda a}\delta_{ij} + f_\varepsilon(ia,ja) \qquad i,j \in \mathbb{Z}, \\ C_{\pi\pi}(x,y) &= \frac{\Lambda}{2}\delta(x-y) + g_\varepsilon(x,y) \quad &\longrightarrow\ (C_{\pi\pi})_{ij} &= \frac{\Lambda a}{2}\delta_{ij} + a^2 g_\varepsilon(ia,ja) \qquad i,j \in \mathbb{Z}. \end{aligned}$$

From here we numerically compute the entanglement entropy profile $S(x)$. We must insist on the fact that this method is based on an approximation. The actual theory is defined

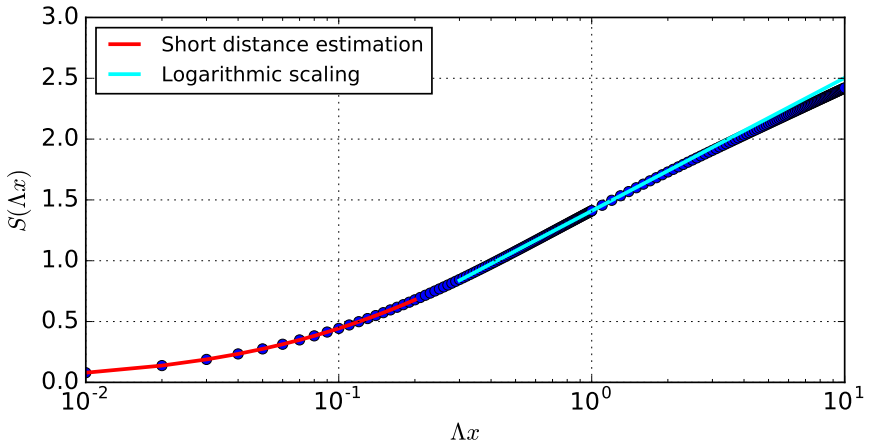

Figure 3.3: Numerical computation of the entanglement entropy profile ($\Lambda a = 0.01$, $\varepsilon = 10^{-6}$) for a 1+1 dimensional Klein-Gordon theory. The short range theoretical estimation and the long distance logarithmic scaling have been superimposed.

in the continuum, and we are applying a sampling operation that produces discretized versions of the continuous operator kernels $C(x, y)$, in the hope that their spectra will be captured well enough by those of their discretizations in the limit of small a. Note that, for example, the spectra of the discretized operators will in general not be fully compatible with the constraints on the spectra of discrete correlation matrices. This will force us to discard a fraction of the eigenvalues of the constructed operators, relying on the assumption that their deviation from allowed values approaches zero as a does (an assumption that we corroborate numerically). Crucially, progressive fine-graining of the lattice discretization (that is, reducing the lattice spacing a) reveals convergence of the entanglement entropy $S(x)$ to a finite value, rather than the divergence seen in the entanglement entropy of the CFT. Specifically, Figure 3.4 shows that for $a \ll 1/\Lambda$, the entanglement entropy of an interval converges to its finite value for $a = 0$ quadratically in a, $S_a(x) = S(x) + O(a^2)$. We will take this value as our approximation to the entanglement entropy.

The converged entropy profile can be seen in Figure 3.3. We observe two clearly different regimes: one for interval sizes x significantly smaller than the UV cutoff $1/\Lambda$, and one for sizes x comparable to and larger than $1/\Lambda$ (but smaller than the IR cutoff $1/(\varepsilon\Lambda)$, which is not shown). In this second region, the scaling of entanglement entropy reproduces the CFT logarithmic growth of (3.45). The numerical fit of the central charge c in the region

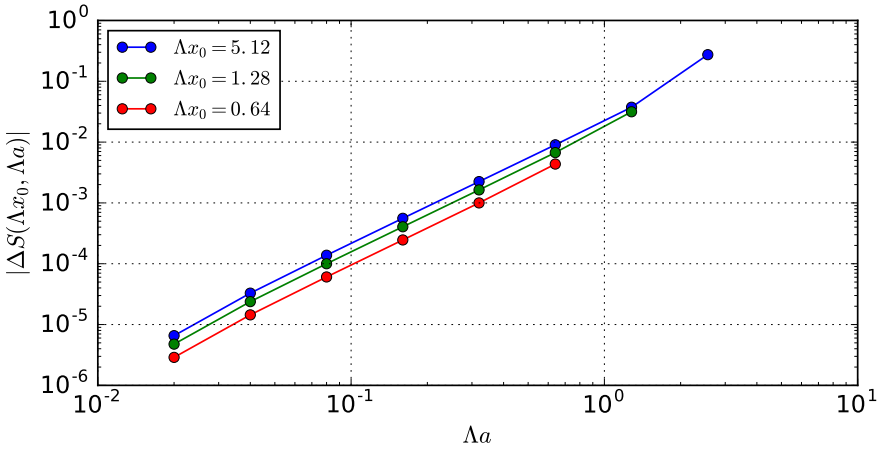

Figure 3.4: Plot of the difference $|S(\Lambda x_0, \Lambda a) - S(\Lambda x_0, \Lambda a = 0.01)|$ that shows the convergence of this particular value of entropy upon iterative fine-graining of the sampling parameter used as a tool to compute it. The plotted difference goes to zero approximately quadratically with Λa.

around $x \sim 1/\Lambda$ gives a value of the central charge

$$c \approx 0.987 \tag{3.54}$$

which is very close to the exact value $c = 1$. At larger distances the growth of the entropy is slightly smaller than the one dictated by (3.45) with $c = 1$, which we believe to be an effect of the IR regulator. Figure 3.3 also shows a theoretical estimate, derived in Appendix B.3, for the scaling of the cMERA entanglement entropy for a small interval size x, $x \ll 1/\Lambda$.

We have thus seen that the scaling of correlations and of entanglement entropy in the cMERA state $|\Psi^\Lambda\rangle$ mimic those of the target CFT ground state at long distances $x \gg 1/\Lambda$. However, at short distances $x \ll 1/\Lambda$, the correlators tend to a constant and the entanglement entropy (which is finite for any finite interval) vanishes. Similar results will be obtained below for $d = 2$ spatial dimensions and for free fermion CFTs. This is the sense in which the cMERA state $|\Psi^\Lambda\rangle$ has a built-in UV cutoff at distance $x \approx 1/\Lambda$.

cMERA fixed point $|\Psi^\Lambda\rangle$ (2+1 dimensions)

In more than one spatial dimension, the free massless boson field theory does not need to be IR regularized. However, the numerical cost of computing the correlations and, especially,

the entanglement entropy becomes much larger. Fortunately, this does not prevent us from being able to numerically characterize the scaling at short distances $x \ll 1/\Lambda$, confirm once more the presence of the UV cutoff, and justify both analytically and numerically the transition to the asymptotic CFT-like behaviour.

The cMERA two-point correlation functions are again given in momentum space by (3.22), and in position space by their Fourier transform:

$$\begin{aligned}\langle\phi(\vec{x})\phi(\vec{y})\rangle &= \frac{1}{2\Lambda}\delta(\vec{x}-\vec{y}) + \int_{\mathbb{R}^2} d\vec{k}\, \frac{e^{i\vec{k}\cdot(\vec{x}-\vec{y})}}{(2\pi)^2}\left(\frac{1}{2\alpha(k)} - \frac{1}{2\Lambda}\right) \\ &= \frac{1}{2\Lambda}\delta(\vec{x}-\vec{y}) + \int_0^\infty \frac{k\, dk}{2\pi}\left(\frac{1}{2\alpha(k)} - \frac{1}{2\Lambda}\right)\int_0^{2\pi} d\varphi \frac{e^{ik|\vec{x}-\vec{y}|\cos\varphi}}{2\pi} \\ &= \frac{1}{2\Lambda}\delta(\vec{x}-\vec{y}) + \int_0^\infty \frac{k\, dk}{2\pi}\left(\frac{1}{2\alpha(k)} - \frac{1}{2\Lambda}\right) J_0(k|\vec{x}-\vec{y}|) \\ &= \frac{1}{2\Lambda}\delta(\vec{x}-\vec{y}) + f(|\vec{x}-\vec{y}|) \end{aligned} \tag{3.55}$$

where J_0 is the zeroth Bessel function of the first kind. Similarly,

$$\begin{aligned}\langle\pi(\vec{x})\pi(\vec{y})\rangle &= \frac{\Lambda}{2}\delta(\vec{x}-\vec{y}) + \int_0^\infty \frac{k\, dk}{2\pi}\left(\frac{\alpha(k)-\Lambda}{2}\right) J_0(k|\vec{x}-\vec{y}|) \\ &= \frac{\Lambda}{2}\delta(\vec{x}-\vec{y}) + g(|\vec{x}-\vec{y}|). \end{aligned} \tag{3.56}$$

These two-point correlation functions consist of on-site deltas plus smooth terms[6] that only depend on the distance $|\vec{x}-\vec{y}|$. Their asymptotic behaviour for long distances can again be inferred from their momentum space representation (3.22). $\langle\phi(\vec{x})\phi(\vec{y})\rangle$ decays as $|\vec{x}-\vec{y}|^{-1}$ at long distances due to the $|\vec{k}|^{-1}$ singularity at the origin of the function $\alpha(\vec{k})^{-1}$ (see Appendix B.1). On the other hand, $\langle\pi(\vec{x})\pi(\vec{y})\rangle$ decays as $|\vec{x}-\vec{y}|^{-3}$ since the function $\alpha(\vec{k})$ goes as $|\vec{k}|$ near $\vec{k}=0$. Note again how the fact that the cMERA construction preserves the low momentum character of the target CFT manifestly leads to the preservation of the long distance behaviour of the two-point functions of the theory. The leading order asymptotic cMERA corrections to these can be seen to go like

$$|\langle\phi(\vec{x})\phi(\vec{y})\rangle_{\text{cMERA}} - \langle\phi(\vec{x})\phi(\vec{y})\rangle_{\text{CFT}}| \sim |\vec{x}-\vec{y}|^{-3} \tag{3.57}$$

$$|\langle\pi(\vec{x})\pi(\vec{y})\rangle_{\text{cMERA}} - \langle\pi(\vec{x})\pi(\vec{y})\rangle_{\text{CFT}}| \sim |\vec{x}-\vec{y}|^{-5} \tag{3.58}$$

[6]Notice that we repeat the notation f, g for these terms, which should not be mistaken for their 1+1-dimensional analogues (which we had regularized with ε because of the IR divergence).

i.e., decaying in both cases two orders faster than the leading term.

We plot the numerically obtained functions f and g in Figure 3.5. As in the one dimensional case, we observe a short distance regime $|\vec{x}-\vec{y}| \ll 1/\Lambda$, where the correlators are practically constant, and a long distance regime $|\vec{x}-\vec{y}| \gg 1/\Lambda$, where the shape of the correlators reproduces the CFT power law decay with the right exponents:

$$f(x) \sim \frac{1}{x^{2p_1}}, \qquad p_1 = 0.4998 \quad (\approx 0.5 = \Delta_\phi), \qquad \Lambda x \gg 1, \tag{3.59}$$

$$g(x) \sim \frac{1}{x^{2p_2}}, \qquad p_2 = 1.502 \quad (\approx 1.5 = \Delta_\pi), \qquad \Lambda x \gg 1. \tag{3.60}$$

Let us now turn to the entanglement entropy. In $2+1$ dimensions we compute the entanglement entropy of discs of increasing radius x. The technical details of this computation are presented in Appendix B.2. In short, we work in polar coordinates and consider modes indexed by the radial coordinate r and with a definite angular momentum given by an integer $l \in \mathbb{Z}$. Different angular momentum modes are uncorrelated, so they contribute independently to the entanglement entropy. Only the modes with smallest angular momentum are found to contribute at short distances, with the corrections due to larger angular momenta becoming more relevant at longer distances [66].

We approximately compute the entanglement entropy by the same procedure as in the 1+1-dimensional case: we sample the correlators with some lattice spacing a and build discrete versions of the continuum operators $C_{\phi\phi}, C_{\pi\pi}$, from which we numerically extract an approximation to the entanglement entropy $S(x)$. In addition, Appendix B.3 derives a theoretical estimate of $S(x)$ for $x \ll 1/\Lambda$, restricted to the contribution from the zero angular momentum mode.

Two remarks are in order. The first refers to the convergence of the profile $S(x)$ above with respect to contributions coming from different angular momenta. Figure 3.6, shows the partial entropy $S_{l_{\max}}(x)$ of a disc of radius x obtained by adding the contributions from all angular momentum l such that $|l| \leq l_{\max}$. We see that, indeed, $S_{l_{\max}}(x)$ is essentially independent of $l_{\max}$ for $x \leq 1/\Lambda$. For $x \approx 2/\Lambda$ convergence is roughly obtained for $l_{\max} \geq 1$, for $x \approx 3/\Lambda$ convergence is roughly obtained for $l_{\max} \geq 2$, etc. These results are sufficient to see the onset of the area law at $x \approx 1/\Lambda$, as expected in the CFT, see Eq. (3.44).

Our second remark refers to the convergence of these results with respect to the sampling parameter a used to discretize the correlation functions. Figure 3.7 shows that, once more, $S(x)$ tends to a finite profile when we reduce a. Notice also the agreement between the numerical values and the zero angular momentum estimate at short distances $x \ll 1/\Lambda$.

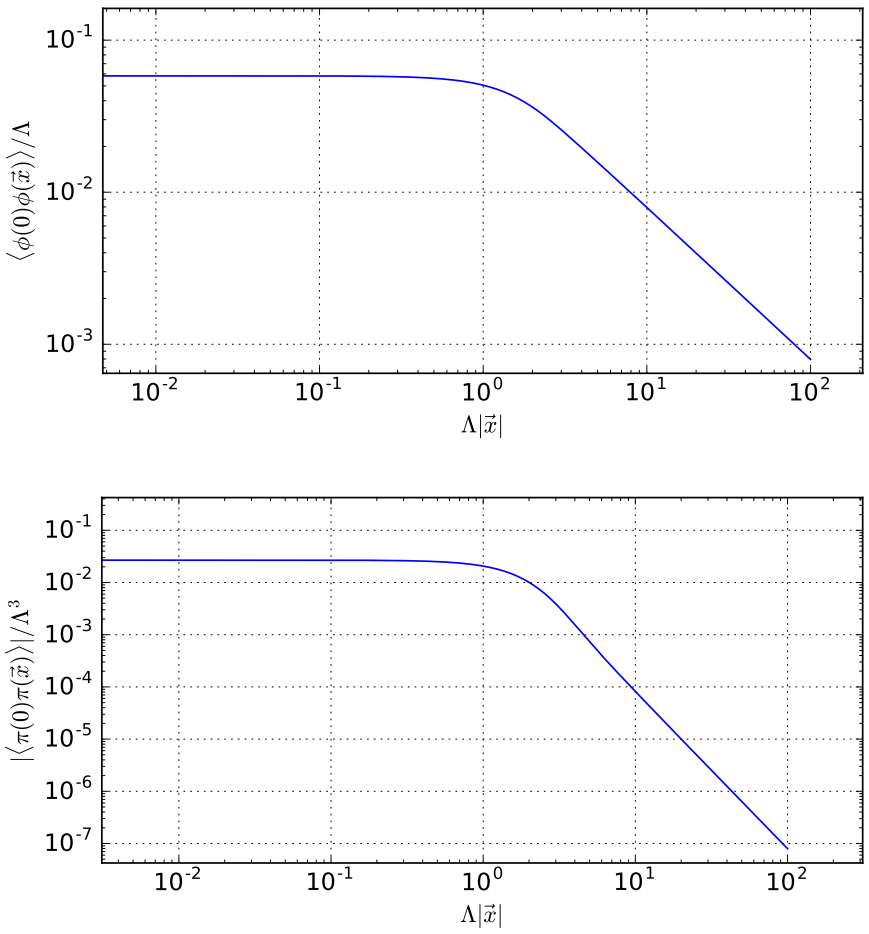

Figure 3.5: $\langle\phi(0)\phi(\vec{x})\rangle$ (top) and $\langle\pi(0)\pi(\vec{x})\rangle$ (bottom) correlators computed for the 2+1-dimensional bosonic cMERA.

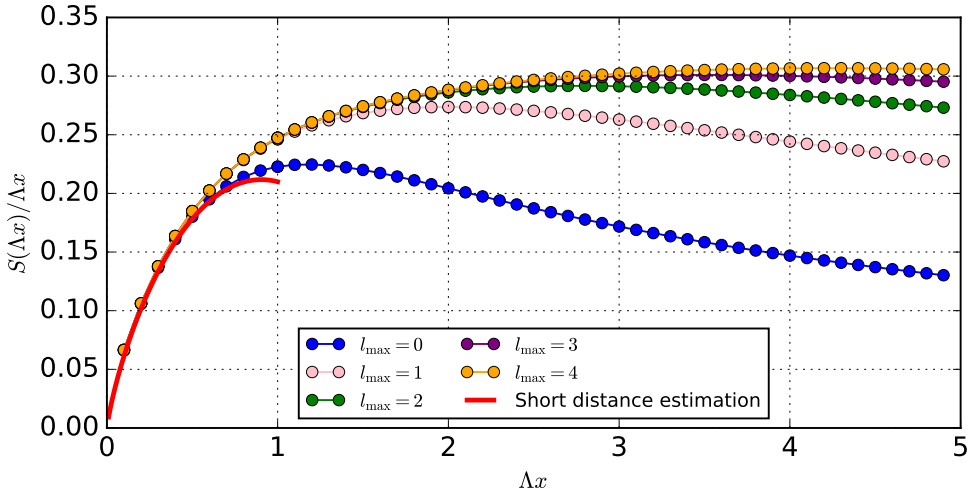

Figure 3.6: Numerical computation of the entanglement entropy profile ($\Lambda a = 0.01$) for the 2+1 dimensional bosonic cMERA.

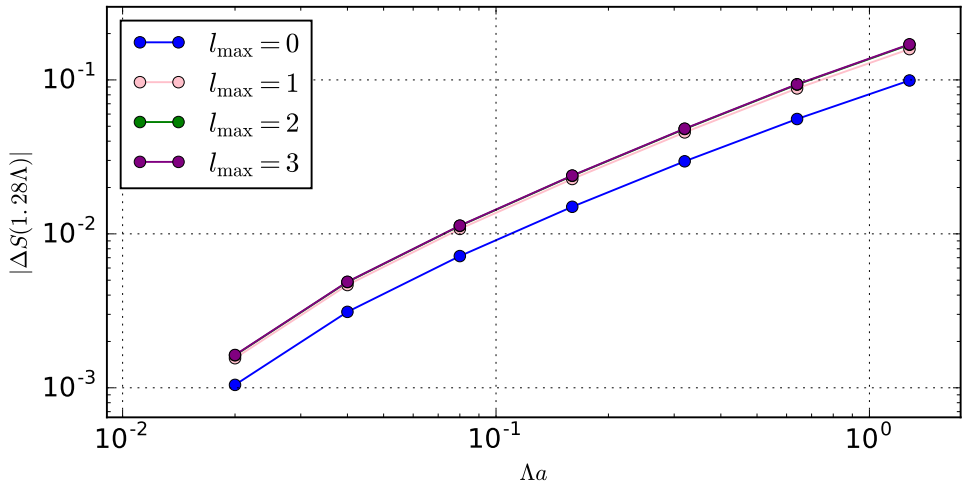

Figure 3.7: Plot of the difference $|S(1.28\Lambda, \Lambda a) - S(1.28\Lambda, \Lambda a = 0.01)|$, for different values of $l_{\max}$ that shows the convergence of this particular value of entropy upon iterative fine-graining of the sampling used as a tool to compute it. Note how truncating at higher values of l does not affect the rate of convergence in a.

3.4.3 A comment on finite s cMERA states

So far we have been focusing on the asymptotic fixed point cMERA state $|\Psi^\Lambda\rangle$, and we have learned that it can be understood as a UV regularized version of the target state of the cMERA, due to the fact that the entangling evolution introduces correlations almost entirely at length scales above the UV cutoff Λ^{-1}. On that basis, there are a couple of things we can expect from cMERA states $|\Psi^\Lambda(s)\rangle$ that result from evolving for a finite "pseudotime",

$$|\Psi^\Lambda(s)\rangle = \mathcal{P}\exp\left(-i\int_0^s ds'\ [L + K(s')]\right)|\Omega\rangle. \tag{3.61}$$

First, most of their correlations should be present within the length scale window $[\Lambda^{-1}, e^s\Lambda^{-1}]$. A way to see this comes from thinking of the entangling evolution in a Trotterized fashion, i.e., as alternating infinitesimal evolutions by the generator L and K. If we evolve only until pseudotime s, the longest-range correlations present in the state will be those that we introduced right at the start of the evolution (recall that K introduces correlations mostly at length scale Λ^{-1}) and then progressively rescaled by a total factor of e^s. In conclusion, in a similar fashion that Λ^{-1} is a UV cutoff, $e^s\Lambda^{-1}$ is an IR cutoff, i.e. an effective correlation length, for $|\Psi^\Lambda(s)\rangle$.

Secondly, in the cases we have been dealing with, the entangler is independent of scale. That means that the correlations we have been introducing in the window between our cutoffs should roughly match the ones present in the fixed point state $|\Psi^\Lambda\rangle$ (and hence in the target state $|\Psi\rangle$, if the cMERA is optimized) in that same window. This is so because, even if that entanglement would have been rescaled to become longer range entanglement if we continued the evolution, it would have been replaced by identical correlations due to scale invariance. Hence the convergence to the fixed point state in a scale invariant cMERA can be interpreted as the lifting of an IR cutoff, and $|\Psi^\Lambda(s)\rangle$ should behave as $|\Psi^\Lambda\rangle$ at all scales below $e^s\Lambda^{-1}$.

When speaking of an IR cutoff for the free boson theory, the first one that comes to mind is the one obtained by adding a mass term $m^2\phi^2(x)$ to the Hamiltonian. How do its effects compare to the cutoff induced by an "unfinished" cMERA? The effects of both IR cutoffs in the correlation measures of $|\Psi^\Lambda(s)\rangle$ will in principle be qualitatively similar, modifying the CFT-like behaviours into those of a gapped theory at length scales above the effective correlation length: former power-law correlators should decay exponentially and the entanglement entropy should saturate to a constant. However, quantitatively, the IR behaviour of the massive free boson ground state of mass $m = \Lambda e^{-s}$ need not be well approximated by $|\Psi^\Lambda(s)\rangle$.

The reader might remember that in Section 2.6 we spoke about *magic* cMERAs: a particular subclass of entanglers that gave rise to cMERAs with interesting properties, among them the compatibility with cMPS simulation. It so happens that finite s magic cMERAs are very good at approximating massive ground states. This will be one of the key insights from Chapter 4, so we will leave the topic of intermediate cMERA states for now and retake it then.

3.5 Free fermion cMERA

In this section we investigate the entanglement structure of the cMERA introduced in 2.5 for the ground state of the free Dirac fermion CFT, following the same approach as in the bosonic case. Once again we will restrict ourselves to $1+1$ and $2+1$ spacetime dimensions, and we will focus on the cMERA fixed point. This is the only section we devote in the thesis to the fermionic cMERA: in the rest of the upcoming chapters we will be entirely focusing on bosonic cMERAs.

3.5.1 Meeting our fermionic Gaussian states

Throughout this section, $\vec{\psi}(\vec{x})$ denotes a 2-component Dirac spinor, with components $\psi_1(x)$ and $\psi_2(x)$ obeying anticommutation relations

$$\left\{\psi_i(\vec{x}), \psi_j^\dagger(\vec{y})\right\} = \delta_{i,j}\delta(\vec{x}-\vec{y}), \qquad \left\{\psi_i(\vec{x}), \psi_j(\vec{y})\right\} = 0.$$

Similarly, $\vec{\psi}(\vec{k})$ denotes the Fourier component of the Dirac spinor,

$$\psi_i(\vec{k}) \equiv \frac{1}{(2\pi)^{d/2}} \int d^d x \; e^{-i\vec{k}\cdot\vec{x}} \psi_i(\vec{x}), \qquad i = 1, 2. \tag{3.62}$$

with

$$\left\{\psi_i(\vec{k}), \psi_j^\dagger(\vec{q})\right\} = \delta_{i,j}\delta(\vec{k}-\vec{q}), \qquad \left\{\psi_i(\vec{k}), \psi_j(\vec{q})\right\} = 0.$$

Recall that the free fermion cMERA aims at approximating the ground state of the free massless Dirac fermion Hamiltonian in $d = 1, 2$ spatial dimensions:

$$H = \int d^d x \; \psi^\dagger(\vec{x})\gamma^0(-i\vec{\gamma}\cdot\vec{\partial})\psi(\vec{x}). \tag{3.63}$$

Once again we denote this target state by $|\Psi\rangle$.

Fermionic Gaussian states

We consider Gaussian states $|\Phi\rangle$ characterized by their annihilation operators

$$\tilde{\psi}_1(\vec{k})|\Phi\rangle = 0, \qquad \tilde{\psi}_2^\dagger(\vec{k})|\Phi\rangle = 0, \qquad \forall \vec{k} \in \mathbb{R}^d, \tag{3.64}$$

where $\tilde{\psi}_1(\vec{k})$ and $\tilde{\psi}_2(\vec{k})$ are related to the original momentum space spinor components $\psi_1(\vec{k})$ and $\psi_2(\vec{k})$ by a $\vec{k}$-dependent unitary transformation $M(\vec{k})$

$$\tilde{\psi}_i(\vec{k}) = M_{ij}(\vec{k})\psi_j(\vec{k}). \tag{3.65}$$

For all the states of interest in this section, this transformation can be parametrized by an angular function $\theta(\vec{k}) = \theta(k)$ of the modulus of the momentum, according to

$$M[\theta(k)] \equiv \cos\theta(k)\ \mathbb{1} + \sin\theta(k)\ \vec{\gamma}\cdot\hat{k} = \exp\left(\ \theta(k)\ \vec{\gamma}\cdot\hat{k}\ \right). \tag{3.66}$$

Here $\hat{k} \equiv \vec{k}/k$ is a normalized vector and $\vec{\gamma}$ is the vector of space-like Dirac matrices, which are skew-Hermitian, so $M[\theta(k)]$ is unitary. The two-point functions[7] of such a state can be written in terms of $\theta(k)$ via the change of variables:

$$\begin{pmatrix} \langle\psi_1^\dagger(\vec{k})\psi_1(\vec{q})\rangle & \langle\psi_1^\dagger(\vec{k})\psi_2(\vec{q})\rangle \\ \langle\psi_2^\dagger(\vec{k})\psi_1(\vec{q})\rangle & \langle\psi_2^\dagger(\vec{k})\psi_2(\vec{q})\rangle \end{pmatrix} = M[-\theta(\vec{k})]^* \begin{pmatrix} 0 & 0 \\ 0 & \delta(\vec{k}-\vec{q}) \end{pmatrix} M[-\theta(\vec{k})]^t. \tag{3.67}$$

where t denotes matrix transposition. Once we pick a representation for the γ matrices we will be able to give more explicit expressions.

We proceed to find the parametrization in terms of $\theta(k)$ of the target, initial and fixed point states. The Dirac Hamiltonian (3.63) can be diagonalized in momentum space:

$$H = \int d^dk\ \psi^\dagger(\vec{k})\ \gamma^0\left(\vec{\gamma}\cdot\vec{k}\right)\psi(\vec{k}). \tag{3.68}$$

Indeed, the quadratic form $\gamma^0(\vec{\gamma}\cdot\vec{k})$ is Hermitian and can thus be diagonalized by a unitary transformation. If we pick

$$\gamma^0 \equiv \sigma_z = \begin{pmatrix} 1 & 0 \\ 0 & -1 \end{pmatrix},$$

[7]Note that these states are all $U(1)$ symmetric under $\vec{\psi}(\vec{x}) \to e^{i\zeta}\vec{\psi}(\vec{x})$, thus all correlators of the form $\langle\psi_i(\vec{x})\psi_j(\vec{y})\rangle$ vanish.

then said unitary turns out to be of the form (3.66) for

$$\theta(k) = \pi/4 \qquad \text{(target CFT ground state } |\Psi\rangle\text{)}\,. \tag{3.69}$$

Indeed,

$$\tilde{\psi}(\vec{k}) = \frac{\mathbb{1} + \vec{\gamma}\cdot\hat{k}}{\sqrt{2}}\psi(\vec{k}) \implies H = \int d^d k\; k\; \tilde{\psi}^\dagger(\vec{k})\gamma^0\tilde{\psi}(\vec{k}). \tag{3.70}$$

Thus we have diagonalized the Hamiltonian and we can identify the structure of the ground state $|\Psi\rangle$, which shall be annihilated by the operators $\tilde{\psi}_1(\vec{k})$ and $\tilde{\psi}_2^\dagger(\vec{k})$, that is, the operators that annihilate particles with positive energy and create particles with negative energy.

The initial unentangled state for this cMERA was given by (2.15), which in momentum space reads

$$\psi_1(\vec{k})|\Omega\rangle = 0, \quad \psi_2^\dagger(\vec{k})|\Omega\rangle = 0, \quad \forall\vec{k}. \tag{3.71}$$

Thus the state can be characterized by annihilation operators $\tilde{\psi}_1 = \psi_1, \tilde{\psi}_2^\dagger = \psi_2^\dagger$, that is,

$$\theta(k) = 0 \qquad \text{(initial unentangled state } |\Omega\rangle\text{)}\,. \tag{3.72}$$

To find the annihilation operators for the cMERA fixed point, we use a similar technique to the bosonic case. Define $\theta(k,s)$ in the analogous way

$$M_{1j}[\theta(k,s)]\psi_j(\vec{k})|\Psi^\Lambda(s)\rangle = \Big(M_{2j}[\theta(k,s)]\psi_j(\vec{k})\Big)^\dagger|\Psi^\Lambda(s)\rangle = 0. \tag{3.73}$$

The cMERA evolution generators in momentum space read

$$L = i\int d^d k\; \psi_j^\dagger(\vec{k})\left(\vec{k}\cdot\vec{\nabla} + \frac{d}{2}\right)\psi_j(\vec{k}), \tag{3.74}$$

$$K = -i\int d^d k\; g(k)\vec{\psi}^\dagger(\vec{k})\left(\vec{\gamma}\cdot\hat{k}\right)\vec{\psi}(\vec{k}). \tag{3.75}$$

where, to keep with the conventions in the literature, we have defined $g(k) \equiv -kh(k)$, $h(k)$ being the Fourier transform of the profile $h(x)$ from (2.16). With them we can evolve the spinor

$$-i[L+K, \vec{\psi}(\vec{k})] = -\left(\vec{k}\cdot\vec{\nabla}_{\vec{k}} + \frac{d}{2} - g(\vec{k})\,\hat{k}\cdot\vec{\gamma}\right)\vec{\psi}(\vec{k}), \tag{3.76}$$

and obtain a partial differential equation for $\theta(k,s)$:

$$\partial_s\theta(k,s) = k\partial_k\theta(k,s) + g(k,s). \tag{3.77}$$

The solution to this equation gives

$$\theta(k,s) = \theta(ke^s, 0) + \int_0^s du\; g(ke^u) \tag{3.78}$$

and replacing the value $\theta(k,0) = 0$ from the initial state:

$$\theta(k,s) = \int_0^s du\; g(ke^u). \tag{3.79}$$

The fixed point is then characterized by

$$\theta(k) = \int_0^\infty du\; g(ke^u) \qquad \left(\text{cMERA fixed point}|\Psi^\Lambda\rangle\right). \tag{3.80}$$

Ideally, a successful cMERA would be given by a θ function that interpolates between those of $|\Omega\rangle$ and $|\Psi\rangle$, as we saw for the free boson:

$$\theta(k) \sim \begin{cases} \pi/4 & k \ll \Lambda \\ 0 & k \gg \Lambda \end{cases} \tag{3.81}$$

Following [56], we consider the family of Gaussian cutoff functions:

$$g_n(k) = C_n \left(\frac{k}{\Lambda}\right)^{2n+1} e^{-\frac{k^2}{\Lambda^2}}, \tag{3.82}$$

where n is a nonnegative integer and C_n is a normalization constant. Using (3.80), the resulting cMERA fixed points are given by

$$\theta_n(k) = \frac{C_n}{2}\,\Gamma\left(n+\frac{1}{2}, \left(\frac{k}{\Lambda}\right)^2\right), \tag{3.83}$$

where $\Gamma(a,x)$ is the upper incomplete gamma function. We choose

$$C_n = \frac{\pi}{4}\frac{2}{\Gamma\left(n+\frac{1}{2}\right)} = \frac{2^{n-1}\sqrt{\pi}}{(2n-1)!!}, \tag{3.84}$$

so that $\theta(0) = \pi/4$, and using the properties of the incomplete gamma function, we obtain

$$\theta_n(k) = \frac{\pi}{4}\left(1 - \operatorname{erf}\left(\frac{k}{\Lambda}\right)\right) + \frac{\sqrt{\pi}}{4}e^{-k^2}\sum_{j=1}^{n}\frac{2^j k^{2j-1}}{(2j-1)!!} \tag{3.85}$$

We observe a similar interpolating character as the one found in the bosonic case. In what follows we will mostly focus on the simplest case $n = 0$ and drop the subindex.

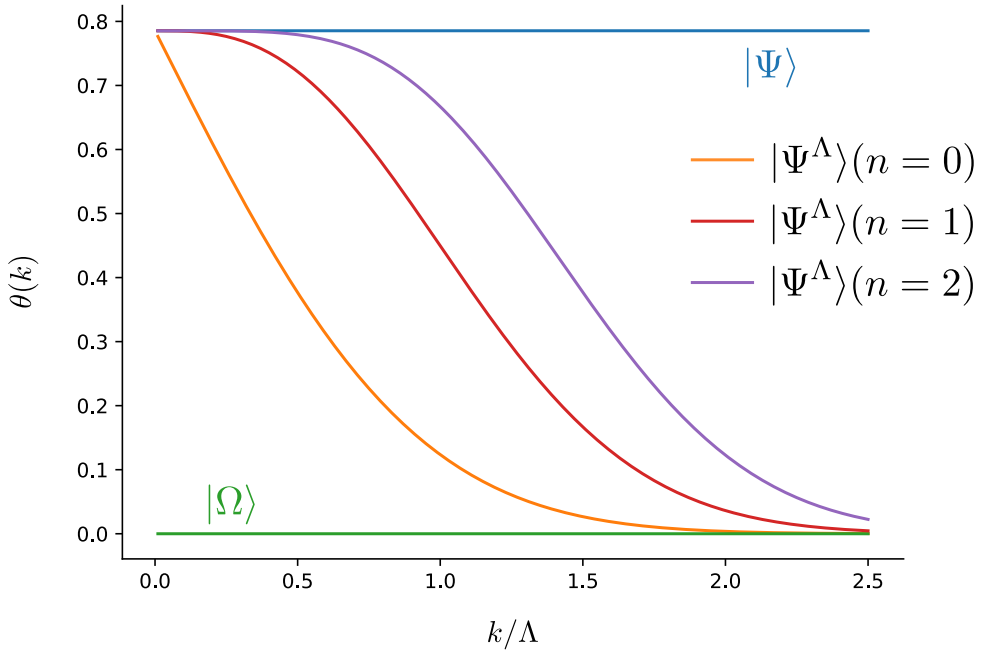

Figure 3.8: $\theta(k)$ function for the states $|\Psi\rangle$, $|\Omega\rangle$, and $\theta_n(k)$ function for $|\Psi^\Lambda\rangle$, for $n = 0, 1, 2$.

3.5.2 Entanglement structure of the cMERA state

We proceed as in the previous section: first we review the entanglement structure for the target and initial states, then we do the computation for the cMERA fixed points and compare the results. We will use the following representations of the Dirac matrices in 1+1d and 2+1d:

$$\gamma^0 \equiv \sigma_z, \qquad \gamma^1 \equiv i\sigma_y \qquad \text{(1+1 dimensions)}, \tag{3.86}$$

$$\gamma^0 \equiv \sigma_z, \qquad \gamma^1 \equiv -i\sigma_x, \qquad \gamma^2 \equiv -i\sigma_y \qquad \text{(2+1 dimensions)}, \tag{3.87}$$

which are written in terms of the Pauli matrices

$$\sigma_x = \begin{pmatrix} 0 & 1 \\ 1 & 0 \end{pmatrix}, \qquad \sigma_y = \begin{pmatrix} 0 & -i \\ i & 0 \end{pmatrix}, \qquad \sigma_z = \begin{pmatrix} 1 & 0 \\ 0 & -1 \end{pmatrix}. \tag{3.88}$$

With these representations, Eq. (3.67) reduces to

$$\left(\langle \psi_i^\dagger(k)\psi_j(q)\rangle\right) = \begin{pmatrix} \sin^2\theta(k) & -\frac{1}{2}\operatorname{sign} k \sin 2\theta(k) \\ \frac{1}{2}\operatorname{sign} k \sin 2\theta(k) & \cos^2\theta(k) \end{pmatrix} \delta(k-q) \tag{3.89}$$

in 1+1 dimensions, and

$$\left(\langle\psi_i^\dagger(\vec{k})\psi_j(\vec{q})\rangle\right) = \begin{pmatrix} \sin^2\theta(k) & -\frac{i}{2}e^{i\phi_{\vec{k}}}\sin 2\theta(k) \\ \frac{i}{2}e^{-i\phi_{\vec{k}}}\sin 2\theta(k) & \cos^2\theta(k) \end{pmatrix}\delta(\vec{k}-\vec{q}) \tag{3.90}$$

in 2+1 dimensions, where the phase $\phi_{\vec{k}}$ is defined by

$$|\vec{k}|e^{i\phi_{\vec{k}}} = k_x + ik_y. \tag{3.91}$$

In what follows, we will only pay attention to the $\langle\psi_1^\dagger(k)\psi_1(q)\rangle$ and $\langle\psi_1^\dagger(k)\psi_2(q)\rangle$ correlators, since the rest can be easily expressed in terms of them.

Target state $|\Psi\rangle$

In the CFT ground state, the two-point correlation functions are

$$\langle\psi_1^\dagger(\vec{x})\psi_1(\vec{y})\rangle = \frac{1}{2}\delta(\vec{x}-\vec{y}), \qquad \langle\psi_1^\dagger(x)\psi_2(y)\rangle = \frac{i}{2\pi}\frac{1}{x-y}, \tag{3.92}$$

in 1+1 dimensions, and

$$\langle\psi_1^\dagger(\vec{x})\psi_1(\vec{y})\rangle = \frac{1}{2}\delta(\vec{x}-\vec{y}), \qquad \langle\psi_1^\dagger(\vec{x})\psi_2(\vec{y})\rangle = \frac{i}{2\pi}\frac{e^{i\phi_{\vec{x}-\vec{y}}}}{|\vec{x}-\vec{y}|^2}, \tag{3.93}$$

in 2+1 dimensions. In both cases, the correlator between fermions of the same species is a delta function, while that between different species decays as a power-law, as befits a CFT.

The central charge of a single 1+1d free massless fermion is $c = \frac{1}{2}$. Because we have two species of fermions in the Dirac spinor, and central charge is additive, the total central charge of the theory is $c = 1$. Thus the entanglement entropy in the 1+1d theory scales logarithmically as

$$S(L) = \frac{1}{3}\log\frac{L}{a}. \tag{3.94}$$

In 2+1 dimensions, it follows an area law, scaling as the linear size x of the region

$$S(x) \sim \left(\frac{x}{a}\right). \tag{3.95}$$

In both cases we keep a to denote a UV cutoff.

Initial state $|\Omega\rangle$

The correlation functions for the initial unentangled state read:

$$\langle\psi_1^\dagger(\vec{x})\psi_1(\vec{y})\rangle = 0, \qquad \langle\psi_1^\dagger(x)\psi_2(y)\rangle = 0. \tag{3.96}$$

Indeed, the only non-vanishing two-point function is

$$\langle\psi_2^\dagger(\vec{x})\psi_2(\vec{y})\rangle = \delta(x-y) \tag{3.97}$$

The entanglement entropy in such a state once again vanishes.

cMERA fixed point $|\Psi^\Lambda\rangle$ (1+1 dimensions)

To obtain the cMERA state correlation functions, we just need to plug $\theta_n(k)$ from Eq. (3.85) into Eq. (3.89) and Fourier transform back numerically into position space. Their long-distance behaviour can be however directly inferred from their momentum space representation, as we did for the boson theories (see Appendix B.1).

The single-species correlator $\langle\psi_1^\dagger(x)\psi_1(y)\rangle$, will display a leading decay of $(x-y)^{-(2n+2)}$ at long distances. This is due to the first discontinuous derivative of the function $\sin^2(\theta_n(k))$ being the $(2n+1)$-th, which is discontinuous at the origin. This discontinuity was *not* present in the target state, and is the only example we present here, together with its 2-dimensional counterpart, of a cMERA qualitatively differing from the target state at long distances. The spurious power-law decay of this correlator, not present in the CFT, can be made faster by choosing a higher n, so that $\theta_n(k)$ coincides to higher and higher order with the exact $\theta(k)$ from the CFT in the $k \to 0$ (infrared) limit [56].

On the other hand, the dominant term in the asymptotic expansion of the two-species correlator $\langle\psi_1^\dagger(x)\psi_2(y)\rangle$ can be seen to decay like $(x-y)^{-1}$. This reflects the fact that the function $\mathrm{sign}(k)\sin(2\theta_n(k))$ is discontinuous at the origin, independently of the value of n. This matches the behaviour of the target CFT ground state (3.92). What does depend on n is the leading decay order of the difference between the CFT and cMERA correlators, which gets faster as n grows and $\theta_n(k)$ approximates the CFT $\theta(k)$ better in the infrared:

$$|\langle\psi_1^\dagger(x)\psi_2(y)\rangle_{\text{cMERA}} - \langle\psi_1^\dagger(x)\psi_2(y)\rangle_{\text{CFT}}| = \frac{(4j+2)!\pi}{16\Lambda^{4j+2}\Gamma\left(\frac{3}{2}+j\right)^2}|x-y|^{-(4j+3)} + \dots \tag{3.98}$$

Fig. 3.9 displays the numerically computed correlation functions. At short distances $x \ll 1/\Lambda$, the single-species correlator goes to a constant while the two-species correlator

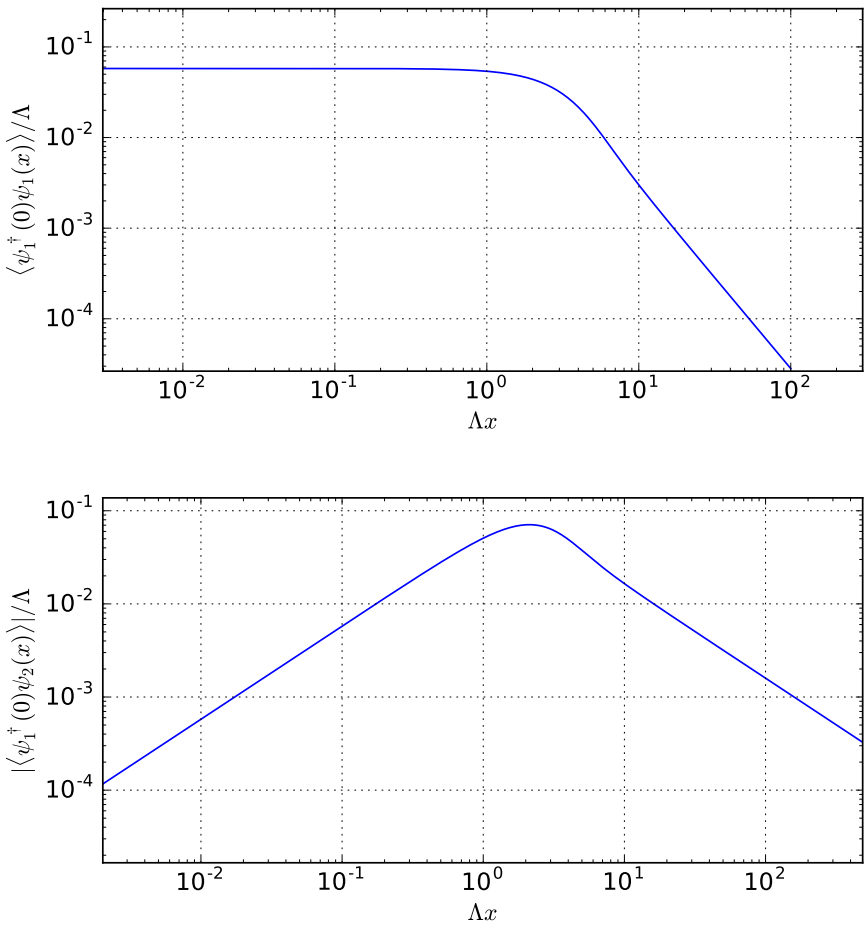

Figure 3.9: Correlation functions $\langle\psi_1^\dagger(0)\psi_1(x)\rangle$ (top) $\langle\psi_1^\dagger(0)\psi_2(x)\rangle$ (bottom, in absolute value) and computed for a cMERA defined by $\theta(k)$ as in (3.85) for $n = 0$. Notice the existence of two clearly different regimes delimited by $\Lambda x \sim 1$.

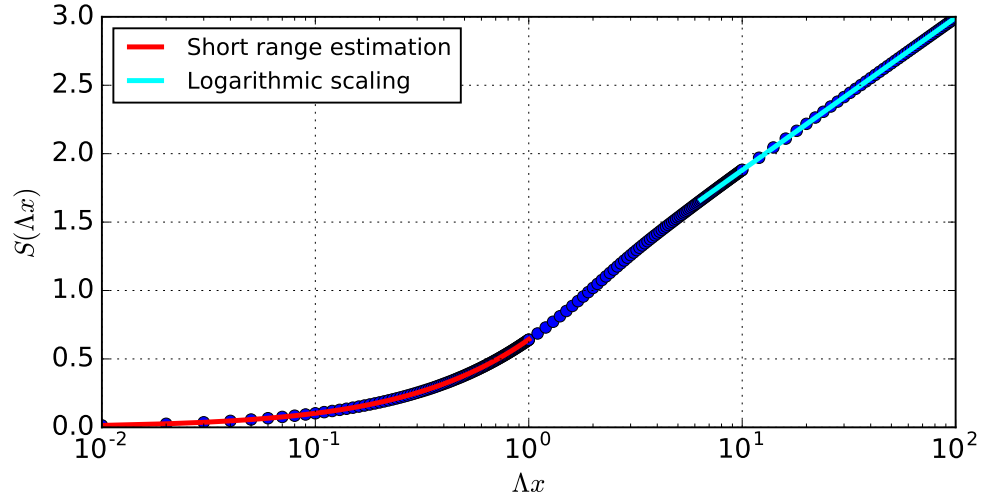

Figure 3.10: Entanglement entropy profile obtained for $\Lambda a = 0.01$ ($\Lambda x < 10$) and $\Lambda a = 0.1$ ($\Lambda x > 10$). We superpose the short distance estimation and the fit to logarithmic scaling at distances much larger than the cutoff, which provides a value of the central charge $c \approx 1.003$.

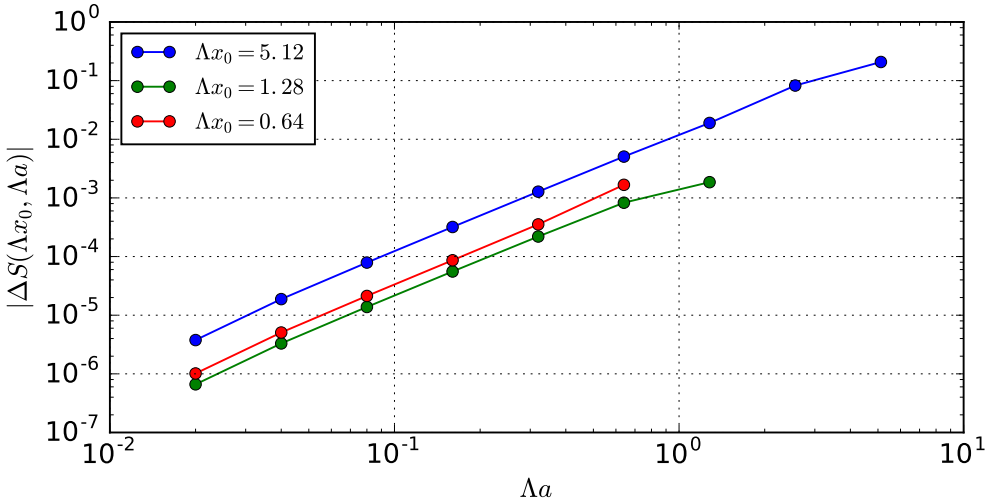

Figure 3.11: Plot of the difference $|S(\Lambda x_0, \Lambda a) - S(\Lambda x_0, \Lambda a = 0.01)|$ that shows the convergence of this particular value of entropy upon iterative fine-graining of the sampling parameter. The plotted difference goes to zero approximately quadratically with Λa.

vanishes as $(x-y)^p$, where the exponent is numerically estimated to be $p = 0.9992$ (the correlator vanishes linearly as $x - y \to 0$).

At large distances $x \gg 1/\Lambda$, both the single-species and two-species correlators exhibit power-law decay, with exponents numerically determined to be $p = -2.002$ and $p = -1.004$ respectively, confirming the previous asymptotic analysis.

As for the free boson, we perform the numerical computation of entanglement entropy in cMERA by sampling the correlators with a certain lattice spacing a, which produces discrete versions of the corresponding continuum correlation operators, to which we apply the usual prescription from Section 3.3. Once more we find finite values of the entropy to which our results converge when $a \to 0$, hinting at the removal of short scale entanglement, see Figure 3.11. Figure 3.10 shows the results of the numerical computation of entanglement entropy. As expected, two differentiated regimes are visible. For small intervals $x \ll 1/\Lambda$, the entanglement entropy $S(L)$ is seen to vanish as $L \to 0$, with the numerics matching an analytical estimation derived in Appendix B.3. For large intervals $a \gg 1/\Lambda$, the expected logarithmic scaling of $S(x)$ is recovered. The value obtained for the central charge from fitting the curve is very close to our expectation,

$$c \approx 1.003 \approx 1. \tag{3.99}$$

cMERA fixed point $|\Psi^\Lambda\rangle$ (2+1 dimensions)

The long distance decay properties of the two-point functions can once again be deduced from their momentum space representation (3.90) by means of the methods reviewed in Appendix B.1. For the single-species correlators, the cMERA again displays a spurious power-law decay $|\vec{x}-\vec{y}|^{-2n-3}$, which was not present in the CFT. This is a consequence of the behaviour of the function $\sin^2(\theta_n(\vec{k}))$ around $\vec{k} = 0$: it goes as $|\vec{k}|^{2n+1}$. In the case of the two-species correlator, however, we infer a leading decay given by $|\vec{x}-\vec{y}|^{-2}$, independently of n, which matches the CFT exponent. The next-to-leading term gives the leading order cMERA correction to the CFT correlator, and goes like:

$$|\langle\psi_1^\dagger(\vec{x})\psi_2(\vec{y})\rangle_{\text{cMERA}} - \langle\psi_1^\dagger(\vec{x})\psi_2(\vec{y})\rangle_{\text{CFT}}| \sim |x-y|^{-(4n+4)}. \tag{3.100}$$

Figure 3.12 shows how correlations behave for this cMERA, again for $n = 0$. The usual two regimes are observed: at distances smaller that $1/\Lambda$, the single-species correlator is practically constant, and the two-species correlator grows linearly (as a power law $|\vec{x}-\vec{y}|^p$

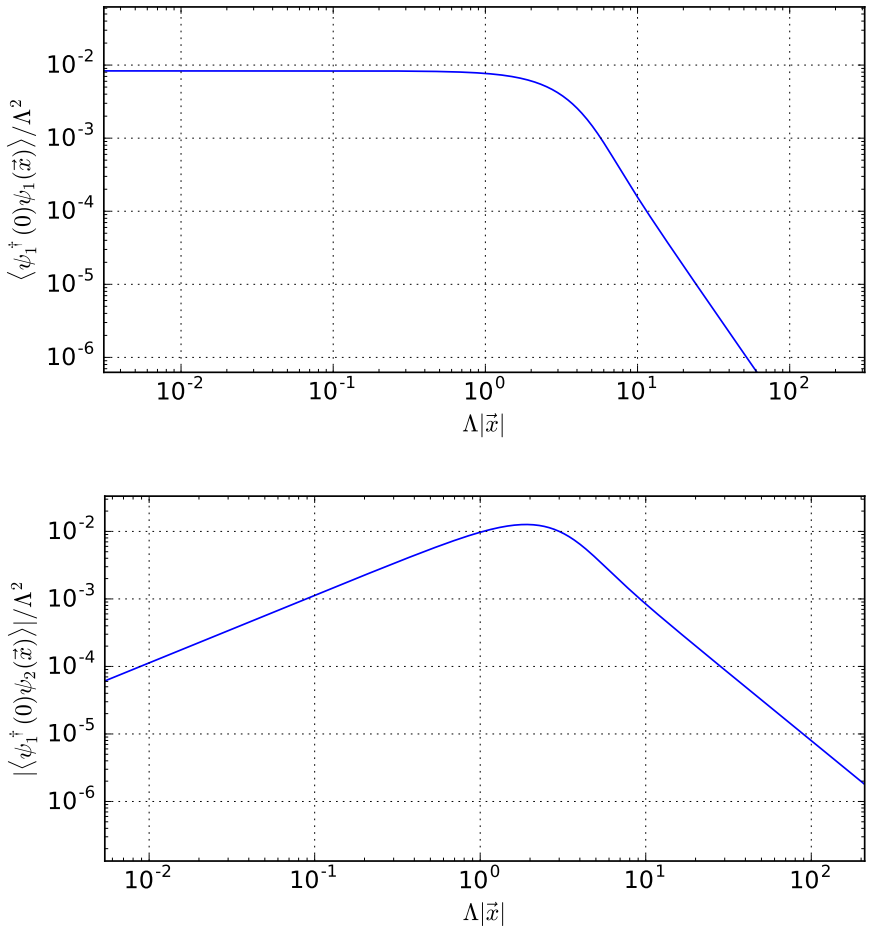

Figure 3.12: Correlation functions $\langle\psi_1^\dagger(0)\psi_1(\vec{x})\rangle$ (top) $\langle\psi_1^\dagger(0)\psi_2(\vec{x})\rangle$ (bottom, in absolute value) and computed for the 2+1 dimensional fermionic cMERA with $j = 0$.

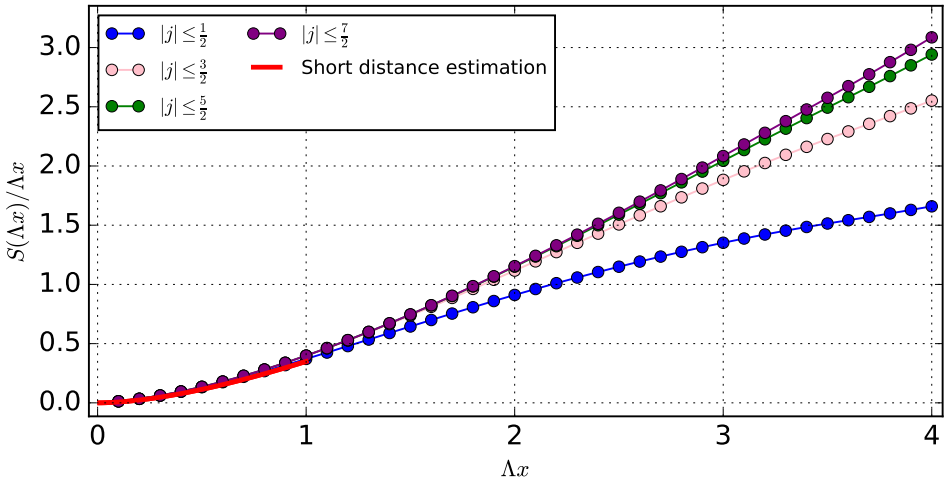

Figure 3.13: Entanglement entropy profile obtained for $\Lambda a = 0.01$ ($x < 4/\Lambda$). Convergence upon increase of the maximum value of $|j|$ is observed. We lack numerical data to comment on how reliably the long distance behaviour reproduces an area law.

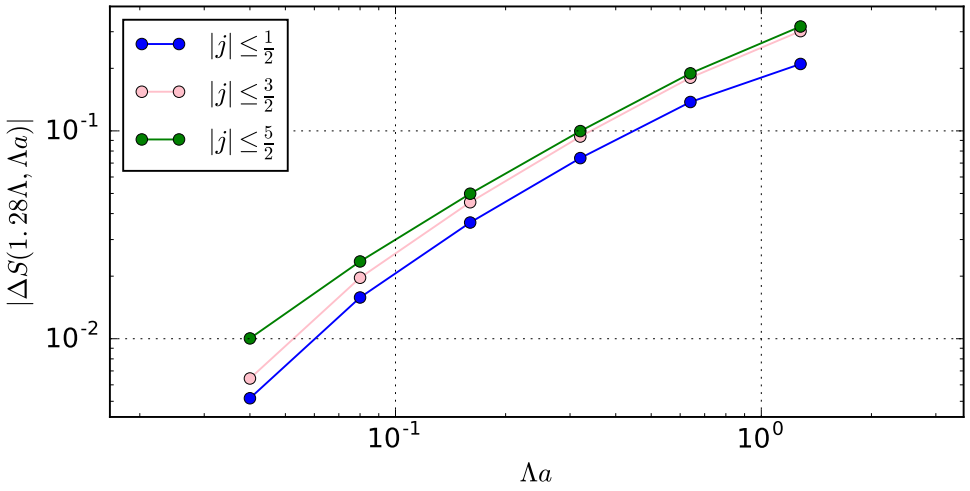

Figure 3.14: Plot of the difference $|S(1.28\Lambda, \Lambda a) - S(1.28\Lambda, \Lambda a = 0.02)|$, for different maximum values of $|j|$ that shows the convergence of this particular value of entropy upon iterative fine-graining of the sampling parameter a. Note how truncating at higher values of $|j|$ does not affect very noticeably the rate of convergence in a.

with $p \approx 0.9994 \approx 1$) with distance. Once the cutoff length scale is surpassed, the single-species correlator decays with exponent $p \approx -3.008 \approx -3$, while the two-species correlator decays with exponent $p \approx -2.005 \approx -2$, which is in accordance with the argumentation at the beginning of this paragraph.

As in the 2+1 dimensional bosonic case discussed earlier, we will study the scaling of entanglement entropy $S(x)$ by taking discs of increasing radii x and tracing out the rest of the system. We do so by again changing to polar coordinates and taking into account only the modes with small angular momentum, which provide the main contributions. The details of the computation are presented in Appendix B.2.

Figures 3.13 and 3.14 show that the main features we have been observing in this paper prevail in the 2d fermionic case: the entropy converges to a finite value upon fine-graining of the sampling of the correlators. However, the numerical computation becomes too heavy before we can assert with enough confidence the presence of two differentiated regimes, or the recovery of the area law (note that the onset of the area law in Figure 3.10 can only be clearly appreciated past $x \sim 3/\Lambda$, where we stop having converged data in the 2d case). Nevertheless, we can still give a good analytical estimation of the scaling of the entropy (see Appendix B.3) for small radii $x \ll 1/\Lambda$.

This chapter's takeaways:

- Scale invariant cMERA fixed point states can be interpreted as *UV regularized* versions of their target states: they *interpolate* between their target CFT ground state at long distances, and their initial unentangled state at short distances.
- More precisely, this property is reflected in the *correlation functions* and the scaling of *entanglement entropy* of these states: both display two different regimes, separated by the cutoff length scale Λ^{-1}, above which they reproduce CFT behaviour. The entanglement entropy computed via discretization converges to a finite value upon fine-graining.
- Finite s states of scale invariant cMERAs may be expected to behave as the corresponding fixed point and target states in the length scale window between the UV cutoff Λ^{-1} and the *effective IR cutoff* $\Lambda^{-1}e^s$, where the entangling evolution has introduced correlations.

Chapter 4

cMERA for gauge theories

This chapter's goal: In this chapter we explain how to generalize the cMERA framework to *gauge invariant* quantum fields, following the example of the free massless vector boson, a $U(1)$ gauge theory.

4.1 Introduction

Gauge theories stand among the most successful theories of physical reality, describing a wide range of phenomena – from the standard model of particle physics [67,68] and general relativity [69] to topological phases of quantum matter [70]. They are characterized by an explicit redundancy in the choice of degrees of freedom used to represent the physical system. This redundancy is the price to be paid in order to retain a more tractable and intuitive description, for instance one in terms of a local Hamiltonian. Gauge theories fit into the more general framework of *constrained theories*, whose quantization is itself a rich and interesting subject [71]. A quantum gauge theory can be formulated so that physical states are confined to a particular, *gauge invariant* subspace of the total Hilbert space of the theory.

To go beyond perturbative treatments of gauge theory, one must often resort to numerical simulations. In lattice gauge theory [72, 73], spacetime is discretized into a lattice in such a way that gauge invariance is preserved. Then stochastic methods, such as Monte Carlo sampling, are used to study certain aspects of the discretized theory. For instance, and most prominently, such techniques have been used to successfully extract the mass

spectrum of quantum chromodynamics (QCD) [74, 75]. In spite of their remarkable success, simulation strategies based on stochastic sampling suffer from the fermionic sign and complex action problems at finite fermionic density [76, 77] and, more generally, are not capable of simulating dynamics. For such important problems, alternative formulations are still much needed.

Much work has been devoted to applying tensor network algorithms to lattice gauge theories [78–129], with the expectation of advancing our numerical capabilities past the breaking points of standard techniques, such as the sign problem mentioned above in the case of Monte Carlo simulation (see [128, 129] for a recent review). Successful simulations in one spatial dimension [78–112] and partial success in two spatial dimensions [113–124] are certainly encouraging. However, very significant improvements will be required before e.g. QCD in three spatial dimensions can be meaningfully tackled. For lattice gauge theories in the Hamiltonian formalism, MERA has been seen to offer a proper framework to represent gauge invariant ground states [113,114]. In this case the renormalization group transformations exactly preserve the gauge constraints along the flow.

So far we have worked with cMERAs for scalar bosons and for fermions. In this chapter we take a step further and extend the cMERA formalism to gauge invariant quantum fields. Our main motivation is simple. If, as we expect, the cMERA program is to eventually give rise to a useful numerical simulation framework for interacting QFTs, then understanding how to handle gauge invariant quantum fields is a priority, given the central role gauge theories play in modern physics. A second motivation for our work comes from current applications of cMERA as a toy models for the AdS/CFT correspondence. There the CFT theory is often taken to be a gauge theory with a large gauge group. Therefore a gauge invariant cMERA could also be useful to build improved toy models of the AdS/CFT correspondence.

We will illustrate how the cMERA formalism can be extended to gauge theories by considering the simple case of noninteracting $U(1)$ gauge theory, or electromagnetism without matter fields, in $d+1$ spacetime dimensions as a proof-of-principle example. $U(1)$ gauge theory is ideal for our purposes, because the Hamiltonian is quadratic and this allows us to show, explicitly and exactly, how the *local* linear constraints in Hilbert space implementing gauge invariance can coexist with the *quasi-local* character of the *entangler* that generates the cMERA wavefunctional. Our eventual goal is to address interacting gauge theories, where the interaction may be due to either coupling to matter fields or to considering non-Abelian gauge groups (or to both at the same time). We expect that the compatibility between the quasi-local character of the cMERA and the local character of the gauge constraints, as demonstrated here for a non-interacting theory, will work in a similar way in the interacting case.

This chapter is organized as follows. We begin in Section 4.2 with a review of the target theories that will be of interest for us: the massless and massive free vector boson. As constrained theories, their quantization procedure involves a few choices that we will show and justify. Section 4.3 reviews the magic entanglement renormalization paradigm, from which we derive some inspiration for Section 4.4 where we present our proposal for a gauge invariant cMERA and analyze it in detail.

4.2 Massless and massive free vector boson theory

The field theories we deal with in this chapter are special in the sense that they involve constraints due to the Lagrangian not being regular. There are several nuances that should be taken into account when quantizing a constrained system, and in general there might not be a unique way of doing so: for instance, gauge theories, which provide a subclass of constrained theories, can be quantized with a variety of different gauge-fixing conditions. In what follows, we describe the general (Dirac) formalism for the quantization of constrained theories, and then apply it in turn to the massless and massive free vector boson theories. We will choose a quantization scheme that makes the massive and massless theories "compatible", in a sense that we will specify below.

4.2.1 Quantization of constrained theories

Given a family of position and velocity variables $\{q^i, \dot{q}^i = \partial_t q^i\}$, where i is an abstract index, a Lagrangian $\mathcal{L}(q^i, \dot{q}^i)$ is called *irregular* if the map that defines the canonical momenta p_i,

$$p_j = \frac{\partial \mathcal{L}(q^i, \dot{q}^i)}{\partial \dot{q}^j}, \tag{4.1}$$

is not invertible, in the sense that one cannot define an inverse map $(q^i, p_i) \mapsto (q^i, \dot{q}^i)$, because the positions q^i and momenta p_i are not independent variables: rather, they have to satisfy some dependency relations called *constraints*. These take the place of some of the equations of motion and specify a constrained submanifold of the phase space where the dynamics is allowed to take place. Gauge theories are a class of constrained theories. In fact the consequences of gauge symmetry are even more dramatic, since the underlying redundancy of degrees of freedom that gives rise to it is reflected in the appearance of arbitrary functions of time in the solutions of the equations of motion.

The following are the steps we will be following to quantize the vector boson theories, whose Lagrangians are irregular. For a more in-depth explanation of the quantization of constrained theories we refer the reader to a specialized textbook such as [71].

1. Given an irregular Lagrangian, find all the constraints to be imposed in the Hamiltonian formalism. This includes *primary* constraints (dependency relations between coordinates and momenta) and *secondary* constraints (constraints derived from demanding that other constraints are preserved by the time evolution generated by the Hamiltonian).

2. Once all constraints have been found, classify them as *first-class* (if they Poisson-commute with all other constraints) or *second-class* (if they don't).

3. First-class constraints generate gauge transformations. We choose if we want to add additional constraints in order to "fix the gauge" and turn them into second-class constraints.

4. We impose second-class constraints as operator equations in the algebra of operators (technically speaking, what we do is replacing Poisson brackets by Dirac brackets when defining the algebra of operators, but for all practical purposes we can think of this step as stated above).

5. Any remaining first-class constraints are imposed on the Hilbert space as gauge invariance conditions, so that only gauge invariant states are physical.

4.2.2 Free massless vector boson (U(1) gauge theory)

The free massless vector boson theory, which is used to describe electromagnetism, is a theory of a vector field $A_\mu(x)$ given by the Maxwell Lagrangian density

$$\mathcal{L} = -\frac{1}{4} F_{\mu\nu} F^{\mu\nu} \tag{4.2}$$

where

$$F_{\mu\nu} \equiv \partial_\mu A_\nu - \partial_\nu A_\mu \tag{4.3}$$

is the field strength tensor. Let us follow the steps above:

1. When we compute the conjugate momenta to the field components in the usual way

$$\Pi^0 \equiv \frac{\partial \mathcal{L}}{\partial(\partial_0 A_0)} = 0 \tag{4.4}$$

$$\Pi^i \equiv \frac{\partial \mathcal{L}}{\partial(\partial_0 A_i)} = -F^{0i} = \partial_0 A_i - \partial_i A_0 \tag{4.5}$$

we find a single primary constraint: $\Pi^0 = 0$. This constraint is now included in the Hamiltonian by means of a Lagrange multiplier u:

$$\mathcal{H} = \partial_0 A_\mu \Pi^\mu - \mathcal{L} + u\Pi^0 \tag{4.6}$$

$$= \frac{1}{2}\Pi_i \Pi^i + \frac{1}{4} F_{ij} F^{ij} - A_0 \partial_i \Pi^i + u\Pi^0 \tag{4.7}$$

We look for secondary constraints by imposing the preservation of the primary constraint under time evolution:

$$\partial_0 \Pi^0 = \{\Pi^0, \mathcal{H}\} = 0 \implies \partial_i \Pi^i = 0. \tag{4.8}$$

Thus we obtain a secondary constraint, that we identify as Gauss's law[1]. We look for additional secondary constraints and find that

$$\partial_0(\partial_i \Pi^i) = \{\partial_i \Pi^i, \mathcal{H}\} = 0 \tag{4.9}$$

holds without any additional assumptions. Thus we have found all the constraints.

2. The two constraints we obtained are first-class since their Poisson bracket vanishes:

$$\{\Pi^0(\vec{x}), \partial_i \Pi^i(\vec{y})\} = 0 \tag{4.10}$$

First-class constraints are a consequence of gauge invariance, which it is well-known that the Maxwell field exhibits.

[1]Indeed, when using this theory to describe electromagnetism, the components of the electric field are given in terms of the electromagnetic field strength tensor as

$$E^i = F^{0i} = -\Pi^i$$

thus the secondary constraint we found reads $\partial_i E^i = \vec{\nabla} \cdot \vec{E} = 0$, one of Maxwell's equations, also known as Gauss's law.

3. We now make the choice to quantize in the *temporal gauge*. We add the (partially) gauge-fixing constraint $A_0 = 0$ (temporal gauge), and check its consistency:

$$\dot{A}_0 = \{A_0, \mathcal{H}\} = \frac{\partial \mathcal{H}}{\partial \Pi^0} = u. \tag{4.11}$$

Hence we can impose the preservation of the gauge fixing just by a condition on the Lagrange multiplier. The new set of constraints includes a first-class constraint

$$\partial_i \Pi^i = 0 \tag{4.12}$$

and a pair of second-class constraints

$$A_0 = \Pi^0 = 0. \tag{4.13}$$

4. Upon quantization, the second pair of constraints can be imposed (à la Dirac) as operator equations: the operator representation of A_0 and Π^0 vanishes identically.

5. The remaining first-class constraint generates ("residual") gauge transformations:

$$A_i \longmapsto A_i + \partial_i \epsilon(x). \tag{4.14}$$

These transformations do not affect the physical degrees of freedom, and any two states that differ by one of them should be identified. Consequently, we define the physical Hilbert space as the subspace of the total Hilbert space whose elements are invariant under $\partial_i \Pi^i$:

$$\partial_i \Pi^i |\text{phys}\rangle = 0. \tag{4.15}$$

In conclusion, the relevant operator algebra is just the one generated by the *spatial* components of fields and momenta A_i, Π^i, with the usual canonical commutation relations:

$$[A_i(\vec{x}), \Pi^j(\vec{y})] = i\delta_{ij}\delta(\vec{x} - \vec{y}). \tag{4.16}$$

This algebra is represented on the Hilbert space of the theory, of which only the subspace given by (4.15) is physical.

In this setting we can now write down and diagonalize the Hamiltonian operator:

$$H_{\text{U(1)}} \equiv \frac{1}{2} \int d^d x \ \left[\Pi_i(\vec{x})\Pi^i(\vec{x}) - A^i(\vec{x}) \left(\delta_{ij}\Delta - \partial_i\partial_j\right) A^j(\vec{x})\right] \tag{4.17}$$

$$= \frac{1}{2} \int d^d k \ \left[\Pi_i(-\vec{k})\Pi^i(\vec{k}) + A^i(-\vec{k}) \left(\delta_{ij}k^2 - k_i k_j\right) A^j(\vec{k})\right], \tag{4.18}$$

where $k = |\vec{k}|$. H can be diagonalized by changing to a basis consistent of the *longitudinal* polarization

$$A_\parallel(\vec{k}) = \frac{k^i A_i(\vec{k})}{k}, \quad \Pi_\parallel(\vec{k}) = \frac{k^i \Pi_i(\vec{k})}{k} \tag{4.19}$$

and the $d-1$ orthogonal *transversal* polarizations[2]

$$A_{\perp,n}(\vec{k}), \quad \Pi_{\perp,n}(\vec{k}), \qquad n = 1, \ldots, d-1. \tag{4.20}$$

(Summation over any repeated index n for this basis will be implied throughout this chapter.) This basis is additionally helpful because the longitudinal polarization is precisely the gauge degree of freedom, while the transversal polarizations are the physical (gauge invariant) degrees of freedom, as can be seen by performing a gauge transformation:

$$A_j(\vec{x}) \to A_j(\vec{x}) + \partial_j \omega(\vec{x}) \implies \begin{cases} A_\parallel(\vec{k}) & \to \quad A_\parallel(\vec{k}) + ik\omega(\vec{k}), \\ A_{\perp,n}(\vec{k}) & \to \quad A_{\perp,n}(\vec{k}). \end{cases} \tag{4.21}$$

Consequently, the gauge constraint (4.15) becomes

$$\Pi_\parallel(\vec{k})|\text{phys}\rangle = 0. \tag{4.22}$$

The Hamiltonian $H_{\text{U}(1)}$ restricted to the gauge invariant subspace reads

$$H_{\text{U}(1)} = \int d^d k \ \left(\Pi_{\perp,n}(-\vec{k}) \Pi_{\perp,n}(\vec{k}) + k^2 A_{\perp,n}(-\vec{k}) A_{\perp,n}(\vec{k}) \right) \tag{4.23}$$

$$= \int d^d k \ k \ a^\dagger_{\perp,n}(\vec{k}) a_{\perp,n}(\vec{k}), \tag{4.24}$$

where

$$a_{\perp,n}(\vec{k}) \equiv \sqrt{\frac{k}{2}} A_{\perp,n}(\vec{k}) + i \sqrt{\frac{1}{2k}} \Pi_{\perp,n}(\vec{k}), \tag{4.25}$$

and we have removed an infinite constant term from the Hamiltonian in the usual way. What remains is nothing but the Hamiltonian for $d-1$ free bosons, whose ground state $|\Psi_{\text{U}(1)}\rangle$ is defined via the annihilation operators:

$$a_{\perp,n}(\vec{k})|\Psi_{\text{U}(1)}\rangle = 0 \qquad \forall \vec{k}, \ n = 1, \ldots, d-1. \tag{4.26}$$

[2]There is a subtlety here involving the fact that the zero mode subspace of the operator algebra, generated by $A_i(\vec{k}=0), \Pi_i(\vec{k}=0)$ cannot be separated in longitudinal and transversal sectors. Since this will however not be very relevant to the discussion, we will mostly ignore the zero modes in what follows.

Notice that both Eq. (4.26) and the gauge constraint (4.22) are constraints that are expressed in terms of operators that are linear in the field operators $A_i(\vec{x})$ and $\Pi_i(\vec{x})$. These constraints completely determine the ground state $|\Psi_{\mathrm{U}(1)}\rangle$, which is therefore a Gaussian state. For later reference, we parametrize the annihilation operators $a_\parallel(\vec{k})$ and $a_\perp(\vec{k})$ in terms of two functions $\alpha_\parallel(k), \alpha_{\perp,n}(k)$ in an analogous fashion to what we did in Section 3.4 on the previous chapter:

$$a_\parallel(\vec{k})|\Psi_{\mathrm{U}(1)}\rangle = 0, \qquad a_{\perp,n}(\vec{k})|\Psi_{\mathrm{U}(1)}\rangle = 0, \tag{4.27}$$

$$a_\parallel(\vec{k}) \equiv \sqrt{\frac{\alpha_\parallel(k)}{2}} A_\parallel(\vec{k}) + i\sqrt{\frac{1}{2\alpha_\parallel(k)}} \Pi_\parallel(\vec{k}), \tag{4.28}$$

$$a_{\perp,n}(\vec{k}) \equiv \sqrt{\frac{\alpha_\perp(k)}{2}} A_{\perp,n}(\vec{k}) + i\sqrt{\frac{1}{2\alpha_\perp(k)}} \Pi_{\perp,n}(\vec{k}). \tag{4.29}$$

We see that in order to recover (4.22) and (4.26) from the more general formulation (4.27)-(4.29), we just need to make the particular choice of functions $\alpha_\parallel(k), \alpha_\perp(k)$ given by

$$\alpha_\parallel(k) = 0, \qquad \alpha_\perp(k) = k \qquad \text{(massless ground state } |\Psi_{\mathrm{U}(1)}\rangle\text{)}. \tag{4.30}$$

Given the similarity in the description of the free massless scalar and free vector boson ground states, it may seem that a straightforward generalization of the cMERA for the former (thoroughly analyzed in Section 3.4) should give rise to a cMERA for the latter. This cMERA would keep $\alpha_\parallel(k) = 0$ during the whole evolution, which amounts to preserving gauge invariance, and would give rise to the same kind of interpolatory $\alpha_\perp(k, s)$ that we observed in the free scalar. However, early on this path we would run into trouble. As early as $s = 0$ in fact, for the annihilation operators defining the initial state $|\Omega\rangle$ would turn out not to be the limit of local lattice annihilation operators, leaving such initial state outside the formalism. It suffices to take a look at one of them, the gauge invariance constraint, to convince oneself, since it involves derivatives that should come from finite differences on a lattice[3]:

$$\sum_i \Big(\Pi^i(x + a\hat{i}) - \Pi^i(x)\Big)|\Omega\rangle = 0 \longrightarrow \partial_i \Pi^i(x)|\Omega\rangle = 0. \tag{4.31}$$

The same would generically happen for the other annihilation operators of $|\Omega\rangle$. In fact, the only state in the gauge invariant subspace that satisfies the conditions for a cMERA

[3]Usually in lattice gauge theory, gauge field variables are defined on the edges rather than the vertices of the lattice, as it may be naïvely assumed from this expression, but the finite difference argument still applies.

initial state is the zero electric field state, which is rather anomalous and hard to work with:

$$\Pi^i(x)|\Omega\rangle = 0 \qquad \forall i. \tag{4.32}$$

Fortunately for us, there exists an alternative cMERA construction, which we propose below in this chapter, that gives rise to a gauge invariant fixed point cMERA state. In this proposal, the entangling evolution happens outside the gauge invariant subspace. As a bonus, we will show that finite s cMERA states give good approximations to ground states of *massive* vector boson theories, which would not be possible in a fully gauge invariant cMERA. In preparation for that, we review these theories next.

4.2.3 Free massive vector boson

The massive vector boson theory is given by the Proca Lagrangian

$$\mathcal{L} = -\frac{1}{4}F_{\mu\nu}F^{\mu\nu} - \frac{1}{2}m^2 A_\mu A^\mu. \tag{4.33}$$

The nonvanishing mass term spoils gauge invariance[4], but this does not mean that the Lagrangian is regular, so we follow the same steps as in the massless theory.

1. When computing the conjugate momenta, we obtain the same primary constraint

$$\Pi^0 \equiv \frac{\partial \mathcal{L}}{\partial(\partial_0 A_0)} = 0, \tag{4.34}$$

which we include with a Lagrange multiplier u:

$$\begin{aligned}\mathcal{H} &= \dot{A}_\mu \Pi^\mu - \mathcal{L} + u\Pi^0 \\ &= \frac{1}{2}\Pi_i\Pi^i + \frac{1}{4}F_{ij}F^{ij} + \frac{1}{2}m^2 A_\mu A^\mu - A_0\partial_i\Pi^i + u\Pi^0.\end{aligned} \tag{4.35}$$

Looking for secondary constraints, we find

$$\partial_0\Pi^0 = 0 \implies m^2 A_0 + \partial_i\Pi^i = 0, \tag{4.36}$$

$$\partial_0(m^2 A_0 + \partial_i\Pi^i) = 0 \implies u = \partial_i A_i, \tag{4.37}$$

thus the theory presents two constraints.

[4]Massive vector bosons can arise in gauge invariant theories where we couple them to an additional scalar, the Higgs field. In the symmetry broken phase where the Higgs field acquires a vacuum expectation value, the non-interacting part of the Lagrangian for the vector boson can effectively look like (4.33). Names for this mechanism vary in inclusiveness, the most comprehensive one to our knowledge being "ABEGHHK'tH mechanism", for Anderson, Brout, Englert, Guralnik, Hagen, Higgs, Kibble, and 't Hooft.

2. The constraints are second-class (there is no gauge invariance), since their Poisson bracket does not vanish:

$$\{\Pi^0(\vec{x}), m^2 A_0(\vec{y}) + \partial_i \Pi^i(\vec{y})\} = -m^2 \delta(\vec{x} - \vec{y}). \tag{4.38}$$

3. There are no first-class constraints.

4. We impose the second-class constraints "à la Dirac" as operator equations, which effectively removes A_0, Π^0 as independent operators, and write canonical commutation relations for the rest of operators:

$$\Pi^0 = 0,\ A_0 = -\frac{\partial_i \Pi^i}{m^2}, \tag{4.39}$$

$$[A_i(\vec{x}), \Pi^j(\vec{y})] = \delta_{ij} \delta(\vec{x} - \vec{y}). \tag{4.40}$$

5. We do not need to impose any constraints on the Hilbert space.

Now the Hamiltonian of this theory reads,

$$H_m \equiv H_{\mathrm{U}(1)} + \frac{1}{2} \int d^d x \ \left[\frac{(\partial_i \Pi^i)^2}{m^2} + m^2 A_i(x) A^i(x) \right] \tag{4.41}$$

and can be diagonalized in the polarization basis (4.19)-(4.20) as in the massless case. The lack of a gauge invariance constraint now implies that the longitudinal component $A_\parallel(\vec{k})$, $\Pi_\parallel(\vec{k})$ is a legitimate propagating degree of freedom, instead of a gauge degree of freedom. The ground state of the theory is again of the form (4.27)-(4.29), this time with functions $\alpha_\parallel(k), \alpha_\perp(k)$ given by

$$\alpha_\parallel(k) = \frac{m^2}{\sqrt{k^2 + m^2}}, \qquad \alpha_\perp(k) = \sqrt{k^2 + m^2} \qquad \text{(massive ground state } |\Psi_m\rangle\text{)}. \tag{4.42}$$

Note that in the limit $m \to 0$, (4.42) reduces to (4.30).

When choosing the respective quantization schemes for the massless and massive theories, we have kept in mind that we are aiming to build a cMERA evolution that can give rise to approximations to the ground states of both. Our choices will make our task easier because

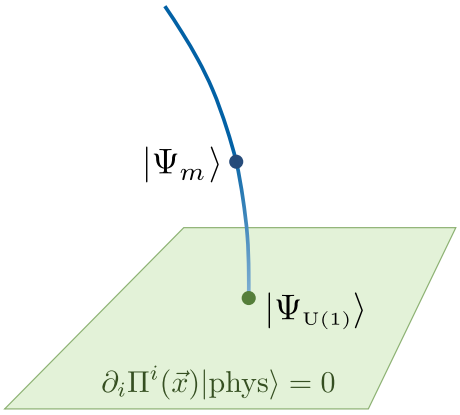

Figure 4.1: The ground state $|\Psi_m\rangle$ of the massive vector boson Hamiltonian H_m depends on the mass m and is not gauge invariant. However, in the limit $m \to 0$ we recover the massless vector boson Hamiltonian $H_{\mathrm{U}(1)}$, whose ground state $|\Psi_{U(1)}\rangle$ is gauge invariant. The green surface represents the gauge invariant subspace, or physical subspace, of the Hilbert space.

- The relevant operator algebras are identical: in both cases they are generated by A_i, Π_i, the spatial components of the field and their momenta, and they satisfy canonical commutation relations. This would not be the case had we chosen, for example, the Coulomb gauge quantization for the gauge theory, where the commutation relations of the operators are modified from the canonical case.

- The Hilbert spaces where these observable algebras are represented are also taken to be the same, with the caveat that for the massless case only a subspace of the total Hilbert space is physical, since the number of physical degrees of freedom is reduced by gauge invariance.

This will allow for a cMERA evolution to be defined consistently in a way that $|\Psi^\Lambda(s)\rangle$ is a massive vector boson state for finite s and a massless vector boson state for $s = \infty$. We said in Chapter 3 that finite s cMERA states do show an IR cutoff similar to the one induced by a mass. We also mentioned that this statement can be made in a more precise manner for the particular case of "magic" cMERAs, briefly introduced in 2.6. Since this will be helpful for us later in this chapter, the time has arrived to delve a bit deeper into the properties of these magic cMERAs, which we do in what follows.

4.3 Magic entanglement renormalization

Let us go back to the free scalar cMERA for this section. Remember that the variational parameters in cMERA correspond to different choices of the entangler K. Even if we restrict ourselves to quadratic entanglers, as we are allowed to do when addressing non-interacting theories, there is a lot of freedom in choosing an entangler K that gives rise to a good long distance approximation to a fixed target state. This begs the question of whether one may be able to use this freedom to identify particularly useful subclasses of entanglers.

The magic cMERA, which already came up shortly in Section 2.6, is a free boson cMERA in one spatial dimension, with a particular choice of the entangler that presents additional properties. Denote the relativistic free *massless* boson CFT ground state $|\Psi^{\text{CFT}}\rangle$. Consider as well more generally a relativistic free *massive* boson QFT, with Hamiltonian

$$H_m \equiv H^{\text{CFT}} + \frac{m^2}{2}\int dx\ \phi(x)^2, \tag{4.43}$$

and ground state $|\Psi_m\rangle$. For the sake of brevity, let us introduce the notation $\overset{\text{LD}}{\sim}$ to denote states that approximate each other at long distances, in the sense that we have been observing for cMERA. It was recently shown [58] that the choice of entangler profile

$$g(x,s) \equiv g(x) = \frac{\Lambda}{4}e^{-\Lambda|x|} \qquad \left(\implies g(k) = \frac{1}{2}\frac{\Lambda^2}{k^2+\Lambda^2}\right) \tag{4.44}$$

in the free boson cMERA introduced in Section 2.5 leads to cMERA wavefunctionals $|\Psi^\Lambda\rangle$ and $|\Psi^\Lambda(s)\rangle$ with

$$|\Psi^\Lambda\rangle \overset{\text{LD}}{\sim} |\Psi^{\text{CFT}}\rangle, \qquad |\Psi^\Lambda(s)\rangle \overset{\text{LD}}{\sim} |\Psi_{m(s)}\rangle, \tag{4.45}$$

where $|\Psi_{m(s)}\rangle$ is the relativistic massive ground state $|\Psi_m\rangle$ for mass

$$m(s) \equiv \Lambda e^{-s}. \tag{4.46}$$

The α function characterizing these states is given by

$$\alpha(k,s) = \Lambda\sqrt{\frac{k^2+\Lambda^2 e^{-2s}}{k^2+\Lambda^2}} \quad \xrightarrow{s\to\infty} \quad \alpha(k) = \Lambda\frac{|k|}{\sqrt{k^2+\Lambda^2}}. \tag{4.47}$$

Moreover, the magic cMERA wavefunctional has two remarkable properties:

(i) *Compatibility with cMPS:* $|\Psi^\Lambda(s)\rangle$ has the same UV structure as a *continuous matrix product state* (cMPS) [58]. As a result, cMPS techniques [36, 38, 130–140] can be used to numerically manipulate the cMERA wavefunctional efficiently. Most importantly, these cMPS techniques work equally well for both Gaussian and non-Gaussian wavefunctionals. Therefore they provide a much needed numerical avenue for producing strongly correlated (i.e. highly non-Gaussian) cMERA wavefunctionals for interacting QFTs, as demonstrated in Ref. [141].

(ii) *Exact ground state of local Hamiltonian:* The magic cMERA $|\Psi^\Lambda(s)\rangle$ is the exact ground state of a strictly local QFT Hamiltonian $H^\Lambda(s)$, see Eq. (4.50) below. This is unexpected. Indeed, it can be seen that a generic choice of quasi-local entangler produces a wavefunctional that is the ground state of a Hamiltonian which is, at best, quasi-local [58].

Let us elaborate a bit more on this last property, since it will play a role in our discussion of the $U(1)$ gauge invariant cMERA in the rest of the chapter. We introduce the local Hamiltonian

$$H^\Lambda \equiv H^{\text{CFT}} + A^\Lambda_{\text{UV}} \tag{4.48}$$

for the massless case, where

$$A^\Lambda_{\text{UV}} \equiv \frac{1}{2\Lambda^2}\int dx\ (\partial_x \pi(x))^2, \tag{4.49}$$

and the local Hamiltonian

$$H^\Lambda(s) \equiv H_{m(s)} + A^\Lambda_{\text{UV}}, \tag{4.50}$$

in the massive case, where $H_{m(s)}$ is the relativistic massive Hamiltonian H_m of Eq. (4.43) for mass $m(s)$ given by (4.46). Then Ref. [58] showed that $|\Psi^\Lambda\rangle$ is the exact ground state of H^Λ and $|\Psi^\Lambda(s)\rangle$ is the exact ground state of $H^\Lambda(s)$.

The parent Hamiltonian $H^\Lambda(s)$ is thus obtained from the relativistic massive $H_{m(s)}$ by adding the non-relativistic UV regulator A^Λ_{UV}, which breaks Lorentz invariance and primarily affects the UV physics by modifying the dispersion relation for momenta above the cutoff scale Λ. On the other hand, the mass term in $H^\Lambda(s)$ introduces a mass gap in the low energy spectrum. Thus, for $s > 0$, that is $m < \Lambda$, we can think of m and Λ in $H^\Lambda(s)$ as providing IR and UV regulators to the relativistic, massless Hamiltonian H^{CFT}, respectively.

In case the reader is wondering, the magic cMERA formalism also exists for the fermionic case. It will not be relevant for us in what follows, since we are working with bosonic degrees of freedom, but we have included a brief description for the interested reader in Appendix C.1.

4.4 Gauge invariant cMERA

We are now ready to present the main result of this chapter: a cMERA wavefunctional $|\Psi^{\Lambda}_{\mathrm{U}(1)}\rangle$ that approximates the ground state $|\Psi_{\mathrm{U}(1)}\rangle$ of Hamiltonian $H_{\mathrm{U}(1)}$ in Eq. (4.17) for the U(1) *gauge invariant*, *massless* free vector boson. Similarly to the ones studied in the previous chapter, this is a scale invariant cMERA: $|\Psi^{\Lambda}_{\mathrm{U}(1)}\rangle$ is the fixed point of an entangling evolution in scale generated by a constant entangler K starting from an unentangled state $|\Omega\rangle$. Our construction is an extension to gauge fields of the *magic* cMERA of Ref. [58]. It has the following three key properties:

(i) *Gauge invariance*: the wavefunctional $|\Psi^{\Lambda}_{\mathrm{U}(1)}\rangle$ is explicitly U(1) gauge invariant, that is, it fulfills the constraint (4.22);

(ii) *Correct large distance physics (I)*: the wavefunctional $|\Psi^{\Lambda}_{\mathrm{U}(1)}\rangle$ accurately approximates the behaviour (e.g. correlators, see Fig. 4.2) of the ground state $|\Psi_{\mathrm{U}(1)}\rangle$ of $H_{\mathrm{U}(1)}$ at distances $x \gg \Lambda^{-1}$, or

$$|\Psi^{\Lambda}_{\mathrm{U}(1)}\rangle \overset{\mathrm{LD}}{\sim} |\Psi_{\mathrm{U}(1)}\rangle; \tag{4.51}$$

(iii) *Ground state of a local Hamiltonian (I)*: the cMERA $|\Psi^{\Lambda}\rangle$ is the exact ground state of a Hamiltonian $H^{\Lambda}_{\mathrm{U}(1)}$, see Eq. (4.85) below, that is *local* and can be understood as a UV regulated version of $H_{\mathrm{U}(1)}$.

Moreover, and justifying all our previous foreshadowing in this chapter, the intermediate cMERA wavefunctional $|\Psi^{\Lambda}(s)\rangle$ for any finite $s \in [0, \infty)$ is related to the massive vector boson in the following ways:

(iv) *Correct large distance physics (II)*: the wavefunctional $|\Psi^{\Lambda}(s)\rangle$ accurately approximates the behaviour (e.g. correlators, see Fig. 4.2) of the ground state $|\Psi_{m(s)}\rangle$ of the relativistic massive vector boson Hamiltonian $H_{m(s)}$ in Eq. (4.41) for mass $m(s) = \Lambda e^{-s}$, that is

$$|\Psi^{\Lambda}(s)\rangle \overset{\mathrm{LD}}{\sim} |\Psi_{m(s)}\rangle. \tag{4.52}$$

(v) *Ground state of a local Hamiltonian (II)*: the cMERA $|\Psi^{\Lambda}(s)\rangle$ is the exact ground state of a Hamiltonian $H^{\Lambda}(s)$, see Eq. (4.82) below, that is *local* and can be understood as a UV regulated version of $H_{m(s)}$ for mass $m(s) = \Lambda e^{-s}$.

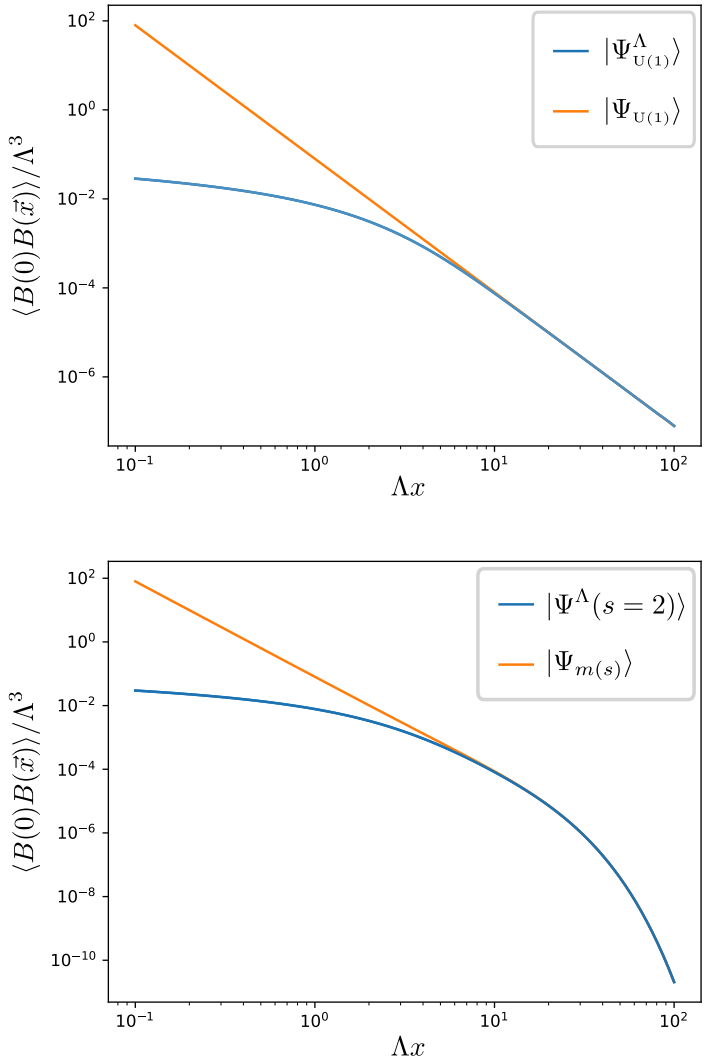

Figure 4.2: Correlator $\langle B(0)B(\vec{x})\rangle$ as a function of $x \equiv |\vec{x}|$ in 2+1 dimensions, where $B \equiv \partial_1 A_2 - \partial_2 A_1$, for both a target state and the corresponding cMERA approximation, which matches the correlator of its target state for $\Lambda x \gg 1$. (top) Gauge invariant target state $|\Psi_{\mathrm{U}(1)}\rangle$ and the corresponding cMERA $|\Psi^{\Lambda}_{\mathrm{U}(1)}\rangle$. The cMERA correlator has a distributional contribution $\frac{1}{2\Lambda}\left(\Delta + \frac{\Lambda^2}{2}\right)\delta(\vec{x})$ localized at the origin, not visible in the figure. (bottom) Massive target state $|\Psi_{m(s)}\rangle$ for $m(s) = \Lambda e^{-s}$ and the corresponding cMERA $|\Psi^{\Lambda}(s)\rangle$. The cMERA correlator has a distributional contribution $\frac{1}{2\Lambda}\left(\Delta + \frac{\Lambda^2 - m(s)^2}{2}\right)\delta(\vec{x})$ localized at the origin, not visible in the figure.

We emphasize that in our construction, for any finite s (finite mass $m(s)$) the cMERA wavefunctional $|\Psi^\Lambda(s)\rangle$ is not gauge invariant, and gauge invariance is only attained in the large s limit. That is, the entangling evolution in scale takes place outside the gauge invariant subspace of the Hilbert space. However, as shown in Fig. 4.4, an approximation to $|\Psi^\Lambda\rangle$ (e.g. in terms of correlators) can already be obtained from $|\Psi^\Lambda(s)\rangle$ at finite $s \gg 1$, since the IR cutoff above which the two states differ significantly is $m(s)^{-1} = \Lambda^{-1}e^s$. Notice that this situation closely mimics the relativistic gauge invariant vector boson we are targeting: at finite mass m, the theory is not gauge invariant, and gauge invariance is only attained in the massless limit $m \to 0$. Fig. 4.3 summarizes diagramatically the relations between cMERA states and the ground states they target.

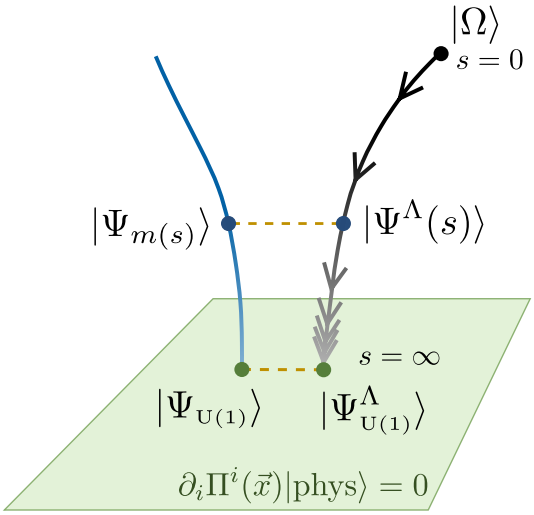

Figure 4.3: The massive vector boson ground state $|\Psi_{m(s)}\rangle$ for $m(s) = \Lambda e^{-s}$ is approximated by the cMERA state $|\Psi^\Lambda(s)\rangle$. None of these wavefunctionals are gauge invariant. The massless vector boson ground state $|\Psi_{\mathrm{U}(1)}\rangle$ is approximated by the scale-invariant cMERA state $|\Psi^\Lambda_{\mathrm{U}(1)}\rangle$. These two wavefunctionals are gauge invariant.

4.4.1 Definition

Let us begin by defining our gauge invariant cMERA, for which we will have to specify the initial unentangled state $|\Omega\rangle$ and the generators of the entangling evolution L and K. Because our target theories are noninteracting, our proposal is once more a Gaussian cMERA. We will thus be able to rely on the formalism of Gaussian states laid out in the previous chapter: states will be characterized by their annihilation operators, which

are themselves parametrized by two momentum-space functions $\alpha_\parallel(k), \alpha_\perp(k)$ as in Eqs. (4.27)-(4.29); and K will be quadratic in the field modes, so as to preserve the manifold of Gaussian states.

Unentangled state $|\Omega\rangle$

We begin by defining annihilation operators

$$\psi_i(\vec{x}) \equiv \sqrt{\frac{\Lambda}{2}} A_i(\vec{x}) + i\sqrt{\frac{1}{2\Lambda}} \Pi_i(\vec{x}). \tag{4.53}$$

We then consider the unentangled state $|\Omega\rangle$ given by

$$\psi_i(\vec{x})|\Omega\rangle = 0, \quad i = 1, \ldots, d. \tag{4.54}$$

This will be the starting point of our entangling evolution. For later convenience, we write (4.54) in the basis of polarizations in momentum space:

$$\psi_\parallel(\vec{k})|\Omega\rangle = 0, \tag{4.55}$$

$$\psi_{\perp,n}(\vec{k})|\Omega\rangle = 0, \quad n = 1, \ldots, d-1, \tag{4.56}$$

where we have defined

$$\psi_\parallel(\vec{k}) \equiv \sqrt{\frac{\Lambda}{2}} A_\parallel(\vec{k}) + i\sqrt{\frac{1}{2\Lambda}} \Pi_\parallel(\vec{k}), \tag{4.57}$$

$$\psi_{\perp,n}(\vec{k}) \equiv \sqrt{\frac{\Lambda}{2}} A_{\perp,n}(\vec{k}) + i\sqrt{\frac{1}{2\Lambda}} \Pi_{\perp,n}(\vec{k}), \qquad n = 1, \cdots, d-1. \tag{4.58}$$

This initial state $|\Omega\rangle$ is clearly of the Gaussian form (4.27)-(4.29), with both functions $\alpha_\parallel(k), \alpha_\perp(k)$ set to a constant:

$$\alpha_\parallel(k) = \Lambda, \qquad \alpha_\perp(k) = \Lambda \qquad \text{(initial unentangled state } |\Omega\rangle\text{)}. \tag{4.59}$$

Entangling evolution in scale

Our next step is to define the generator of scale transformations as

$$L \equiv \frac{1}{2} \int d^d\vec{x}\, \Pi_i(\vec{x}) \left(-\vec{x} \cdot \vec{\nabla} - \frac{d}{2} \right) A^i(\vec{y}) + \text{h.c.} \tag{4.60}$$

$$= \int d^d\vec{k}\, \Pi_i(-\vec{k}) \left(\vec{k} \cdot \vec{\nabla}_{\vec{k}} + \frac{d}{2} \right) A^i(\vec{k}) + \text{h.c.}, \tag{4.61}$$

which assigns non-relativistic scaling dimensions $\Delta_{A_i} = d/2$ and $\Delta_{\Pi_i} = d/2$ to the fields, and consider an entangler of the form

$$K = \frac{-i}{2}\int d^d\vec{x}\; g^{ij}(\vec{x}-\vec{y})\;\psi_i(\vec{x})\psi_j(\vec{y}) + \text{h.c.} \tag{4.62}$$

$$= \frac{-i}{2}\int d^d\vec{k}\; g^{ij}(\vec{k})\;\psi_i(-\vec{k})\psi_j(\vec{k}) + \text{h.c.} \tag{4.63}$$

which is the natural generalization to vector bosons of the scalar boson entangler (2.12). We choose a rotation covariant form for the profile $g^{ij}(\vec{k}) = g(k)\delta^{ij} + f(k)k^ik^j$, and rewrite

$$K = \frac{-i}{2}\int d^d\vec{k}\;\left[g_\parallel(k)\;\psi_\parallel(-\vec{k})\psi_\parallel(\vec{k}) + g_\perp(k)\;\psi_{\perp,n}(-\vec{k})\psi_{\perp,n}(\vec{k})\right] + \text{h.c.} \tag{4.64}$$

where we have defined

$$g_\perp(k) \equiv g(k), \qquad g_\parallel(k) \equiv g(k) + k^2 f(k). \tag{4.65}$$

In our case, we choose

$$g_\parallel(k) = 1 - \frac{1}{2}\frac{\Lambda^2}{\Lambda^2+k^2}, \qquad g_\perp(k) = \frac{1}{2}\frac{\Lambda^2}{\Lambda^2+k^2}. \tag{4.66}$$

To have a picture of what these profiles look like in position space, notice that by inverse Fourier transforming we obtain

$$\mathcal{F}^{-1}\left[\frac{1}{\Lambda^2+k^2}\right](x) \propto \frac{K_{\frac{d-2}{2}}(\Lambda x)}{(\Lambda x)^{\frac{d-2}{2}}}, \tag{4.67}$$

where $x = |\vec{x}|$ and K_n is the n-th modified Bessel function of the second kind. This implies that the position space profile of the entangler decays exponentially at large distances, and for $d > 1$ it diverges at the origin. In particular, in 1+1 spacetime dimensions, $g_\perp(x)$ is the same profile as that in Eq. (4.44).

Having made our choices for $|\Omega\rangle$, L and K, the family of ansatz states $|\Psi^\Lambda(s)\rangle$ is defined by the cMERA evolution. The procedure here will be entirely familiar to the reader since it is the same as in Chapter 3: since K is a quadratic operator in the fields, and we start from a Gaussian state $|\Omega\rangle$, the whole evolution takes place in the manifold of Gaussian states, and each $|\Psi^\Lambda(s)\rangle$ is of the form (4.27)-(4.29), i.e., it is given by a set of scale-dependent annihilation operators

$$a^\Lambda_\parallel(\vec{k},s)|\Psi^\Lambda(s)\rangle = 0, \quad \forall\vec{k}\in\mathbb{R}^d, \tag{4.68}$$

$$a^\Lambda_{\perp,n}(\vec{k},s)|\Psi^\Lambda(s)\rangle = 0, \quad \forall\vec{k}\in\mathbb{R}^d, \quad n = 1,\cdots,d-1, \tag{4.69}$$

that are characterized by a pair of scale-dependent functions $\alpha_{\parallel}(k,s)$, $\alpha_{\perp}(k,s)$,

$$a^{\Lambda}_{\parallel}(\vec{k},s) = \sqrt{\frac{\alpha_{\parallel}(k,s)}{2}} A_{\parallel}(\vec{k}) + i\sqrt{\frac{1}{2\alpha_{\parallel}(k,s)}}\Pi_{\parallel}(\vec{k}), \tag{4.70}$$

$$a^{\Lambda}_{\perp,n}(\vec{k},s) = \sqrt{\frac{\alpha_{\perp}(k,s)}{2}} A_{\perp,n}(\vec{k}) + i\sqrt{\frac{1}{2\alpha_{\perp}(k,s)}}\Pi_{\perp,n}(\vec{k}). \tag{4.71}$$

We can then solve for $\alpha_{\parallel}(k,s)$ and $\alpha_{\perp}(k,s)$ in terms of $g_{\parallel}(k,s)$ and $g_{\perp}(k,s)$:

$$\alpha_{\parallel}(k,s) = \Lambda \exp\left(-2\int_0^s du\; g_{\parallel}(ke^{s-u})\right), \tag{4.72}$$

$$\alpha_{\perp}(k,s) = \Lambda \exp\left(-2\int_0^s du\; g_{\perp}(ke^{s-u})\right). \tag{4.73}$$

For our particular choice of entangler given by Eq (4.66), we have

$$\alpha_{\parallel}(k,s) = \frac{m(s)^2}{\Lambda}\sqrt{\frac{k^2+\Lambda^2}{k^2+m(s)^2}}, \tag{4.74}$$

$$\alpha_{\perp}(k,s) = \Lambda\sqrt{\frac{k^2+m(s)^2}{k^2+\Lambda^2}}, \qquad \text{(cMERA state } |\Psi^{\Lambda}(s)\rangle\text{)}, \tag{4.75}$$

where $m(s) = \Lambda e^{-s}$. Since for the transversal modes of the vector boson we used the same entangler as the one for a scalar boson in Ref. [58], $\alpha_{\perp}(k,s)$ is the same function from Eq. (4.47).

4.4.2 Properties

Now that we have characterized our cMERA states, we proceed to check on the properties (i)-(v) we claimed at the beginning of this section.

(i): Fixed-point wavefunctional and gauge invariance

In the limit $s \to \infty$, the constraint from Eq. (4.68) becomes the gauge invariance condition (4.22), so that the fixed-point state $|\Psi^{\Lambda}_{\mathrm{U}(1)}\rangle$ belongs to the gauge invariant subspace. It is

fully characterized (up to a global phase) by the gauge constraint and the $s \to \infty$ limit of the annihilation operators of the transversal modes:

$$\Pi_{\parallel}(\vec{k})|\Psi^{\Lambda}\rangle = 0, \tag{4.76}$$

$$a^{\Lambda}_{\perp,n}(\vec{k},\infty)|\Psi^{\Lambda}\rangle = 0. \tag{4.77}$$

The state defined by the conditions (4.76)-(4.77) is a fixed point of the evolution generated by $L+K$. This can be shown in the same way as it was shown in Chapter 3 for the scalar boson. There is an important subtlety here regarding the $s \to \infty$ limit, due to the fact that the theories for $s < \infty$ and $s = \infty$ are fundamentally distinct. We elaborate on this in Appendix C.2.

(ii) and (iv): Comparing Gaussian wavefunctionals

The fact that all states involved in this discussion are Gaussian, of the form (4.27)-(4.29), facilitates comparison among them, since it can be conducted at the level of α functions. Recall from Chapter 3 that annihilation operators for noninteracting cMERA states interpolate between those of the target state at small momenta $k \ll \Lambda$ and those of the unentangled initial state at large momenta $k \gg \Lambda$. As we then checked numerically, this leads to correlation functions with the corresponding interpolating behaviours. Indeed, the two-point functions of $|\Psi^{\Lambda}(s)\rangle$, which for Gaussian states encode all the other correlators, are related to $\alpha_{\parallel}(k,s)$ and $\alpha_{\perp}(k,s)$ by the analogue of Eq. (3.22):

$$\langle A_{\parallel}(\vec{k})A_{\parallel}(\vec{q})\rangle = \frac{1}{2}\frac{\delta(\vec{k}+\vec{q})}{\alpha_{\parallel}(\vec{k},s)}, \qquad \langle A_{\perp,n}(\vec{k})A_{\perp,n}(\vec{q})\rangle = \frac{1}{2}\frac{\delta(\vec{k}+\vec{q})}{\alpha_{\perp}(\vec{k},s)}, \tag{4.78}$$

$$\langle \Pi_{\parallel}(\vec{k})\Pi_{\parallel}(\vec{q})\rangle = \frac{\alpha_{\parallel}(\vec{k},s)}{2}\delta(\vec{k}+\vec{q}), \qquad \langle \Pi_{\perp,n}(\vec{k})\Pi_{\perp,n}(\vec{q})\rangle = \frac{\alpha_{\perp}(\vec{k},s)}{2}\delta(\vec{k}+\vec{q}). \tag{4.79}$$

In the particular case of our current proposal, it follows from Eqs. (4.74)-(4.75) that

$$\alpha_{\parallel}(k,s) \sim \begin{cases} \dfrac{m(s)^2}{\sqrt{k^2+m(s)^2}} & k \ll \Lambda, \\ \dfrac{m(s)^2}{\Lambda} & k \gg \Lambda, \end{cases} \qquad \alpha_{\perp}(k,s) \sim \begin{cases} \sqrt{k^2+m(s)^2} & k \ll \Lambda, \\ \Lambda & k \gg \Lambda. \end{cases} \tag{4.80}$$

We see that for $k \ll \Lambda$ these functions reproduce the target state's behaviour from Eq. (4.42), while for $k \gg \Lambda$ they become constant, which is the behaviour seen for the unentangled initial state $|\Lambda\rangle$, as in Eq. (4.59) (notice the longitudinal case is special since the

constant is rescaled along the evolution from Λ at $s = 0$ to 0 at $s = \infty$). This leads to the correlation functions having the same IR behaviour for our cMERA states and their target states, as was already shown in Fig. 4.2. Notice that this also implies that correlation functions of finite s states $|\Psi^\Lambda(s)\rangle$ will behave as the correlation functions of the fixed point $|\Psi^\Lambda(s)\rangle$ at length scales smaller than their corresponding IR cutoff $m(s)^{-1}$, and as a consequence they will show convergence to the latter as $s \to \infty$, since in that limit the IR cutoff is lifted. Fig. 4.4 shows the correlator $\langle B(0)B(\vec{x})\rangle$ for $|\Psi^\Lambda(s)\rangle$ in 2+1 dimensions as a function of s. We see that the correlators for large s converge[5] to those of the fixed point wavefunctional $|\Psi^\Lambda_{\mathrm{U}(1)}\rangle$. Thus, we can learn about the properties of the gauge invariant $|\Psi^\Lambda_{\mathrm{U}(1)}\rangle$ by studying the non-gauge invariant $|\Psi^\Lambda(s)\rangle$ at finite but large s. This feature, which is a straight consequence of the fact that the entangling evolution of cMERA introduces correlations scale by scale, could be exploited in the setting of numerical implementations, where running an evolution for an infinite amount of time would be impossible, but where the result of a finite evolution would contain physical information below a certain correlation length.

(iii) and (v): Local Hamiltonians with relativistic IR physics

In order to prove statements (iii) and (v) from the beginning of this section, consider the following family of Hamiltonians:

$$H^\Lambda(s) \equiv H_{m(s)} + B^\Lambda_{\mathrm{UV}}(s) \tag{4.82}$$

where $H_{m(s)}$ is the massive Hamiltonian from (4.41) with $m(s) = \Lambda e^{-s}$ and

$$B^\Lambda_{\mathrm{UV}}(s) \equiv \frac{1}{\Lambda^2}\int d^dx\ \Pi^i(\delta_{ij}\Delta - \partial_i\partial_j)\Pi^j + \frac{m(s)^2}{\Lambda^2}\int d^dx\ (\partial_i A^i)^2. \tag{4.83}$$

For every $s \in [0,\infty]$, $H^\Lambda(s)$ is quadratic and can hence be easily diagonalized. We then find that $|\Psi^\Lambda(s)\rangle$ is the ground state of $H^\Lambda(s)$. The term $B^\Lambda_{\mathrm{UV}}(s)$ in (4.82) can be seen as a UV regulator for $H_{m(s)}$. Notice that the first term in (4.83) involves the transversal degrees of freedom, while the second term involves the longitudinal one:

$$B^\Lambda_{\mathrm{UV}}(s) = \frac{1}{\Lambda^2}\int d^dk\ k^2\,\Pi_{\perp,n}(-\vec{k})\Pi_{\perp,n}(\vec{k}) + \frac{m(s)^2}{\Lambda^2}\int d^dk\ k^2 A_\parallel(-\vec{k})A_\parallel(\vec{k}). \tag{4.84}$$

[5]The distributional terms at the origin, which are not shown in Figure 4.4, also converge in s:

$$\frac{1}{2\Lambda}\left(\Delta + \frac{\Lambda^2 - m(s)^2}{2}\right)\delta(\vec{x}) \xrightarrow{s\to\infty} \frac{1}{2\Lambda}\left(\Delta + \frac{\Lambda^2}{2}\right)\delta(\vec{x}). \tag{4.81}$$

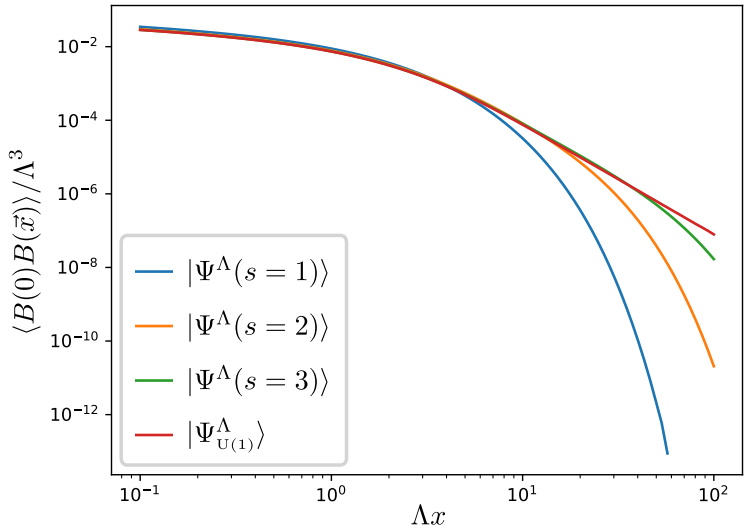

Figure 4.4: Two-point correlator $\langle B(0)B(\vec{x})\rangle$ for state $|\Psi^\Lambda(s)\rangle$ for $s = 1, 2, 3$ and for the fixed point wavefunctional $|\Psi^\Lambda_{\mathrm{U}(1)}\rangle$ in 2+1 dimensions (see also Fig. 4.2). Distributional delta-like terms at the origin are not shown.

The UV regulator term for the transversal modes is once again equivalent to the one found in [58]. In the limit $s \to \infty$, the longitudinal degree of freedom is restricted by the gauge constraint, and $|\Psi^\Lambda_{\mathrm{U}(1)}\rangle$ can be given a rather compact parent Hamiltonian:

$$H^\Lambda_{\mathrm{U}(1)} \equiv H_{\mathrm{U}(1)} + \frac{1}{\Lambda^2}\int d^dx\ \Pi_i(x)\Delta\Pi^i(x). \tag{4.85}$$

with $H_{\mathrm{U}(1)}$ the Maxwell Hamiltonian from (4.17).

This concludes the list of properties of the gauge invariant cMERA that we introduced in this chapter. The reader should be aware, that, much as in the case of all noninteracting cMERAs, its merit does not come from its ability to approximate its completely solvable target theory, but rather as a source of theoretical insight. How much of this example can be imported without modification to the interacting case is an open question as of now, but it can be expected that the kind of compatibility between local gauge constraints and quasi-local entangling evolution that we have seen here will be replicated also in more complicated examples. This construction also gives a step further in the direction of building cMERAs whose intermediate states can be directly applied to approximating theories resulting from the fixed point target theory by a relevant perturbation (in this case, a mass).

So far, we have focused on the long distance behaviour of the cMERA states, without

saying much about what happens at distances below the UV cutoff Λ^{-1}. We conclude this chapter by studying the UV structure of the proposed gauge invariant cMERA in more detail.

4.4.3 UV regularization of correlation functions

In Chapter 3 the existence of the short distance limit of two-point functions of cMERA states was used as a witness for UV regularization. These correlation functions usually take the following form in cMERA states:

$$\langle \mathcal{O}(\vec{x})\mathcal{O}(\vec{y})\rangle = C\delta(\vec{x}-\vec{y}) + f(|\vec{x}-\vec{y}|), \tag{4.86}$$

with C a constant and f some function such that

$$\lim_{\vec{x}\to\vec{y}} \langle \mathcal{O}(\vec{x})\mathcal{O}(\vec{y})\rangle < \infty, \tag{4.87}$$

that is, the short-distance limit of the correlator of two fields is finite, barring the on-site delta divergence. In our particular example, and focusing on the A fields in the polarization basis[6], the two-point functions are given in terms of the α functions by (4.79). Removing the constant factor responsible for the δ functions, the corresponding limits are given by

$$\lim_{\vec{x}\to\vec{y}} \langle A_{\parallel}(\vec{x})A_{\parallel}(\vec{y})\rangle = \int d^dk \left(\frac{1}{\alpha_{\parallel}(k,s)} - \frac{\Lambda}{m(s)^2}\right) \tag{4.88}$$

$$\lim_{\vec{x}\to\vec{y}} \langle A_{\perp,n}(\vec{x})A_{\perp,n}(\vec{y})\rangle = \int d^dk \left(\frac{1}{\alpha_{\perp}(k,s)} - \frac{1}{\Lambda}\right) \tag{4.89}$$

where the expectation values are taken with respect to $|\Psi(k,s)\rangle$. For the α functions from (4.74)-(4.75) we have

$$\frac{1}{\alpha_{\parallel}(k,s)} \sim \frac{\Lambda}{m(s)^2}\left(1 - \frac{\Lambda^2 - m(s)^2}{2k^2} + \dots\right), \tag{4.90}$$

$$\frac{1}{\alpha_{\perp}(k,s)} \sim \frac{1}{\Lambda}\left(1 + \frac{\Lambda^2 - m(s)^2}{2k^2} + \dots\right), \tag{4.91}$$

[6] Admittedly, this is an unusual choice of fields to focus on: the Fourier transforms of $A_{\parallel}(\vec{k})$ and $A_{\perp,n}(\vec{k})$ do not yield any of the position space fields that we usually talk about in QFT. Rather, it is $ikA_{\parallel}(\vec{k})$ that Fourier transforms to $\partial_i A^i$, and $ikA_{\perp,n}(\vec{k})$ that Fourier transforms to a linear combination of magnetic field components. Hopefully, this will not lead to confusion: the analysis can be carried out in a similar fashion for these other fields, the only difference being in the counting of powers of k, and the fact that the distributional contribution in the correlators will include a differential operator acting on the delta function (as we mentioned in the caption to Figure 4.2). Keeping $A_{\parallel}$ and $A_{\perp,n}$ also has the small advantage of making the analogy with the same analysis for the d-dimensional free boson more straightforward.

and the UV divergence is removed in $d = 1$, but it remains in higher dimensions. Notice that since

$$\alpha_{\parallel}(k,s) = \frac{m(s)^2}{\alpha_{\perp}(k,s)}, \tag{4.92}$$

and both functions asymptote to constants, their asymptotic behaviour is very much related, as can be seen in the expansions above.

If needed, we can build cMERAs where these states are more strongly UV regulated, at the cost of adding extra derivatives to the entangler and the parent Hamiltonians. Consider an entangler of the form (4.64) whose momentum space profile is given by

$$g_{\perp}(k) = \frac{1 + n\kappa^{2n-2}}{2\left(1+\kappa^{2n-2}\right)\left(1+\kappa^2+\kappa^{2n}\right)}, \quad \kappa \equiv \frac{k}{\Lambda}, \tag{4.93}$$

$$g_{\parallel}(k) = 1 - g_{\perp}(k) \tag{4.94}$$

for $n > 1$. $g_{\perp}(k)$ is a rational function of k^2 that goes to $\frac{1}{2}$ at $k = 0$ and decays as k^{-2n} at long distances. Its Fourier transform, namely the real space profile of the entangler, is therefore integrable for dimensions $d < 2n$. The resulting α functions corresponding to this entangler, if applied on the same initial state, are

$$\alpha_{\perp}(k,s) = \Lambda\sqrt{\frac{k^{2n}+k^2\Lambda^{2n-2}}{k^{2n}+k^2\Lambda^{2n-2}+\Lambda^{2n}}}\sqrt{\frac{k^{2n}+k^2m(s)^{2n-2}+m(s)^{2n}}{k^{2n}+k^2m(s)^{2n-2}}}, \tag{4.95}$$

$$\alpha_{\parallel}(k,s) = \frac{m^2(s)}{\alpha_{\perp}(k,s)}, \tag{4.96}$$

with asymptotic fixed-points:

$$\alpha_{\perp}(k) = \Lambda\sqrt{\frac{k^{2n}+k^2\Lambda^{2n-2}}{k^{2n}+k^2\Lambda^{2n-2}+\Lambda^{2n}}}, \tag{4.97}$$

$$\alpha_{\parallel}(k) = 0. \tag{4.98}$$

These states are more strongly UV regularized, as can be checked by expanding

$$\frac{1}{\alpha_{\parallel}(k,s)} \sim \frac{\Lambda}{m(s)^2} + \frac{\Lambda\left(m(s)^{2n}-\Lambda^{2n}\right)}{2m(s)^2k^{2n}} + \ldots, \tag{4.99}$$

$$\frac{1}{\alpha_{\perp}(k,s)} \sim \frac{1}{\Lambda} + \frac{\Lambda^{2n}-m(s)^{2n}}{2\Lambda k^{2n}} + \ldots, \tag{4.100}$$

Indeed, the short distance limit of the corresponding two-point functions will be finite for $d < 2n$, while their long distance behaviour can still be seen to approximate that of the

target state correlation functions by performing the expansion around small k rather than large k.

This chapter's takeaways:

- We provide a scale invariant cMERA whose fixed point state is *gauge invariant* and approximates the ground state of the free massless vector boson, i.e. the Maxwell field.
- Additionally, finite s states of this cMERA approximate the ground state of the free *massive* vector boson theory, for a mass $m(s) = \Lambda e^{-s}$ (and are consequently not gauge invariant).
- Our proposal generalizes the magic cMERA to the vector boson case, and shares with it the property that all cMERA states have a *strictly local parent Hamiltonian*, which differs from their target state's parent Hamiltonian by a *UV regulating term*.
- This approach to gauge invariant cMERAs has the potential to generalize to the interacting case, in which case it would provide a *prescription* to tackle gauge theories when suitable interacting cMERA algorithms become available in the future.

Chapter 5

cMERA with boundaries and defects

This chapter's goal: In this chapter we explain how to generalize the cMERA framework to deal with boundaries and localized defects, following examples from the free boson theory.

5.1 Introduction

One of the ways we can probe a quantum theory is by placing it on a manifold with a boundary. The well-definedness of the variational principle then requires that we impose adequate boundary conditions on the fields. More generally, we can think of introducing defects into the theory. Classifying boundary conditions and defects which satisfy certain symmetries, in particular conformal symmetry in the case of a CFT, is an important problem, which has been solved to various degrees of completeness depending on the theory at hand.

As we have seen in previous chapters, a cMERA wavefunctional is defined as the result of evolving a reference state with a unitary evolution generated by a *quasi-local* entangler. This makes the generalization of the formalism to the case where boundaries and defects are present nontrivial: intuitively, a modification will be needed when the spatial smearing profile of the entangling operator hits, for instance, a boundary, on the other side of which there are no degrees of freedom to have support on; or a defect, which can be interpreted as an interface or domain wall between two theories (or two instances of the same theory).

In the present chapter, we explain how this situation can be tackled. We also point out a related property of cMERA that reproduces known results on its lattice counterpart. Boundary critical phenomena were first addressed with entanglement renormalization techniques in [50]. Later, in [142], Evenbly and Vidal analyze in detail the problem of finding MERA representations of systems with boundaries and defects (which they also call impurities). They state (and provide strong evidence for) the following conjecture[1]:

Minimal update (MERA) A MERA for a system with a defect (in particular a boundary) can be obtained from a MERA for a system without the defect by only modifying the tensors within the causal cone of the defect.

The causal cone $C(\mathcal{R})$ of a spatial region $\mathcal{R}$ in a MERA is made of all the tensors involved in the computation of the reduced density matrix $\rho_{\mathcal{R}}$ (conversely, the modification of a tensor outside $C(\mathcal{R})$ does not affect $\rho_{\mathcal{R}}$). Consequently, in Figure 5.1 (left), $\rho_{\mathcal{R}}$ can be obtained exactly from the sole knowledge of the reduced density matrix $\rho_{\mathcal{R}'}$ of region $\mathcal{R}'$ plus the tensors contained between them in $C(\mathcal{R})$. The latter are used to define the so-called *descending superoperator* [49], which maps $\rho_{\mathcal{R}'} \mapsto \rho_{\mathcal{R}}$ without the need to compute the whole pure state. Thanks to the structure of the MERA, and the unitarity and isometric constraints on its tensors, the causal cone of any given region has constant width as we move up in the network, see Figure 5.1 (right).

This conjecture has important consequences both from a theoretical and a practical point of view. On the one hand, it teaches us about the structure of ground state wavefunctions of systems with impurities, and relates to Wilson's renormalization-based study of impurity problems that we briefly alluded to in Chapter 2 [53]. On the other hand, consider the case of an impurity perturbing an otherwise homogeneous system (whose MERA representation would consist of the same tensors repeated along the spatial direction, the number of parameters in each layer thus being independent of the system size). In spite of the explicit breaking of translation symmetry, if the conjecture holds we only need to change a constant number of tensors per layer from the homogeneous case, leading to a much more favorable scaling of parameters with the system size than in a generic translation noninvariant state. In the particular case where both the unperturbed system and the impurity are scale-invariant, the number of parameters is constant and the system can be directly studied in the thermodynamic limit, avoiding finite size effects.

In some particular cases, the properties of the defect allow for even more structure. Such is the case of topological defects, whose representation on the tensor network is not

[1] This conjecture is named after the *theory of minimal updates* by the same authors [143].

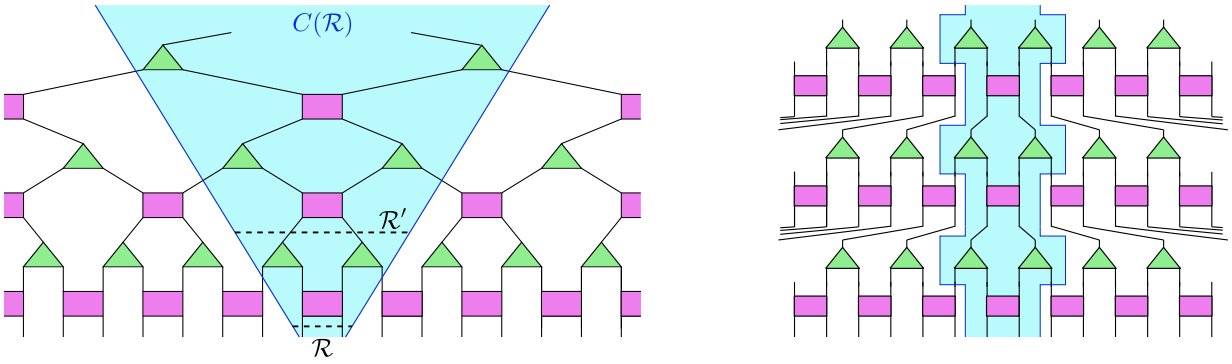

Figure 5.1: (left) The causal cone of a two-site region $\mathcal{R}$ in the MERA. $\rho_{\mathcal{R}}$ can be computed from just $\rho_{\mathcal{R}'}$ and the tensors between them in $C(\mathcal{R})$ (right) The same causal cone, but in the picture where we rescale after each layer of MERA to keep the lattice spacing constant (as we do in cMERA with Λ^{-1}). In this picture, it is patent that the width of the causal cone is constant as we move up the network.

unique, featuring tensors that can be moved around. This feature is explored, e.g., in [144] for the topological defects of the Ising model (where MERAs are obtained from partition functions by means of TNR, an algorithm we will review in Chapter 7); and in [145], where topological defects are implemented by symmetry MPOs acting on the virtual bonds of the MERA. In a different direction, the authors of [146] explore additional consequences of the minimal update conjecture in AdS/CFT, including situations where it would not be applicable, for which they introduce a more generic ansatz called the *rayed MERA*. More recently, the theory of minimal updates in MERA was used in the interpretation of results concerning the holographic complexity of a 2d CFT with a conformal defect [147].

In this chapter, we are going to be building cMERA evolutions for non-interacting theories with boundaries and defects, in particular for the 1+1d free boson theory. Our examples provide ground for the following general prescription, analogous to the lattice statement, and expected to hold equally for interacting theories:

Minimal update (cMERA) A cMERA for a system with a defect (in particular a boundary) can be obtained from a cMERA for a system without the defect by modifying the entangler quasi-locally at the "causal cone" of the defect, i.e., with a perturbation supported mostly within a distance $\sim \Lambda^{-1}$ of it.

Recall that in cMERA Λ^{-1} plays the role of the lattice spacing, thus setting the natural length scale to define a causal cone. Of course, due to the quasi-locality of the entangler,

there is no such a thing as a sharp causal cone in the cMERA, but rather a quasi-local one. This is enough to have a descending superoperator that can map reduced density matrices to reduced density matrices further down the entangling evolution, not exactly but with an error that decays as regions become large compared to Λ^{-1} [148]. Thus we cannot expect the modification of the entangler due to a defect to be sharply supported on a compact interval. Instead, we will see that, in the examples we deal with, the term we have to add to the entangler shares the same quasi-locality of the entangler itself.

This chapter is structured as follows: in Section 5.2 we provide a review of the kinds of boundaries and defects for the free boson CFT that we will be considering[2]. Then, in Section 5.3 we build example cMERAs for the free boson in the presence of a boundary (placing the theory on the semi-infinite line) and a defect, providing evidence for the claims made above. We finish in Section 5.4 with a small discussion.

5.2 Boundaries and defects for the free boson CFT

For the cMERAs that we will be working with in the next section, we need to review how the free scalar field theory is modified when we add boundaries and defects. We will not be exhaustive in studying all the possible instances of a boundary or a defect that we can find for the free boson, since a few examples should be enough to justify our claims. We restrict ourselves to 1+1d.

Recall the standard method to solve the free scalar field theory: we exploit the decomposition of the field in terms of momentum modes

$$\phi(x,t) = \int \frac{dk}{2\sqrt{\pi}|k|} \left(a_k e^{i(kx-|k|t)} + a_k^\dagger e^{-i(kx-|k|t)} \right) \tag{5.1}$$

which can be easily written in terms of the Fourier components of the field:

$$a_k = \sqrt{\frac{|k|}{2}}\phi(k) + i\sqrt{\frac{1}{2|k|}}\pi(k). \tag{5.2}$$

Then, thanks to the fact that the Hamiltonian is diagonal in these modes, we can express the (Gaussian) ground state in terms of them,

$$H = \int dk\; E_k\, a_k^\dagger a_k \qquad \Longrightarrow \qquad a_k|\Psi\rangle = 0 \qquad \forall k \in \mathbb{R}, \tag{5.3}$$

[2]Technically, we could restrict ourselves to presenting the defect formalism, since boundaries are particular kinds of defects, and their treatment is no different. We expect however that proceeding in a gradual fashion will make the presentation more accessible for the unfamiliar reader.

and the correlation functions then easily follow through. Now, note that these modes arise from considering the *plane wave* basis of complex solutions of the classical equation of motion:

$$\Box\phi(x,t) = 0 \qquad (\Box = \partial_t^2 - \partial_x^2) \tag{5.4}$$

given by

$$\frac{1}{\sqrt{2\pi}} e^{i(kx-|k|t)}, \ \frac{1}{\sqrt{2\pi}} e^{-i(kx-|k|t)}. \tag{5.5}$$

In this section we are going to be dealing with situations in which an additional condition, such as a boundary condition, is added to the equation of motion, resulting in a different set of momentum modes. However, once we have identified a suitable basis to play a role analogous to (5.5), the quantization procedure follows through in an equivalent fashion, and we will be able to recover analogous expressions (5.2)-(5.3), from where we can proceed to propose cMERA approximations to the ground state wavefunctional.

5.2.1 A boundary at the origin: the free boson on the half-line

CFTs such as the free boson are endowed with a large amount of symmetries. However, the moment we include a boundary in our manifold, we are definitely going to lose some of them: we may only keep, in principle, those that leave the new manifold invariant. *Conformal* boundary conditions are those that are also invariant under these symmetries. If we impose a conformal boundary condition, the resulting system is described by a boundary conformal field theory or BCFT[3].

Let us place a free scalar field on the half-line $\mathbb{R}_+ = \{x > 0\}$. We are going to focus on the following two (conformal) boundary conditions (b.c.):

$$\phi(0) = 0 \qquad \text{(Dirichlet b.c.)} \tag{5.6}$$

$$\partial_x\phi(0) = 0 \qquad \text{(Neumann b.c.)} \tag{5.7}$$

As discussed above, these boundary conditions modify the allowed momentum modes we can use to expand the field. For instance, for Dirichlet b.c., consider the classical e.o.m. (massless Klein-Gordon equation) with the corresponding boundary conditions:

$$\Box\phi = 0 \tag{5.8}$$

$$\phi(0) = 0 \tag{5.9}$$

[3]BCFT will be one of the stars in Chapter 6.

The addition of the boundary condition restricts us to a subspace of the space of solutions to the equation. Indeed, if we take the general solution (5.1) and impose the boundary condition, we obtain:

$$0 = \int_{-\infty}^{\infty} \frac{dk}{2\sqrt{\pi}|k|} \left(a_k e^{-i|k|t} + a_k^* e^{i|k|t}\right) \tag{5.10}$$

We need $a_k = -a_{-k}$. The mode expansion of the field then looks as follows

$$\phi(x,t) = \int_0^{\infty} \frac{dk}{\sqrt{\pi|k|}} \left(a_k \sin kx\, e^{-i|k|t} + a_k^* \sin kx\, e^{i|k|t}\right) \tag{5.11}$$

We then define

$$\phi(k) \equiv \frac{2}{\sqrt{\pi}} \int_0^{\infty} dx\ \sin kx\, \phi(x), \qquad \pi(k) \equiv \frac{2}{\sqrt{\pi}} \int_0^{\infty} dx\ \sin kx\, \pi(x), \tag{5.12}$$

so that we have

$$a_k \equiv \sqrt{\frac{|k|}{2}}\phi(k) + i\sqrt{\frac{1}{2|k|}}\pi(k) \tag{5.13}$$

and the following canonical commutation relations are satisfied

$$[\phi(k), \pi(q)] = i\delta(k-q), \qquad [a_k^\dagger, a_q] = \delta(k-q). \tag{5.14}$$

Note that, as opposed to the case of the full real line (e.g. in Section 3.4), here $\phi(k)$ and $\pi(k)$ are Hermitian, and the commutation relation between them involves a $\delta(k-q)$ instead of $\delta(k+q)$. The Klein-Gordon Hamiltonian on the half line

$$H = \int_0^{\infty} dx\ \left(\pi(x)^2 + (\partial_x \phi(x))^2\right), \tag{5.15}$$

can again be brought to diagonal form, in terms of the momentum modes we just defined. Thus, the ground state is defined by the corresponding annihilation operators:

$$H = \int_0^{\infty} dk\ |k|\, a_k^\dagger a_k \qquad \Longrightarrow \qquad a_k |\Psi\rangle_{\text{BCFT}} = 0 \qquad \forall k > 0. \tag{5.16}$$

From here the correlation functions between momentum modes follow:

$$\langle \phi(k)\phi(q)\rangle = \frac{\delta(k-q)}{2k}, \qquad \langle \pi(k)\pi(q)\rangle = \frac{k\delta(k-q)}{2}. \tag{5.17}$$

To go back to real space, we use Eq. (5.12):

$$\begin{aligned}\langle\phi(x)\phi(y)\rangle &= \int_0^\infty\int_0^\infty \frac{2dkdq}{\pi k}\delta(k-q)\sin kx\sin qy = \int_0^\infty \frac{2dk}{\pi k}\sin kx\sin ky \\ &= \frac{1}{\sqrt{2\pi}}\left(\mathcal{F}^{-1}\left[\frac{1}{2k}\right](x-y) - \mathcal{F}^{-1}\left[\frac{1}{2k}\right](x+y)\right) \\ &= -\frac{1}{2\pi}\log|x-y| + \frac{1}{2\pi}\log(x+y) \\ &= -\frac{1}{2\pi}\log\frac{|x-y|}{x+y}. \end{aligned} \tag{5.18}$$

where $\mathcal{F}^{-1}[f]$ is the inverse Fourier transform of f. Note that the correlation function is made of two pieces: the original correlator on the real line, a function of $x-y$, minus the same function evaluated at $x+y$, which enforces the b.c. and breaks translation invariance[4]. The same happens for $\pi(x)$:

$$\begin{aligned}\langle\pi(x)\pi(y)\rangle &= \frac{1}{\sqrt{2\pi}}\left(\mathcal{F}^{-1}\left[\frac{k}{2}\right](x-y) - \mathcal{F}^{-1}\left[\frac{k}{2}\right](x+y)\right) \\ &= -\frac{1}{2\pi}\frac{1}{(x-y)^2} + \frac{1}{2\pi}\frac{1}{(x+y)^2} \\ &= \frac{1}{\pi}\frac{2xy}{(x^2-y^2)^2}. \end{aligned} \tag{5.19}$$

Figure 5.2 depicts examples of these correlators. Neumann b.c. can be addressed in a similar manner (replacing sines by cosines). Following the previous remark, the BCFT correlators can be written compactly

$$\begin{aligned}\langle\phi(x)\phi(y)\rangle &= \mathcal{C}_{\phi\phi}(x-y) + \xi\,\mathcal{C}_{\phi\phi}(x+y), \\ \langle\pi(x)\pi(y)\rangle &= \mathcal{C}_{\pi\pi}(x-y) + \xi\,\mathcal{C}_{\pi\pi}(x+y). \end{aligned} \tag{5.20}$$

where $\xi = 1$ for Neumann b.c. and $\xi = -1$ for Dirichlet b.c., and we have abbreviated the CFT correlation functions,

$$\mathcal{C}_{\phi\phi}(x) = -\frac{1}{2\pi}\log|x|, \qquad \mathcal{C}_{\pi\pi}(x) = -\frac{1}{2\pi}\frac{1}{x^2}. \tag{5.21}$$

[4]This extra term can be interpreted as the (negative) correlation function between a field at x and a field at $-y$ which is the "reflection" of the field at y (or the same with y and $-x$). In fact, there is an actual formalism, the *method of images* or *doubling trick* [46], that allows for the computation of BCFT correlators as CFT correlators involving image fields, reflected along the boundary. In spite of its beauty, we will not delve into it in this thesis.

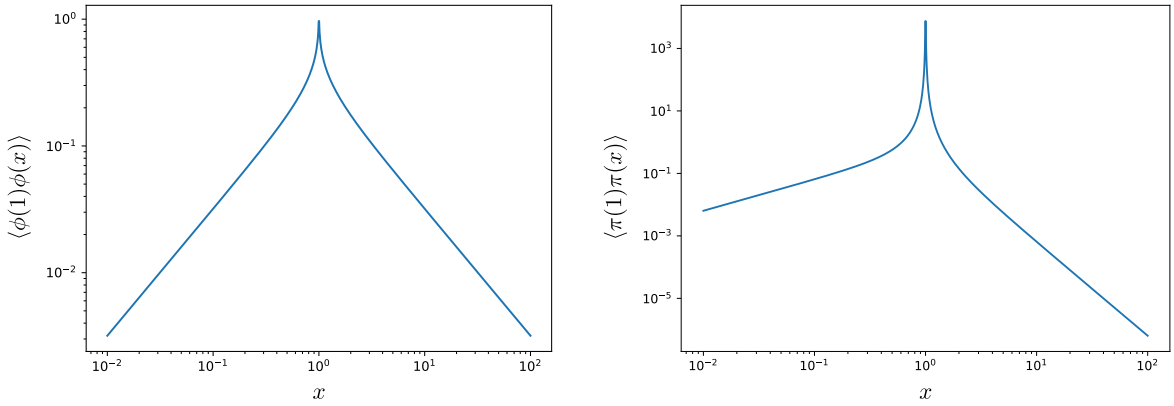

Figure 5.2: $\langle\phi(1)\phi(x)\rangle$ and $\langle\pi(1)\pi(x)\rangle$ for the free boson with Dirichlet boundary conditions.

5.2.2 A defect at the origin: conformal defects of the free boson

A *conformal defect* can be understood as an interface between two CFTs, a junction that is itself scale invariant. Here we will consider the setting of a single defect, sitting at the origin of the real line, between two free boson theories in each of the half-lines, much like a domain wall, resulting in a defect conformal field theory or DCFT. A pair of conformal b.c. like the ones we explored above, one for each theory, constitutes an example of such a defect, yet a very specific one. That would be called a *totally reflective* or *factorising* defect: the two theories do not talk to each other, particles incoming to the defect are reflected backwards. More generally, we can consider *permeable* defects, which let incident waves be partially transmitted to the other side. These range up to the case of the trivial defect, which transmits everything perfectly. Such a defect simply amounts to not inserting anything and having a single theory defined on the real line; it is an example of a *totally transmissive* defect[5]. For these conformal defects, reflection and transmission coefficients $\mathcal{R}$ and $\mathcal{T}$ can be defined [149], which satisfy $\mathcal{R}+\mathcal{T}=1$, and such that totally reflective and totally transmissive defects respectively have $\mathcal{R}=1$ and $\mathcal{T}=1$.

In our study we are going to focus on a particular family of local conformal defects for the free boson, one of the two[6] introduced in [150], which is parametrized by an angular

[5]It may seem that the term "totally transmissive" would be reserved for this kind of defect. However, it is applied in general to all *topological* defects, whose presence cannot be detected in correlators of the stress-energy tensor, and which can thus be deformed without affecting the values of general correlators, as long as they do not cross field insertions [149].

[6]The second family of defects can be obtained from the first one by composing with a "chiral" defect,

variable. These defects are characterized by the *gluing* conditions for the field on both sides of the interface:

$$\left(\begin{array}{c} \partial_x \phi(x,t) \\ \partial_t \phi(x,t) \end{array} \right) \Big|_{x=0^-} = M(\theta) \left(\begin{array}{c} \partial_x \phi(x,t) \\ \partial_t \phi(x,t) \end{array} \right) \Big|_{x=0^+}, \tag{5.22}$$

where

$$M(\theta) = \left(\begin{array}{cc} \tan\theta & 0 \\ 0 & \cot\theta \end{array} \right), \qquad \theta \in \left(-\frac{\pi}{2}, \frac{\pi}{2} \right]. \tag{5.23}$$

Such a defect allows particles to either bounce off or be transmitted, with respective probabilities given by the coefficients $\mathcal{R}$ and $\mathcal{T}$, which of course depend on θ:

$$\mathcal{R} = \cos^2(2\theta), \qquad \mathcal{T} = \sin^2(2\theta). \tag{5.24}$$

Note that, e.g., $\theta = \pi/4$ is a perfect transmitter (it is the trivial defect) and $\theta = 0, \pi/2$ are perfect reflectors, equivalent to placing Neumann boundary conditions on the left field and Dirichlet boundary conditions on the right field ($\theta = 0$) and vice versa ($\theta = \pi/2$).

Upon placing a defect with parameter θ at the origin, the momentum mode expansion of the field is modified, since Eq. (5.22) constrains the allowed solutions to the equation of motion. We thus have to look for an orthonormal basis of solutions to the Klein-Gordon. We define the ansatz modes

$$f_k(x) e^{-i|k|t}, \;\; f_k^*(x) e^{i|k|t} \tag{5.25}$$

where

$$f_k(x) \equiv \left(\alpha_k \, e^{ikx} + \beta_k \, e^{-ikx} \right) \oplus \left(\alpha'_k \, e^{ikx} + \beta'_k \, e^{-ikx} \right). \tag{5.26}$$

Here we are using the direct sum notation as shorthand to separate the behaviour of a function on both sides of the defect

$$f(x) \oplus g(x) \equiv \begin{cases} f(x) & x < 0, \\ g(x) & x > 0, \end{cases} \tag{5.27}$$

a notation that comes from seeing $f_k(x)$ as an element of $C^\infty(\mathbb{R}^-) \oplus C^\infty(\mathbb{R}^+)$. The coefficients $\alpha_k, \beta_k, \alpha'_k, \beta'_k$ can then be determined by imposing orthonormality

$$\int dx \; f_k^*(x) f_q(x) = \delta(k - q) \tag{5.28}$$

which flips the sign of either left-moving or right-moving excitations (but not both). Their treatment is more complicated so we omit them here.

and the gluing conditions (5.22). After some computation that we relegate to Appendix D, we finally arrive at one such basis of functions

$$f_k(x) = \frac{e^{i\frac{\pi}{4}}}{2\sqrt{\pi}} \left((\sin 2\theta - i)e^{ikx} - i\cos 2\theta e^{-ikx}\right) \oplus \left((1 - i\sin 2\theta)e^{ikx} - \cos 2\theta e^{-ikx}\right) \quad (5.29)$$

We can now expand the field

$$\phi(x,t) = \int \frac{dk}{\sqrt{2|k|}} \left(a_k f_k(x) e^{-i|k|t} + a_k^\dagger(t) f_k^*(x) e^{i|k|t}\right), \quad (5.30)$$

and define the analogue of the momentum space fields

$$\phi(k) = \int dx\ f_k^*(x)\phi(x), \qquad \pi(k) = \int dx\ f_k^*(x)\pi(x), \quad (5.31)$$

in terms of which the creation-annihilation operators have a familiar form:

$$a_k = \sqrt{\frac{|k|}{2}}\phi(k) + i\sqrt{\frac{1}{2|k|}}\pi(k). \quad (5.32)$$

Note however that the familiar relation from the case without defect

$$\phi(k)^\dagger = \phi(-k) \quad (5.33)$$

is now replaced by

$$\phi(k)^\dagger = \sin 2\theta\, \phi(-k) - i\cos 2\theta\, \phi(k) \quad (5.34)$$

and similarly for $\pi(k)$, due to the presence of the defect. The momentum space commutation relations read

$$[\phi(k), \pi^\dagger(q)] = i\delta(k-q) \quad (5.35)$$

which are the same as in the real line and the half-line, barring the fact that the Hermitian conjugate of $\pi(q)$ in those cases could be written as $\pi(-q)$ or $\pi(q)$ respectively, as opposed to a linear combination of the two as is the case now.

In these variables, and after the subtraction of the usual infinite constant, the Hamiltonian is diagonalized and its ground state is defined as the common kernel of annihilation operators of the desired form:

$$H = \int dk\ |k| a_k^\dagger a_k \quad \Longrightarrow \quad a_k|\Psi\rangle_{\text{DCFT}} = 0 \qquad \forall k \in \mathbb{R}. \quad (5.36)$$

Following the standard procedure we can then compute the correlation functions between the momentum modes:

$$\langle\phi(k)\phi(q)\rangle = \frac{1}{2|k|}\left(\sin 2\theta\,\delta(k+q) + i\cos 2\theta\,\delta(k-q)\right), \tag{5.37}$$

$$\langle\pi(k)\pi(q)\rangle = \frac{|k|}{2}\left(\sin 2\theta\,\delta(k+q) + i\cos 2\theta\,\delta(k-q)\right), \tag{5.38}$$

and go back to position space:

$$\langle\phi(x)\phi(y)\rangle = \begin{cases} \mathcal{C}_{\phi\phi}(x-y) + \cos 2\theta\,\mathcal{C}_{\phi\phi}(x+y) & x,y<0, \\ \sin 2\theta\,\mathcal{C}_{\phi\phi}(x-y) & xy<0, \\ \mathcal{C}_{\phi\phi}(x-y) - \cos 2\theta\,\mathcal{C}_{\phi\phi}(x+y) & x,y>0, \end{cases} \tag{5.39}$$

$$\langle\pi(x)\pi(y)\rangle = \begin{cases} \mathcal{C}_{\pi\pi}(x-y) + \cos 2\theta\,\mathcal{C}_{\pi\pi}(x+y) & x,y<0, \\ \sin 2\theta\,\mathcal{C}_{\pi\pi}(x-y) & xy<0, \\ \mathcal{C}_{\pi\pi}(x-y) - \cos 2\theta\,\mathcal{C}_{\pi\pi}(x+y) & x,y>0, \end{cases} \tag{5.40}$$

where we have again used the abbreviations from (5.21). The reader can check from the expressions above that the cases $\theta = 0, \frac{\pi}{4}, \frac{\pi}{2}$ reproduce what we know from the CFT and BCFT cases. Figure 5.3 shows some example correlation functions for different values of θ.

Before moving on, we note that Eqs. (5.39)-(5.40) can be written more compactly as

$$\langle\phi(x)\phi(y)\rangle = \mathcal{C}_{\phi\phi}(x-y) + c_\theta(x,y)\,\mathcal{C}_{\phi\phi}(|x|+|y|) \tag{5.41}$$

$$\langle\pi(x)\pi(y)\rangle = \mathcal{C}_{\pi\pi}(x-y) + c_\theta(x,y)\,\mathcal{C}_{\pi\pi}(|x|+|y|) \tag{5.42}$$

by defining a piecewise constant function $c_\theta(x,y)$:

$$c_\theta(x,y) \equiv \begin{cases} \cos 2\theta & x,y<0, \\ \sin 2\theta - 1 & xy<0, \\ -\cos 2\theta & x,y>0. \end{cases} \tag{5.43}$$

This notation will come in handy in what follows.

5.3 Boundaries and defects in cMERA

We now move on to the proposal of cMERA approximations for the ground states $|\Psi\rangle_{\text{BCFT}}$ and $|\Psi\rangle_{\text{DCFT}}$ of the theories presented in the previous section. As the reader might expect,

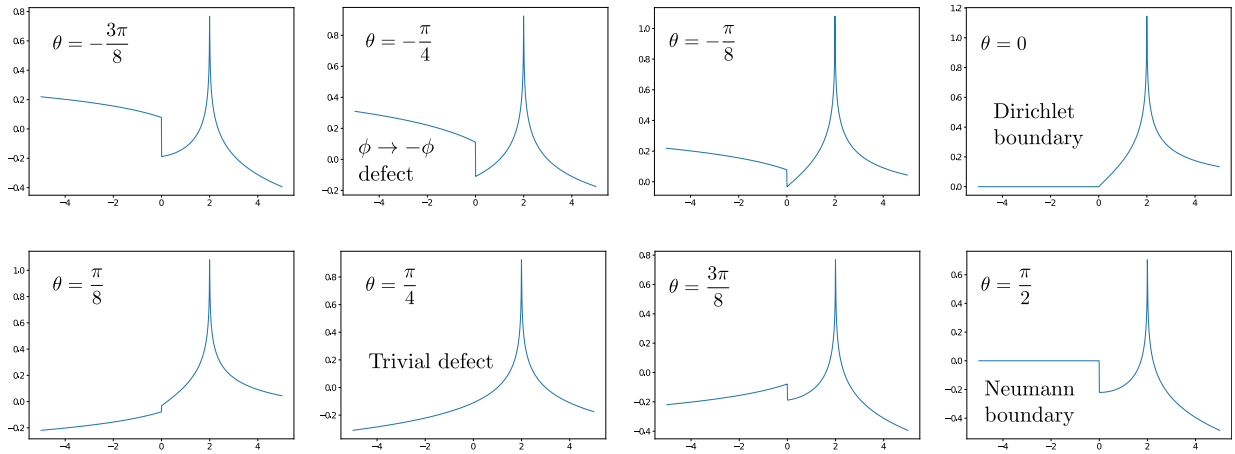

Figure 5.3: $\langle\phi(2)\phi(x)\rangle$ correlator as a function of x, for several values of θ. Note the discontinuity caused by the defect at the origin.

all these constructions will be heavily inspired by the free boson cMERA. Indeed, for each case we will use essentially the same unentangled initial state $|\Omega\rangle$ and scaling generator L, and the entangler K will be that of the CFT, modified by an extra term that will have support only close to the boundary or defect. With all that, we will obtain a long-distance approximation to each target state as the fixed point $|\Psi^\Lambda\rangle$ of the corresponding cMERA.

5.3.1 Boundary cMERA

Consider the free boson theory on the half-line with Dirichlet or Neumann boundary conditions at the origin. The ground state of this BCFT is given in terms of annihilation operators by (5.16). We now propose an initial unentangled state $|\Omega\rangle$, a generator of scale transformations L and an entangler K such that the fixed point of the corresponding cMERA evolution approximates $|\Psi\rangle_{\text{BCFT}}$ at long distances.

Initial state

We define $|\Omega\rangle$ in terms of local annihilation operators, in a completely analogous way to the CFT case (Eqs. (2.10) and (3.26)), so that it can be interpreted as the continuum limit of a product state on a semi-infinite lattice:

$$\left(\sqrt{\frac{\Lambda}{2}}\phi(x) + i\sqrt{\frac{1}{2\Lambda}}\pi(x)\right)|\Omega\rangle = 0 \qquad \forall x > 0. \tag{5.44}$$

In terms of momentum modes this reads

$$\left(\sqrt{\frac{\Lambda}{2}}\phi(k) + i\sqrt{\frac{1}{2\Lambda}}\pi(k)\right)|\Omega\rangle = 0 \qquad \forall k > 0. \tag{5.45}$$

Generator of scale transformations

Note that the half-line is invariant with respect to scale transformations centered at the origin, so we do not need to keep redefining our set of degrees of freedom as we rescale space. Both Dirichlet and Neumann b.c., being conformal b.c., are invariant under scaling as well. We can thus use the restriction to the half-line of the scaling generator L from the CFT cMERA:

$$L\big|_{\mathbb{R}^+} \equiv \int_0^\infty dx\ \pi(x)\left(x\partial_x + \frac{1}{2}\right)\phi(x) + \text{h.c.} \tag{5.46}$$

$$= \int_0^\infty dk\ \pi(k)\left(k\partial_k + \frac{1}{2}\right)\phi(k) + \text{h.c.} \tag{5.47}$$

Entangler

We propose an entangling operator made out of two contributions:

$$K_{\text{BCFT}} \equiv K_{\text{CFT}}\big|_{\mathbb{R}^+} + K_{\text{bdy}}. \tag{5.48}$$

The first term is nothing but the restriction to the half-line of the entangler (2.12) of the free boson cMERA, which we write here in terms of $\phi(x)$ and $\pi(x)$

$$K_{\text{CFT}}\big|_{\mathbb{R}^+} = \frac{1}{2}\int_{x,y>0} dx\,dy\ g(x-y)\phi(x)\pi(y) + \text{h.c.}, \tag{5.49}$$

while the second term looks quite similar to the first but with a key sign difference:

$$K_{\text{bdy}} = \frac{\xi}{2}\int_{x,y>0} dx\,dy\ g(x+y)\phi(x)\pi(y) + \text{h.c.}, \tag{5.50}$$

where ξ again depends on the boundary conditions, $\xi = 1$ for Neumann and $\xi = -1$ for Dirichlet. The addition of this second term modifies the original entangler only within distance $\sim \Lambda^{-1}$ from the origin, where the boundary is located. Indeed, this follows from the quasi-locality of the profile g, since $g(x+y)$ will be negligible whenever $x \gg \Lambda^{-1}$ or

$y \gg \Lambda^{-1}$, and is in line with the cMERA minimal update conjecture. The reader is also invited to observe the analogy between the structure of K_{BCFT} and the correlators in (5.20).

The justification behind our boundary cMERA proposal is simple, and we already hinted at it as we defined $|\Omega\rangle$ and $L\big|_{\mathbb{R}^+}$: when expressed in momentum modes (5.12), K_{BCFT} is manifestly analogous to the free boson cMERA entangler (3.30):

$$K_{\text{BCFT}} = \frac{1}{2}\int dk\; g(k)\phi(k)\pi(k) + \text{h.c.} \tag{5.51}$$

As a consequence, the cMERA evolution of the momentum modes of the boundary theory mirrors (3.32):

$$\partial_s \phi(k,s) = -i[L\big|_{\mathbb{R}^+} + K_{\text{BCFT}}, \phi(k,s)] = -\left(k\partial_k + \frac{1}{2} + g(k)\right)\phi(k,s), \tag{5.52}$$

$$\partial_s \pi(k,s) = -i[L\big|_{\mathbb{R}^+} + K_{\text{BCFT}}, \pi(k,s)] = -\left(k\partial_k + \frac{1}{2} - g(k)\right)\pi(k,s), \tag{5.53}$$

and boundary cMERA states can be given a characterization

$$\left(\sqrt{\frac{\alpha(k,s)}{2}}\phi(k) + i\sqrt{\frac{1}{2\alpha(k,s)}}\pi(k)\right)|\Psi^\Lambda(s)\rangle_{\text{BCFT}} = 0. \tag{5.54}$$

which is identical to that of the cMERA states on the real line (3.28), barring the use of a different set of momentum modes, with $\alpha(k,s)$ once again given in terms of $g(k)$ by (3.35). From all these analogies it follows that the correlation functions in the boundary cMERA fixed point $|\Psi^\Lambda\rangle_{\text{BCFT}}$ are, in momentum space,

$$\langle\phi(k)\phi(q)\rangle = \frac{\delta(k-q)}{2\alpha(k)}, \qquad \langle\pi(k)\pi(q)\rangle = \frac{\alpha(k)\delta(k-q)}{2}. \tag{5.55}$$

and thus are related to those of the original free boson cMERA similarly to (5.20):

$$\begin{aligned}\langle\phi(x)\phi(y)\rangle &= \mathcal{C}^\Lambda_{\phi\phi}(x-y) + \xi\,\mathcal{C}^\Lambda_{\phi\phi}(x+y),\\ \langle\pi(x)\pi(y)\rangle &= \mathcal{C}^\Lambda_{\pi\pi}(x-y) + \xi\,\mathcal{C}^\Lambda_{\pi\pi}(x+y),\end{aligned} \tag{5.56}$$

where $C^\Lambda_{\phi\phi}(x), C^\Lambda_{\pi\pi}(x)$ are now the corresponding original cMERA correlators (3.47)-(3.48). This is a powerful statement, since all properties proved for the original cMERA now follow for the boundary cMERA, in particular:

- $|\Psi^{\Lambda}\rangle_{\text{BCFT}} \overset{\text{LD}}{\simeq} |\Psi\rangle_{\text{BCFT}}$, i.e., the long distance physics of the boundary cMERA fixed point approximates that of its target, the ground state $|\Psi\rangle_{\text{BCFT}}$ of the BCFT.
- $|\Psi^{\Lambda}\rangle_{\text{BCFT}}$ is UV regularized at length scales below the cutoff Λ^{-1}, in the sense we studied in Chapter 3.

To corroborate these statements, Figures 5.4 and 5.5 show examples of boundary cMERA correlators, obtained with the entangler profile (3.38), for Dirichlet boundary conditions. In both Figures we can see the boundary cMERA correlators approximating the BCFT correlators in the limit of long distances (with respect to the cutoff length scale Λ^{-1}) between the two field insertions. In the opposite limit, the BCFT correlators diverge, while the boundary cMERA correlators are UV regularized and tend to a constant. Most cMERA correlators have an onsite delta function term when the two field insertions coincide: the Dirichlet b.c. correlators are special in that these deltas do not appear, since they cancel in Eq. 5.56 between the two summands[7]. The boundary cMERA correlators always satisfy the boundary conditions (in this case, they go to zero when one of the field insertions approaches the boundary, where the field vanishes); on the other hand, how well they approximate the BCFT correlator when one field insertion is near the boundary depends on whether the other one is far away (as in Fig. 5.4, where the correlator is accurately approximated near the boundary) or nearby (as in Fig. 5.5, where near the boundary we have a short distance correlator, which is not as accurate).

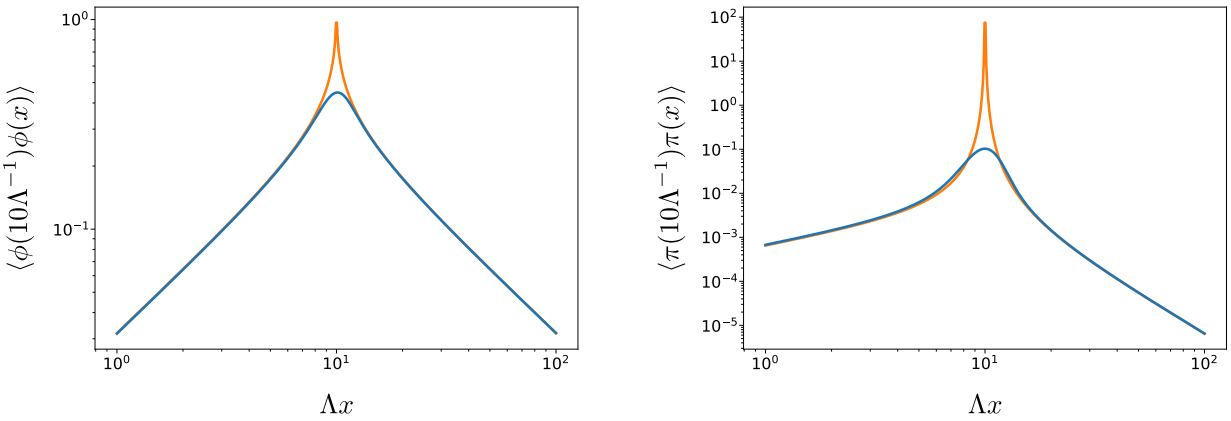

Figure 5.4: $\langle\phi(10\Lambda^{-1})\phi(x)\rangle$ and $\langle\pi(10\Lambda^{-1})\pi(x)\rangle$ correlators for the boundary cMERA fixed point with Dirichlet b.c. (blue) and for the corresponding BCFT (orange).

[7]The same happens for the arbitrary additive constant of the $\phi\phi$ correlator: in fact the Dirichlet b.c. breaks the shift symmetry of the field $\phi(x) \to \phi(x) + a, \quad a \in \mathbb{R}$.

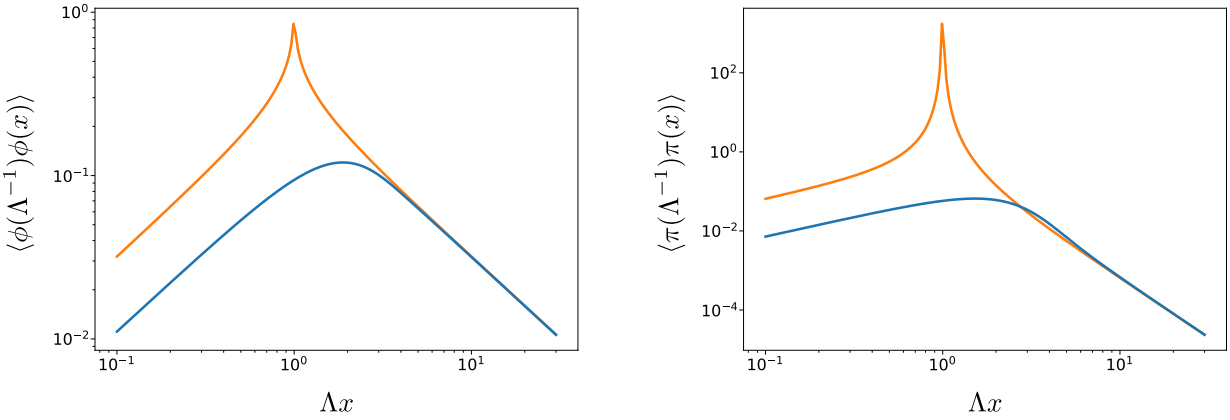

Figure 5.5: $\langle\phi(\Lambda^{-1})\phi(x)\rangle$ and $\langle\pi(\Lambda^{-1})\pi(x)\rangle$ correlators for the boundary cMERA fixed point with Dirichlet b.c. (blue) and for the corresponding BCFT (orange).

5.3.2 Defect cMERA

Consider now the insertion of a conformal defect from the family we discussed in Section 5.2.2 at the origin of the real line. We again propose an initial unentangled state, a scaling generator and an entangler such that the resulting cMERA fixed point approximates the ground state $|\Psi\rangle_{\text{DCFT}}$ at long distances.

Initial state and generator of scale transformations

We use exactly the same initial state $|\Omega\rangle$ and the same generator L than for the free boson without the defect. Notice that L will not displace the defect, since it is sitting at the origin. In terms of the momentum modes (5.31) of the DCFT, the expression for $|\Omega\rangle$ is analogous to the CFT one:

$$\left(\sqrt{\frac{\Lambda}{2}}\phi(k) + i\sqrt{\frac{1}{2\Lambda}}\pi(k)\right)|\Omega\rangle = 0, \qquad k \in \mathbb{R}, \tag{5.57}$$

while the expression of L in momentum modes

$$L = \int dk\, \pi^\dagger(k)\left(k\partial_k + \frac{1}{2}\right)\phi(k) + \text{h.c.}, \tag{5.58}$$

is also entirely analogous.

Entangler

As in the BCFT case, we propose for the defect case an entangler obtained by adding to the entangler K_{CFT} of the free boson on the real line a piece that modifies it in the vicinity of the defect,

$$K_{\text{DCFT}} = K_{\text{CFT}} + K_{\text{defect}}(\theta). \tag{5.59}$$

The latter has the following form in terms of the profile $g(x)$:

$$K_{\text{defect}}(\theta) = \frac{1}{2}\int_{x,y>0} dx\, dy\; c_\theta(x,y)\, g(|x|+|y|)\, \phi(x)\pi(y) + \text{h.c.} \tag{5.60}$$

where $c_\theta(x,y)$ is precisely the function defined in (5.43). This time we invite the reader to compare the structure of K_{DCFT} with the correlators in (5.42). Note that $K_{\text{defect}}(\theta)$ is indeed localized around the defect, since the argument of the profile function is $|x|+|y|$, that is, the sum of the distances to the defect of the two operator insertions $\phi(x)\pi(y)$. From the quasi-locality property of g it follows at distances much larger than Λ^{-1} from the defect,

$$K_{\text{DCFT}} \sim K_{\text{CFT}}, \tag{5.61}$$

resulting in the cMERA version of a minimal update, as depicted in Figure 5.6. For instance, if we pick the entangler from (3.38), $K_{\text{defect}}(\theta)$ will be localized by a Gaussian of width $\sim \Lambda^{-1}$ around the defect, since

$$g(|x|+|y|) \propto e^{-\frac{\sigma\Lambda^2}{4}(|x|+|y|)^2}, \tag{5.62}$$

whereas if we use the entangler from the magic cMERA (4.44), $K_{\text{defect}}(\theta)$ becomes exponentially localized, since in that case

$$g(|x|+|y|) \propto e^{-\Lambda(|x|+|y|)}. \tag{5.63}$$

Notice as well that for $\theta = \pi/4$, $K_{\text{defect}}(\theta)$ vanishes, since for that value of θ there is no defect, and the theory is identical to the free boson. On the other hand, it can be checked that for $\theta = 0$ or $\theta = \pi/2$, corresponding to perfectly reflecting defects, the entangler splits into two parts, each acting on a half-line, without any coupling between the two,

$$K_{\text{DCFT}} = K_{\text{CFT}} + K_{\text{defect}}(\theta) = \left(K_{\text{CFT}}\big|_{\mathbb{R}^-} + K_{\text{bdy, left}}\right) + \left(K_{\text{CFT}}\big|_{\mathbb{R}^+} + K_{\text{bdy, right}}\right). \tag{5.64}$$

These two half-line entanglers are exactly like the ones we proposed above, in Eqs. (5.48)-(5.50).

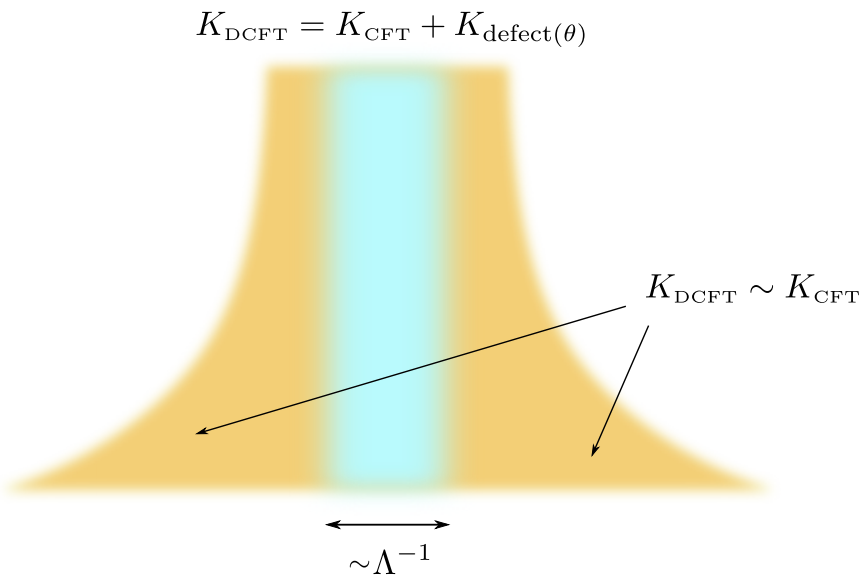

Figure 5.6: Our cMERA for the DCFT only differs from the cMERA for the CFT within distances $\sim \Lambda^{-1}$ of defect. Compare as well with Figure 5.1 (right).

As for the BCFT case above, the analogy between this cMERA and the original one for the CFT becomes transparent in the language of momentum modes (5.31), where the DCFT entangler reads

$$K_{\text{DCFT}} = \frac{1}{2}\int dk\; g(k)\,\phi(k)\pi(k)^\dagger + \text{h.c.}, \tag{5.65}$$

thus mimicking Eq. (3.30). Together, L and K_{DCFT} generate, for the new momentum modes, the same cMERA evolution from (3.32),

$$\partial_s \phi(k,s) = -i[L + K_{\text{DCFT}}, \phi(k)] = -\left(k\partial_k + \frac{1}{2} + g(k)\right)\phi(k,s), \tag{5.66}$$

$$\partial_s \pi(k,s) = -i[L + K_{\text{DCFT}}, \pi(k)] = -\left(k\partial_k + \frac{1}{2} - g(k)\right)\pi(k,s), \tag{5.67}$$

and once more, the cMERA state can be defined during the evolution by annihilation operators of a certain familiar form:

$$\left(\sqrt{\frac{\alpha(k,s)}{2}}\phi(k) + i\sqrt{\frac{1}{2\alpha(k,s)}}\pi(k)\right)|\Psi^\Lambda(s)\rangle_{\text{DCFT}} = 0 \tag{5.68}$$

with $\alpha(k,s)$ given in terms of the entangler profile $g(k)$ by (3.35). The same line of reasoning as above allows now to find the correlation functions for $|\Psi^\Lambda\rangle_{\text{DCFT}}$, in terms of those of the original cMERA:

$$\langle\phi(x)\phi(y)\rangle = \mathcal{C}^\Lambda_{\phi\phi}(x-y) + c_\theta(x,y)\,\mathcal{C}^\Lambda_{\phi\phi}(|x|+|y|), \tag{5.69}$$

$$\langle\pi(x)\pi(y)\rangle = \mathcal{C}^\Lambda_{\pi\pi}(x-y) + c_\theta(x,y)\,\mathcal{C}^\Lambda_{\pi\pi}(|x|+|y|), \tag{5.70}$$

and the same conclusions thus apply to the defect cMERA: its fixed point succeeds at approximating the long distance physics of its target state

$$|\Psi^\Lambda\rangle_{\text{DCFT}} \overset{\text{LD}}{\sim} |\Psi\rangle_{\text{DCFT}}, \tag{5.71}$$

while its short distance behaviour is regulated by the UV cutoff.

Figures 5.7 and 5.8 show examples of defect cMERA correlators to provide evidence for these claims. They were obtained using the Gaussian entangler profile (3.38) from Chapter 3. Note that since we are taking the absolute value to be able to make the vertical axis logarithmic, we cannot distinguish the defects that differ on a sign flip, namely those with opposite values of θ. Thus, we only include plots for $\theta \in (0, \pi/2)$. In both figures, we observe how the cMERA reproduces the correlator accurately at long distances (as always, in terms of Λ^{-1}), far from the limit where both field insertions coincide. On the other hand, in this limit, the defect cMERA correlator deviates from the DCFT correlator and goes to a constant, while the latter shows a UV divergence. As we argued in Chapter 3, this provides evidence of the UV regularized character of the cMERA state. (Remember that cMERA correlators do show a delta function divergence when the two field insertions coincide. This term corresponds to the UV structure of the initial state $|\Omega\rangle$ they were made from, and is not shown in the figures). The part of the correlator where one field insertion is close to the defect will be accurately described if the other field insertion is far away, as in Figure 5.7, and not so much if the other field insertion is within Λ^{-1} of the defect, as in Figure 5.8.

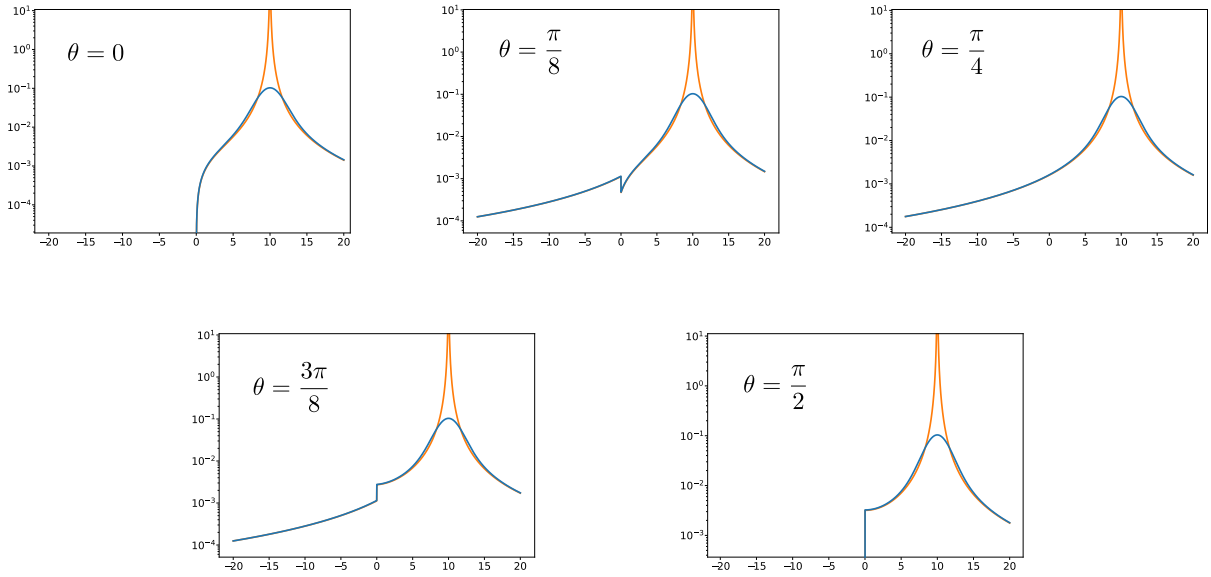

Figure 5.7: $|\langle\pi(10\Lambda^{-1})\pi(x)\rangle|$ correlator as a function of Λx for the defect cMERA (blue) and the defect CFT (orange). Delta functions in the cMERA correlator are not shown.

5.4 Discussion

In this chapter we have seen the very basics of both boundary cMERA and defect cMERA: how the sharp cut of a boundary or interface can be reconciled with the quasi-local nature of the entangler, how the theory of minimal updates for MERA generalizes to the continuum, and how the resulting cMERA fixed point states display the usual interpolatory character between the physics of the target state in the IR and that of the initial unentangled state in the UV. There are still, however, many interesting additional aspects of these constructions that can be studied [3]. One of them is, e.g., their application to the study of boundary critical phenomena. Much like fixed point cMERA states, fixed point boundary cMERA states support a full representation of the subgroup of conformal symmetries that characterize their target BCFT, where, for instance, the generator of scale transformations replaced by the generator of the boundary cMERA evolution. This allows for the extraction of conformal data from the BCFT in an analogous fashion to the cMERA. The same applies for the defect cMERA. In fact, once we are able to include defects in the formalism, their fusion rules can be studied, running the cMERA evolution backwards to coarse-grain space: once the defects get within a distance $\sim \Lambda^{-1}$ of each other, the cMERA should stop

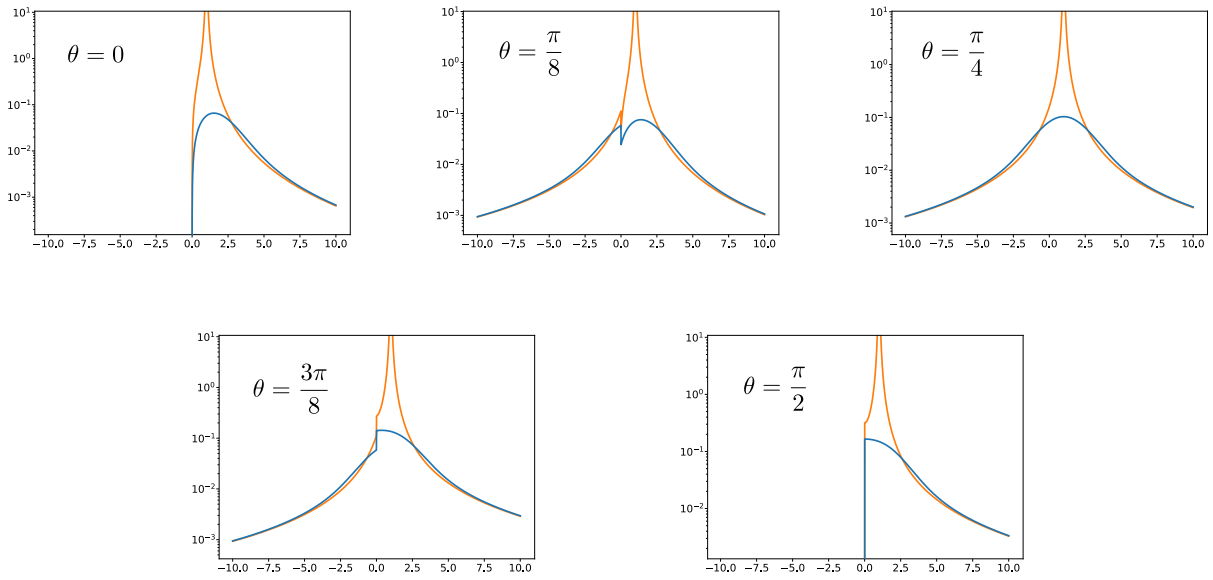

Figure 5.8: $|\langle\pi(\Lambda^{-1})\pi(x)\rangle|$ correlator as a function of Λx for the defect cMERA (blue) and the defect CFT (orange). Delta functions in the cMERA correlator are not shown.

resolving them, giving rise to defect fusion[8]. Of course, for that to happen, we have to allow for defects sitting in places other than the origin: the cMERA scale transformations will then move such defects around, and the entangler K_{DCFT} will have to acquire an s-dependence to follow them.

Although we have been focusing on noninteracting examples, because they are the ones we know how to work with, we expect that the minimal update conjecture for cMERA will hold similarly in the interacting case. Along these lines, another interesting facet of these constructions is their interplay with the magic cMERA (recall Sections 2.6 and 4.3). It turns out, boundary and defect cMERAs built from the magic free boson cMERA inherit its features. In particular, it is possible to write the modified entanglers as continuous matrix product operators (cMPOs), leaving thus the door open to studying interacting theories numerically also in the presence of boundaries and defects.

[8]This same principle is used in the MERA to study the fusion algebra of scaling operators in critical systems, bringing them to distances of the order of the lattice spacing by coarse-graining [51].

This chapter's takeaways:

- We have built examples of cMERAs for the massless free boson in the presence of *conformal boundaries* and *defects*. Their fixed point states serve as long distance approximations to the ground states of their target boundary/defect CFT.
- Our examples provide evidence for the cMERA version of the *minimal update conjecture*: the modification required by the entangler is mostly supported within distance $\sim \Lambda^{-1}$ of the defect, in what could constitute the continuum version of a MERA *causal cone*. We expect this conjecture to also hold in the interacting case.

Chapter 6

Emergent universal entanglement algebra in critical lattice systems

This chapter's goal: In this chapter we study a manifestation of universality in critical lattice systems: an emergent approximate representation of the Virasoro algebra on the eigenvectors of reduced density matrices in lattice systems at criticality.

6.1 Introduction

The study of entanglement structures in quantum many-body systems is such a broad topic that, while staying within its boundaries, in this chapter we completely change gears with respect to the rest of this thesis: we are going to be presenting results about lattice systems, and the analysis we present is going to be practically devoid of tensor network references (even though we could expect tensor network techniques to be of use in future studies, since they already have been very successful in related approaches to conformal data extraction from quantum critical systems [151–153]). Therefore, we invite the reader to enjoy the interlude.

In this chapter we are going to be talking about *emergence of universal behaviour*: the appearance in critical lattice systems of structures that only depend on the universality class of the quantum phase transition, and are therefore independent of the particular microscopic realization thereof. In particular, we will be focusing on the appearance of such structure in the entanglement patterns of one-dimensional systems, more specifically

on the spectral decomposition of reduced density matrices. Since the universality classes of quantum phase transitions in 1+1 dimensions are labeled by 2d CFTs, these universal emergent structures will be dependent on the associated *conformal data* (which were introduced in Section 1.4). A few examples follow that will be useful to both clarify what we are referring to and motivate the research in this chapter.

The most paradigmatic example of an entanglement-related quantity exhibiting universal behaviour at criticality is one that we have already mentioned in previous chapters. The scaling of the entanglement entropy of an interval of size L is logarithmic with a universal prefactor given in terms of the central charge of the underlying CFT [44, 45, 154]:

$$S(L) \sim \frac{c}{3} \log L. \tag{6.1}$$

This phenomenon can be used to both identify critical systems and obtain an approximation to the central charge of the CFT that describes them, just from the knowledge of the entanglement entropy for different interval sizes.

Entanglement entropy is just a coarse-grained version of the information contained in the spectrum of the reduced density matrices, the so-called *entanglement spectrum*. If we know the full spectrum of the reduced density matrices, we can access the low-lying spectrum of a *boundary* conformal field theory that describes the system [155–159]. A justification of this fact is given in one of the review sections in this chapter.

Here we give one step further and take a look at the eigenvectors of the reduced density matrix. In a (B)CFT, from the same argument that links entanglement spectrum and scaling dimensions, the eigenvectors turn out to be a natural basis for a representation on the interval of the Virasoro algebra, that we can write in terms of the Hamiltonian and momentum densities of the theory. On the lattice, and in the long distance/low energy limit (where we can expect the correspondence between the continuum description and the discrete realization) this results in an emergent non-trivial set of relations between the operators in the lattice Hamiltonian and the eigenvectors of the reduced density matrix, which we name the *entanglement algebra*.

This chapter is organized as follows: in Section 6.2 we review boundary conformal field theories, which will be needed in Section 6.3, where we review the computations that we need to justify the presence of the emergent entanglement algebra in the eigenvectors of critical lattice systems. Then we translate these statements to approximate lattice versions and check them in the example of the Ising model in Section 6.4.

6.2 Boundary conformal field theory

We have already come across the notion of a boundary conformal field theory in the previous chapter, with the example of the free boson. Let us know delve a little bit deeper into the mathematical structure of BCFTs. It is not our aim here to be exhaustive or fully rigorous; the reader in search for a more comprehensive review is invited to consult [39, 40, 46, 160–162].

Conformal field theory: Virasoro generators and the energy-momentum tensor

Recall from Chapter 1 that CFTs are quantum field theories that are symmetric under the conformal group. This makes them particularly useful to describe critical systems, which are scale invariant. In the particular case of 2d CFTs, conformal invariance gives rise to an infinite dimensional algebra of infinitesimal symmetries, given by the tensor product of two copies of the Virasoro algebra Vir, respectively spanned by the Virasoro generators $\{L_n\}_{n\in\mathbb{Z}}$ and $\{\bar{L}_n\}_{n\in\mathbb{Z}}$:

$$\begin{aligned}
[L_m, L_n] &= (n+m)L_{n+m} + \frac{c}{12}m(m^2-1)\delta_{m+n,0}, \\
[L_m, \bar{L}_n] &= 0, \\
[\bar{L}_m, \bar{L}_n] &= (n+m)\bar{L}_{n+m} + \frac{c}{12}m(m^2-1)\delta_{m+n,0}.
\end{aligned}$$

L_n and $\bar{L}_n$ act on the Hilbert space of the theory and generate infinitesimal conformal transformations (which in 2d amounts to generating infinitesimal holomorphic maps). For instance, in the radial quantization scheme we use below, $L_0 + \bar{L}_0$ is the generator of scale transformations and its eigenvalues $\{\Delta_\alpha\}$ are the scaling dimensions of the theory, while $i(L_0 - \bar{L}_0)$ is the generator of rotations and its eigenvalues $\{is_\alpha\}$ are (i times) the conformal spins of the theory. The common eigenvectors of L_0 and $\bar{L}_0$ are thus in correspondence to the scaling fields (this is an aspect of the so-called *state-operator correspondence*), and provide a natural basis for the Hilbert space of the CFT, which, in the language of Lie algebra theory, is made of highest-weight representations with highest-weight vectors associated to the primary fields.

The Virasoro generators are intimately related to the energy-momentum tensor $T_{\mu\nu}$ of the theory, so let us talk a little bit about it. The energy-momentum tensor $T_{\mu\nu}$, the conserved current associated to translation symmetry, is a crucial field present in any CFT. In 2d CFTs, we usually work in complex coordinates:

$$z \equiv x + iy, \qquad z \equiv x - iy, \tag{6.2}$$

so that

$$T_{zz} = \frac{1}{4}\left(T_{xx} - T_{yy}\right) + \frac{1}{4i}\left(T_{xy} + T_{yx}\right), \tag{6.3}$$

$$T_{\bar{z}\bar{z}} = \frac{1}{4}\left(T_{xx} - T_{yy}\right) - \frac{1}{4i}\left(T_{xy} + T_{yx}\right). \tag{6.4}$$

Conformal invariance forces the other two components to vanish (requiring the tracelessness of the stress-energy tensor), as well as

$$\partial_{\bar{z}} T_{zz} = \partial_z T_{\bar{z}\bar{z}} = 0, \tag{6.5}$$

which imply that T_{zz} is a *holomorphic* field (it can be taken to depend only on z as a complex variable) and $T_{\bar{z}\bar{z}}$ is an *antiholomorphic field* (it depends only on $\bar{z}$, i.e. it is a holomorphic function with respect to $x - iy$, rather than $x + iy$). It is then usual to work with the so-called *renormalized* energy-momentum tensor components[1]

$$T(z) \equiv -2\pi T_{zz}, \qquad \bar{T}(\bar{z}) \equiv -2\pi T_{\bar{z}\bar{z}}. \tag{6.6}$$

In *radial quantization* we foliate $\mathbb{R}^2$ by circumferences centered at the origin $z = 0$, and define the Hilbert space of the theory on them. The Virasoro generators are then defined as the Laurent modes of these components,

$$L_n \equiv \frac{1}{2\pi i}\oint dz\; z^{n+1} T(z), \qquad \bar{L}_n \equiv \frac{1}{2\pi i}\oint d\bar{z}\; \bar{z}^{n+1} \bar{T}(z), \tag{6.7}$$

where the integration happens along a circle around the origin. It is thus fair to say that, through its mode decomposition, the energy-momentum tensor generates all infinitesimal conformal transformations on the Hilbert space.

$T(z)$ and $\bar{T}(\bar{z})$ are not primary fields. Instead of (1.16), they satisfy a modified transformation law under holomorphic maps $z \mapsto w(z)$:

$$T'(w) = \left(\frac{dw}{dz}\right)^{-2}\left(T(z) - \frac{c}{12}\{w; z\}\right), \qquad \bar{T}'(\bar{w}) = \left(\frac{d\bar{w}}{d\bar{z}}\right)^{-2}\left(T(\bar{z}) - \frac{c}{12}\{\bar{w}; \bar{z}\}\right), \tag{6.8}$$

which are the transformation laws of a primary field with conformal dimensions $(h, \bar{h}) = (2, 0)$ and $(h, \bar{h}) = (0, 2)$, for T and $\bar{T}$ respectively, with an additional term proportional to the central charge c and the *Schwarzian derivative*:

$$\{w; z\} \equiv \left(\frac{d^3 w}{d^3 z}\right)\left(\frac{dw}{dz}\right)^{-1} - \frac{3}{2}\left(\frac{d^2 w}{d^2 z}\right)^2\left(\frac{dw}{dz}\right)^{-2}. \tag{6.9}$$

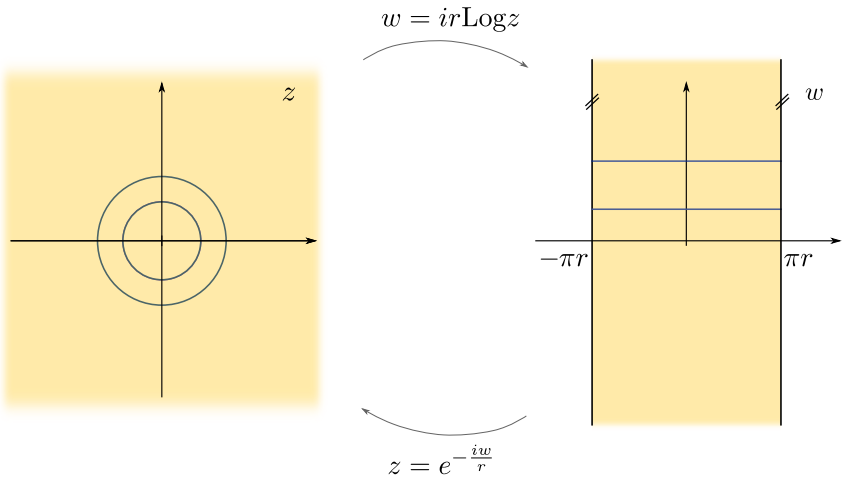

Figure 6.1: Conformal mappings between the complex plane and the infinite cylinder.

Knowing the transformation properties of the energy-momentum tensor allows us to map the Virasoro generators between geometries related by a conformal transformation. One of the most well-known examples of this procedure involves the mapping between the theory on the complex plane (in radial quantization) to the theory on a cylinder of radius r, obtained by the conformal map

$$z = e^{-\frac{iw}{r}}, \tag{6.10}$$

where z is the complex coordinate parametrizing the plane and w the one parametrizing the cylinder (note that its real part should be understood as being $2\pi r$-periodic). For example, the generator of scale transformations $L_0 + \bar{L}_0$ on the plane is related to the Hamiltonian operator H_{cyl} that generates translations along the cylinder:

$$\begin{aligned} L_0 + \bar{L}_0 &= \frac{1}{2\pi}\int_0^{2\pi} dt \left(e^{2it}T(e^{it}) + e^{-2it}\bar{T}(e^{-it})\right) \\ &= \frac{c}{12} - \frac{r^2}{2\pi}\int_{-\pi r}^{\pi r} dx \left(T'(x) + \bar{T}'(x)\right) \\ &= \frac{c}{12} + rH_{\text{cyl}} \end{aligned} \tag{6.11}$$

[1]We warn the reader that some references may adopt a convention in which the minus signs in this definition are dropped.

Here the first equality comes from Eq. (6.7). The second one follows from applying the transformation rules (6.8) for T and $\bar{T}$ (here $T', \bar{T}'$ represent the stress-energy tensor of the cylinder, and x parametrizes the circumference around it). Finally, the third equality comes from identifying the Hamiltonian operator as the integral of the Hamiltonian density:

$$h(x) \equiv -\frac{T'(x) + \bar{T}'(x)}{2\pi}, \qquad H_{\text{cyl}} \equiv \int_{-\pi r}^{\pi r} dx\, h(x) \tag{6.12}$$

Equation 6.11 relates the spectrum of scaling dimensions of the CFT with that of the Hamiltonian on the cylinder, and has therefore been extensively used. In particular, it underlies the extraction of conformal data from the diagonalization of the Hamiltonian of a lattice model on the circle [163–167]; and together with analogous expressions for other Virasoro operators [168] it has been proved useful to identify the conformal towers of the CFT, also in a lattice context [151].

Boundary conformal field theory: half of the above

In Chapter 5 we already introduced boundary conformal field theories (BCFTs), as the result of placing a CFT on a manifold with a boundary, where a conformal boundary condition is imposed. Its study was initiated by Cardy, and Cardy and Lewellen in [46, 169–171]. Good introductions can be found in [160, 162, 172]. The reason BCFT is going to be important for us in this chapter is that the reduced density matrix of an interval can be represented via a path integral on a manifold with boundaries, as we will see below.

A 2d BCFT is similar in many aspects to a 2d CFT, but due to the presence of the boundary, it presents only half of the symmetry. The paradigmatic example of a BCFT is that of a CFT defined on the upper half-plane $H = \{(x, y)|y > 0\} \subset \mathbb{R}^2$. Such a theory keeps translation invariance along the x-axis, but not along the y-axis, because of the presence of the boundary. Similarly, scale invariance is preserved but rotation invariance is lost. Doing the counting, the symmetry algebra of a BCFT turns out to be *a single copy* of the Virasoro algebra, rather than two copies: it is consequently generated on the Hilbert space by a single family of generators L_n.

Radial quantization can be performed on the upper half-plane. The Hilbert space now is associated with semicircles that end at the conformal boundaries $\mathbb{R}^+$ and $\mathbb{R}^-$, and depends on the choice of boundary conditions (b.c.). For the real axis to be a conformal boundary, the energy-momentum tensor components have to satisfy:

$$T(x) = \bar{T}(x) \qquad x \in \mathbb{R} \tag{6.13}$$

The boundary conditions allow for a definition of the stress-energy tensor on the *lower* half-plane, via analytic continuation. Indeed, $T(z)$ is a holomorphic (i.e., analytic) function of z, and $\bar{T}(\bar{z})$ is a holomorphic function of $\bar{z}$, both of which coincide on a subset of the complex plane (the boundary $\mathbb{R}$) which has an accumulation point. It follows that the analytic continuation to the lower half-plane of T is given by the values of $\bar{T}$ in the upper half-plane (this is a bit confusing to write in the usual notation so, inspired by [160], for this equation we write both arguments of T and $\bar{T}$):

$$T(z, z^*) = \bar{T}(z^*, z) \qquad \forall z \in \mathbb{C}. \tag{6.14}$$

This allows us to keep the original definitions of L_n and $\bar{L}_n$ as modes of the energy-momentum tensor, even if the integration contour around the origin has to leave the upper half-plane at some point, since we can define the values of T on the lower half-plane via those of $\bar{T}$ on the upper half-plane and vice versa:

$$L_n \equiv \frac{1}{2\pi i} \int_{\mathcal{C}} \left[dz \; z^{n+1} T(z) - d\bar{z} \; \bar{z}^{n+1} \bar{T}(\bar{z}) \right], \tag{6.15}$$

where the integration contour $\mathcal{C}$ is a semicircle in the upper half-plane going counterclockwise around the origin. Under this definition, L_n can be seen to be identical to $\bar{L}_n$ for all $n \in \mathbb{Z}$, resulting in the aforementioned reduction to a single copy of Vir, the symmetry algebra of a BCFT. The spectrum of a BCFT is now given by the eigenvalues of L_0, as the generator of scale transformations, and depends on the boundary conditions. This is the spectrum that, as mentioned in the introduction to this chapter, can be seen emerging in the entanglement spectrum of reduced density matrices. We can justify this by means of a mapping of Virasoro generators to a different geometry, much as the example from (6.11), but for that we will have to move on to the next section.

6.3 BCFT and reduced density matrices

The object of our interest in this chapter is the reduced density matrix ρ of an interval of the real line, in the ground state of a critical theory. An important operator is the *entanglement Hamiltonian*, defined as

$$H_E \equiv -\frac{1}{2\pi} \log \rho \qquad \Longrightarrow \; \rho = e^{-2\pi H_E}. \tag{6.16}$$

Sometimes the term "entanglement spectrum" may be used to talk about the spectrum of H_E instead of ρ_I, which is not too much of a problem since they are related by the

definition above. In a CFT, the entanglement Hamiltonian can be expressed as a spatial integral of energy-momentum components [173, 174]:

$$H_E = \frac{-1}{2\pi}\int_I dx \frac{(R^2-x^2)}{2R}\big(T(x)+\bar{T}(x)\big), \tag{6.17}$$

which should be understood as an equality up to a constant that ensures the normalization of ρ_I. The entanglement Hamiltonian can be related to the Virasoro generator L_0 of an associated BCFT, thus connecting the entanglement spectrum with the spectrum of the BCFT. In this section we are going to see how this can be done, and how we can obtain expressions analogous to (6.17) not only for L_0 but for all Virasoro generators.

In two-dimensional QFT, the reduced density matrix ρ_I of an interval $I = (-R, R)$ can be written by means of a Euclidean path integral. To see how, consider $\mathbb{R}^2$ with Euclidean coordinates (x, τ). Recall that the Euclidean path integral on a half-plane gives rise, up to normalization, to the ground state of the theory.

$$\langle\varphi(x)|0\rangle = \int_{\phi(x,0)=\varphi(x)} [D\phi]_{\tau<0}\, e^{-S[\phi]}, \tag{6.18}$$

where $|\varphi(x)\rangle$ is the corresponding field configuration eigenstate:

$$\phi(x)|\varphi(x)\rangle = \varphi(x)|\varphi(x)\rangle. \tag{6.19}$$

This is justified by the fact that the Hamiltonian H is the generator of Euclidean time evolution, so we have

$$\langle\varphi(x)|e^{-\Delta\tau\, H}|\varphi'(x)\rangle = \int_{\substack{\phi(x,0)=\varphi(x)\\ \phi(x,-\Delta\tau)=\varphi'(x)}} [D\phi]_{\tau\in(-\Delta\tau,0)}\, e^{-S[\phi]}, \tag{6.20}$$

and to get (6.18) we just need to make $\Delta\tau \to \infty$ so that $e^{-\Delta\tau H}$ effectively "projects" onto the ground state. Thus, the density matrix $|0\rangle\langle 0|$ for the full ground state can be represented by juxtaposing the representations of $|0\rangle$ and $\langle 0|$ on the lower and upper half-planes, respectively:

$$\langle\varphi^-(x)|0\rangle\langle 0|\varphi^+(x)\rangle = \int_{\phi^-(x,0)=\varphi^-(x)} [D\phi^-]_{\tau<0}\, e^{-S[\phi^-]} \int_{\phi^+(x,0)=\varphi^+(x)} [D\phi^+]_{\tau>0}\, e^{-S[\phi^+]}, \tag{6.21}$$

where we have used superindices $\pm$ to distinguish the two fields we integrate over (one on each half-plane), and their two boundary conditions on the horizontal line $\tau = 0$. Now to

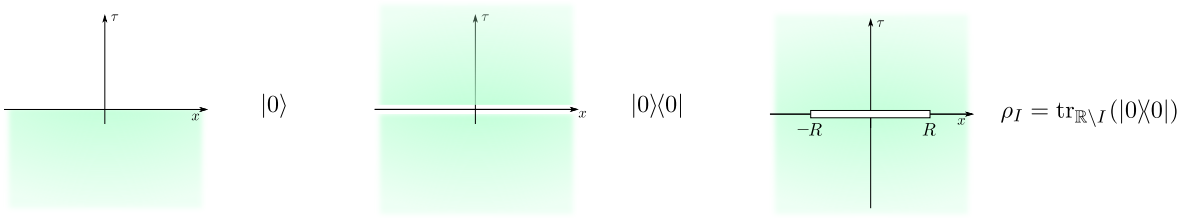

Figure 6.2: Path integral representations of the vacuum, the vacuum density matrix, and the reduced density matrix.

obtain the reduced density matrix ρ_I we just need to trace out (i.e., integrate over) the field outside the interval I:

$$\langle \varphi_I^-(x)|\rho_I|\varphi_I^+(x)\rangle = \int_{\mathcal{B}} [D\phi^-]_{\tau<0}[D\phi^+]_{\tau>0}\, e^{-S[\phi^-]-S[\phi^+]}, \tag{6.22}$$

where the boundary conditions are

$$\mathcal{B} \equiv \begin{cases} \phi^+(x,0) = \varphi_I^+(x), \quad \phi^-(x,0) = \varphi_I^-(x) & x \in I, \\ \phi^+(x,0) = \phi^-(x,0) & x \notin I. \end{cases} \tag{6.23}$$

Thus the path integral over this manifold produces the reduced density matrix of the ground state on I. If we tried to compute the entanglement entropy from it, however, it would turn out to be divergent for usual QFTs without UV cutoffs, as we already mentioned in Chapter 3. This is due to the contribution of arbitrarily short-range entanglement close to the interval's boundaries $x = \pm R$. To regularize it, we follow [157, 159] and remove from the path integral two discs of radius ϵ centered at the extremes of the interval. This step introduces boundaries in the system, and is responsible for us having to invoke BCFT. These boundaries will carry some conformal boundary conditions (which will contribute the universal Affleck-Ludwig correction to the entanglement entropy [175]).

The manifold over which we path integrate to obtain ρ_I can be obtained by a conformal map from a semiannulus, the area of the upper half-plane between two semicircumferences centered at the origin [157]. This is good news because it allows us to relate L_0 and ρ_I. Indeed, on the upper half-plane, L_0 is the generator of scale transformations that map semicircumferences to other semicircumferences. The path integration over the semiannulus is thus generated by L_0, in the same way that the Hamiltonian, being the generator of time translations, gave rise to the path integral in (6.20).

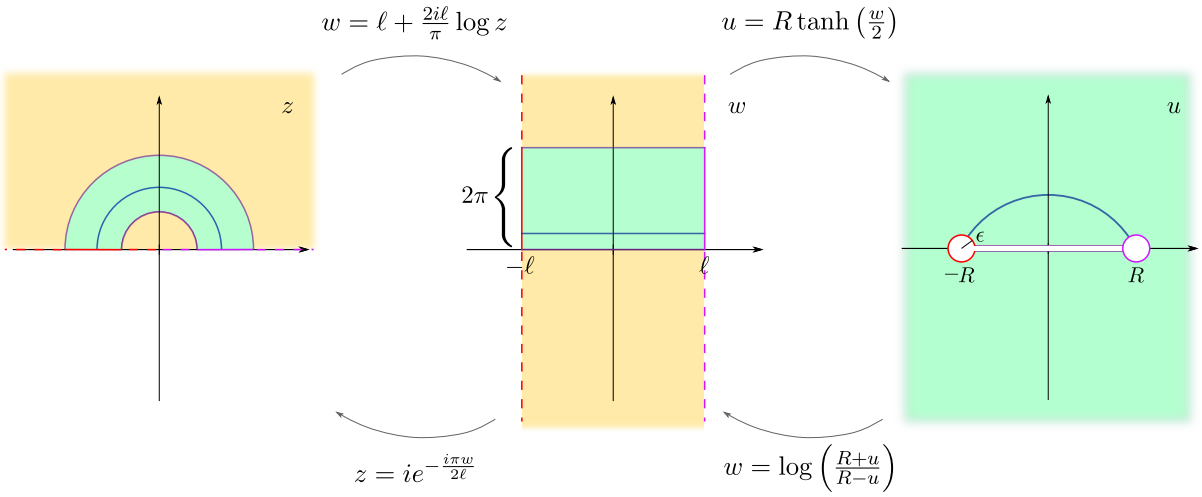

Figure 6.3: Conformal mappings between the upper half-plane, the infinite strip, and the path integral representation of ρ_I regularized by removing two discs at the entanglement cut.

The actual mapping is easier to follow as a two-step process, depicted in Figure 6.3. First, we map the upper half-plane (complex coordinate z) to an infinite strip of width 2ℓ (complex coordinate w), by

$$w = \ell + \frac{2i\ell}{\pi} \log z. \tag{6.24}$$

The original semiannulus is then mapped to a rectangle. This map is similar to the one we used in (6.10) to map the complex plane to the cylinder. Secondly, we map the rectangle to the manifold over which we path integrate to obtain ρ_I (complex coordinate u). This is accomplished by the map

$$u = R \tanh\left(\frac{w}{2}\right). \tag{6.25}$$

To be completely precise, the boundaries of the rectangle ($\mathrm{Re}\, w = \pm\ell$) get mapped to circumferences

$$\pm R\left(1 + \frac{2}{e^{2\ell} - 1} + \frac{2e^{\ell+it}}{e^{2\ell} - 1}\right) \qquad t \in (0, 2\pi), \tag{6.26}$$

which for $\ell \gg 1$ reduce to

$$\pm R\left(1 + 2e^{-\ell+it}\right) \qquad t \in (0, 2\pi). \tag{6.27}$$

This approximates well enough the geometry we obtained by removing two disks of radius

$$\epsilon = 2e^{-\ell}R \tag{6.28}$$

around the entangling points $\pm R$. Note that ℓ, the width of the intermediate strip, ends up controlling our UV cutoff ϵ.

Now the Virasoro generators can be "sent over" these conformal maps: the goal is to obtain a representation of L_n on the Hilbert space of the interval I, as spatial integrals of energy-momentum tensor components. We use for that the transformation rules from (6.8). The first mapping takes

$$L_n = \frac{1}{2\pi}\int_0^\pi dt\, \left[e^{i(n+2)t}\, T(e^{it}) + e^{-i(n+2)t}\, \bar{T}(e^{it})\right] \tag{6.29}$$

to

$$L_n = -\frac{\ell}{\pi^2}\int_{-\ell}^{\ell} dx\, \left[e^{-\frac{in\pi}{2\ell}(x-\ell)}\, T(x) + e^{\frac{in\pi}{2\ell}(x-\ell)}\, \bar{T}(x)\right] + \frac{c}{24}\delta_{n,0}. \tag{6.30}$$

The first integral is over the semicircumference $z = e^{it},\ t \in (0,\pi)$ and the second one over the interval $w = x,\ x \in (-\ell, \ell)$. Here we have dropped the primes in the energy-momentum tensor components, but of course in (6.29) $T, \bar{T}$ denote the energy-momentum tensor on the upper half-plane, while in (6.30) they denote the one on the strip, which is related to the previous one by (6.8). Note that the case $n = 0$ is similar to how we related $L_0 + \bar{L}_0$ to the cylinder Hamiltonian in Section 6.2: now we are mapping L_0 to the Hamiltonian on the strip, which is written in terms of the Hamiltonian density on the strip in a way analogous to (6.11). We then apply the second map to obtain

$$\begin{aligned} L_n = -\frac{\ell}{\pi^2}\int_{-R+\epsilon}^{R-\epsilon} dx\, \frac{R^2 - x^2}{2R}\, \left[e^{-\frac{in\pi}{2\ell}\left(\log\left(\frac{R+x}{R-x}\right)-\ell\right)} T(x) + e^{\frac{in\pi}{2\ell}\left(\log\left(\frac{R+x}{R-x}\right)-\ell\right)} \bar{T}(x)\right] \\ + \frac{c}{24}\left(1 + \frac{4\ell^2}{\pi^2}\right)\delta_{n,0} \end{aligned} \tag{6.31}$$

in terms of the stress-energy tensor components in the u geometry. Here the variable x is used to parametrize the interval I: note that we integrate over $(-R+\epsilon, R-\epsilon)$ because of the disks we removed. Setting $n = 0$ gives an affine relation between L_0 and the entanglement Hamiltonian given by (6.17), as announced. This implies that not only their eigenvalues are related, but also their eigenvectors are the same: the eigenvectors of the reduced density matrix thus provide a natural basis for the representation of the Virasoro algebra given by (6.31), which we call the *entanglement algebra*. These eigenvectors will be mapped to each other by the L_n operators following the rules dictated by the operator content of the BCFT. In the next section, we propose an approach to try to observe this structure emerging on the lattice, following the example of the critical Ising model.

6.4 Emergent entanglement algebra in the Ising model

The critical Ising model on an infinite 1d lattice of spin-$\frac{1}{2}$ degrees of freedom is defined by the Hamiltonian

$$H = -\frac{1}{2}\sum_{j\in\mathbb{Z}} (X_j X_{j+1} + Z_j) \tag{6.32}$$

where X_j, Z_j are the Pauli operators at site j. We set the lattice spacing to 1, and consider the reduced density matrices of intervals of N sites:

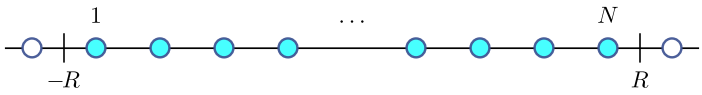

The underlying CFT for the Ising model is a minimal model with two nonidentity primary fields: the spin density σ, and the energy density ε, whose conformal dimensions are

$$h_\sigma = \bar{h}_\sigma = \frac{1}{16}, \quad h_\varepsilon = \bar{h}_\varepsilon = \frac{1}{2}. \tag{6.33}$$

As explained in the main text, the Hilbert space of the CFT on a manifold with boundaries depends on the boundary conditions. The Ising CFT admits three conformal boundary conditions that correspond in the statistical spin model to fixing the boundary spins to be up or down, or leaving them free. It is the latter that should be observed in our circumstances [158], and indeed we observe results compatible with the presence of free boundary conditions on both entanglement cuts. The Hilbert space consists then of the conformal towers of the identity and energy density operators. Figure 6.4 represents the 18 lowest energy states.

In order to realize the entanglement algebra on a lattice model, it seems natural to try to apply some discretization procedure to the continuum operators. Let us first rewrite (6.31) in terms of the Hamiltonian and momentum densities:

$$h(x) = -\frac{1}{2\pi}\left(T(x) + \bar{T}(x)\right), \tag{6.34}$$

$$p(x) = \frac{1}{2\pi}\left(\bar{T}(x) - T(x)\right). \tag{6.35}$$

We obtain

$$L_n = \frac{\ell}{\pi R}\int_{-R+\epsilon}^{R-\epsilon} dx\, \left(R^2 - x^2\right)\left[\cos n\theta(x)\, h(x) + i \sin n\theta(x)\, p(x)\right] + \left(\frac{c}{24} + \frac{c\ell^2}{6\pi^2}\right)\delta_{n,0}, \tag{6.36}$$

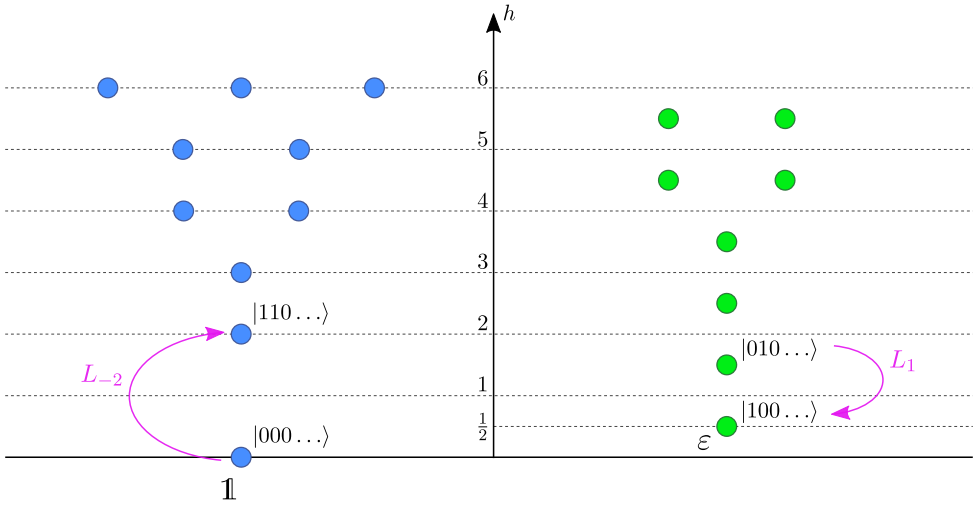

Figure 6.4: Operator content of the Ising CFT with free boundary conditions. The Hilbert space decomposes into the direct sum of two modules, or conformal towers, each of them closed under the action of the Virasoro generators L_n. We use the horizontal axis only to resolve degeneracies. Note that in the free fermion language the two towers correspond to the two sectors of different fermion parity.

where we abbreviated

$$\theta(x) \equiv \frac{\pi}{2\ell} \log\left(\frac{R+x}{R-x}\right) - \frac{\pi}{2}. \tag{6.37}$$

To turn these integrals into discrete sums we need thus a discretization for h and p. The local Hamiltonian terms from (6.32) are a natural candidate for h, though they leave the door open for ambiguities, while for p we could apply the technique from Appendix A in [151]. Since we are working with the Ising model, however, we proceed in a slightly more sophisticated manner and import the results from [153], where a relation is established between lattice operators at given effective positions and series of CFT operators of increasing scaling dimensions. The authors of this work propose a method to obtain the coefficients of the series via numerical optimization. In the Supplementary Material, however, they also compute the coefficients analytically for the particular case of the critical Ising model, thanks to its free fermion representation. We shall hence use the following

expansions from [153]:

$$Z_i\,[i] \sim \frac{2}{\pi}\mathbb{1} - h + \frac{1}{\pi}\varepsilon, \tag{6.38}$$

$$X_iX_{i+1}\left[i+\frac{1}{2}\right] \sim \frac{2}{\pi}\mathbb{1} - h - \frac{1}{\pi}\varepsilon, \tag{6.39}$$

$$X_iY_{i+1}\left[i+\frac{3}{4}\right] \sim -2p + \frac{i}{2\pi}\partial_\tau\varepsilon, \tag{6.40}$$

$$Y_iX_{i+1}\left[i+\frac{1}{4}\right] \sim 2p + \frac{i}{2\pi}\partial_\tau\varepsilon, \tag{6.41}$$

where we indicate the effective position of the lattice operator in square brackets. We thus establish approximate discretizations

$$h \sim \frac{2}{\pi}\mathbb{1} - \frac{1}{2}X_iX_{i+1}\left[i+\frac{1}{2}\right] - \frac{1}{2}Z_i\,[i]\,, \qquad p \sim \frac{1}{2}Y_iX_{i+1}\left[i+\frac{1}{4}\right] - \frac{1}{2}X_iY_{i+1}\left[i+\frac{3}{4}\right] \tag{6.42}$$

and use them to discretize (6.31). This way we define

$$\begin{aligned} L_n^{\text{lat}} \equiv \frac{\ell}{N\pi}\Bigg\{ &-\sum_{j=1}^{N}\left[\left(\frac{N^2}{4}-x_j^2\right)\cos\left(n\theta(x_j)\right)Z_j\right] \\ &-\sum_{j=1}^{N-1}\left[\left(\frac{N^2}{4}-x_{j+\frac{1}{2}}^2\right)\cos\left(n\theta(x_{j+\frac{1}{2}})\right)X_jX_{j+1}\right. \\ &\quad+\frac{i}{2}\left(\frac{N^2}{4}-x_{j+\frac{3}{4}}^2\right)\sin\left(n\theta(x_{j+\frac{3}{4}})\right)X_jY_{j+1} \\ &\quad\left.-\frac{i}{2}\left(\frac{N^2}{4}-x_{j+\frac{1}{4}}^2\right)\sin\left(n\theta(x_{j+\frac{1}{4}})\right)Y_jX_{j+1}\right]\Bigg\}, \end{aligned} \tag{6.43}$$

where $x_j = -(N+1)/2 + j$, and we have dropped the constant terms. To compute these operators we need to fix ℓ, or equivalently ϵ. As a first approximation, one can set $\epsilon = 1/2$, equal to half the lattice spacing. However, the accuracy of the represention can be improved dramatically, by optimizing over possible choices of ϵ [4]. In the results below we use the value resulting of an optimization of the first eigenvalue of the entanglement Hamiltonian, $\epsilon = 0.0369$ [176].

Another advantage of this example is that the Ising model can be solved by mapping it to free fermions on the lattice. This greatly increases the system sizes that we can study for

a given computational power. The details of this formulation are explained in Appendix E. If we then map the spin to complex fermion operators $c_j, c_j^\dagger$, satisfying anticommutation relations

$$\{c_j, c_k\} = \{c_j^\dagger, c_k^\dagger\} = 0, \quad \{c_j, c_k^\dagger\} = \delta_{jk}, \tag{6.44}$$

then the reduced density matrix ρ_I can be expressed as a Gaussian thermal state:

$$\rho_I \propto e^{-2\pi \sum_{j=1}^N e_j c_j^\dagger c_j}, \qquad 0 < e_1 < e_2 < \cdots, \tag{6.45}$$

where $\{e_j\}$ is the single particle spectrum of the entanglement Hamiltonian H_E. In this language, the 2^N eigenstates of ρ_I are of the form:

$$\left(\prod_{j\in J} c_j^\dagger\right)|0\rangle \qquad J \subseteq \{1, \ldots, N\}, \tag{6.46}$$

where $|0\rangle$ is the vacuum

$$c_j|0\rangle = 0 \qquad j = 1, \ldots, N. \tag{6.47}$$

These eigenstates can be identified with the operators of the CFT, see Figure 6.4. Those with an even number of fermions are in the tower of the identity, while those with an odd number of fermions are in the tower of ε. The operators L_n^{lat} from (6.43) should be the ones to (approximately) map states within the same conformal tower to each other. They can be expressed as quadratic polynomials of the $c_j, c_j^\dagger$, and their matrix elements computed. We will do so for a few values of N to study how accurate this representation is.

Figures 6.5, 6.6, 6.7 show the numerical results for some matrix elements of the lattice representation. Figure 6.5 shows diagonal elements of L_0^{lat} (off-diagonal elements are zero to machine precision, which matches expectations since L_0 and ρ_I have the same eigenvectors). Figures 6.6 and 6.7 show the behaviour of matrix elements of L_1^{lat} and L_2^{lat}, that should be nonzero and zero. In most cases we find the accuracy increase with N, which points to at least some of the error being due to finite size effects. One possible reason these are quite relevant is given by the mapping between the w and u geometries involving a logarithm (see Figure 6.3), which may reduce the effective number of sites that the generators see from N to $\sim \log N$.

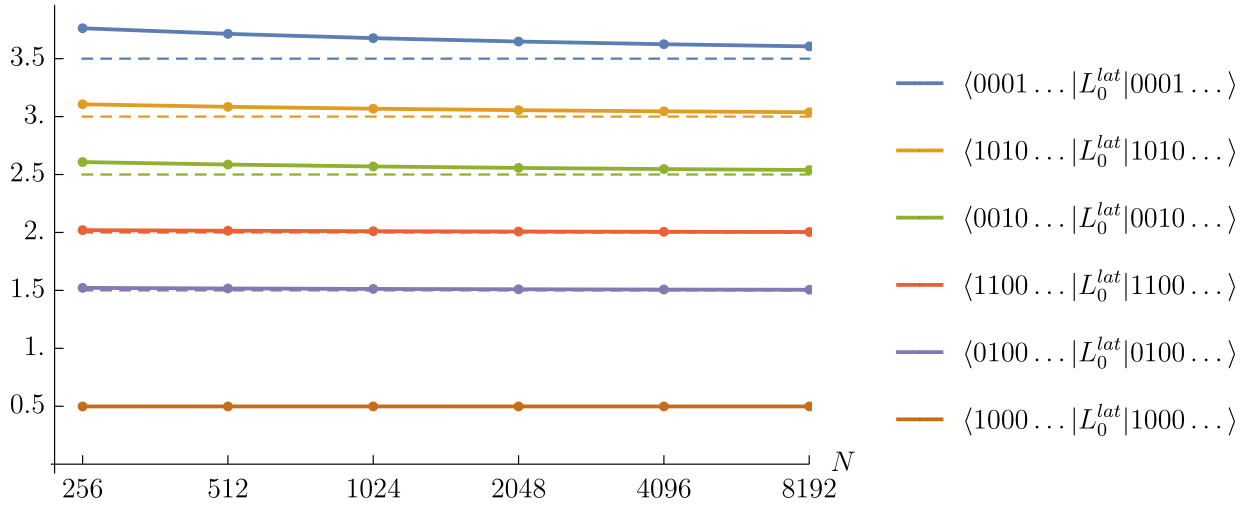

Figure 6.5: Diagonal elements of L_0^{lat}.

This chapter's takeaways:

- Entanglement structures of critical lattice systems can display *universal behaviour*: signatures of the underlying CFT that are independent of the microscopic realization. The entanglement entropy and entanglement spectrum of reduced density matrices show this kind of behaviour.
- We have proposed another emergent universal property to be investigated in critical lattice systems, which we call the *entanglement algebra*: an approximate representation of the Virasoro algebra on the eigenvectors of the reduced density matrix. Its existence is a natural consequence of the same kind of BCFT argument that explains the universal behaviour of entanglement spectra.
- We have built and tested numerically the entanglement algebra of the critical Ising model. The results agree with the predictions, and *finite size effects* can be improved upon a lot by optimizing over a parameter (ϵ) related to how we regularize the entanglement entropy in the continuum theory.

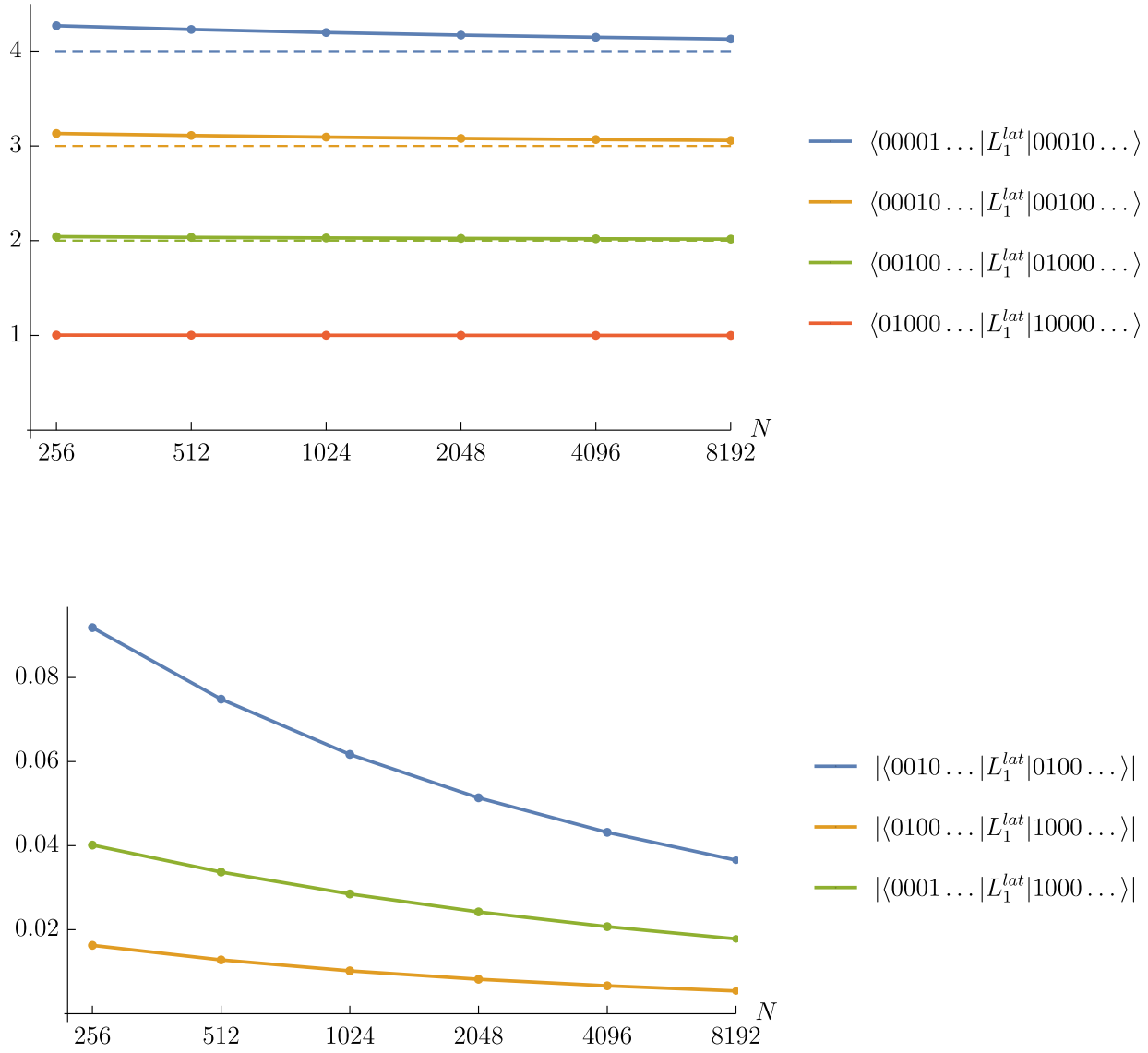

Figure 6.6: L_1^{lat} matrix elements expected to be nonzero (top) and zero (bottom).

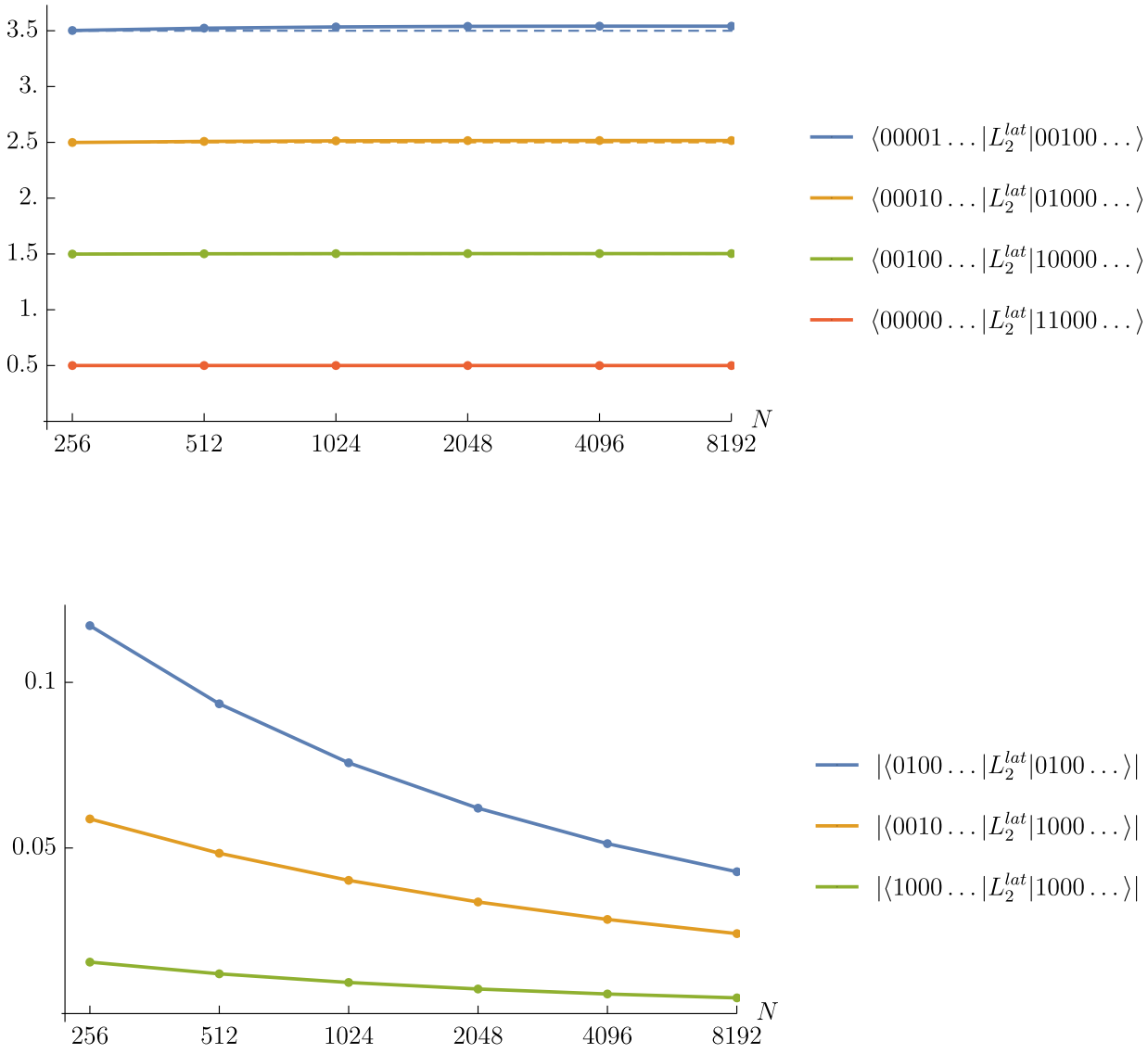

Figure 6.7: L_2^{lat} matrix elements expected to be nonzero (top) and zero (bottom).

Chapter 7

Continuous tensor network renormalization

This chapter's goal: In this chapter we introduce a proposal for the continuous version of the lattice algorithm called tensor network renormalization (TNR), which coarse-grains tensor network representations of partition functions and path integrals.

7.1 Introduction

Barring the slight digression in the previous chapter, so far in this thesis we have been focusing on the continuous analogue of the MERA, which is a tensor network that provides the renormalization group flow of a lattice quantum state, and can be applied also to coarse-grain operators. This could be dubbed as entanglement renormalization *in the Hamiltonian picture*. However, the paradigm of entanglement renormalization also has a tensor network realization *in the Lagrangian picture*, where the relevant objects are partition functions and path integrals. On the lattice, we can obtain a renormalization group flow for two-dimensional partition functions expressed as a tensor network using algorithms such as the tensor renormalization group (TRG) [177] and tensor network renormalization (TNR) [178].

Our goal here is to present a proposal for the continuous version of the TNR algorithm, which we consequently dub continuous TNR or cTNR. Our scheme operates on a particular kind of UV-regularized partition functions, which present a UV cutoff length scale Λ^{-1} much as cMERA states do (recall Chapter 3), and is based on the continuous flow generated

by a *scaling* operator L and a quasi-local *disentangling* operator K, which are direct analogues of the generators of the cMERA evolution. Thus the reader will find here many familiar ideas from previous chapters of this thesis. In a further display of continuity, we will use our by now beloved free boson theory as a proof-of-point example: we will see how cTNR can give rise to a fixed point of the RG flow from which conformal data can be correctly extracted.

This chapter is organized as follows: we begin in Section 7.2 by reviewing RG flows on tensor network representations of lattice partition functions (in particular TNR, the algorithm that we intend to extend to the continuum, and TRG, the original algorithm on which it is based). We then introduce cTNR in Section 7.3, and apply it to the free boson algorithm as an example in Section 7.4.

7.2 Tensor Renormalization Group and Tensor Network Renormalization

Before the passage to the continuum, let us review the lattice algorithms: tensor renormalization group (TRG) and tensor network renormalization (TNR).

The object to be coarse-grained is a two-dimensional statistical partition function (equivalently, a discrete Euclidean path integral in two spacetime dimensions) that has been expressed as a two-dimensional tensor network[1], arising from the repeated contraction of a tensor A, which encodes local Boltzmann weights (see the rightmost network in Figure 7.1). To see how we arrive to such a representation, consider the usual example of a classical 2d nearest-neighbour Ising model on a square lattice, where a classical spin variable σ_i that can take values ± 1 sits on top of each vertex of the lattice. The Hamiltonian function is given by

$$H[\{\sigma_i\}] = -\sum_{<i,j>} J\sigma_i\sigma_j, \tag{7.1}$$

where the sum runs over nearest neighbours and $J \in \mathbb{R}$ is the coupling constant. The partition function of this system is then

$$Z(\beta) = \sum_{\{\sigma_i\}} e^{-\beta H[\{\sigma_i\}]} = \sum_{\{\sigma_i\}} \prod_{<i,j>} e^{\beta J\sigma_i\sigma_j}. \tag{7.2}$$

[1]We will be working with square lattices for our convenience, but the algorithms we talk about can be adapted to other kinds of lattices.

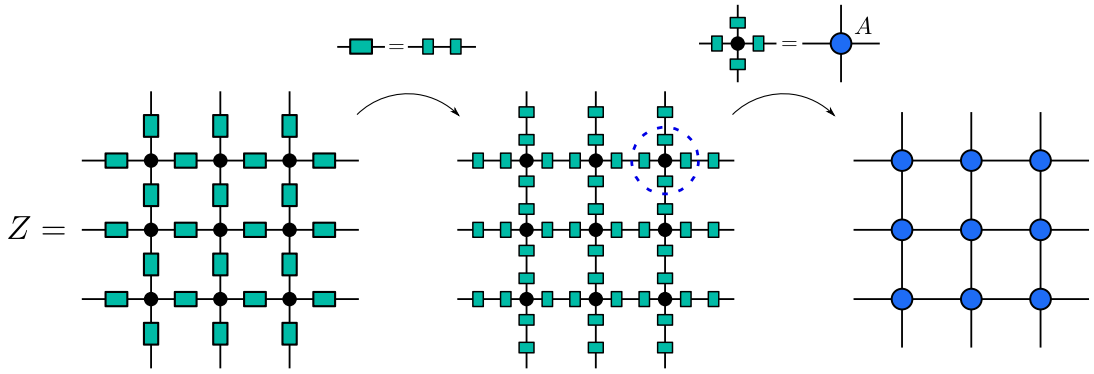

Figure 7.1: Tensor network representation of the Ising partition function.

This can be written as a tensor network with two types of tensors: two-legged tensors (matrices of Boltzmann weights) on the edges :

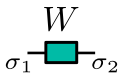

$$W_{\sigma_1\sigma_2} = e^{\beta J \sigma_1 \sigma_2} \tag{7.3}$$

and four-legged tensors on the vertices that ensure that each configuration we sum over has a unique definite value for the spin on that vertex:

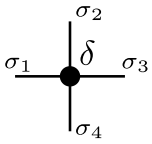

$$\delta_{\sigma_1\sigma_2\sigma_3\sigma_4} = \begin{cases} 1 & \sigma_1 = \sigma_2 = \sigma_3 = \sigma_4, \\ 0 & \text{otherwise.} \end{cases} \tag{7.4}$$

The resulting tensor network can be seen in Figure 7.1, where it is shown that, by taking the square root of the W matrices, we can rewrite it as the contraction of a single kind of four-legged tensor A. To arrive at such a representation in the case of a Euclidean path integral of a 1d lattice system, we would have to discretize the imaginary time evolution into timesteps

$$e^{-\tau H} = \left(e^{-\frac{\tau}{N}H}\right)^N, \tag{7.5}$$

then find a matrix product operator (MPO) representation of the timestep evolution operator:

$e^{-\frac{\tau}{N}H} =$ 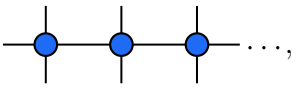

(7.6)

which will give rise to the 2d tensor network by iterative composition with itself.

In the same spirit of the real space renormalization group methods seen in Section 2.2, the algorithms we present here work by blocking degrees of freedom, and coarse-graining

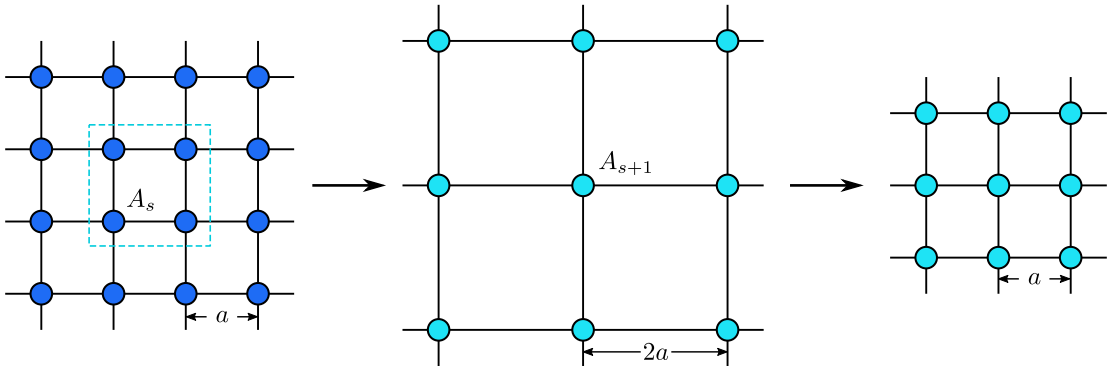

Figure 7.2: A coarse-graining step effectively blocks four tensors A_s at scale s into a single tensor A_{s+1} at scale $s+1$ (TRG and TNR differ in the way this effective tensor is chosen). After that, the lattice spacing is rescaled so that it stays constant along the flow.

each block into an effective description of itself. In this case, we will obtain an RG flow in the space of tensors: each coarse-graining step will effectively map a block of four tensors A_s at scale s into a single tensor A_{s+1} at scale $s+1$. After that, space is rescaled by a factor of $1/2$, so as to reset the lattice spacing $2a$ of the coarse-grained network back to the original lattice spacing a. This lattice spacing a of the model serves as a short-distance cutoff, hence by keeping it constant we are able to compare the partition functions at different stages as objects with the same UV regulator. Figure 7.2 summarizes this process.

The first version of the *tensor renormalization group* (TRG) algorithm was introduced by Levin and Nave in [177], and over the years it was joined by many related algorithms [179–184]. Here we review the original formulation, based on a factorization of the A tensors as the contraction of two three-legged tensors:

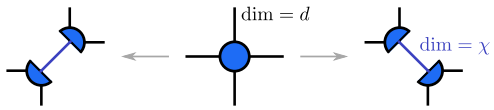

This decomposition can be performed by means of the singular value decomposition (SVD). The dimension χ of the bond that appears would generically have to be the square of the bond dimension d of the original tensors in order for the decomposition to be exact. However, that would cause the bond dimension of the new effective tensors to keep growing, since we would not be throwing away any information along the RG. Thus, the algorithm operates by truncating that index to some value $\chi < d^2$ and thus generating an approximate decomposition (this is equivalent to taking only the largest singular values in the SVD,

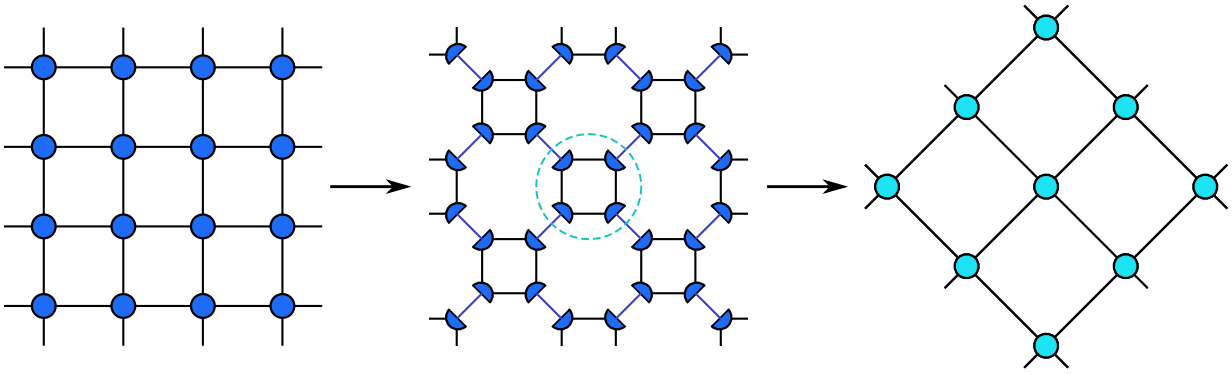

Figure 7.3: A half-step of the TRG algorithm: truncated SVD is used to decompose the original tensors, the factors are then regrouped to form a 45° tilted lattice, to which the same process will then be applied a second time.

and thus is very close to the philosophy of DMRG (see Section 2.2)). The algorithm then proceeds in "half-steps" such as the one depicted in Figure 7.3. Eeach half-step rotates the original network by 45° and increases the lattice spacing by a factor of $\sqrt{2}$, so after two of them we are back to the initial orientation with twice the lattice spacing, and the original tensor A_s has been replaced with A_{s+1}. After a number of iterations the algorithm will usually reach a fixed point tensor A_*.

The TRG algorithm as presented above, together with all its variants, is a powerful numerical tool: coarse-graining a large tensor network prior to its contraction can significantly reduce computational costs, allowing us to compute expectation values of observables and other quantities of physical interest for much larger system sizes. However, as already pointed out in [177], it does face trouble when applied to systems at criticality, where keeping the accuracy of the method becomes increasingly costly in terms of bond dimension due to the accumulation of short-range entanglement that is not removed by the coarse-graining steps. Additionally, the algorithm will fail to capture the correct structure of fixed points of the phase diagram of the system under study, in the sense that initial microscopic tensors that lie within the same phase will generically reach different fixed points, which thus contain non-universal, short-range information that should have been discarded during the RG flow.

If the reader finds that some of the problems we just mentioned sound familiar, that is totally right. We encountered similar issues when speaking of real-space renormalization methods in the Hamiltonian picture, such as DMRG, in Section 2.3 and in Appendix A. There we found they could be successfully addressed by the inclusion of a disentangling

step by local unitaries (which we called disentanglers) before each coarse-graining transformation. The algorithm of *tensor network renormalization* (TNR) arises in a similar way: it involves *disentanglers* and *isometries*, borrowing the technology of MERA to first decouple, and then eliminate, short-distance degrees of freedom from the partition function, in such a way as to generate a proper RG flow with the correct structure of fixed points.

In order to better visualize how the disentanglers are the key difference between TRG and TNR, we make the following remark: the TRG factorization step can be seen to be equivalent to the insertion in the network of a series of approximate resolutions of the identity (projectors) built from isometric tensors

(7.7)

that are chosen so that they satisfy

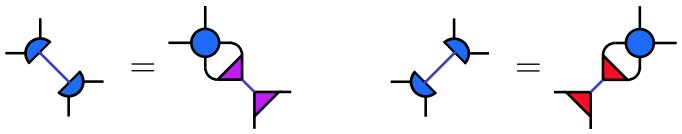

(7.8)

As a result, the middle network from Figure 7.3 is equivalent[2] to this one

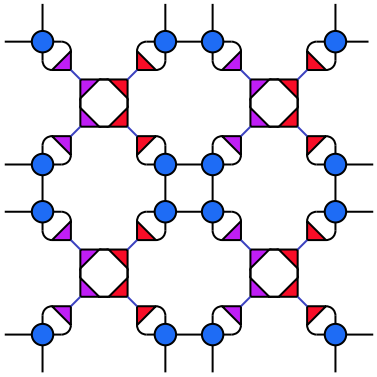

[2]What we mean here is that the two networks are the same up to a *gauge transformation*. A gauge transformation in a tensor network is a transformation of the tensors that leaves the contracted network invariant (i.e., in the case of a fully contracted network such as this one, it does not change its numerical value). It involves multiplying two tensors by a matrix X and its inverse X^{-1} respectively along a contracted index:

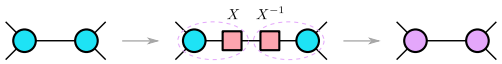

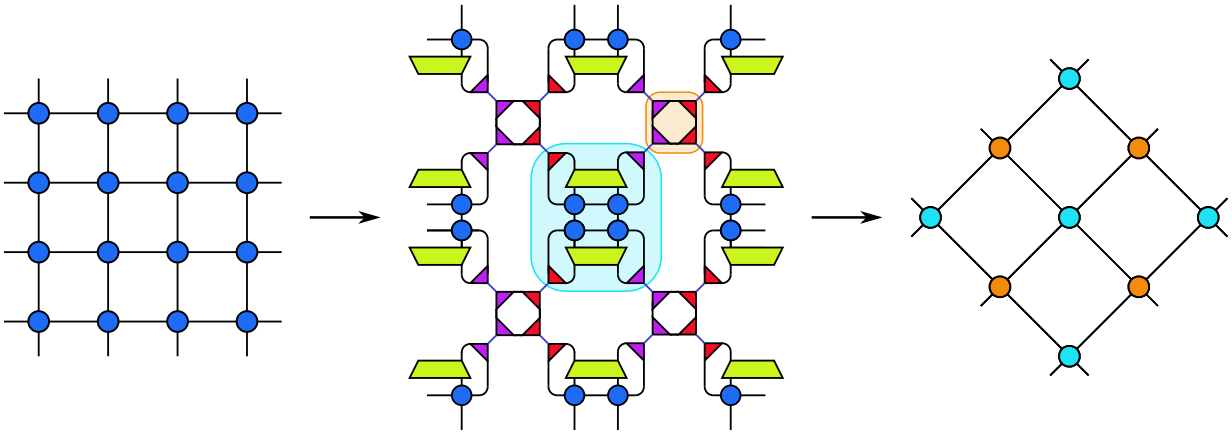

Figure 7.4: The first half-step of TNR in its original formulation. Disentanglers and isometries are introduced in the network, and new tensors are obtained from contracting them with the original ones, giving rise to a tilted lattice with translational invariance broken down to two sublattices. A second half-step identical to TRG brings the lattice to its original orientation and restores translation symmetry.

where we can see the coarse-graining isometries in action. The TNR coarse-graining step includes the disentangling step into this picture, by means of local unitaries:

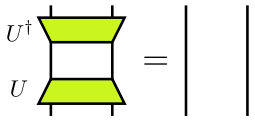

(7.9)

Figure 7.4 shows[3] the first half-step of TNR step, in its original formulation. The second

[3]They way we are presenting these algorithms, we are making the technical assumption that, for a row of A tensors, exchanging top and bottom indices amounts to complex conjugation, which is a property that follows from the Hermiticity of the Hamiltonian in Euclidean path integrals and from reflection invariance along the horizontal axis in classical partition functions. If this holds, then via a gauge transformation (see previous footnote) on every second row of tensors, we can have the tensors that make up the coarse-graining projector acting on the top and bottom indices of a row of A tensors be conjugate to each other:

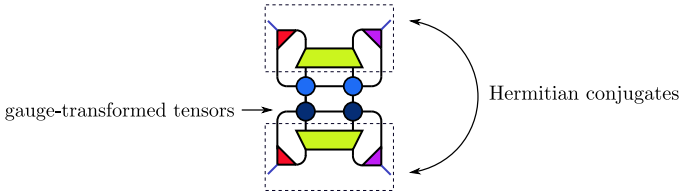

A proper discussion of these and other technicalities can be found in [185].

half-step (to obtain a lattice oriented as the original one) is left to be the same as in TRG. The disentanglers and isometries are determined variationally at each step, minimizing the truncation error for a given bond dimension

$$U, I_1, I_2 = \arg\min_{U,I_1,I_2}$$ 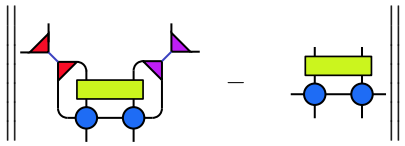

(7.10)

while satisfying constraints (7.7) and (7.9).

At each step of TNR, the disentanglers provide a *local rearrangement of degrees of freedom*, removing short-range correlations to facilitate coarse-graining. TNR has been proved successful at reproducing the phase diagram and fixed-point structure of 1+1d many-body Hamiltonians, as well as tackling systems at quantum phase transitions accurately without the need of a growing bond dimension. Additionally, conformal data of the underlying CFT can be extracted [186]. In fact, TNR is intimately related to the MERA, since the latter arises from applying the former to a manifold with a boundary [187]. After TNR was proposed, many similar algorithms have been put forward [188–191]. Its generalization to higher dimensions, while conceptually not very hard, presents too high a computational cost, to the point that to date we cannot speak of an efficient numerical implementation in three or higher dimensions.

7.3 Continuous tensor network renormalization

We now move to quantum field theory (QFT), and describe our proposal for a generalization of the TNR scheme to the continuum. First we describe the kind of regularized path integrals it applies to, where a UV cutoff Λ similar to the one in cMERA plays the role of a lattice spacing. Then we move on to describing the generators of the continuous transformation analogous to the coarse-graining and rescaling steps of TNR. Since in the next section we will see them applied to the case of the free boson in 1+1 dimensions, we will already use for convenience the notation of a scalar field for the elements introduced in this section.

7.3.1 Regularized path integrals

For this whole chapter we stay in Euclidean signature, so that the partition function for a QFT of a field $\phi(\vec{x})$ in d dimensions is given by

$$Z = \int [D\phi]\, e^{-S[\phi]}, \tag{7.11}$$

where $S[\phi]$ is the Euclidean action, taken to be the integral of a local Lagrangian density, a function of the field and its derivative:

$$S[\phi] = \int d^d x\ \mathcal{L}\Big(\phi(\vec{x}), \Delta\phi(\vec{x})\Big). \tag{7.12}$$

We assume $\mathcal{L}$ to be both translation and $O(d)$ rotation invariant, and generically, interacting. We will define a regularized version of this path integral via a *smeared action*

$$S^\Lambda[\phi] \equiv S[\phi^\Lambda] \tag{7.13}$$

where ϕ^Λ denotes a smeared field

$$\phi^\Lambda(\vec{x}) \equiv \int d^d y\ \mu(|\vec{x}-\vec{y}|)\phi(\vec{y}), \qquad \int d^d x\ \mu(|\vec{x}|) = 1, \tag{7.14}$$

where $\mu : \mathbb{R} \to \mathbb{R}$, with $x \equiv |\vec{x}|$, is a normalized, O(d) rotation invariant smearing profile which decays quickly (*e.g.* exponentially) to zero for distances x larger than a characteristic smearing length scale Λ^{-1}, see Fig. 7.7 (left) for an example. The smeared action S^Λ is the integral of a *quasi-local* Lagrangian

$$\mathcal{L}^\Lambda\Big(\phi(\vec{x}), \Delta\phi(\vec{x})\Big) \equiv \mathcal{L}\Big(\phi^\Lambda(\vec{x}), \Delta\phi^\Lambda(\vec{x})\Big), \tag{7.15}$$

and the corresponding partition function

$$Z^\Lambda \equiv \int [d\phi]\ e^{-S^\Lambda[\phi]} = \int [d\phi]\ e^{-S[\phi^\Lambda]} \tag{7.16}$$

is analogous to a tensor network like the ones discussed above, in the sense that it presents a UV cutoff: fluctuations of $\phi(\vec{x})$ at distances smaller than Λ^{-1} (the analogue of the lattice spacing a) have been suppressed thanks to the smearing. This translates, for instance, in the absence of the usual UV divergence in the correlator for the (unsmeared) field $\phi(\vec{x})$,

$$\langle\phi(\vec{x})\phi(\vec{y})\rangle_\Lambda \equiv \frac{1}{Z^\Lambda}\int [d\phi]\ e^{-S^\Lambda[\phi]}\ \phi(\vec{x})\phi(\mathbf{0}) \tag{7.17}$$

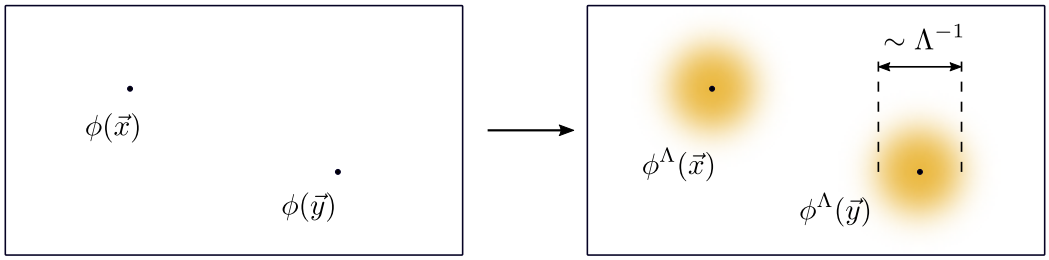

Figure 7.5: The smearing process yields a UV regularized path integral with cutoff length scale Λ^{-1}.

in the limit $\vec{x} \to \vec{y}$. Instead, we may have

$$\langle \phi(\vec{x})\phi(\vec{y})\rangle_\Lambda \sim \text{const.} \qquad 0 < |\vec{x} - \vec{y}| \ll \Lambda^{-1} \tag{7.18}$$

that is, the correlator tends to a constant at distances smaller than the UV cutoff (though we allow, and in general will have, an on-site distributional contribution, such as a delta function, that does not affect the $\vec{x} \to \vec{y}$ limit), see Fig. 7.7 (right). Recall from Chapter 3 that these were the UV regularization properties of the correlators in cMERA states.

7.3.2 cTNR evolution

As in the case of the entangling evolution of cMERA, the RG flow in cTNR is continuous in a parameter s (scale). During this flow, we need to perform an analogue of the local rearrangement of degrees of freedom that the disentanglers and isometries[4] produced on the lattice. Additionally, we need to keep rescaling the system in order to keep the cutoff scale Λ^{-1} constant in s, in the same way we kept the lattice spacing a fixed for TNR.

Our proposal of how to make these intuitive ideas concrete is very much inspired on the cMERA. We define a flow generated infinitesimally by an operator acting on field configurations, which is made of two contributions, denoted analogously to their Hamiltonian picture counterparts:

$$\delta\phi(\vec{x}) = (L + K(s))\phi(\vec{x}). \tag{7.19}$$

[4]Remember from MERA that an isometry $I : \mathcal{H} \to \mathcal{H} \otimes \mathcal{H}$ can be seen as a unitary $U_I : \mathcal{H} \otimes \mathcal{H} \to \mathcal{H} \otimes \mathcal{H}$ where one of the inputs has been fixed to a reference state (see Section 2.3), or, read in the opposite direction, a unitary that disentangles one of the degrees of freedom and places it in a product state with the rest of the system. This interpretation is more akin to the continuum version where we do not discard degrees of freedom: the Hilbert spaces involved do not change during the evolution.

Indeed, L is here the generator of scale transformations,

$$L\phi(\vec{x}) = (-\vec{x}\cdot\nabla_{\vec{x}} - \Delta_\phi)\phi(\vec{x}), \tag{7.20}$$

with $\Delta_\phi \equiv (d-2)/2$ the classical scaling dimension of the field $\phi(\vec{x})$. On the other hand, $K(s)$ is the *disentangling*[5] operator. We demand it to act quasi-locally at scale Λ^{-1}, and to preserve the translation and rotation symmetries of the theory. Without further constraints, we can write it in terms of some (generically nonlinear) function F:

$$K(s)\phi(\vec{x}) = F\Big(s, \phi^\Lambda(\vec{x}), \Delta\phi^\Lambda(\vec{x}), \Delta^2\phi^\Lambda(\vec{x}), \dots\Big), \tag{7.21}$$

where $\phi^\Lambda(\vec{x})$ is the smeared field from (7.14). Once we have defined a flow on the space of field configurations, we can define an s-dependent partition function Z_s^Λ and an s-dependent action $S_s[\phi]$. We write symbolically,

$$Z_s^\Lambda \;\equiv\; \mathcal{P}e^{\int_0^s du\ (L+K_u)}\ Z^\Lambda = \int [D\phi] e^{-S_s^\Lambda[\phi]}, \tag{7.22}$$

where $S_s[\phi]$ should include the change of the integration measure as we keep performing field redefinitions. Since both L and $K(s)$ are acting (quasi-)locally, there should exist a Lagrangian density $\mathcal{L}_s^\Lambda$ that is quasi-local over a length-scale Λ^{-1} such that:

$$S_s^\Lambda[\phi] = \int d^dx\ \mathcal{L}_s^\Lambda\Big(\phi(\vec{x}), \Delta\phi(\vec{x}), \Delta^2\phi(\vec{x}), \dots\Big). \tag{7.23}$$

How does this cutoff length scale stay constant along the RG flow? It is due to the interplay of the two generators L and $K(s)$. Imagine evolving with each of them alternatively, as would happen if we apply a Lie-Trotter-Suzuki approximation to the evolution from (7.22). Under evolution by L, both space and the cutoff are rescaled: zooming out causes the cutoff length-scale to get smaller; then the evolution under K_s performs a local field redefinition that restores the cutoff to its original value, without affecting space (i.e., without moving points around). This is depicted in Figure 7.6.

As in the case of cMERA, L is fixed by the field content of the theory we are working with, and $K(s)$ contains all the parameters that should be determined variationally (note the considerable amount of freedom that its definition allows for). This makes sense, since $K(s)$ is the continuum analogue of the lattice isometries and disentanglers at scale s. The

[5]Notice that its cMERA counterpart is was the *entangler* because we defined the forward direction in s as the one where entanglement was introduced on the state, which in terms of RG is running backwards.

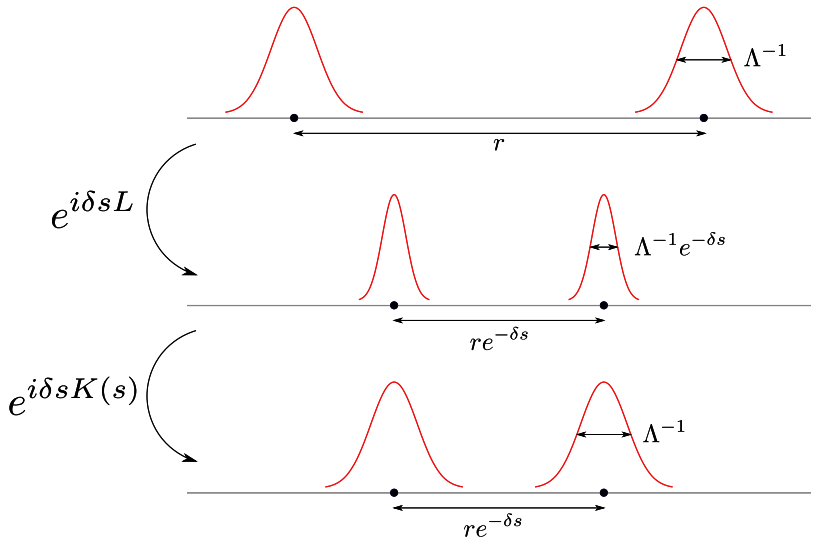

Figure 7.6: The action of L rescales the cutoff along with space, while the action of $K(s)$ locally reorganizes degrees of freedom, removing short distance information, and bringing the cutoff back to its original value.

latter are determined by demanding that the truncation introduced when coarse-graining causes the smallest error possible in the corresponding local part of the network, as per Eq. (7.10). It seems reasonable that a practical cTNR algorithm should therefore determine $K(s)$ by minimizing the "local" difference between the path integral given by $\mathcal{L}_s^\Lambda$ and $\mathcal{L}_{s+\delta s}^\Lambda$ (note that $\mathcal{L}_s^\Lambda$ contains information analogous to that of the tensors A that made the network on the lattice). Here we do not propose a specific algorithm, leaving this important aspect for future work. Instead, we now turn to the example of the 2d free boson theory, which, due to its solvability, allows for an easy analysis, while hopefully also displaying some key features of the construction that generalize to the interacting case.

7.4 cTNR for the free boson

7.4.1 Regularized path integral

For our computations with the free boson theory we will exploit its momentum space represention, in terms of Fourier modes

$$\phi(\vec{k}) \equiv \int \frac{d^2x}{2\pi} e^{-i\vec{k}\cdot\vec{x}} \phi(\vec{x}). \tag{7.24}$$

The action of the free massive boson theory in two Euclidean dimensions then reads

$$S[\phi] = \frac{1}{2}\int d^2x \left(-\phi(\vec{x})\Delta\phi(\vec{x}) + m^2\phi(\vec{x})^2\right) \tag{7.25}$$

$$= \frac{1}{2}\int d^2k \ (k^2+m^2)\phi(\vec{k})\phi(-\vec{k}), \tag{7.26}$$

and the partition function Z is defined as in the previous section. Our first step is to find a "continuous tensor network" representation thereof, that is, a regularized partition function with a UV cutoff Λ^{-1} on which the generators of the RG flow will be acting. In momentum space, the convolution (smearing) operation from Eq. (7.14) becomes just pointwise multiplication by the Fourier transform of the smearing profile:

$$\phi(\vec{k}) \longrightarrow \phi^\Lambda(\vec{k}) = \mu(k)\phi(\vec{k}), \tag{7.27}$$

where $\mu(k)$ only depends on $k = |\vec{k}|$ because of rotational invariance. This leaves

$$S^\Lambda[\phi] \equiv S[\phi^\Lambda] = \frac{1}{2}\int d^2k \ \mu(k)^2(k^2+m^2)\phi(\vec{k})\phi(-\vec{k}). \tag{7.28}$$

An appropriate choice of $\mu(\vec{k})$ should be able to regularize short-distance fluctuations. We have learned from cMERA that a possible indicator of such behaviour is the finiteness of the short-distance limit of the two-point function, which can be computed from Eq. (7.28) by Gaussian integration:

$$\langle\phi(\vec{k})\phi(\vec{q})\rangle_\Lambda = \frac{\delta(\vec{k}+\vec{q})}{\mu(k)^2(k^2+m^2)} \tag{7.29}$$

Inspired by the cMERA, we demand this correlator to have a similar UV behaviour to those we computed in Chapter 3: a finite short-distance limit with at most a delta contact term[6].

[6]Note that the term proportional to a delta function is precisely the kind of correlator we would expect in a "product partition function", the partition function of a theory whose action has no derivatives, which

To that end, we know that the momentum space correlator should tend to a constant fast enough. Since we also want to preserve the long-distance (small momentum) behaviour, it is natural to impose the following conditions on $\mu(k)$:

$$\begin{aligned} \mu(k) &\sim 1 \qquad k \ll \Lambda, \\ \mu(k) &\sim \Lambda/k \qquad k \gg \Lambda, \end{aligned}$$

$$\left| \int_\Lambda^\infty \left(\frac{1}{(k^2+m^2)} \frac{1}{\mu(k)^2} - \frac{1}{\Lambda^2} \right) \right| < \infty. \tag{7.31}$$

Indeed, the first condition implies the preservation of the correlator in the IR (low momenta). In fact, $\mu(k=0)=1$ was already given to us since it is nothing but the normalization condition from (7.14), which makes sense, since this condition is necessary for the long distance behaviour of the smeared fields to be equal to that of the sharp (unsmeared) fields, i.e. for the long distance physics of $S^\Lambda[\phi]$ to be the same than for $S[\phi]$. The second condition makes the momentum space correlator tend to a constant Λ^{-2} in the UV, and the third condition makes this convergence "fast enough" so that the UV limit of the position space correlator is finite[7] (the Fourier transform integral back to position space is absolutely convergent). Note that we include only the integral from $k=\Lambda$ instead of $k=0$: this is due to the fact that, in the case $m=0$, the IR divergence of the 2d free massless boson kicks in, and the correlator diverges even if the UV is regulated, requiring an additional IR regulator.

We could now start looking for functions $\mu(k)$ that satisfy (7.31)-(7.31), so as to give rise to good regularized path integrals. An example, depicted in Figure 7.7 is

$$\mu(k) = \frac{\Lambda}{k} \exp\left(\frac{1}{2} \mathrm{Expi}\left(-\frac{k^2}{\sigma \Lambda^2} \right) \right), \tag{7.32}$$

where $\mathrm{Expi}(x)$ is the exponential integral function and $\sigma = e^\gamma \approx 1.78$ (where γ is the Euler-Mascheroni constant), both of which the reader may recall from Section 3.4. In fact, going

thus (formally) factorizes in position space as the product of partition functions for each single degree of freedom $\phi(x)$, for example:

$$S[\phi] = \int d^2x \; \Lambda^2 \phi(\vec{x})^2 \implies Z \sim \prod_{\vec{x}} \int d\phi(\vec{x}) \; e^{-\Lambda^2 \phi(x)^2 dx} \tag{7.30}$$

[7]Remember that in the 2d free boson theory the correlator diverges logarithmically in the ultraviolet, which can also be checked just by setting $\mu(k)=1$ and Fourier transforming Eq. (7.29).

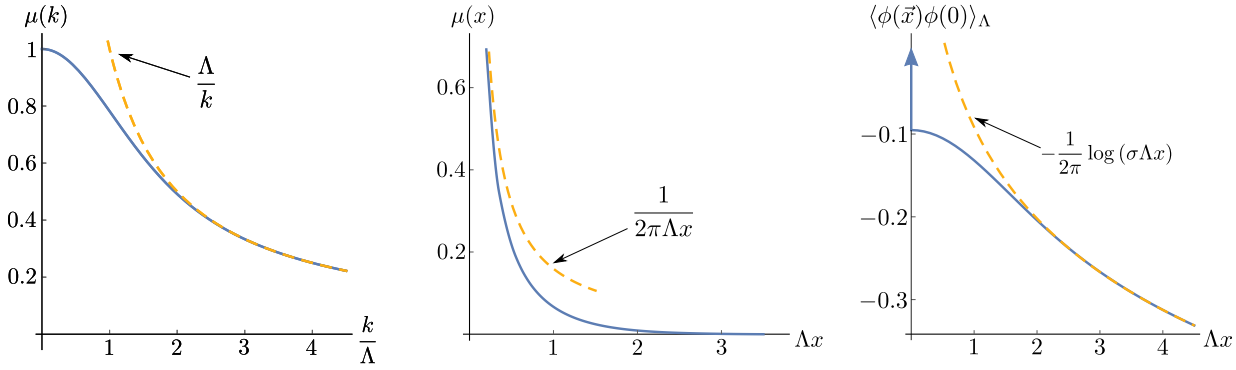

Figure 7.7: (left) Smearing profile $\mu(k)$ in momentum space; the dashed line shows its power law behaviour for large k. (center) Smearing profile $\mu(x)$ in position space; the dashed line shows its power law behaviour for small x. (right) Two-point correlator in the regularized theory for $m = 0$; the dashed line shows the same correlator in the original theory, with the UV divergence present. The delta function at the origin is represented by an arrow.

back to that section, it is not hard to guess a way to arrive at this example: comparing the requirements for the functions $\alpha(k)$ (Eq. (3.37)) and $\mu(k)$ (Eq. (7.31)) suggests picking

$$\mu(k) = \frac{\alpha(k)}{k}, \tag{7.33}$$

and this last equation relates indeed Eqs. (3.39) and (7.32). Importantly, it can be seen that $\mu(x)$ is indeed a quasi-local profile, bounded by an exponentially decaying function as $x \to \infty$ (the proof of this fact is rather technical and can be found in the appendix to [5]). This is important to carry on the analogy with between the UV regulator and the lattice spacing and to keep a certain degree of locality (at scale Λ^{-1}) in the structure of the regularized partition function. At short distances, $\mu(x)$ diverges as x^{-1}, which is an integrable divergence in 2d.

Seeing (7.33), and remembering about Eq. (3.38), the reader's intuition would be correct in guessing that in this example we will be looking at disentanglers with Gaussian profiles, but for that we will have to move on to the next section.

7.4.2 cTNR evolution

As explained in Section 7.3, of the two operators L and $K(s)$, the first one is already determined by the field content of the theory, and is given by (7.20), while all the parameters

of the scheme are contained in $K(s)$. To begin with, we consider the massless case $m = 0$. We are going to make a couple of assumptions similar to those we made for cMERA.

First, we impose $K(s) \equiv K$, i.e., the disentangling operator is scale-independent, which seems reasonable since the massless free boson is a conformal field theory, hence scale invariant. In fact, we are going to use this property to argue for the choice of disentangler we will make, by imposing a fixed point condition.

Secondly, we will propose an ansatz for K that is linear in the field:

$$K\phi(\vec{x}) = \int d^2y\, g(|\vec{x} - \vec{y}|)\phi(\vec{y}), \tag{7.34}$$

where $g(x)$ is a translation and rotation invariant profile, that is quasi-local with characteristic length scale Λ^{-1}, so that K satisfies the guidelines from Section 7.3. Choosing K to be linear in $\phi(\vec{x})$ restricts the evolution to happen within the space of quadratic actions, much in the same manner that the linear entanglers of the free cMERAs keep their evolutions within the corresponding manifold of Gaussian states. Quadratic actions, which include the original free boson action (7.25) and its regularized version (7.28), are easy to compute with, and will suffice to deal with a non-interacting theory, which should stay so along the RG flow.

With all these assumptions let us now impose the fixed point condition of the regularized massless free boson action $S^{\Lambda}_{m=0}[\phi]$ under the cTNR flow, and see what it implies for μ and g. We will do the computation in momentum space, where the action of the generators on the field is

$$L\phi(\vec{k}) = (\vec{k} \cdot \vec{\nabla}\phi(\vec{k}) + 2)\phi(\vec{k}), \tag{7.35}$$

$$K\phi(\vec{k}) = g(k)\phi(\vec{k}). \tag{7.36}$$

Additionally, we have to take into account the change in the path integral measure $[D\phi]$ due to the field redefinition. We will assume[8] that both L and K leave the measure invariant

[8]This is justified by the fact that, formally, scaling results in a permutation of the integration variables

$$\phi(\vec{k}) \mapsto \lambda^{-\Delta}\phi(\lambda\vec{k}) \qquad d\phi(\vec{k}) \mapsto \lambda^{-\Delta}d\phi(\lambda\vec{k}) \qquad [D\phi] \mapsto D[\lambda^{-\Delta}\phi(\lambda\cdot)] \propto [D\phi]$$

while K is diagonal in momentum space and just multiplies each integration variable by some number

$$\phi(\vec{k}) \mapsto g(k)\phi(\vec{k}) \qquad d\phi(\vec{k}) \mapsto g(k)d\phi(\vec{k}) \qquad [D\phi] \mapsto \left(\prod_{\vec{k}} g(\vec{k})\right)[D\phi].$$

up to a constant factor (independent of $\phi(\vec{k})$) that we will henceforth drop. We have

$$(L+K)S^{\Lambda}_{m=0}[\phi] = \int d\vec{k}\, k^2 \mu(k) \left[\big(-k\partial_k + g(k) \big) \mu(k) \right] \phi(\vec{k})\phi(-\vec{k}) \tag{7.37}$$

where we have used $\vec{k}\cdot\vec{\nabla} = k\partial_k$. The fixed point condition then gives $g(k)$ in terms of $\mu(k)$ or vice versa:

$$g(k) = \frac{k\partial_k \mu(k)}{\mu(k)}. \tag{7.38}$$

For the particular choice from (7.32) we have

$$g(k) = -1 + e^{-\frac{k^2}{\sigma\Lambda^2}} \implies g(\vec{x}) = -4\pi^2\delta(\vec{x}) + e^{-\frac{\sigma(\Lambda x)^2}{4}}, \tag{7.39}$$

which is a sensible profile for the disentangling operator, with a delta term at the origin and a Gaussian decay of characteristic length $\sim \Lambda^{-1}$, see Figure 7.7 (center). Now that we have this example we will explore two aspects of it: the extraction of conformal data, and the extension to the massive case.

7.4.3 Conformal data

On the lattice, TNR is able to retrieve conformal data by building lattice versions of *local scaling operators*. These are common eigenoperators of the scaling generator L, and the rotation generator R, given by

$$R\phi(\vec{x}) = (x_1\partial_2 - x_2\partial_1)\phi(\vec{x}). \tag{7.40}$$

The corresponding eigenvalues are the scaling dimensions and conformal spins:

$$L\mathcal{O}_\alpha(0) = -\Delta_\alpha \mathcal{O}_\alpha(0), \tag{7.41}$$
$$R\mathcal{O}_\alpha(0) = s_\alpha \mathcal{O}_\alpha(0). \tag{7.42}$$

For the free boson, the primary scaling fields are given by the identity, the holomorphic and antiholomorphic derivatives of the field and the vertex operators

$$\mathbb{1}, \quad \partial\phi(\vec{x}) \equiv \frac{1}{2}\left(\partial_{x_1} - i\partial_{x_2}\right)\phi(\vec{x}), \quad \bar{\partial}\phi(\vec{x}) \equiv \frac{1}{2}\left(\partial_{x_1} + i\partial_{x_2}\right)\phi(\vec{x}), \quad V_\alpha(\vec{x}) \equiv :e^{-i\alpha\phi(\vec{x})}: \tag{7.43}$$

with scaling dimensions and conformal spins given by

$$(\Delta_{\mathbb{1}}, s_{\mathbb{1}}) = (0,0), \qquad (\Delta_{\partial\phi}, s_{\partial\phi}) = (1,1), \tag{7.44}$$

$$(\Delta_{\bar{\partial}\phi}, s_{\bar{\partial}\phi}) = (1,-1), \qquad (\Delta_{V_\alpha(\vec{x})}, s_{V_\alpha(\vec{x})}) = \left(\frac{\alpha^2}{4\pi}, 0\right). \tag{7.45}$$

Naïvely, all the structure of the CFT, reliant as they are on scale invariance, should be affected by the regularization process, since it introduces a scale in the theory (that of the cutoff Λ) and thus eliminates the theory's scale symmetry. This is however not the case: it can be argued that our regularized theory supports an entire representation of the conformal group, just one where the generators of conformal transformations are not all the traditional ones[9]. In particular, here it is $L + K$, rather than L, the operator we should take as the generator of scale transformations. Indeed, $L + K$ generates the RG flow that moves us between scales while keeping the cutoff in place. In the same fashion that L generates the appropriate kind of scale transformations in the space of unregulated quantum field theories, it is $L + K$, which can be interpreted as a deformation of L in the UV, the generator of the correct notion of scale transformations on the space of quantum field theories with cutoff Λ.

This is not an entirely new notion: lattice critical systems do not obey the kind of scale symmetry of their underlying CFTs, which cannot even sensibly apply because arbitrary scale transformations cannot be represented on the lattice. However, emergent universality (of which we have seen an example in Chapter 6) evidences that the structure of the CFT is very much present despite the lack of strict scale symmetry. Tensor network techniques such as MERA and TNR provide a suitable notion of scale transformations on the lattice that allow for the extraction of conformal data [51, 186], while the implementation of more general conformal transformations on the lattice has also been successfully carried out [151, 192–194].

As opposed to the lattice case, however, in the case we are studying in this chapter we can obtain exact conformal data, and an exact representation of the conformal group. Then key to this statement is that the corresponding structures from the unregularized CFT case can be imported to the regularized case via smearing. This results, for instance, in the existence a quasi-local scaling operator $\mathcal{O}^\Lambda$ for each scaling operator of the original theory $\mathcal{O}$:

$$\mathcal{O}^\Lambda(\vec{x}) \equiv \int d^2y\ \mu(\vec{x} - \vec{y})\mathcal{O}(\vec{y}) \tag{7.46}$$

Indeed, it can be proved that if $\mathcal{O}$ satisfies Eqs. (7.41)-(7.42), then

$$(L + K)\mathcal{O}^\Lambda_\alpha(0) = -\Delta_\alpha \mathcal{O}^\Lambda_\alpha(0), \tag{7.47}$$

$$R\mathcal{O}^\Lambda_\alpha(0) = s_\alpha \mathcal{O}^\Lambda_\alpha(0) \tag{7.48}$$

holds, for K the disentangler given by (7.38). Note that we did not have to change R, since rotation invariance is preserved by the smearing. Thus we get the exact spectrum of

[9] The same situation takes place in the cMERA setting, as was first discussed in [57].

scaling dimensions and conformal spins of the theory, each paired with the corresponding quasi-local scaling operator. This is independent of the choice of the smearing profile $\mu(x)$ used to regularize the theory, provided that we pick K so that (7.38) is satisfied. Apart from those in the global conformal group, more general conformal transformations can also be quasi-locally represented: they are generated by the smeared components of the stress-energy tensor $T^\Lambda, \bar{T}^\Lambda$, giving rise to a quasi-local version of the full CFT machinery. Here we will not pursue it further, but the interested reader can consult the Supplemental Material in Reference [5].

7.4.4 RG flow of the massive theory

We now turn to a different observation, concerning the massive theory $m \neq 0$. In this case, we do not have an argument of scale invariance to determine the disentangling generator. We can, however, study what happens if we use the same K that we obtained in the massless case. The massive action is not a fixed-point, rather it evolves in s: we can integrate the infinitesimal evolution equation

$$\partial_s S_s^\Lambda[\phi] = (L + K) S_s[\phi], \tag{7.49}$$

to obtain

$$S_s^\Lambda[\phi] = \int d^2k \, \mu(k)^2 (k^2 + (me^s)^2) \phi(\vec{k}) \phi(-\vec{k}). \tag{7.50}$$

The result is a regularized massive free boson theory with an s-dependent mass $m(s) = me^s$. We can interpret the mass as an IR cutoff, imposing a correlation length $\sim m(s)^{-1}$. We then arrive at a picture where correlations exist in the theory at length scales in a window between the UV cutoff Λ^{-1} and the IR cutoff $m(s)^{-1}$. As we perform the RG flow, we remove correlations; since we keep rescaling to leave the UV cutoff fixed, the net result is the correlation length becoming shorter and shorter as the width of the window where correlations exist becomes smaller. This is depicted in Figure 7.8, where we compare the momentum space correlation function $\langle \phi(\vec{k}) \phi(-\vec{k}) \rangle$ before and after the evolution generated by $L + K$ with what would happen if we evolved only with L, which would rescale both cutoffs without reducing the width of the window between them.

What we obtained applying the disentangler from the massless theory to coarse-grain the massive theory matches what one would expect from an RG flow in a non-interacting theory: the action flows to a trivial massive fixed point of infinite mass as we zoom out. One could argue that this makes certain sense, since the task of the disentangler is to remove short-range correlations as we coarse-grain, and, sufficiently above the IR cutoff

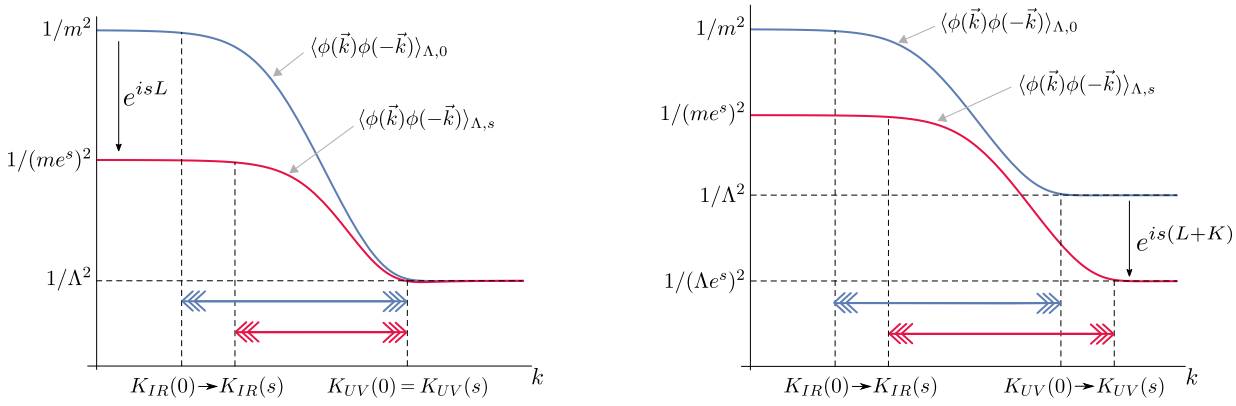

Figure 7.8: Evolution of the momentum space correlation function, its IR cutoff K_{IR} and its UV cutoff K_{UV}, generated by $L + K$ (left) and L alone (right), in loglog scale. In the first case, the UV cutoff is kept constant, but the IR cutoff grows as we remove correlations, so the width of the window between them decreases along the RG flow. In the second case, the width of the window between both cutoffs does not change.

given by the mass, both the massless and massive free boson theories have the same UV entanglement structure, so the same disentangler should be able to unravel both. Note however that after $s \sim \log(\Lambda/m)$ the RG flow and the interpretation we presented stop being trustworthy: the IR cutoff moves past the UV cutoff and the disentangler starts introducing spurious correlations, a sign that it is most likely not optimal at this stage of the RG flow. We remind the reader that the way we arrived at the disentangler K was not necessarily one that could be pursued in a generic situation, since we exploited the knowledge that a particular partition function should be a fixed point of the RG flow, and found the disentangler within an ansatz class (scale invariant operators that are linear in the field) that guaranteed it. Expectedly, in a practical implementation of the cTNR scheme, the disentangler should be determined at each moment of the evolution via some variational optimization.

This chapter's takeaways:

- TNR is an algorithm that implements a *renormalization group flow* on tensor network representations of classical partition functions and quantum Euclidean path integrals.
- cTNR is a proposed *continuous* version of this algorithm, acting on *regularized* versions of path integrals.
- Though cTNR is not yet at a stage where it can be applied to arbitrary theories, we can build an example for the massless free boson and prove it yields the *correct fixed point behaviour* and even reproduces a reasonable RG flow when applied to the massive case.

Epilogue

At this point, we have just finished surveying research carried out during four years. It is probably worth it to take a step back now, after having gone through it all, and briefly contemplate.

In this thesis, abstractly speaking, we have been searching for understanding about the underlying structure of quantum correlations that makes many-body and field theoretic states complex and interesting. This is of course a worthwhile goal on its own, but undeniably motivated by previous instances of improved understanding bringing along greater computational abilities. We have dwelled nevertheless very much on the analytical side of things, with numerics being used occasionally to support our arguments, rather than being the subject thereof.

In our particular case, this abstract program has taken concrete realization at the crossroads between continuous and discrete formulations. The fixed point cMERA states and fixed point cTNR partition functions are continuous objects that pretend to have a lattice spacing and to be conformally invariant, and achieve both by doing neither in the usual way. We have spent time investigating the signatures of the "dual" continuous-discrete character of these objects: the UV regularization, the representation of smeared scaling operators. We have also established comparisons with the actually discrete constructions that inspire them. In the case of cMERA, its properties can either have a clear analogue on the MERA or not have one. The minimal update conjecture for boundary and defect cMERA is an example of the first, while the construction of the gauge invariant cMERA via massive vector boson cMERAs could be argued to be an example of the second. Both are interesting, since it is worth being able to tell apart essential features of the family of quantum states versus aspects that depend on the choice of continuous vs. discrete. The entanglement algebra representation is on the other hand a more traditional example of the continuum-discretuum interplay, being a lattice system where we can observe signatures of an underlying continuous description in terms of a BCFT, signatures that appear in the entanglement degrees of freedom, the ones that represent the correlations in the system.

However conclusive these last paragraphs may be expected to sound, the reader will have noticed that many chapters in this thesis are phrased as commencements. We have been giving the first examples of gauge invariant, boundary and defect cMERAs, and we also have started the program of cTNR. We have done that, correspondingly, by giving baby steps, though in a teleological fashion, as a means to an end: the natural gravitating center for all these research lines is interacting quantum field theory. This is why we have phrased a few of our conclusions as prescriptions: what to do if, in the future where working continuous tensor network algorithms are commonplace, one faces a cMERA simulation on, e.g., a manifold with a boundary. It seems almost clear that the big breakthroughs in that direction will come from the numerical side. However, we are of the impression that there definitely would be interest in finding an analytical model of interacting cMERA or cTNR on which we can have as firm of a grasp as we do for the noninteracting models we have presented, in spite of the potentially fine-tuned nature of such a construction, which we foresee would most likely arise in the context of integrable or conformal systems. Purely theoretical questions keep driving research in this field as in many others: our study of boundaries and defects was actually partially motivated by the question of relating cMERA and cTNR, in an analogous way to the fact that applying TNR to a manifold with a boundary generates the MERA.

We conclude here. We hope the reader found something of value in this document, and we would like to finish by expressing our gratitude for the time devoted to it.

Waterloo, First Snowfall of Spring, 2020

References

[1] A. Franco-Rubio and G. Vidal, *Entanglement and correlations in the continuous multi-scale entanglement renormalization ansatz*, *Journal of High Energy Physics* (2017) [1706.02841].

[2] A. Franco-Rubio and G. Vidal, *Entanglement renormalization for gauge invariant quantum fields*, arXiv:1910.11815v1.

[3] A. Franco-Rubio, *Entanglement renormalization for quantum fields in the presence of boundaries and defects*, *to appear* .

[4] Q. Hu, A. Franco-Rubio and G. Vidal, *Emergent Universal Entanglement Algebra in Critical Lattice Systems*, *to appear* .

[5] Q. Hu, A. Franco-Rubio and G. Vidal, *Continuous tensor network renormalization for quantum fields*, arXiv:1809.05176v1.

[6] M. Fannes, B. Nachtergaele and R. F. Werner, *Finitely correlated states on quantum spin chains*, *Communications in Mathematical Physics* (1992) .

[7] F. Verstraete and J. I. Cirac, *Renormalization algorithms for Quantum-Many Body Systems in two and higher dimensions*, 0407066.

[8] G. Vidal, *Class of Quantum Many-Body States That Can Be Efficiently Simulated*, *Physical Review Letters* **101** (2008) 110501 [0610099].

[9] R. Orús, *A practical introduction to tensor networks: Matrix product states and projected entangled pair states*, *Annals of Physics* **349** (2014) 117.

[10] J. C. Bridgeman and C. T. Chubb, *Hand-waving and interpretive dance: an introductory course on tensor networks*, *Journal of Physics A: Mathematical and Theoretical* **50** (2017) 223001.

[11] G. Evenbly, "Tensors.net."

[12] J. Maldacena, *The large N Limit of superconformal field theories and supergravity*, *Advances in Theoretical and Mathematical Physics* **2** (1998) 231 [9711200].

[13] B. Swingle, *Constructing holographic spacetimes using entanglement renormalization*, *arXiv preprint arXiv:1209.3304* **02138** (2012) 1 [arXiv:1209.3304v1].

[14] B. Swingle, *Entanglement renormalization and holography*, *Physical Review D - Particles, Fields, Gravitation and Cosmology* **86** (2012) [0905.1317].

[15] M. Nozaki, S. Ryu and T. Takayanagi, *Holographic geometry of entanglement renormalization in quantum field theories*, *Journal of High Energy Physics* **2012** (2012) [1208.3469].

[16] A. Mollabashi, M. Naozaki, S. Ryu and T. Takayanagi, *Holographic geometry of cMERA for quantum quenches and finite temperature*, *Journal of High Energy Physics* **2014** (2014) [1311.6095].

[17] M. Miyaji, S. Ryu, T. Takayanagi and X. Wen, *Boundary states as holographic duals of trivial spacetimes*, *Journal of High Energy Physics* **2015** (2015) [1412.6226].

[18] M. Miyaji, T. Numasawa, N. Shiba, T. Takayanagi and K. Watanabe, *Continuous Multiscale Entanglement Renormalization Ansatz as Holographic Surface-State Correspondence*, *Physical Review Letters* **115** (2015) 171602 [1506.01353].

[19] M. Miyaji and T. Takayanagi, *Surface/state correspondence as a generalized holography*, *Progress of Theoretical and Experimental Physics* **2015** (2015) [1503.03542].

[20] J. Molina-Vilaplana, *Information geometry of entanglement renormalization for free quantum fields*, *Journal of High Energy Physics* **2015** (2015) [1503.07699].

[21] N. Bao, C. Cao, S. M. Carroll, A. Chatwin-Davies, N. Hunter-Jones, J. Pollack et al., *Consistency conditions for an AdS multiscale entanglement renormalization ansatz correspondence*, *Physical Review D - Particles, Fields, Gravitation and Cosmology* **91** (2015) 125036 [1504.06632].

[22] F. Pastawski, B. Yoshida, D. Harlow and J. Preskill, *Holographic quantum error-correcting codes: toy models for the bulk/boundary correspondence*, *Journal of High Energy Physics* (2015) [1503.06237].

[23] P. Hayden, S. Nezami, X. L. Qi, N. Thomas, M. Walter and Z. Yang, *Holographic duality from random tensor networks*, *Journal of High Energy Physics* (2016) [1601.01694].

[24] X. Wen, G. Y. Cho, P. L. S. Lopes, Y. Gu, X. L. Qi and S. Ryu, *Holographic entanglement renormalization of topological insulators*, *Physical Review B - Condensed Matter and Materials Physics* **94** (2016) [1605.07199].

[25] B. Czech, L. Lamprou, S. McCandlish and J. Sully, *Tensor networks from kinematic space*, *Journal of High Energy Physics* **07** (2016) 100 [1512.01548].

[26] W. C. Gan, F. W. Shu and M. H. Wu, *Thermal geometry from CFT at finite temperature*, *Physics Letters, Section B: Nuclear, Elementary Particle and High-Energy Physics* **760** (2016) 796 [1605.05999].

[27] M. Miyaji, T. Takayanagi and K. Watanabe, *From Path Integrals to Tensor Networks for AdS/CFT*, 1609.04645.

[28] J. R. Fliss, R. G. Leigh and O. Parrikar, *Unitary Networks from the Exact Renormalization of Wave Functionals*, 1609.03493.

[29] J. Molina-Vilaplana, *Entanglement renormalization and two dimensional string theory*, *Physics Letters, Section B: Nuclear, Elementary Particle and High-Energy Physics* **755** (2016) 421 [1510.09020].

[30] P. Caputa, N. Kundu, M. Miyaji, T. Takayanagi and K. Watanabe, *Liouville action as path-integral complexity: from continuous tensor networks to AdS/CFT*, *Journal of High Energy Physics* (2017) [1706.07056].

[31] G. Evenbly, *Hyperinvariant Tensor Networks and Holography*, *Physical Review Letters* (2017) [1704.04229].

[32] P. Caputa, N. Kundu, M. Miyaji, T. Takayanagi and K. Watanabe, *AdS from Optimization of Path-Integrals in CFTs*, *Physical Review Letters* **119** (2017) 071602 [1703.00456].

[33] B. Czech, *Einstein Equations from Varying Complexity*, *Physical Review Letters* (2018) [1706.00965].

[34] J. Molina-Vilaplana and A. del Campo, *Complexity functionals and complexity growth limits in continuous MERA circuits*, *Journal of High Energy Physics* (2018) [1803.02356].

[35] M. Campos, G. Sierra and E. López, *Tensor renormalization group in bosonic field theory*, *Physical Review B* (2019) [1902.02362].

[36] F. Verstraete and J. I. Cirac, *Continuous matrix product states for quantum fields*, *Physical Review Letters* (2010) [1002.1824].

[37] A. Tilloy and J. I. Cirac, *Continuous Tensor Network States for Quantum Fields*, *Physical Review X* (2019) [1808.00976].

[38] M. Ganahl and G. Vidal, *Continuous matrix product states for nonrelativistic quantum fields: A lattice algorithm for inhomogeneous systems*, *Physical Review B* (2018) [1801.02219].

[39] P. Di Francesco, P. Mathieu and D. Sénéchal, *Conformal Field Theory*. Springer-Verlag, 1997, 10.1007/978-1-4612-2256-9.

[40] P. H. Ginsparg, *Applied Conformal Field Theory*, in *Les Houches Summer School in Theoretical Physics: Fields, Strings, Critical Phenomena Les Houches, France, June 28-August 5, 1988*, pp. 1–168, 1988, 9108028.

[41] S. Rychkov, *EPFL Lectures on Conformal Field Theory in D >= 3 Dimensions*, SpringerBriefs in Physics. Springer International Publishing, Cham, 2017, 10.1007/978-3-319-43626-5, [1601.05000].

[42] M. Schottenloher, *A Mathematical Introduction to Conformal Field Theory*. Springer-Verlag, 2 ed., 2008, 10.1007/978-3-540-68628-6.

[43] A. Belavin, A. Polyakov and A. Zamolodchikov, *Infinite conformal symmetry in two-dimensional quantum field theory*, *Nuclear Physics B* **241** (1984) 333.

[44] C. Holzhey, F. Larsen and F. Wilczek, *Geometric and renormalized entropy in conformal field theory*, *Nuclear Physics, Section B* (1994) [9403108].

[45] P. Calabrese and J. L. Cardy, *Entanglement entropy and quantum field theory*, *Journal of Statistical Mechanics: Theory and Experiment* **2004** (2004) P06002 [0405152].

[46] J. L. Cardy, *Conformal invariance and surface critical behavior*, *Nuclear Physics B* **240** (1984) 514.

[47] G. Vidal, *Entanglement Renormalization*, *Physical Review Letters* **99** (2007) 220405 [0512165].

[48] V. Giovannetti, S. Montangero and R. Fazio, *Quantum multiscale entanglement renormalization ansatz channels*, *Physical Review Letters* **101** (2008) [0804.0520].

[49] R. N. C. Pfeifer, G. Evenbly and G. Vidal, *Entanglement renormalization, scale invariance, and quantum criticality*, *Physical Review A - Atomic, Molecular, and Optical Physics* **79** (2009) [0810.0580].

[50] G. Evenbly, R. N. Pfeifer, V. Picó, S. Iblisdir, L. Tagliacozzo, I. P. McCulloch et al., *Boundary quantum critical phenomena with entanglement renormalization*, *Physical Review B - Condensed Matter and Materials Physics* (2010) [0912.1642].

[51] G. Evenbly and G. Vidal, *Quantum Criticality with the Multi-scale Entanglement Renormalization Ansatz*, 1109.5334.

[52] K. G. Wilson, *Renormalization Group and Critical Phenomena. I. Renormalization Group and the Kadanoff Scaling Picture*, *Physical Review B* **4** (1971) 3174.

[53] K. G. Wilson, *The renormalization group: Critical phenomena and the Kondo problem*, *Reviews of Modern Physics* **47** (1975) 773.

[54] L. P. Kadanoff, *Scaling laws for Ising models near Tc*, *Physics Physique Fizika* **2** (1966) 263.

[55] S. R. White, *Density matrix formulation for quantum renormalization groups*, *Physical Review Letters* **69** (1992) 2863.

[56] J. Haegeman, T. J. Osborne, H. Verschelde and F. Verstraete, *Entanglement Renormalization for Quantum Fields in Real Space*, *Physical Review Letters* **110** (2013) 100402 [1102.5524v1].

[57] Q. Hu and G. Vidal, *Spacetime symmetries and conformal data in the continuous multi-scale entanglement renormalization ansatz*, 1703.04798.

[58] Y. Zou, M. Ganahl and G. Vidal, *Magic entanglement renormalization for quantum fields*, 1906.04218.

[59] J. S. Cotler, J. Molina-Vilaplana and M. T. Mueller, *A Gaussian Variational Approach to cMERA for Interacting Fields*, 1612.02427.

[60] J. Cotler, M. R. M. Mozaffar, A. Mollabashi and A. Naseh, *Renormalization Group Circuits for Weakly Interacting Continuum Field Theories*, *Fortschritte der Physik* (2019) [1806.02831].

[61] J. S. Cotler, M. Reza Mohammadi Mozaffar, A. Mollabashi and A. Naseh, *Entanglement renormalization for weakly interacting fields*, *Physical Review D* (2019) [1806.02835].

[62] J. J. Fernández-Melgarejo, J. Molina-Vilaplana and E. Torrente-Lujan, *Entanglement renormalization for interacting field theories*, *Physical Review D* (2019) [1904.07241].

[63] H. Casini and M. Huerta, *Entanglement entropy in free quantum field theory*, *Journal of Physics A: Mathematical and Theoretical* **42** (2009) 504007 [0905.2562].

[64] I. Peschel and V. Eisler, *Reduced density matrices and entanglement entropy in free lattice models*, *Journal of Physics A: Mathematical and Theoretical* **42** (2009) 504003 [0906.1663].

[65] J. Eisert, M. Cramer and M. B. Plenio, *Area laws for the entanglement entropy - a review*, *Reviews of Modern Physics* **82** (2008) 277 [0808.3773].

[66] M. Srednicki, *Entropy and area*, *Physical Review Letters* **71** (1993) 666 [9303048].

[67] S. Weinberg, *The Quantum Theory of Fields, Vol. 2 (Modern Applications)*, 1995. 10.1126/science.269.5231.1742.

[68] M. D. Schwartz, *Quantum Field Theory and the Standard Model*. Cambridge University Press, 2013.

[69] C. W. Misner, K. S. Thorne and J. A. Wheeler, *Gravitation*. W. H. Freeman, 1973.

[70] X.-G. Wen, *Quantum Field Theory of Many-Body Systems: From the Origin of Sound to an Origin of Light and Electrons*. 2007, 10.1093/acprof:oso/9780199227259.001.0001.

[71] M. Henneaux and C. Teitelboim, *Quantization of Gauge System*. Princeton University Press, 1992.

[72] K. G. Wilson, *Confinement of quarks*, *Physical Review D* **10** (1974) 2445.

[73] J. Kogut and L. Susskind, *Hamiltonian formulation of Wilson's lattice gauge theories*, *Physical Review D* **11** (1975) 395.

[74] S. Aoki, G. Boyd, R. Burkhalter, S. Ejiri, M. Fukugita, S. Hashimoto et al., *Quenched light hadron spectrum*, *Physical Review Letters* (2000) [9904012].

[75] S. Dürr, Z. Fodor, J. Frison, C. Hoelbling, R. Hoffmann, S. D. Katz et al., *Ab initio determination of light hadron masses*, *Science* (2008) [0906.3599].

[76] C. Gattringer and K. Langfeld, *Approaches to the sign problem in lattice field theory*, *International Journal of Modern Physics* **31** (2016) 1643007 [arXiv:1603.09517v1].

[77] D. Sexty, *New algorithms for finite density QCD*, in *Proceedings of Science*, 2014, DOI [1410.8813].

[78] T. M. Byrnes, P. Sriganesh, R. J. Bursill and C. J. Hamer, *Density matrix renormalization group approach to the massive Schwinger model*, *Physical Review D - Particles, Fields, Gravitation and Cosmology* (2002) [0202014].

[79] T. Sugihara, *Matrix product representation of gauge invariant states in a Z_2 lattice gauge theory*, *Journal of High Energy Physics* (2005) [0506009].

[80] M. C. Bañuls, K. Cichy, J. I. Cirac and K. Jansen, *The mass spectrum of the Schwinger model with matrix product states*, *Journal of High Energy Physics* (2013) [1305.3765].

[81] B. Buyens, J. Haegeman, K. Van Acoleyen, H. Verschelde and F. Verstraete, *Matrix product states for gauge field theories*, *Physical Review Letters* (2014) [1312.6654].

[82] K. Van Acoleyen, B. Buyens, J. Haegeman and F. Verstraete, *Matrix product states for gauge field theories*, in *Proceedings of The 32nd International Symposium on Lattice Field Theory — PoS(LATTICE2014)*, (Trieste, Italy), p. 308, Sissa Medialab, may, 2015, DOI [1411.0020].

[83] H. Saito, M. C. Bañuls, K. Cichy, J. I. Cirac and K. Jansen, *The temperature dependence of the chiral condensate in the Schwinger model with Matrix Product States*, in *Proceedings of Science*, 2014, DOI [1412.0596].

[84] M. C. Bañuls, K. Cichy, J. I. Cirac, K. Jansen and H. Saito, *Thermal evolution of the Schwinger model with matrix product operators*, *Physical Review D - Particles, Fields, Gravitation and Cosmology* (2015) [1505.00279].

[85] T. Pichler, M. Dalmonte, E. Rico, P. Zoller and S. Montangero, *Real-time dynamics in U(1) lattice gauge theories with tensor networks*, *Physical Review X* (2016) [1505.04440].

[86] S. Kühn, E. Zohar, J. I. Cirac and M. C. Bañuls, *Non-Abelian string breaking phenomena with matrix product states*, *Journal of High Energy Physics* (2015) [1505.04441].

[87] A. Milsted, *Matrix product states and the non-Abelian rotor model*, *Physical Review D* (2016) [1507.06624].

[88] B. Buyens, J. Haegeman, F. Verstraete and K. Van Acoleyen, *Tensor networks for gauge field theories*, in *Proceedings of Science*, 2015, DOI [1511.04288].

[89] H. Saito, M. C. Bañuls, K. Cichy, J. I. Cirac and K. Jansen, *Thermal evolution of the one-flavour Schwinger model using matrix product states*, in *Proceedings of Science*, 2015, DOI [1511.00794].

[90] B. Buyens, J. Haegeman, H. Verschelde, F. Verstraete and K. Van Acoleyen, *Confinement and String Breaking for QED2 in the Hamiltonian Picture*, *Physical Review X* (2016) [1509.00246].

[91] M. C. Bañuls, K. Cichy, K. Jansen and H. Saito, *Chiral condensate in the Schwinger model with matrix product operators*, *Physical Review D* (2016) [1603.05002].

[92] B. Buyens, F. Verstraete and K. Van Acoleyen, *Hamiltonian simulation of the Schwinger model at finite temperature*, *Physical Review D* (2016) [1606.03385].

[93] P. Silvi, E. Rico, M. Dalmonte, F. Tschirsich and S. Montangero, *Finite-density phase diagram of a (1 + 1)-d non-abelian lattice gauge theory with tensor networks*, *Quantum* (2017) [1606.05510].

[94] M. C. Bañuls, K. Cichy, J. I. Cirac, K. Jansen and S. Kühn, *Density Induced Phase Transitions in the Schwinger Model: A Study with Matrix Product States*, *Physical Review Letters* (2017) [1611.00705].

[95] B. Buyens, J. Haegeman, F. Hebenstreit, F. Verstraete and K. Van Acoleyen, *Real-time simulation of the Schwinger effect with matrix product states*, *Physical Review D* (2017) [1612.00739].

[96] B. Buyens, S. Montangero, J. Haegeman, F. Verstraete and K. Van Acoleyen, *Finite-representation approximation of lattice gauge theories at the continuum limit with tensor networks*, *Physical Review D* (2017) [1702.08838].

[97] K. Zapp and R. Orús, *Tensor network simulation of QED on infinite lattices: Learning from (1+1) d, and prospects for (2+1) d*, *Physical Review D* (2017) [1704.03015].

[98] M. C. Bañuls, K. Cichy, J. Ignacio Cirac, K. Jansen and S. Kühn, *Efficient basis formulation for (1 + 1)-dimensional SU(2) lattice gauge theory: Spectral calculations with matrix product states*, *Physical Review X* (2017) [1707.06434].

[99] F. Bruckmann, K. Jansen and S. Kühn, *O(3) nonlinear sigma model in 1+1 dimensions with matrix product states*, *Physical Review D* (2019) .

[100] P. Silvi, Y. Sauer, F. Tschirsich and S. Montangero, *Tensor Network Simulation of compact one-dimensional lattice Quantum Chromodynamics at finite density*, *Physical Review D* **100** (2019) 074512 [arXiv:1901.04403v2].

[101] L. Funcke, K. Jansen and K. Stefan, *Topological vacuum structure of the Schwinger model with matrix product states*, arXiv:1908.00551v2.

[102] Y. Liu, Y. Meurice, M. P. Qin, J. Unmuth-Yockey, T. Xiang, Z. Y. Xie et al., *Exact blocking formulas for spin and gauge models*, *Physical Review D - Particles, Fields, Gravitation and Cosmology* (2013) [1307.6543].

[103] Y. Shimizu and Y. Kuramashi, *Critical behavior of the lattice Schwinger model with a topological term at $\theta=\pi$ using the Grassmann tensor renormalization group*, *Physical Review D - Particles, Fields, Gravitation and Cosmology* (2014) [1408.0897].

[104] Y. Shimizu and Y. Kuramashi, *Grassmann tensor renormalization group approach to one-flavor lattice Schwinger model*, *Physical Review D - Particles, Fields, Gravitation and Cosmology* (2014) [1403.0642].

[105] J. Unmuth-Yockey, Y. Meurice, J. Osborn and H. Zou, *Tensor renormalization group study of the 2d O(3) model*, in *Proceedings of Science*, 2014, DOI [1411.4213].

[106] L. P. Yang, Y. Liu, H. Zou, Z. Y. Xie and Y. Meurice, *Fine structure of the entanglement entropy in the O(2) model*, *Physical Review E* (2016) .

[107] H. Kawauchi and S. Takeda, *Tensor renormalization group analysis of CP (N-1) model*, *Physical Review D* (2016) [1603.09455].

[108] A. Bazavov, Y. Meurice, S. W. Tsai, J. Unmuth-Yockey, L. P. Yang and J. Zhang, *Estimating the central charge from the Rényi entanglement entropy*, *Physical Review D* (2017) .

[109] Y. Shimizu and Y. Kuramashi, *Berezinskii-Kosterlitz-Thouless transition in lattice Schwinger model with one flavor of Wilson fermion*, *Physical Review D* (2018) .

[110] J. Unmuth-Yockey, J. Zhang, A. Bazavov, Y. Meurice and S. W. Tsai, *Universal features of the Abelian Polyakov loop in 1+1 dimensions*, *Physical Review D* (2018) [1807.09186].

[111] A. Bazavov, S. Catterall, R. G. Jha and J. Unmuth-Yockey, *Tensor renormalization group study of the non-Abelian Higgs model in two dimensions*, *Physical Review D* (2019) [1901.11443].

[112] M. Asaduzzaman, S. Catterall and J. Unmuth-Yockey, *Tensor network formulation of two dimensional gravity*, arXiv:1905.13061v1.

[113] M. Aguado and G. Vidal, *Entanglement renormalization and topological order*, *Physical Review Letters* **100** (2008) [0712.0348].

[114] R. König, B. W. Reichardt and G. Vidal, *Exact entanglement renormalization for string-net models*, *Physical Review B - Condensed Matter and Materials Physics* (2009) [0806.4583].

[115] L. Tagliacozzo and G. Vidal, *Entanglement renormalization and gauge symmetry*, *Physical Review B - Condensed Matter and Materials Physics* (2011) [1007.4145].

[116] P. Silvi, E. Rico, T. Calarco and S. Montangero, *Lattice gauge tensor networks*, *New Journal of Physics* (2014) [1404.7439].

[117] L. Tagliacozzo, A. Celi and M. Lewenstein, *Tensor networks for lattice gauge theories with continuous groups*, *Physical Review X* (2014) [1405.4811].

[118] J. Haegeman, K. Van Acoleyen, N. Schuch, J. Ignacio Cirac and F. Verstraete, *Gauging quantum states: From global to local symmetries in many-body systems*, *Physical Review X* (2015) [1407.1025].

[119] E. Zohar, M. Burrello, T. B. Wahl and J. I. Cirac, *Fermionic projected entangled pair states and local U(1) gauge theories*, *Annals of Physics* (2015) [1507.08837].

[120] E. Zohar and M. Burrello, *Building projected entangled pair states with a local gauge symmetry*, *New Journal of Physics* (2016) .

[121] A. Milsted and T. J. Osborne, *Quantum Yang-Mills theory: An overview of a program*, *Physical Review D* (2018) [1604.01979].

[122] E. Zohar, T. B. Wahl, M. Burrello and J. I. Cirac, *Projected Entangled Pair States with non-Abelian gauge symmetries: An SU(2) study*, *Annals of Physics* (2016) [1607.08115].

[123] E. Zohar and J. I. Cirac, *Combining tensor networks with Monte Carlo methods for lattice gauge theories*, *Physical Review D* (2018) [1710.11013].

[124] Y. Kuramashi and Y. Yoshimura, *Three-dimensional finite temperature Z2 gauge theory with tensor network scheme*, *Journal of High Energy Physics* (2019) [1808.08025].

[125] P. Emonts and E. Zohar, *Gauss law, minimal coupling and fermionic PEPS for lattice gauge theories*, *SciPost Physics Lecture Notes* (2020) [1807.01294].

[126] M. C. Bañuls, K. Cichy, J. I. Cirac, K. Jansen and S. Kühn, *Tensor networks and their use for Lattice Gauge Theories*, in *Proceedings of Science*, 2018, DOI [1810.12838].

[127] M. Dalmonte and S. Montangero, *Lattice gauge theory simulations in the quantum information era*, *Contemporary Physics* (2016) [1602.03776].

[128] M. Carmen Bañuls and K. Cichy, *Review on novel methods for lattice gauge theories*, *Reports on progress in physics. Physical Society (Great Britain)* (2020) [1910.00257].

[129] M. C. Bañuls, R. Blatt, J. Catani, A. Celi, J. I. Cirac, M. Dalmonte et al., *Simulating Lattice Gauge Theories within Quantum Technologies*, 1911.00003.

[130] J. Haegeman, J. I. Cirac, T. J. Osborne, H. Verschelde and F. Verstraete, *Applying the variational principle to (1+1)-Dimensional quantum field theories*, *Physical Review Letters* (2010) [1006.2409].

[131] J. Haegeman, J. I. Cirac, T. J. Osborne, I. Pižorn, H. Verschelde and F. Verstraete, *Time-Dependent Variational Principle for Quantum Lattices*, *Physical Review Letters* **107** (2011) 070601 [1103.0936].

[132] D. Draxler, J. Haegeman, T. J. Osborne, V. Stojevic, L. Vanderstraeten and F. Verstraete, *Particles, holes, and solitons: A matrix product state approach*, *Physical Review Letters* (2013) .

[133] F. Quijandría, J. J. García-Ripoll and D. Zueco, *Continuous matrix product states for coupled fields: Application to Luttinger liquids and quantum simulators*, *Physical Review B - Condensed Matter and Materials Physics* (2014) .

[134] S. S. Chung, K. Sun and C. J. Bolech, *Matrix product ansatz for Fermi fields in one dimension*, *Physical Review B - Condensed Matter and Materials Physics* (2015) [1501.00228].

[135] F. Quijandría and D. Zueco, *Continuous-matrix-product-state solution for the mixing-demixing transition in one-dimensional quantum fields*, *Physical Review A - Atomic, Molecular, and Optical Physics* (2015) .

[136] J. Haegeman, D. Draxler, V. Stojevic, I. Cirac, T. Osborne and F. Verstraete, *Quantum Gross-Pitaevskii Equation*, *SciPost Physics* (2017) [1501.06575].

[137] J. Rincón, M. Ganahl and G. Vidal, *Lieb-Liniger model with exponentially decaying interactions: A continuous matrix product state study*, *Physical Review B - Condensed Matter and Materials Physics* (2015) [1508.04779].

[138] D. Draxler, J. Haegeman, F. Verstraete and M. Rizzi, *Continuous matrix product states with periodic boundary conditions and an application to atomtronics*, *Physical Review B* (2017) [1609.09704].

[139] M. Ganahl, *Continuous Matrix Product States for Inhomogeneous Quantum Field Theories: a Basis-Spline Approach*, arXiv:1712.01260v1.

[140] M. Ganahl, J. Rincón and G. Vidal, *Continuous Matrix Product States for Quantum Fields: An Energy Minimization Algorithm*, *Physical Review Letters* (2017) [1611.03779].

[141] Y. Zou, M. Ganahl and G. Vidal, *Interacting cMERA*, *to appear* .

[142] G. Evenbly and G. Vidal, *Algorithms for Entanglement Renormalization: Boundaries, Impurities and Interfaces*, *Journal of Statistical Physics* **157** (2014) 931 [1312.0303].

[143] G. Evenbly and G. Vidal, *Theory of minimal updates in holography*, *Physical Review B* **91** (2015) 205119 [1307.0831].

[144] M. Hauru, G. Evenbly, W. W. Ho, D. Gaiotto and G. Vidal, *Topological conformal defects with tensor networks*, *Physical Review B* (2016) [1512.03846].

[145] J. C. Bridgeman and D. J. Williamson, *Anomalies and entanglement renormalization*, *Physical Review B* **96** (2017) 125104 [1703.07782].

[146] B. Czech, P. H. Nguyen and S. Swaminathan, *A defect in holographic interpretations of tensor networks*, *Journal of High Energy Physics* **2017** (2017) 90 [1612.05698].

[147] S. Chapman, D. Ge and G. Policastro, *Holographic complexity for defects distinguishes action from volume*, *Journal of High Energy Physics* (2019) [1811.12549].

[148] Y. Zou, *private communication*, .

[149] T. Quella, I. Runkel and G. M. Watts, *Reflection and transmission for conformal defects*, *Journal of High Energy Physics* **2007** (2007) 095.

[150] C. Bachas, J. de Boer, R. Dijkgraaf and H. Ooguri, *Permeable conformal walls and holography*, *Journal of High Energy Physics* **2002** (2002) 027 [0111210].

[151] A. Milsted and G. Vidal, *Extraction of conformal data in critical quantum spin chains using the Koo-Saleur formula*, *Physical Review B* **96** (2017) 245105 [1706.01436].

[152] Y. Zou, A. Milsted and G. Vidal, *Conformal Data and Renormalization Group Flow in Critical Quantum Spin Chains Using Periodic Uniform Matrix Product States*, *Physical Review Letters* (2018) [1710.05397].

[153] Y. Zou, A. Milsted and G. Vidal, *Conformal Fields and Operator Product Expansion in Critical Quantum Spin Chains*, *Physical Review Letters* (2020) [1901.06439].

[154] G. Vidal, J. I. Latorre, E. Rico and A. Kitaev, *Entanglement in Quantum Critical Phenomena*, *Physical Review Letters* **90** (2003) 227902 [0211074].

[155] H. Li and F. D. M. Haldane, *Entanglement Spectrum as a Generalization of Entanglement Entropy: Identification of Topological Order in Non-Abelian Fractional Quantum Hall Effect States*, *Physical Review Letters* **101** (2008) 010504.

[156] A. M. Läuchli, *Operator content of real-space entanglement spectra at conformal critical points*, 1303.0741.

[157] J. L. Cardy and E. Tonni, *Entanglement Hamiltonians in two-dimensional conformal field theory*, *Journal of Statistical Mechanics: Theory and Experiment* **2016** (2016) 123103.

[158] K. Ohmori and Y. Tachikawa, *Physics at the entangling surface*, *Journal of Statistical Mechanics: Theory and Experiment* **2015** (2015) P04010.

[159] G. Y. Cho, A. W. W. Ludwig and S. Ryu, *Universal entanglement spectra of gapped one-dimensional field theories*, *Physical Review B* **95** (2017) 115122 [1603.04016].

[160] I. Runkel, *Boundary Problems in Conformal Field Theory. Chapter 2. Boundary Conformal Field Theory*, Ph.D. thesis, University College London, 2000.

[161] J. L. Cardy, *Boundary Conditions in Conformal Field Theory*, in *Integrable Systems in Quantum Field Theory*, pp. 127–148, 1989, DOI.

[162] J. L. Cardy, *Boundary Conformal Field Theory*, 0411189.

[163] J. L. Cardy, *Conformal invariance and universality in finite-size scaling*, *Journal of Physics A: Mathematical and General* **17** (1984) L385.

[164] J. L. Cardy, *Operator content of two-dimensional conformally invariant theories*, *Nuclear Physics B* **270** (1986) 186.

[165] H. W. J. Blöte, J. L. Cardy and M. P. Nightingale, *Conformal invariance, the central charge, and universal finite-size amplitudes at criticality*, *Physical Review Letters* **56** (1986) 742.

[166] J. L. Cardy, *Logarithmic corrections to finite-size scaling in strips*, *Journal of Physics A: Mathematical and General* **19** (1986) L1093.

[167] I. Affleck, *Universal term in the free energy at a critical point and the conformal anomaly*, *Physical Review Letters* **56** (1986) 746.

[168] W. Koo and H. Saleur, *Representations of the Virasoro algebra from lattice models*, *Nuclear Physics B* **426** (1994) 459.

[169] J. L. Cardy, *Effect of boundary conditions on the operator content of two-dimensional conformally invariant theories*, *Nuclear Physics B* **275** (1986) 200.

[170] J. L. Cardy, *Boundary conditions, fusion rules and the Verlinde formula*, *Nuclear Physics B* **324** (1989) 581.

[171] J. L. Cardy and D. C. Lewellen, *Bulk and boundary operators in conformal field theory*, *Physics Letters B* **259** (1991) 274.

[172] R. Blumenhagen and E. Plauschinn, *Boundary Conformal Field Theory*, in *Lecture Notes in Physics*, pp. 205–256, (2009), DOI.

[173] H. Casini, M. Huerta and R. C. Myers, *Towards a derivation of holographic entanglement entropy*, *Journal of High Energy Physics* **2011** (2011) 36 [1102.0440].

[174] P. D. Hislop and R. Longo, *Modular structure of the local algebras associated with the free massless scalar field theory*, *Communications in Mathematical Physics* (1982) .

[175] I. Affleck and A. W. W. Ludwig, *Universal noninteger "ground-state degeneracy" in critical quantum systems*, *Physical Review Letters* **67** (1991) 161.

[176] In addition to him being first author of [4], we would like to specify that credit for the optimization procedure and the associated plots should go entirely to Qi Hu.

[177] M. Levin and C. P. Nave, *Tensor renormalization group approach to two-dimensional classical lattice models*, *Physical Review Letters* (2007) [0611687].

[178] G. Evenbly and G. Vidal, *Tensor Network Renormalization*, *Physical Review Letters* (2015) [1412.0732].

[179] Z. C. Gu, M. Levin and X. G. Wen, *Tensor-entanglement renormalization group approach as a unified method for symmetry breaking and topological phase transitions*, *Physical Review B - Condensed Matter and Materials Physics* (2008) .

[180] H. C. Jiang, Z. Y. Weng and T. Xiang, *Accurate Determination of Tensor Network State of Quantum Lattice Models in Two Dimensions*, *Physical Review Letters* (2008) [0806.3719].

[181] Z. Y. Xie, H. C. Jiang, Q. N. Chen, Z. Y. Weng and T. Xiang, *Second renormalization of tensor-network states*, *Physical Review Letters* (2009) [0809.0182].

[182] Z. C. Gu and X. G. Wen, *Tensor-entanglement-filtering renormalization approach and symmetry-protected topological order*, *Physical Review B - Condensed Matter and Materials Physics* (2009) [0903.1069].

[183] H. H. Zhao, Z. Y. Xie, Q. N. Chen, Z. C. Wei, J. W. Cai and T. Xiang, *Renormalization of tensor-network states*, *Physical Review B - Condensed Matter and Materials Physics* (2010) [1002.1405].

[184] B. Dittrich, F. C. Eckert and M. Martin-Benito, *Coarse graining methods for spin net and spin foam models*, *New Journal of Physics* (2012) .

[185] G. Evenbly, *Algorithms for tensor network renormalization*, *Physical Review B* (2017) [1509.07484].

[186] G. Evenbly and G. Vidal, *Local Scale Transformations on the Lattice with Tensor Network Renormalization*, *Physical Review Letters* (2016) [1510.00689].

[187] G. Evenbly and G. Vidal, *Tensor Network Renormalization Yields the Multiscale Entanglement Renormalization Ansatz*, *Physical Review Letters* (2015) [1502.05385].

[188] S. Yang, Z. C. Gu and X. G. Wen, *Loop Optimization for Tensor Network Renormalization*, *Physical Review Letters* (2017) [1512.04938].

[189] L. Ying, *Tensor network skeletonization*, *Multiscale Modeling and Simulation* (2017) [1607.00050].

[190] M. Bal, M. Mariën, J. Haegeman and F. Verstraete, *Renormalization Group Flows of Hamiltonians Using Tensor Networks*, *Physical Review Letters* (2017) [1703.00365].

[191] M. Hauru, C. Delcamp and S. Mizera, *Renormalization of tensor networks using graph-independent local truncations*, *Physical Review B* (2018) [1709.07460].

[192] A. Milsted and G. Vidal, *Tensor networks as conformal transformations*, 1805.12524.

[193] A. Milsted and G. Vidal, *Tensor networks as path integral geometry*, 1807.02501.

[194] A. Milsted and G. Vidal, *Geometric interpretation of the multi-scale entanglement renormalization ansatz*, 1812.00529.

[195] M. Lamoreux, *private communication*, .

APPENDICES

A

Appendix for Chapter 2

In this appendix we show a classic toy example of the difference between real-space renormalization group methods that use or do not use disentanglers. Recall that the disentanglers are unitaries added in the entanglement renormalization algorithm in order to remove short-distance entanglement that the isometries of the coarse-graining transformation might not be able to.

In our example, we present a quantum state for a 1d chain with only nearest-neighbour entanglement. In the philosophy of an RG flow, all of this short-range entanglement should be discarded upon a single coarse-graining iteration, and the state should be mapped to a product state, since at long distances it presents no correlations. However, we will see that coarse-graining just with isometries does not reproduce this expected result: on the contrary, part of the entanglement of the state is mapped to longer range entanglement rather than discarded, and the state itself turns out to be preserved by coarse-graining. Once we introduce the disentanglers, we nevertheless recover the proper RG flow behaviour, and the state does map to a product state after one renormalization step. Let us see how this works.

Consider an infinite 1d lattice, with the Hilbert space of two qubits $\mathcal{H} = \mathbb{C}^2 \otimes \mathbb{C}^2$ at each site. We defined a dimerized state where, for each site i, one of the qubits on i is in a maximally entangled (Bell pair) state with one of the qubits from the preceding site $i-1$, and the other qubit on i is in a Bell pair state with one qubit from the following site $i+1$. We choose the Bell pair state

$$|\Phi^+\rangle = \frac{|00\rangle + |11\rangle}{\sqrt{2}}. \tag{A.1}$$

If we label the qubits on site i by the pairs (i, L) and (i, R), the state is given by

$$|\Psi\rangle = \bigotimes_i \frac{|0\rangle_{i,R}|0\rangle_{i+1,L} + |1\rangle_{i,R}|1\rangle_{i+1,L}}{\sqrt{2}}. \tag{A.2}$$

We can use the following graphical depiction of this state:

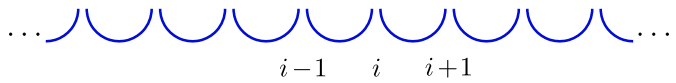

where each line represents a Bell pair[1]. This representation makes it rather easy to see that this state only presents short-range correlations, since there is no entanglement between any two nonconsecutive sites.

A local coarse-graining map acting on two consecutive sites will be able to remove the entanglement between them, but will fail at doing so for the correlations between these sites and their other neighbours, which will go through to the next iteration. To see an example of this best-case scenario, consider the isometry

$$\begin{aligned} I : \quad \mathcal{H} &\longmapsto \mathcal{H} \otimes \mathcal{H} \\ |x_{i,L}\, x_{i,R}\rangle &\longmapsto |x_{i,L}\rangle|\Phi^+\rangle|x_{i,R}\rangle \end{aligned} \tag{A.4}$$

and its adjoint, the coarse-graining map

$$\begin{aligned} I^\dagger : \quad \mathcal{H} \otimes \mathcal{H} &\longmapsto \mathcal{H} \\ |x_{i,L}\, x_{i,R}\, x_{i+1,L}\, x_{i+1,R}\rangle &\longmapsto \langle\Phi^+|x_{i,R}\, x_{i+1,L}\rangle|x_{i,L}\, x_{i+1,R}\rangle \end{aligned} \tag{A.5}$$

which projects the two "internal" qubits onto the Bell state $|\Phi^+\rangle$ and outputs the two "external" qubits as the coarse-grained site (recall that each site hosts two qubits in this example).

[1]This is actually a tensor network representation of this state! Indeed, within a tensor network diagram, "wires" can be thought of as representing an identity matrix in the Hilbert space associated to that wire:

and the tensor that gives the coefficients of our Bell pair state $|\Phi^+\rangle$, up to normalization, is precisely the identity matrix:

$$|00\rangle + |11\rangle = \sum_{ij} \delta_{ij}|ij\rangle \tag{A.3}$$

.

Graphically, we represent[2] this map as follows

Iterative application of this map will thus succeed in removing part of the entanglement, but the coarse-grained states will still present the same structure of nearest-neighbour correlations from the original state. In fact, the state is a fixed point of the RG flow, in spite of it not being scale invariant[3].

Figure A.1a shows the resulting RG flow. Note that in this example the flow is exact (there is no truncation error), i.e., the resulting tree tensor network represents the state exactly, rather than an approximation thereof. The local bond dimension stays constant as the RG progresses because even though we do not get rid of short-range entanglement, there is no entanglement at higher scales to join it. Otherwise, as we coarse-grained more and more, there would be the possibility for new contributions to show up and force us to increase the bond dimension to stay accurate. In a simplified manner, this is in practice what happens when a critical state is treated with a method like DMRG: there are correlations at all length scales, and they keep accumulating rather that being removed properly scale by scale.

This situation can be avoided by the use of the right disentanglers, to help us remove the unaddressed short-range entanglement. For our example, we need a unitary that maps $|\Phi^+\rangle$ to a product state, e.g. $|00\rangle$. An easy choice is

$$\begin{aligned} U &= \mathbb{1} + iY \otimes X \\ &= |00\rangle\langle\Phi^+| + |01\rangle\langle\Phi^+|(\mathbb{1} \otimes X) + |10\rangle\langle\Phi^+|(\mathbb{1} \otimes iY) - |11\rangle\langle\Phi^+|(\mathbb{1} \otimes Z) \end{aligned} \tag{A.6}$$

where X, Y, Z are the Pauli operators

$$X = \begin{pmatrix} 0 & 1 \\ 1 & 0 \end{pmatrix}, \qquad Y = \begin{pmatrix} 0 & -i \\ i & 0 \end{pmatrix}, \qquad Z = \begin{pmatrix} 1 & 0 \\ 0 & -1 \end{pmatrix}. \tag{A.7}$$

We then build disentanglers acting on the Hilbert space of two sites $i, i+1$ that apply U to the internal qubits (i, R and $i+1, L$ which form a Bell pair) and leave the external qubits (i, L and $i+1, R$) untouched.

[2] In the same sense from the previous note, this is a tensor network representation of the linear map (up to normalization).

[3] One could say it is similar to a zero-correlation-length scale invariant state, but technically this state has correlations at the length scale of the lattice spacing, which is finite.

We represent them graphically[4] by

These maps will remove the Bell pairs between sites coarse-grained by different instances of $I^\dagger$, and the partially disentangled state will then be mapped to a product state, as depicted in Fig. A.1b.

Of course, this example is designed *ad hoc* to display the phenomenon in question. In practice, however, it serves as a good illustration of what can happen when numerically performing RG on a given quantum state. Even though the inclusion of disentanglers solves the problem, it also increases the computational cost of the algorithms, hence it is always important to assess the benefits and costs of each particular strategy. As we have said before, the inclusion of disentanglers is particularly helpful when working with critical states, and when getting the correct structure of renormalization group fixed points is important.

[4]This time this is not a proper tensor network representation of the disentangler, which we cannot just write in terms of the identity tensor.

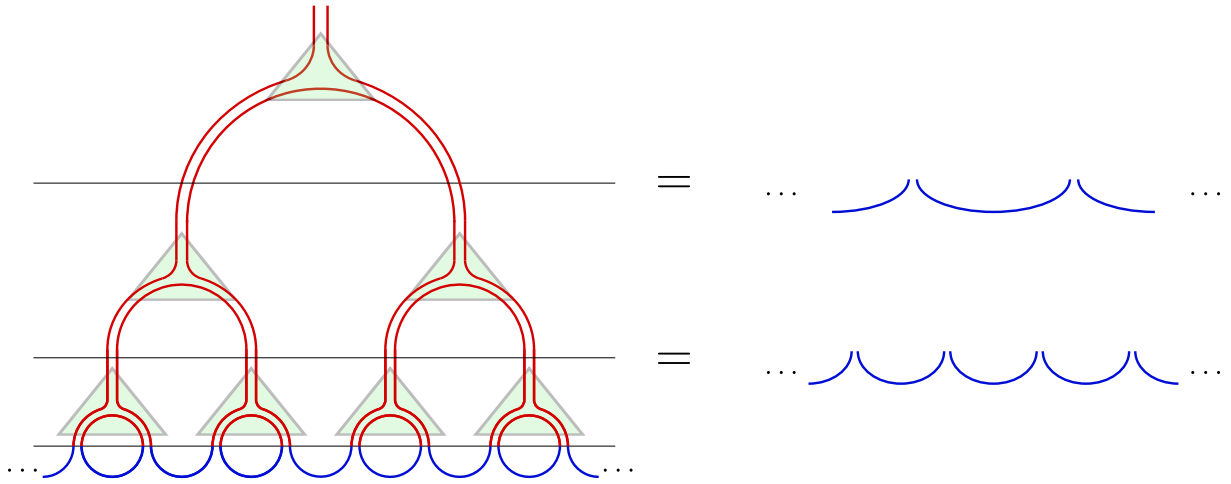

Figure A.1: (a) A coarse-graining scheme consisting only of isometries is incapable of removing all short-range entanglement, which gets promoted to upper levels, giving rise to a spurious fixed point of the RG flow. (b) If we precede the isometries by a row of disentanglers, we are able to remove all short-range entanglement and the state is mapped to a trivial fixed point, a product state, in one step.

B

Appendices for Chapter 3

B.1 Asymptotics of two-point functions

In this appendix we review the analytical determination of the asymptotic decay of two-point functions at long distances. This is done by arguments of asymptotic analysis which we expose in a self-contained manner. All the momentum space two-point functions we find in Chapter 3 are of the form

$$\langle \mathcal{O}(\vec{k})\tilde{\mathcal{O}}(\vec{q})\rangle = f(\vec{k})\delta(\vec{k} \pm \vec{q}), \tag{B.1}$$

the variable sign being + for bosonic theories and – for fermionic theories. The correlator in position space is then given by the inverse Fourier transform of $f(\vec{k})$, up to a proportionality constant:

$$\langle \mathcal{O}(\vec{0})\tilde{\mathcal{O}}(\vec{x})\rangle = (2\pi)^{-d/2}\mathcal{F}^{-1}[f](\vec{x}). \tag{B.2}$$

where d is the spatial dimension. We proceed now to argue how the asymptotic properties of this correlator for large $|\vec{x}|$ can be inferred from the knowledge of $f(\vec{k})$.

B.1.1 1+1 dimensions

Let us first consider the case with one spatial dimension. Assume $f(k)$ is integrable. The Riemann-Lebesgue lemma then states that $\mathcal{F}^{-1}[f](x)$ has to decay to zero at long distances:

$$f \in L^1(\mathbb{R}) \implies \mathcal{F}^{-1}[f](x) = \int \frac{dk}{\sqrt{2\pi}} e^{ikx} f(k) \to 0 \qquad x \to \pm\infty. \tag{B.3}$$

Imposing further conditions on $f(k)$ allows us to be more precise in the characterization of this long distance decay. For example, if we assume that $f'(k)$ exists and is also in $L_1(\mathbb{R})$. Then applying the derivative rule of the Fourier transform gives

$$\mathcal{F}^{-1}[f](x) = \frac{i}{x}\mathcal{F}^{-1}[f'](x). \tag{B.4}$$

But now, by the same Riemann-Lebesgue lemma, $f'(k) \in L^1(\mathbb{R})$ implies that $\mathcal{F}^{-1}[f'](x)$ also vanishes in the limit $|x| \to \infty$. Thus, $\mathcal{F}^{-1}[f]$ itself goes to zero faster than $|x|^{-1}$ when $|x| \to \infty$.

Alternatively, let us consider what would happen if $f(k)$ were differentiable with integrable derivative except at a number of jump discontinuities of size Δ_i at points $\{k_i\}$:

$$\lim_{\varepsilon \to 0^+} f(k_i + \varepsilon) - f(k_i - \varepsilon) = \Delta_i, \tag{B.5}$$

so that $f'(k) = h(k) + \sum_i \Delta_i \delta(k - k_i)$ with $h(k) \in L_1(\mathbb{R})$. Then we have to rewrite B.4 as:

$$\mathcal{F}^{-1}[f](x) = \frac{i}{x}\mathcal{F}^{-1}[f'](x) + \frac{i}{x}\sum_i \frac{\Delta_i e^{ik_i x}}{\sqrt{2\pi}}, \tag{B.6}$$

and the new term on the right hand side becomes the first term in the asymptotic series expansion of $F^{-1}[f](x)$. It will dominate at long distances, decaying as a power law $|x|^{-1}$ together with a certain oscillation[1] dependent on the values of the k_i.

If we are in the situation where $f'(k) \in L^1(\mathbb{R})$, this same argument above can be applied to $f''(k)$, and iteratively to higher derivatives. If $f(k), f'(k), \ldots, f^{(m-1)}(k)$ all exist as continuous integrable functions, but $f^{(m)}(k)$ presents jump discontinuities, we will find the leading order decay of $F^{-1}[f](x)$ at long distances to be $|x|^{-(m+1)}$.

B.1.2 2+1 dimensions

In higher dimensions, $f(\vec{k})$ can display a higher variety of features that translate into asymptotic properties of $\mathcal{F}^{-1}[f](\vec{x})$, and hence of the position space correlator. In Chapter 3 we encounter two different situations, depending on the behaviour of $f(\vec{k})$ around the origin, which is the only point where it is not infinitely differentiable. We review both cases in what follows. Our exposition in this section partially draws from [195].

[1] For instance, this kind of oscillations in the correlators of a fermionic system carry information of the position of the Fermi surface.

First case: $f(\vec{k}) \sim |\vec{k}|^{2m-1}$, $m \geq 0$ **as** $|\vec{k}| \to 0$

The $\langle\phi\phi\rangle$ and $\langle\pi\pi\rangle$ bosonic correlators, and the single-species fermionic correlators all belong to this first case, since close to the origin we have

$$f(\vec{k}) \sim |\vec{k}|^{-1}, \qquad f(\vec{k}) \sim |\vec{k}|, \qquad \text{and} \qquad f(\vec{k}) \sim |\vec{k}|^{2n+1}$$

respectively for each of them. In general, $f(\vec{k}) \sim |\vec{k}|^{2m-1}$ is associated with a $|\vec{x}|^{-2m-1}$ decay. This fits in well with the picture we obtained from the 1+1-dimensional case, since a higher m means higher order for the first discontinuous derivative of $f(\vec{k})$ at the origin.

Let us see it for the particular case of $m = 0$, when $f(\vec{k})$ presents a $1/|\vec{k}|$ singularity at the origin. We define a new function

$$g(\vec{k}) = \frac{e^{-|\vec{k}|^2}}{|\vec{k}|} \in L_1(\mathbb{R}^2), \tag{B.7}$$

which we use to subtract the singularity[2]:

$$f(\vec{k}) = g(\vec{k}) + h(\vec{k}), \tag{B.8}$$

so that the components of $\vec{\nabla} h(\vec{k})$ are integrable (though they might be discontinuous). Then we have

$$\mathcal{F}^{-1}[f](\vec{x}) = \mathcal{F}^{-1}[g](\vec{x}) + \mathcal{F}^{-1}[h](\vec{x}), \tag{B.9}$$

and we can deal with each of the terms individually. For h we have

$$|F^{-1}[h](\vec{x})| = \frac{1}{|\vec{x}|} |\mathcal{F}^{-1}[\vec{\nabla} h](\vec{x})|, \tag{B.10}$$

and the Riemann-Lebesgue lemma again forces the right hand side to decay faster than $|\vec{x}|^{-1}$. However, for $g(\vec{k})$ we have

$$g(\vec{k}) = e^{-|\vec{k}|^2} \cdot \frac{1}{|\vec{k}|} \implies \mathcal{F}^{-1}[g](\vec{x}) = \mathcal{F}^{-1}\left[e^{-|\vec{k}|^2}\right](\vec{x}) * \mathcal{F}^{-1}\left[\frac{1}{|\vec{k}|}\right](\vec{x}) \propto \tag{B.11}$$

$$\propto \int_{\mathbb{R}^2} d^2y \, \frac{e^{-|\vec{y}|^2/4}}{|\vec{x} - \vec{y}|}, \tag{B.12}$$

[2]Of course, if needed we could multiply g by an appropriate constant omitted here.

where $*$ denotes the convolution product. It is easy to see that the result of the convolution decays as $|\vec{x}|^{-1}$ by bounding it above and below. We have

$$\int_{\mathbb{R}^2} d^2y \, \frac{e^{-|\vec{y}|^2/4}}{|\vec{x}-\vec{y}|} = \int_{B\left(\vec{x},\frac{|\vec{x}|}{2}\right)} d^2y \, \frac{e^{-|\vec{y}|^2/4}}{|\vec{x}-\vec{y}|} \quad + \quad \int_{\mathbb{R}^2\setminus B\left(\vec{x},\frac{|\vec{x}|}{2}\right)} d^2y \, \frac{e^{-|\vec{y}|^2/4}}{|\vec{x}-\vec{y}|} \leq$$

$$\leq e^{-|\vec{x}|^2/16} \int_{B\left(\vec{x},\frac{|\vec{x}|}{2}\right)} d^2y \, \frac{1}{|\vec{x}-\vec{y}|} \quad + \quad \frac{2}{|\vec{x}|} \int_{\mathbb{R}^2} d^2y \, e^{-|\vec{y}|^2/4} \leq$$

$$\leq \pi |\vec{x}| e^{-|\vec{x}|^2/16} + \frac{8\pi}{|\vec{x}|}, \tag{B.13}$$

where $B(\vec{a}, r)$ is the ball of radius r centered at $\vec{a}$. Equally,

$$\int_{\mathbb{R}^2} d^2y \, \frac{e^{-|\vec{y}|^2/4}}{|\vec{x}-\vec{y}|} \geq \int_{B\left(-\frac{\vec{x}}{|\vec{x}|},1\right)} d^2y \, \frac{e^{-|\vec{y}|^2/4}}{|\vec{x}-\vec{y}|} \geq \frac{e^{-1}}{|\vec{x}|} \int_{B\left(-\frac{\vec{x}}{|\vec{x}|},1\right)} d^2y = \frac{\pi}{e} \frac{1}{|\vec{x}|}. \tag{B.14}$$

Thus, we have proved that the leading order of decay of $F^{-1}[f](\vec{x})$ is $|\vec{x}|^{-1}$ as claimed.

For higher values of m we can proceed by induction. If $f(\vec{k}) \sim |\vec{k}|^{2m-1}$ we subtract the function:

$$g(\vec{k}) = e^{-\vec{k}^2} |\vec{k}|^{2n-1}, \tag{B.15}$$

and expect the derivatives of $h(\vec{k}) = f(\vec{k}) - g(\vec{k})$ of order up to at least $2n+1$ to be in $L^1(\mathbb{R}^2)$. This assures that $\mathcal{F}^{-1}[h](\vec{x})$ decays faster than $|\vec{x}|^{-(2m+1)}$ by iterating an argument like the one from Eq. B.10. Now, by the induction hypothesis

$$\begin{aligned} \mathcal{F}^{-1}[g](\vec{x}) &= -\frac{\mathcal{F}^{-1}[\Delta g](\vec{x})}{|\vec{x}|^2} = \\ &= -\frac{1}{|\vec{x}|^2} \mathcal{F}^{-1}\left[e^{-|\vec{k}|^2} \left((1-2m)^2 |\vec{k}|^{2m-3} - 8n|\vec{k}|^{2m-1} + 4|\vec{k}|^{2m+1} \right) \right](\vec{x}) = \\ &= O\left(|\vec{x}|^{-(2m+1)} \right). \end{aligned} \tag{B.16}$$

Second case: $f(\vec{k}) \sim k^{2m} e^{i\phi_{\vec{k}}}$, $m \geq 0$ **as** $|\vec{k}| \to 0$

We denote by $\phi_{\vec{k}}$ the angle between $\vec{k}$ and the horizontal axis of the plane. This is the case, with $m = 0$, for the fermionic two-species correlator, and is associated to a $|\vec{x}|^{-(2m+2)}$ decay. To see this, we use a very similar strategy as in the first case. Consider

$$g(\vec{k}) = e^{i\phi_{\vec{k}}} k^{2m} e^{-|\vec{k}|^2}, \tag{B.17}$$

and write

$$f(\vec{k}) = g(\vec{k}) + h(\vec{k}) \qquad \text{with} \qquad \Delta^{m+1} h \in L^1(\mathbb{R}^2). \tag{B.18}$$

The condition on the $(m+1)$-th power of the Laplacian of h guarantees that

$$\mathcal{F}^{-1}[h](\vec{x}) = (-1)^{m+1} \frac{\mathcal{F}^{-1}[\Delta^{m+1} h](\vec{x})}{|\vec{x}|^{2m+2}} \tag{B.19}$$

decays faster than $|\vec{x}|^{-(2m+2)}$. However, for a radially symmetric function $G(\vec{k})$ in two dimensions it holds

$$\mathcal{F}^{-1}[e^{i\phi_k} G(\vec{k})](\vec{x}) = -i\partial_{|\vec{x}|} \mathcal{F}^{-1} \left[\frac{G(\vec{k})}{|\vec{k}|} \right] (\vec{x}), \tag{B.20}$$

provided that $G(k)/|\vec{k}|$ is integrable. Applying this expression for $g(\vec{k}) = e^{i\phi_{\vec{k}}} G(\vec{k})$ already implies $\mathcal{F}^{-1}[g](\vec{x}) = O\left(|\vec{x}|^{-(2m+2)}\right)$, if we use the results from the first case above.

B.2 Computation technicalities in 2+1 dimensions with rotational invariance

In the main text, and also in Appendix B.3, we compute entanglement entropies for concentric discs centered at the origin, so that we can make use of the rotational invariance of the cMERA states. To do so, we perform a canonical transformation that reexpresses our fields in terms of the radial coordinate r and an integer related to angular momentum [66]. In this appendix we specify how this is done for both bosonic and fermionic fields.

B.2.1 Bosonic theories

We define a new set of modes indexed by the radial coordinate r and the integer ℓ that accounts for the angular component:

$$\phi_\ell(r) = \sqrt{\frac{r}{\pi}} \int_0^{2\pi} d\theta \ \cos\left(\ell\theta - \frac{\pi}{4}\right) \ \phi(r\cos\theta, r\sin\theta), \tag{B.21}$$

$$\pi_\ell(r) = \sqrt{\frac{r}{\pi}} \int_0^{2\pi} d\theta \ \cos\left(\ell\theta - \frac{\pi}{4}\right) \ \pi(r\cos\theta, r\sin\theta). \tag{B.22}$$

The new modes defined this way still satisfy bosonic canonical commutation relations (in other words, the transformation is canonical):

$$[\phi_\ell(r), \pi_m(r')] = i\delta(r-r')\delta_{\ell m}, \qquad [\phi_\ell(r), \phi_m(r')] = [\pi_\ell(r), \pi_m(r')] = 0. \tag{B.23}$$

To compute the two-point functions of these new degrees of freedom, we use the following property, which can be proved in a straightforward way. Given any function $h(\zeta)$,

$$\int_0^{2\pi}\int_0^{2\pi} d\theta\, d\theta'\ \cos\left(\ell\theta - \frac{\pi}{4}\right)\cos\left(\ell'\theta' - \frac{\pi}{4}\right) h(|\theta-\theta'|) = \pi\delta_{\ell,\ell'}\int_0^{2\pi} d\zeta\ h(|\zeta|)\cos\ell\zeta. \tag{B.24}$$

Hence we obtain

$$\langle\phi_\ell(r)\phi_{\ell'}(r')\rangle = \delta_{\ell\ell'}\left(\frac{\delta(r-r')}{2\Lambda} + \sqrt{rr'}\int_0^{2\pi} d\zeta\ f\left(\sqrt{r^2+r'^2-2rr'\cos\zeta}\right)\cos\ell\zeta\right). \tag{B.25}$$

We see that, even though ϕ_ℓ is not exactly a mode of definite angular momentum, it still only couples to fields with the same value of ℓ. Something equivalent happens if we include π_ℓ:

$$\langle\phi_\ell(r)\pi_{\ell'}(r')\rangle = i\frac{\delta(r-r')\delta_{\ell\ell'}}{2} = \overline{\langle\pi_\ell(r)\phi_{\ell'}(r')\rangle}, \tag{B.26}$$

$$\langle\pi_\ell(r)\pi_{\ell'}(r')\rangle = \delta_{\ell\ell'}\left(\frac{\delta(r-r')}{2}\Lambda + \sqrt{rr'}\int_0^{2\pi} d\zeta\ g\left(\sqrt{r^2+r'^2-2rr'\cos\zeta}\right)\cos l\zeta\right). \tag{B.27}$$

Hence the correlation matrix is block diagonal:

$$C^{\mathcal{O}\mathcal{O}'}_{\ell,\ell'}(r,r') := \langle\mathcal{O}_\ell(r)\mathcal{O}'_{\ell'}(r')\rangle = \bigoplus_{\ell=-\infty}^{\infty}\langle\mathcal{O}_\ell(r)\mathcal{O}'_\ell(r')\rangle, \qquad \mathcal{O},\mathcal{O}' \in \{\phi,\pi\}. \tag{B.28}$$

When computing entanglement entropies we will make the assumption that the contributions of higher values of $|\ell|$ decay rapidly in magnitude, so that we can truncate the direct sum above at a small value of $|\ell|$ [66].

We will sample the radial indices of the correlation matrix for some lattice spacing a in the same fashion as for 1 dimensional systems (here $\Delta_\mathcal{O}$ represents the mass dimension of the operator $\mathcal{O}$):

$$C^{\mathcal{O}\mathcal{O}'}_{\ell,\ell'}(r,r') \longrightarrow [C^{\mathcal{O}\mathcal{O}'}_{\ell,\ell'}]_{ij} = a^{\Delta_\mathcal{O}+\Delta_{\mathcal{O}'}}C^{\mathcal{O}\mathcal{O}'}_{\ell,\ell'}(ia,ja), \tag{B.29}$$

$$\delta(r-r') \longrightarrow \frac{\delta_{ij}}{a} \qquad i,j\in\mathbb{N}. \tag{B.30}$$

We can then start computing contributions from the terms in the direct sum of (B.28), by the same symplectic diagonalization procedure explained in Section 3.3. We note that indeed the combined sum of all the contributions to $S(x)$ from $|\ell| \leq \ell_{\max}$ converges as $\ell_{\max}$ grows, and it does so earlier for smaller values of x.

B.2.2 Fermionic theories

In the fermionic case, we must take into account that their angular momentum has both an orbital and a spin component. Hence, the irreducible representations of the rotation group SO(2) will be indexed according to the total angular momentum quantum number j. Define

$$\psi_{1,j}(r) = \sqrt{\frac{r}{2\pi}} \int_0^{2\pi} d\theta \; e^{i\left(j+\frac{1}{2}\right)\theta} \psi_1(r\cos\theta, r\sin\theta), \tag{B.31}$$

$$\psi_{2,j}(r) = \sqrt{\frac{r}{2\pi}} \int_0^{2\pi} d\theta \; e^{i\left(j-\frac{1}{2}\right)\theta} \psi_2(r\cos\theta, r\sin\theta), \tag{B.32}$$

for $j \in \mathbb{Z} + \frac{1}{2}$. This change of variables is unitary, thus it preserves the canonical anticommutation relations:

$$\{\psi_{i,j}(r), \psi^\dagger_{i',j'}(r')\} = \delta_{i,i'}\delta_{j,j'}\delta(r-r'), \qquad \{\psi_{i,j}(r), \psi_{i',j'}(r')\} = \{\psi^\dagger_{i,j}(r), \psi^\dagger_{i',j'}(r')\} = 0. \tag{B.33}$$

$\psi_{i,j}(r)$ are hence fermionic modes with definite total angular momentum. The correlation functions in these new variables read:

$$\langle \psi^\dagger_{1,j}(r)\psi'_{1,j'}(r')\rangle = \sqrt{rr'}\delta_{j,j'} \int_0^{2\pi} d\theta \; e^{-i\left(j+\frac{1}{2}\right)\theta} F\left(\sqrt{r^2+r'^2-2rr'\cos\theta}\right) \tag{B.34}$$

$$\langle \psi^\dagger_{1,j}(r)\psi'_{2,j'}(r')\rangle = \sqrt{rr'}\delta_{j,j'} \int_0^{2\pi} d\theta \; e^{i(\xi(r,r',\theta)-j\theta)} G\left(\sqrt{r^2+r'^2-2rr'\cos\theta}\right) \tag{B.35}$$

$$\langle \psi^\dagger_{2,j}(r)\psi'_{2,j'}(r')\rangle = \delta(r-r')\delta_{j,j'} - \langle \psi^\dagger_{1,j-1}(r)\psi'_{1,j'-1}(r')\rangle \tag{B.36}$$

where

$$\xi(r,r',\theta) = \begin{cases} \pi - \dfrac{\theta}{2} - \arctan\dfrac{r\sin\theta}{r'-r\cos\theta}, & r < r', \\ \dfrac{\theta}{2} + \arctan\dfrac{r\sin\theta}{r-r'\cos\theta}, & r > r'. \end{cases} \tag{B.37}$$

Thanks to rotational symmetry, the two-point functions between modes of different angular momentum vanish, and the correlation matrix again decomposes as a direct sum over

different values of j:

$$C^{ab}_{j,j'}(r,r') := \langle \psi^\dagger_{a,j}(r)\psi_{b,j'}(r')\rangle = \bigoplus_{j\in\mathbb{Z}+\frac{1}{2}} \langle \psi^\dagger_{a,j}(r)\psi_{b,j}(r')\rangle \qquad a,b=1,2. \tag{B.38}$$

Now we discretize in the radial variable as done for the bosons. Our expectation is that, for a fixed radius, higher $|j|$ modes will contribute less and less to the entanglement, thus leading to convergence in the entanglement entropy of the disc. This is confirmed by our results displayed in Figure 3.13.

B.3 Analytic approximation of entropy scaling at short distances

In the main text we have stated that expressions can be derived that approximate well the scaling of entanglement entropy in cMERA states for spatial regions $\mathcal{R}$ of small sizes compared to the cutoff $1/\Lambda$. Here we present how this can be achieved. We make use of the techniques reviewed in Section 3.3.

B.3.1 Bosons

Our strategy consists in getting a reasonably good analytical approximation to the operator $C^{\phi\phi}C^{\pi\pi}$ from Eq. (3.10), considering it as an operator on $L^2(\mathcal{R})$ with integral kernel:

$$K(\vec{y},\vec{z}) = \int_{\mathcal{R}} d\vec{w}\; C^{\phi\phi}(\vec{y},\vec{w})C^{\pi\pi}(\vec{w},\vec{z}). \tag{B.39}$$

1+1 dimensions

Let $\mathcal{R}$ be an interval of length x (without loss of generality we consider $\mathcal{R}=[0,x]$). For $\Lambda x \ll 1$, we consider the eigenvalues of the operator of integral kernel

$$\begin{aligned} K(y,z) &= \int_0^x dy\; C^{\phi\phi}(y,w)C^{\pi\pi}(w,z) = \\ &= \int_0^x dy \left(\frac{\delta(y-w)}{2\Lambda} + f_\varepsilon(y-w)\right)\left(\frac{\Lambda\delta(w-z)}{2} + g_\varepsilon(w-z)\right). \end{aligned} \tag{B.40}$$

Since $|y-w|, |z-w| < x \ll 1/\Lambda$, the functions $f_\varepsilon(y-w)$ and $g_\varepsilon(w-z)$ can be well approximated by constants (remember the shape of the correlators in Figure 3.2, so we write

$$f(y,w) \approx A, \qquad g(w,z) \approx B\Lambda^2, \tag{B.41}$$

with A, B dimensionless constants. In practice we will Taylor expand f, g around the origin to zeroth order, meaning $A = f_\varepsilon(0), B = g_\varepsilon(0)/\Lambda^2$. The kernel $K(y,z)$ then becomes

$$K(y,z) \approx \frac{\delta(y-z)}{4} + \frac{(A+B)\Lambda}{2} + AB\Lambda^2 x. \tag{B.42}$$

To look for the eigenvalues of this approximate kernel over a space of square integrable functions $h(z) \in L^2([0,x])$, we write

$$\begin{aligned} &\int_0^x dz \left(\frac{\delta(y-z)}{4} + \frac{(A+B)\Lambda}{2} + AB\Lambda^2 L \right) h(z) = \lambda h(y) \implies \\ &\implies \left(\frac{(A+B)\Lambda}{2} + AB\Lambda^2 x \right) \int_0^x dz\, h(z) = \left(\lambda - \frac{1}{4} \right) h(y). \end{aligned} \tag{B.43}$$

Now the left hand side does not depend on y, so the right hand side must vanish unless $h(y)$ is constant. Thus we find infinitely many eigenvectors[3] with eigenvalue $1/4$ and one extra eigenvector (the constant function) with eigenvalue $1/4 + (A+B)\Lambda x/2 + AB(\Lambda x)^2 = (1+2A\Lambda x)(1+2B\Lambda x)/4$. This is the only one that contributes to the entropy, since by Eq. (3.11):

$$\lambda_i = \frac{1}{4} \implies \zeta_i = 0 \implies \rho_i = |0\rangle\langle 0| \implies S(\rho_i) = 0. \tag{B.44}$$

Thus we approximate the entropy of the interval by

$$S(x) \approx S\left(\lambda = \frac{(1+2A\Lambda x)(1+2B\Lambda x)}{4} \right), \tag{B.45}$$

which turns out to be a very good approximation to the entropy at small length scales, as can be seen in Figure 3.3. More accurate approximations can be found, for example, by going to higher order in the Taylor expansion of the kernel around $\Lambda x = 0$, something that we can do precisely because the correlators in the cMERA state are well-behaved in this limit.

[3] Namely all $L^2([0,x])$ functions whose integral vanishes.

2+1 dimensions

We obtain the estimate by approximating the correlators as in the 1+1-dimensional case, and restricting ourselves to the modes with zero angular momentum, $\ell = 0$ (see Appendix B.2). In fact, the contributions of nonzero values of ℓ vanish for the zeroth order term in the Taylor expansion of the correlators around $|\vec{y} - \vec{z}| = 0$. Again we approximate the functions f, g in the correlators (Eq. (3.55) and (3.56)) by constants

$$f(|\vec{y} - \vec{w}|) \approx f(0) =: A\Lambda, \qquad g(|\vec{w} - \vec{z}|) \approx g(0) =: B\Lambda^3, \tag{B.46}$$

for $|\vec{y} - \vec{w}|, |\vec{w} - \vec{z}| \ll 1/\Lambda$. If we consider $\mathcal{R}$ to be a disc centered at the origin with radius x, we can change to polar coordinates as in Appendix B.2. After selecting to look only at modes of zero angular momentum, we have the following approximate operator kernel:

$$\begin{aligned} K(r, r'') &= \int_0^x dr'\, C^{\phi\phi}_{\ell=\ell'=0}(r, r') C^{\pi\pi}_{\ell'=\ell''=0}(r', r'') \\ &\approx \frac{\delta(r - r'')}{4} + \left(\pi(A + B)\Lambda^2 + 2\pi^2 AB\Lambda^4 R^2\right)\sqrt{rr''} \end{aligned} \tag{B.47}$$

defined on a space of square integrable radial functions $h(r) \in L^2([0, x])$. If we look for the eigenvalues of this approximate kernel over this space, we get

$$\begin{aligned} &\int_0^x dr'' \left[\frac{\delta(r - r'')}{4} + \left(\pi\Lambda^2(A + B) + 2\pi^2 AB\Lambda^4 R^2\right)\sqrt{rr''}\right] h(r'') = \lambda h(r) \implies \\ &\implies \left(\pi\Lambda^2(A + B) + 2\pi^2 AB\Lambda^4 R^2\right)\sqrt{r}\int_0^x dr''\,\sqrt{r''}h(r'') = \left(\lambda - \frac{1}{4}\right)h(r). \end{aligned} \tag{B.48}$$

Again as in the one dimensional case we find infinitely many eigenvectors with eigenvalue $1/4$ and one extra eigenvector (which in this case is proportional to $\sqrt{r}$) with eigenvalue $1/4 + \pi(A + B)(\Lambda x)^2/2 + \pi^2 AB(\Lambda x)^4 = (1 + 2\pi A(\Lambda x)^2)(1 + 2\pi B(\Lambda x)^2)/4$, which is the only one that contributes to the entropy:

$$S(x) \approx S\left(\lambda = \frac{(1 + 2\pi A(\Lambda x)^2)(1 + 2\pi B(\Lambda x)^2)}{4}\right). \tag{B.49}$$

In the regime ($\Lambda x \ll 1$), this expression provides a good approximation to the entropy scaling, as can be seen in Figure 3.6.

B.3.2 Fermions

In the fermionic case, we saw in Section 3.3 that the entropy can be computed as a sum of contributions coming from the spectrum of the correlation matrix

$$C^{ij}(\vec{y},\vec{z}) = \langle \psi_i^\dagger(\vec{y})\psi_j(\vec{z})\rangle\big|_{x,y\in\mathcal{R}}^{i,j=1,2}. \tag{B.50}$$

This we will now see as the kernel of an integral operator over the space $[L^2(\mathcal{R})]^2$ of pairs of square integrable functions $(h_1(\vec{z}), h_2(\vec{z}))$, one per spinor component.

1+1 dimensions

Let $\mathcal{R} = [0, x]$ with $\Lambda x \ll 1$ again and consider the correlation functions at this length scale. The two-point functions can be well approximated by their Taylor expansion to first order around the origin:

$$\langle \psi_1^\dagger(y)\psi_1(z)\rangle \approx A\Lambda \tag{B.51}$$
$$\langle \psi_1^\dagger(y)\psi_2(z)\rangle \approx iB\Lambda^2(x-y), \tag{B.52}$$

with $A, B \in \mathbb{R}$ dimensionless constants. The linear term is zero for the first one, as is the constant term for the second. The eigenvalue equation for the correlation matrix can then be written as

$$\int_0^x C^{ij}(y,z)h_j(z)\,dz = \lambda h_i(y), \tag{B.53}$$

resulting in

$$A\lambda\int_0^x h_1(z)\,dz + iB\lambda^2\int_0^x (y-z)h_2(z)\,dz = \lambda h_1(x) \tag{B.54}$$
$$-iB\lambda^2\int_0^x (y-z)h_1(z)\,dz - A\lambda\int_0^x h_2(z)\,dz = (\lambda-1)h_2(x). \tag{B.55}$$

If $\lambda \neq 0, 1$ (values with don't contribute to the entropy), these equations constrain the eigenvector to be made of linear functions:

$$h_1(z) = a + bz, \qquad h_2(z) = c + dz. \tag{B.56}$$

And upon substitution in the equations above we obtain an eigenvalue problem for a 4-dimensional matrix whose solutions are, in a Taylor expansion to first non-vanishing order

around $\Lambda x = 0$:

$$\lambda_1 \approx A\Lambda x, \qquad \lambda_2 \approx 1 - A\Lambda x,$$
$$\lambda_3 \approx -\frac{B^2(\Lambda x)^4}{12}, \qquad \lambda_4 \approx 1 + \frac{B^2(\Lambda x)^4}{12}. \tag{B.57}$$

The two first eigenvalues are in the right interval $[0, 1]$ and give the only nontrivial contribution to the entropy. The other two eigenvalues are outside of the acceptable range, but they are so due to high order contributions of Λx, what leads us to assume that they are artifacts of the truncation in the correlators and will converge to 0 and 1 respectively if we take more terms in the expansion. Thus our short-range estimation of the entanglement entropy scaling (which ends up being independent of B) is

$$S(x) \approx S(\lambda = A\Lambda x) + S(\lambda = 1 - A\Lambda x) = 2S(\lambda = A\Lambda x) = 2\frac{(1 - \log A\Lambda x)}{\log 2} A\Lambda x. \tag{B.58}$$

As for its bosonic counterpart, were it needed we could improve on this estimate by using more terms of the Taylor expansions of the correlators.

2+1 dimensions

To keep the computations simple, and given the results in the 1+1 dimensional case, we approximate the functions f and g from the two-point functions by their zeroth-order Taylor expansion:

$$f(|\vec{x} - \vec{y}|) \approx f(0) = A\Lambda^2, \qquad g(|\vec{x} - \vec{y}|) \approx g(0) = 0. \tag{B.59}$$

This approximation already implies that the only non-vanishing contributions to the entropy are going to come from the smallest values of angular momentum, namely $j = \pm\frac{1}{2}$ (see Appendix B.3). In particular, they come from the modes of zero *orbital* angular momentum. The eigenvalue problems that we have to solve are those of the approximate kernels:

$$\langle \psi^\dagger_{1,-\frac{1}{2}}(r)\psi_{1,-\frac{1}{2}}(r')\rangle \approx 2\pi A\sqrt{rr'}, \tag{B.60}$$
$$\langle \psi^\dagger_{2,\frac{1}{2}}(r)\psi_{2,\frac{1}{2}}(r')\rangle \approx \delta(r - r') - 2\pi A\sqrt{rr'}. \tag{B.61}$$

So proceeding as for the bosons we get

$$\begin{aligned} S(x) &\approx S(\lambda = \pi A(\Lambda x)^2) + S(\lambda = 1 - \pi A(\Lambda x)^2) = \\ &= -2\left(\pi A(\Lambda x)^2 \log_2\left(\pi A(\Lambda x)^2\right) + (1 - \pi A(\Lambda x)^2)\log_2\left(1 - \pi A(\Lambda x)^2\right)\right) \end{aligned} \tag{B.62}$$

which provides a good estimation in the short distance regime (Figure 3.13).

Notice that in both the bosonic and fermionic case we have approximated the entanglement entropy for that of a theory with flat two point functions. Because we assume such simple situation, the entropy can be computed easily, and we end up with expressions that depend in the same functional way on the volume of the spatial region (Λx in one spatial dimension, $\pi(\Lambda x)^2$ in two spatial dimensions) for each statistics (bosons or fermions).

C

Appendices for Chapter 4

C.1 Fermionic magic cMERA

In this appendix we briefly describe how the magic cMERA looks like for the free Dirac fermion. Consider the entangler (2.16) with

$$h(k) = -\frac{1}{2}\frac{\Lambda}{\Lambda^2 + k^2} \qquad \left(\implies g(k) = \frac{1}{2}\frac{\Lambda k}{\Lambda^2 + k^2} \right), \tag{C.1}$$

i.e., $h(k)$ is up to a sign the same function that gave the magic entangler for the bosonic case (4.44). Consequently, in $d = 1$, the entangler has an exponentially decaying real space profile,

$$h(x) \propto e^{-\Lambda|x|}. \tag{C.2}$$

This, again, should allow to build continuous matrix product operator representations of the evolution generated by K. We can also check that there is a simple way to give parent Hamiltonians to all intermediate states in the cMERA evolution, as well as the fixed point. Starting from $\theta(k) = 0$, and evolving with the $g(k)$ from (C.1), we have:

$$\begin{aligned} \theta(k, s) &= \frac{1}{2}\left(\arctan\frac{\Lambda}{k} - \arctan\frac{\Lambda e^{-s}}{k} \right) \\ &= \frac{1}{2}\arctan k\frac{\Lambda - \Lambda e^{-s}}{k^2 + \Lambda^2 e^{-s}}. \end{aligned} \tag{C.3}$$

Denote the Dirac CFT Hamiltonian

$$H^{\text{CFT}} = \int d^d x \; \psi^\dagger(\vec{x})\gamma^0(-i\vec{\gamma}\cdot\vec{\partial})\psi(\vec{x}), \tag{C.4}$$

and the massive Hamiltonian

$$H_m = H^{\text{CFT}} + \int d^d x \; \psi^\dagger(\vec{x}) m \gamma^0 \psi(\vec{x}). \tag{C.5}$$

It can then be checked that a strictly local parent Hamiltonian is given by

$$H(s) = H_{m(s)} + A^\Lambda_{\text{UV}} - e^{-s} H^{\text{CFT}}, \tag{C.6}$$

where

$$A^\Lambda_{\text{UV}} \equiv \int d^d x \; \frac{\vec{\nabla}\psi^\dagger(\vec{x})\gamma_0 \vec{\nabla}\psi(\vec{x})}{\Lambda} \tag{C.7}$$

is the nonrelativistic UV regulating term, analogous to (4.49) and again $m(s) = \Lambda e^{-s}$. As in the boson case, a mass term appears to represent the IR cutoff going to 0. However, in the fermionic case we also have to slowly "turn on" the Dirac Hamiltonian, which is not present in the product state ($s = 0$) parent Hamiltonian.

C.2 On the continuity of the $s \to \infty$ limit

It is important to point out a subtlety with the $s \to \infty$ limit of the longitudinal degrees of freedom in the cMERA from the main text. A reader familiar with the $m \to 0$ limit of the massive vector boson theory to the massless vector boson theory will find it analogous to what we present here. To be concrete, we study the particular case of 1+1 dimensions, where there are no transversal degrees of freedom. We thus denote $A(\vec{k}) \equiv A_1(\vec{k}) = A_\parallel(\vec{k})$ and $\Pi(\vec{k}) \equiv \Pi_1(\vec{k}) = \Pi_\parallel(\vec{k})$. The massless case theory is pure gauge, having no physical degrees of freedom except for the zero mode $A(\vec{k}=0), \Pi(\vec{k}=0)$ (which gives the quantization of the constant value of the electric field, the only physical degree of freedom of the classical theory). The massless Hamiltonian is given by

$$H = \frac{1}{2}\int dx \; \Pi(x)^2 = \frac{1}{2}\int dk \; \Pi(-k)\Pi(k), \tag{C.8}$$

and its ground state is characterized by

$$\Pi(k)|\Psi\rangle = 0 \tag{C.9}$$

which includes the gauge invariance constraint ($k \neq 0$) and the energy minimization for the single degree of freedom ($k = 0$). It is hard to make statements about the entanglement

properties of this state, since, even though Fourier transformation of (C.9) yields local annihilation operators

$$\Pi(x)|\Psi\rangle = 0, \tag{C.10}$$

as befits an unentangled state, there are no local physical degrees of freedom to speak about their correlations or lack thereof.

Applying the formalism from the main text, we start from the unentangled state

$$\psi(x)|\Lambda\rangle = 0 \tag{C.11}$$

and evolve with an entangler

$$K = \frac{-i}{2}\int dk\; g(k)\psi(-k)\psi(k) + \text{h.c.} \tag{C.12}$$

with

$$g(k) = 1 - \frac{1}{2}\frac{\Lambda^2}{\Lambda^2 + k^2}. \tag{C.13}$$

In position space, this entangler looks like this

$$K = \int dx\; A(x)\Pi(x) - \int dx\, dy\; e^{-\Lambda|x-y|}A(x)\Pi(y), \tag{C.14}$$

that is, it has an onsite part, and a bilocal part which acts at a particular length scale Λ^{-1}. The cMERA states are then characterized by

$$\left(\sqrt{\frac{\alpha(k,s)}{2}}A(k) + i\sqrt{\frac{1}{2\alpha(k,s)}}\Pi(k)\right)|\psi^\Lambda(s)\rangle = 0 \tag{C.15}$$

with

$$\alpha(k,s) = \frac{m(s)^2}{\Lambda}\sqrt{\frac{k^2+\Lambda^2}{k^2+m(s)^2}}. \tag{C.16}$$

Figure C.1 shows a qualitative plot of $\alpha(k,s)$. States at finite values of s are ground states of the following regularized version of the massive vector boson Hamiltonian:

$$H(s) = \int dx\; \left[\frac{\Pi(x)^2}{2} + \frac{m^2}{\Lambda^2}(\partial A(x))^2\right], \tag{C.17}$$

where $m(s) = \Lambda e^{-s}$. These states are entangled, due to the action of K. At any finite time in the evolution, the state has all the entanglement that has been introduced from the

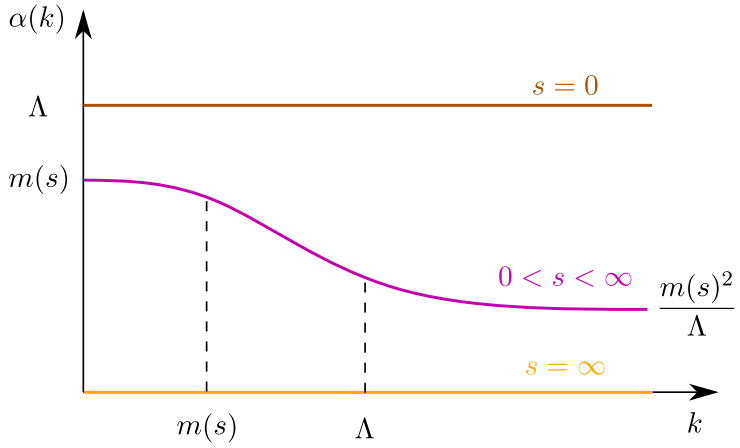

Figure C.1: Evolution of $\alpha(k, s)$ (qualitative plot).

UV cutoff scale Λ^{-1} to the IR cutoff scale $m(s)^{-1}$. This entanglement does not disappear smoothly in the $s \to \infty$ limit because the convergence to the fixed point is not smooth. Take a look at the two-point function for $\Pi(x)$:

$$\langle \Pi(x)\Pi(y)\rangle \propto \mathcal{F}^{-1}[\alpha(k)](x-y) \tag{C.18}$$

Because of the behaviour of $\alpha(k)$ we can decompose this correlator into two parts: an onsite delta and an integrable function of the distance:

$$\langle \Pi(x)\Pi(y)\rangle \sim \frac{m(s)^2}{\Lambda}\delta(x-y) + f_s(x-y) \tag{C.19}$$

As $s \to 0$, we have $\|f_s\|_2 \to 0$ so both terms in the correlator go to zero. However the value at $x = y$, corresponding to the squared norm of $\Pi(x)|\Psi^\Lambda(s)\rangle$ preserves the delta divergence for the whole evolution, while it should be zero in the gauge invariant subspace.

D

Appendix for Chapter 5

In this appendix we are looking for a basis of modes

$$f_k(x)e^{-i|k|t} \qquad k \in \mathbb{R} \tag{D.1}$$

which satisfies the orthonormality property

$$\int dx\ f_k^*(x) f_q(x) = \delta(k-q) \tag{D.2}$$

as well as the matching conditions of the conformal defects that we consider in 5.2.2. We use the ansatz

$$f_k(x) \equiv \left(\alpha_k\, e^{ikx} + \beta_k\, e^{-ikx}\right) \oplus \left(\alpha'_k\, e^{ikx} + \beta'_k\, e^{-ikx}\right). \tag{D.3}$$

This is suitable for us because the matching conditions of the defect will end up relating the primed coefficients to the unprimed ones. The physical motivation behind this ansatz is the fact that the defect, for generic θ, will partially reflect and transmit the incident particles, so if we include modes of momentum k we may also need to include modes of momentum $-k$ for the reflected particles.

We want the modes $f_k(x)e^{-i|k|t}$ to satisfy the defect conditions (5.22). These translate into

$$\alpha_k - \beta_k = \tan\theta\,(\alpha'_k - \beta'_k), \tag{D.4}$$

$$\alpha_k + \beta_k = \cot\theta\,(\alpha'_k + \beta'_k), \tag{D.5}$$

for all $k \neq 0$. If we define η such that

$$\cosh\eta = \frac{\tan\theta + \cot\theta}{2}, \qquad \sinh\eta = \frac{\tan\theta - \cot\theta}{2}, \tag{D.6}$$

then (D.4)-(D.5) imply

$$\begin{pmatrix} \alpha'_k \\ \beta'_k \end{pmatrix} = \begin{pmatrix} \cosh\eta & \sinh\eta \\ \sinh\eta & \cosh\eta \end{pmatrix} \begin{pmatrix} \alpha_k \\ \beta_k \end{pmatrix} \equiv R(\eta)\mathfrak{a}_k, \tag{D.7}$$

where we have defined

$$\mathfrak{a}_k = \begin{pmatrix} \alpha_k \\ \beta_k \end{pmatrix}. \tag{D.8}$$

Once we impose this condition, the primed coefficients are fixed, and the family of functions f_k is given just by the parameters $\mathfrak{a}_k$. Now we want to choose them so that the $f_k(x)$ form an orthonormal basis. To do so we compute the inner product of two such functions:

$$\begin{aligned} \langle f_k, f_q\rangle &= \int_{-\infty}^{\infty} dx\ f_k^*(x) f_q(x) \qquad\qquad (D.9)\\ &= \int_{-\infty}^{0} dx\ \left(\alpha_k^* e^{-ikx} + \beta_k^* e^{ikx}\right)\left(\alpha_q e^{iqx} + \beta_q e^{-iqx}\right) \\ &+ \int_{0}^{\infty} dx\ \left(\alpha_k'^* e^{-ikx} + \beta_k'^* e^{ikx}\right)\left(\alpha'_q e^{iqx} + \beta'_q e^{-iqx}\right) \\ &= \left(\alpha_k^*\alpha_q + \beta_k^*\beta_q + \alpha_k'^*\alpha'_q + \beta_k'^*\beta'_q\right)\pi\delta(k-q) \\ &+ \left(\beta_k^*\alpha_q + \alpha_k^*\beta_q + \beta_k'^*\alpha'_q + \alpha_k'^*\beta'_q\right)\pi\delta(k+q) \\ &+ \left(\alpha_k^*\alpha_q - \beta_k^*\beta_q - \alpha_k'^*\alpha'_q + \beta_k'^*\beta'_q\right)\frac{i}{k-q} + \left(-\beta_k^*\alpha_q + \alpha_k^*\beta_q + \beta_k'^*\alpha'_q - \alpha_k'^*\beta'_q\right)\frac{i}{k+q} \end{aligned}$$

where we have used:

$$\int_{-\infty}^{0} dx\ e^{ikx} = \pi\delta(k) - \frac{i}{k} \tag{D.10}$$

$$\int_{0}^{\infty} dx\ e^{ikx} = \pi\delta(k) + \frac{i}{k} \tag{D.11}$$

Now imposing the gluing condition (D.7) we obtain

$$\begin{aligned} \langle f_k, f_q\rangle &= \mathfrak{a}_k^\dagger\left(\mathbb{1} + R^\dagger(\eta)R(\eta)\right)\mathfrak{a}_q\,\pi\delta(k-q) \\ &+ \mathfrak{a}_k^\dagger\left(X + R^\dagger(\eta)XR(\eta)\right)\mathfrak{a}_q\,\pi\delta(k+q) \\ &+ \mathfrak{a}_k^\dagger\left(Z - R^\dagger(\eta)ZR(\eta)\right)\mathfrak{a}_q\,\frac{i}{k-q} \\ &+ \mathfrak{a}_k^\dagger\left(ZX - R^\dagger(\eta)ZXR(\eta)\right)\mathfrak{a}_q\,\frac{i}{k+q}, \end{aligned}$$

where

$$X = \begin{pmatrix} 0 & 1 \\ 1 & 0 \end{pmatrix}, \qquad Z = \begin{pmatrix} 1 & 0 \\ 0 & -1 \end{pmatrix}. \tag{D.12}$$

Now using $[X, R(\eta)] = 0$ and $R^\dagger(\eta) Z R(\eta) = Z$, we have

$$\begin{aligned} \langle f_k, f_q \rangle = \mathrm{a}_k^\dagger \left(\mathbb{1} + R^\dagger(\eta) R(\eta) \right) \mathrm{a}_q \, \pi \delta(k-q) \\ + \mathrm{a}_k^\dagger X \left(\mathbb{1} + R^\dagger(\eta) R(\eta) \right) \mathrm{a}_q \, \pi \delta(k+q) \end{aligned}$$

To make this into an orthogonal basis, we can simply let a_k be independent of k and such that the second coefficient vanishes. Using a bit of algebra, we conclude that we can use either of the columns of $\mathbb{1} - iR(-\eta)$, since

$$X \left(\mathbb{1} + R^\dagger(\eta) R(\eta) \right) = \left(\mathbb{1} + iR^\dagger(\eta) \right) X \left(\mathbb{1} - iR(\eta) \right), \tag{D.13}$$

and

$$(\mathbb{1} - iR(\eta))^{-1} = \frac{2i}{\cosh \eta} (1 - iR(-\eta)). \tag{D.14}$$

Hence we (arbitrarily) pick the first column, which amounts to

$$\alpha = \frac{\sin 2\theta - i}{2}, \quad \beta = -i \cos 2\theta. \tag{D.15}$$

After all this computation, we have finally arrived at the basis of functions

$$f_k(x) = \frac{1}{2\sqrt{\pi}} \left((\sin 2\theta - i) e^{ikx} - i \cos 2\theta e^{-ikx} \right) \oplus \left((1 - i \sin 2\theta) e^{ikx} - \cos 2\theta e^{-ikx} \right), \tag{D.16}$$

and to obtain the basis from the main text, as shown in (5.29), we just need to multiply f_k by a phase $e^{i\frac{\pi}{4}}$. We do this for convenience, so that in the case $\theta = \frac{\pi}{4}$ (trivial defect), our basis of modes reduces to the plane waves from (5.5).

E

Appendix for Chapter 6

In this appendix we briefly review the free fermion formalism for the critical Ising model, which we used to ease numerical computations.

Via a Jordan-Wigner transformation we can change from spin variables to complex fermion variables:

$$c_j = \left(\prod_{k<j} Z_k\right) \frac{X_j + iY_j}{2} \tag{E.1}$$

in which the Ising Hamiltonian (6.32) takes the form:

$$H = -\frac{1}{2}\sum_j [(c_{j+1} + c_{j+1}^\dagger)(c_j - c_j^\dagger) - 2c_j^\dagger c_j] \tag{E.2}$$

Now we define the fermion operators in Fourier space, and rewrite the Hamiltonian (up to additive constants):

$$c_p = \frac{1}{\sqrt{2\pi}}\sum_j c_j e^{ipj} \qquad \{c_p, c_q^\dagger\} = \delta(p-q) \tag{E.3}$$

$$H = \frac{1}{2}\int_{-\pi}^{\pi} dp \left[(1-\cos p)\left(c_p^\dagger c_p + c_{-p}^\dagger c_p\right) + i\sin p\,\left(c_{-p}c_p + c_{-p}^\dagger c_p^\dagger\right)\right] \tag{E.4}$$

The Hamiltonian can then be diagonalized in momentum space by means of the Bogoliubov transformation

$$c_p = \cos\theta(p)\; b_p - i\sin\theta(p)\; b_{-p}^\dagger, \tag{E.5}$$

$$c_{-p} = \cos\theta(p)\; b_{-p} + i\sin\theta(p)\; b_p^\dagger, \tag{E.6}$$

with $\theta(p) = \frac{\pi - p}{4}, p \in [0, \pi]$. Again up to an additive constant, we have

$$H = \int_{-\pi}^{\pi} dp \ \left|\sin\left(\frac{p}{2}\right)\right| \ b_p^\dagger b_p. \tag{E.7}$$

The ground state correlation functions are therefore

$$\langle b_p b_q \rangle = 0, \tag{E.8}$$

$$\langle b_p b_q^\dagger \rangle = \delta(p - q). \tag{E.9}$$

Hence

$$\langle c_p c_q \rangle = \frac{i}{2} \cos\left(\frac{p}{2}\right) \mathrm{sign}(p) \delta(p + q), \tag{E.10}$$

$$\langle c_p c_q^\dagger \rangle = \frac{1}{2}\left(1 + \left|\sin\left(\frac{p}{2}\right)\right|\right) \delta(p - q), \tag{E.11}$$

which implies, back to position space

$$\langle c_n c_m \rangle = \frac{1}{\pi} \frac{2(n-m)}{4(n-m)^2 - 1}, \tag{E.12}$$

$$\langle c_n c_m^\dagger \rangle = \frac{1}{2}\delta_{nm} - \frac{1}{\pi} \frac{1}{4(n-m)^2 - 1}. \tag{E.13}$$

Now we can obtain the spectrum of the density matrix ρ for N sites by diagonalizing a $2N \times 2N$ correlation matrix, which is a significant improvement with respect to the exponential growth of the dimensionality of ρ. The procedure is as follows: we let v_c be the (column) vector of the $2N$ creation-annihilation operators on the sites of the interval whose reduced density matrix we want to compute,

$$v_c = \begin{pmatrix} c_1^\dagger \\ \vdots \\ c_N^\dagger \\ c_1 \\ \vdots \\ c_N \end{pmatrix}, \tag{E.14}$$

and we build the (Hermitian, positive semidefinite) correlation matrix,

$$\Gamma \equiv \langle v_c v_c^\dagger \rangle = \begin{pmatrix} \langle c_i^\dagger c_j \rangle & \langle c_i^\dagger c_j^\dagger \rangle \\ \langle c_i c_j \rangle & \langle c_i c_j^\dagger \rangle \end{pmatrix} \tag{E.15}$$

and diagonalize it via a canonical transformation of the modes, i.e., a linear map

$$c_i \longrightarrow \tilde{c}_i = A_{ij} c_j + B_{ik} c_k^\dagger \tag{E.16}$$

$$c_i^\dagger \longrightarrow \tilde{c}_i^\dagger = B_{ik}^* c_k + A_{ij}^* c_j^\dagger \tag{E.17}$$

under which Hermitian conjugates are mapped to Hermitian conjugates and the canonical anticommutation relations are preserved. The group of such transformations is isomorphic to $O(2N)$ (which can be more easily seen by rewriting it in terms of Majorana fermions). This way we find a set of N uncorrelated fermionic degrees of freedom $\{\tilde{c}_i, \tilde{c}_i^\dagger\}_{i=1}^N$ (related to the original ones by a nonlocal transformation), and the density matrix factorizes as the tensor product of density matrices associated to each of them:

$$\rho = \bigotimes_{i=1}^{N} \rho_i. \tag{E.18}$$

The entanglement spectrum can be obtained from the eigenvalues of Γ, which naturally come in pairs $(\lambda_i, 1 - \lambda_i)$.